INVESTIGATION OF WIND PROTECTIVE SYSTEMS ON MODELS OF SINGLE STORY STRUCTURES

By

RONALD JAY GADDIS

Bachelor of Science
Oklahoma State University
Stillwater, Oklahoma
1957

Master of Science
Oklahoma State University
Stillwater, Oklahoma
1971

Submitted to the Faculty of the Graduate College
of the Oklahoma State University
in partial fulfillment of the requirements
for the Degree of
DOCTOR OF PHILOSOPHY
July, 1977

Thesis
1977D
G123i
cop. 2

OKLAHOMA STATE UNIVERSITY LIBRARY

INVESTIGATION OF WIND PROTECTIVE SYSTEMS

ON MODELS OF SINGLE STORY STRUCTURES

Thesis Approved:

Thesis Adviser

Dean of the Graduate College

997258

ACKNOWLEDGMENTS

The research reported in this study was supported by funds from the Oklahoma Agricultural Experiment Station, Cooperative State Research Service of the United States Department of Agriculture and by the National Science Foundation.

I wish to extend my sincere thanks to many on the Oklahoma State University Faculty and Staff for their help, inspiration and encouragement throughout my graduate program. Especially to my major overseers, Dr. Allen F. Butchbaker, who was my mainstay during the beginning and Dr. George W. A. Mahoney, my present major adviser -- a hearty thanks! To Professor Jay G. Porterfield, now Head of the Agricultural Engineering Department, I express my thanks for aid in procuring and scheduling equipment and for guidance dating back to my early years in Agricultural Engineering. To David G. Batchelder go thanks for assistance in solving still more equipment procurement problems. The counsel and friendship of Dr. Bobby L. Clary is gratefully acknowledged.

To the members of both my former and present advisory committees, Dr. Gerald H. Brusewitz, Committee Chairman, Dr. John Lloyd, Dr. Charles Rice, and Dr. Rao K. Munshi, I express my gratitude for their concern, their patience, their advice and for the many ways they went above and beyond the call of duty in showing interest in what I was attempting to do.

Sincere appreciation is extended to four long time friends: to

George Cook, Clyde Skoch and Norvil Cole for their advice on constructing and setting up the equipment. Jack Fryrear's assistance with the photography and drafting has been invaluable.

Undergraduate help for the project resulted in more friends to whom thanks are certainly in order; Joe Brungardt, Mike McClure, and Mark Kiner to name a few.

To Professor E. W. Schroeder, now retired, formerly Head of the Oklahoma State Agricultural Engineering Department, for his guidance, encouragement and assistance in obtaining financial support, I express my gratitude and my respect.

To my fellow graduate students whose comraderie through all the trials and tribulations helped to make the whole endeavor worthwhile, thank you.

To my fellow faculty members and coworkers at the University of Nebraska, without whose constant understanding, encouragement and sacrifice I could never have completed such a demanding task, I shall forever be indebted.

To my father, who with his PhD in the world of experience, came from retirement with his practical advice and patiently gave his time and skill to help fabricate hundreds of little pieces of equipment of one kind or another, to help take data far into the night and generally encourage his son in this wild undertaking, -- I owe a debt of gratitude truly impossible to express. The memory of his help and his fellowship will be with me as long as I live.

Last of all, to all my family whose sacrifice to this cause has been far greater than even I will ever be able to comprehend, I say, "Hurray! It is finished?"

TABLE OF CONTENTS

Chapter		Page
I.	INTRODUCTION	1
	Protection from Wind Damage	1
	This Investigation	3
II.	LITERATURE REVIEW	4
	Wind Description	4
	Velocity Magnitude	5
	Velocity Variation with Height Above the Ground	6
	Fluid Flow and the Building	10
	Simulation and Modeling	17
	Fluidic Similarity	17
	Similarity of the Wind Profile	19
	Similarity of Building and Its Surroundings	20
	Buckingham Pi Theorem	21
	Force Measuring Methods	23
	Flow Visualization Techniques	24
III.	THE INVESTIGATION	27
	Objectives	27
	Scope of the Investigation	28
	Method	28
	Qualitative Investigation	31
	Objectives	31
	Method	31
	Equipment-Smoke Tunnel and Models	32
	Entrance Section	36
	Smoke Chamber	38
	Exhaust Section	40
	Smoke Generating Equipment	40
	Lighting	46
	Jig for Models	46
	Procedure	49
	Discussion of Results	49
	Conclusions	50
	Duct Systems	53
	Airfoil Systems	55
	Venting System	57
	Deflector System	61

Chapter Page

Summary 61
Quantitative Investigation 63
Objectives. 63
Method. 63
Experimental Design 65
Pertinent Quantities 65
Pi Terms 69
Pi Terms Not Included. 72
Equipment 73
Wind Tunnel. 73
The Model. 79
The Cantilever Beams 82
Strain Gage Circuitry. 85
Equipment and Circuitry for the Wind Characteristics. 93
Analog Circuitry 98
Calibrations. 102
Cantilever Beam Calibration. 103
Comparisons of Initial and Final Calibrations 104
Calibration of Hot Wire Anemometer 110
The Establishment of the Velocity Profile. . 110
Reynolds Number Investigations 120
Conclusions 124
Procedure 126
Variations in the Standard Procedure 128
Sealing Tests. 129
Deflectors. 132
Objective. 132
Method 133
Equipment Unique to the Deflector Investigation. 133
Procedure. 137
Results - First Deflector Series, Unsealed Model 141
Supplemental Tests - Deflectors, Unsealed Model 156
Conclusions - Deflectors, Unsealed Model. 164
Deflectors, Sealed Model 169
Results - Deflectors, Sealed Model 170
Conclusions - Deflectors, Sealed Model . . . 191
Airfoils. 194
Objective. 194
Method 194
Equipment Unique to the Airfoil Investigation. 195
Procedure. 199
Results - Airfoils, Unsealed Model 200
The Two Additional Tests 202
Conclusions - Airfoils, Unsealed Model . . . 206

Chapter Page

Airfoils, Sealed Model 209
Results - Airfoils, Sealed Model 210
Conclusions - Airfoils, Sealed Model 217
Ducts 218
Objective. 218
Method 219
Equipment Unique to the Duct Investigation. 219
Procedure. 220
Results - Ducts, Unsealed Model. 222
Conclusions - Ducts, Unsealed Model. 227
Results - Ducts, Sealed Model. 227
Conclusions - Ducts, Sealed Model. 231
Eave Overhang, Sealed Model 235
Objective. 235
Method 235
Equipment Unique to the Eave Overhang Investigation. 235
Procedure. 238
Results - Eave Overhang. 239
Conclusions - Eave Overhang. 243
Results - Eave Overhang with Holes 243
Conclusions - Eave Overhang with Holes . . . 248
Results - Eave Overhang, Bent. 249
Conclusions - Eave Overhang, Bent. 252
Conclusions for the Complete Eave Overhang Series. 253
Venting 253
Objective. 253
Method 254
Equipment Unique to the Venting Investigation. 254
Procedure. 255
Results - Venting, Unsealed Model. 255
Conclusions - Venting, Unsealed Model. . . . 264
Results - Venting, Sealed Model. 265
Conclusions - Venting, Sealed Model. 266
Duct - Final Investigation. 269
Method 269
Equipment. 269
Procedure. 273
Sample Calculations. 274
Discussion of Results. 281
Sample Calculation to Obtain Drag or Lift Coefficient 303
Conclusions. 307

IV. SUMMARY 310

Method, Procedure and Equipment Critique 310

Chapter Page

Findings and Conclusions 312
Deflectors, Unsealed Model. 312
Deflectors, Sealed Model. 313
Airfoils, Unsealed Model. 313
Airfoils, Sealed Model. 314
Ducts, Unsealed Model 314
Ducts, Sealed Model 314
Eave Overhang, Sealed Model 315
Venting, Unsealed Model 315
Venting, Sealed Model 316
Ducts, Final Option 316
Future Study 317

REFERENCES CITED 318

APPENDICES 321

APPENDIX A - SMOKE TUNNEL OPERATION 322

APPENDIX B - CONTINUOUS DATA ANALYSIS USING THE ANALOG COMPUTER 327

APPENDIX C - ANALOG CIRCUITS. 336

APPENDIX D - CANTILEVER BEAM CALIBRATIONS 338

APPENDIX E - TEST DATA. 340

APPENDIX F - COMPUTER PROGRAM FOR FINAL INVESTIGATION 353

LIST OF TABLES

Table		Page
I.	List of Pertinent Quantities.	66
II.	Pi Terms.	68
III.	Strain Gauge Circuitry Resistance Values.	91
IV.	Calibration Differences	108
V.	Velocity Profile Data	120
VI.	Change in Strain Due to Sealing Joints.	130
VII.	Unsealed Test Series for Alternative I.	140
VIII.	Summary of Partially Reduced Data, Deflectors--Unsealed Model.	148
IX.	Supplemental Tests - I-11 and I-8 Percent Change with Respect to Control Model.	157
X.	I-26 - I-28 - I-27, Percent Difference.	158
XI.	Test Series - Alternative I, Sealed Model	170
XII.	Summary of Partially Reduced Data, Deflectors--Sealed Model	175
XIII.	Summary of Partially Reduced Data, Airfoils--Unsealed Model	207
XIV.	Summary of Partially Reduced Data, Airfoils--Sealed Model	215
XV.	Summary of Partially Reduced Data, Ducts--Unsealed Model	223
XVI.	Comparisons of Partially and Fully Corrected Data for Beam Calibration.	225
XVII.	Summary of Partially Reduced Data, Ducts--Sealed Model.	232

Table		Page
XVIII.	Summary of Partially Reduced Data Venting Tests--Unsealed Model	260
XIX.	Identification Order of Tests--ANGOPNG	274
XX.	Analysis of Variance--F Values	282
XXI.	Models Using ROP1	300
XXII.	Models Using OP1	301
XXIII.	Predicted Values of Dimensionless Force Coefficients--ANGOPNG Tests	306
XXIV.	Cantilever Beam Calibrations	339
XXV.	Deflectors, Unsealed Model, I-Series	341
XXVI.	Deflectors, Sealed Model, I(s)-Series	343
XXVII.	Airfoils, Unsealed Model, II-Series	348
XXVIII.	Ducts, Unsealed Model, III-Series	349
XXIX.	Ducts, Sealed Model, III(s)-Series	350
XXX.	Venting, Unsealed Model	352

LIST OF FIGURES

Figure		Page
1.	Turbulent Pipe Flow Used as a Model for Turbulent Boundary Layer Flow.	8
2.	Wind Velocity Variation Data	11
3.	ASAE Standards - Shape Coefficients.	15
4.	Effects of Angular Air Flow.	16
5.	Four Systems Investigated.	29
6.	Front View of the Two Dimensional Smoke Tunnel Showing a Building Model in the Flow Viewing Chamber	33
7.	Detail Drawing of the Smoke Tunnel	34
8.	Perspective of Smoke Chamber, Without Door, Viewed from the Back	35
9.	Back View of the Smoke Tunnel.	36
10.	Smoke Rakes.	37
11.	Smoke Chamber with Door Open and Model in Place.	39
12.	Exhaust Chamber Showing Access Door Open and Entrance Groove for Smoke Chamber	39
13.	Exhaust Fan with Butterfly Control and Early Version of Air Supply for Smoke Generator	41
14.	Vapor Generation Equipment	41
15.	Flow Chart for Vapor Generator	42
16.	Exhaust Section, Exhaust Fan and Butterfly Control. Also Shows Variac Unit and Final Version of Air Supply for Smoke Generator.	44
17.	15 cfm Fan for Final Version of Air Supply for Smoke Generator.	44

Figure Page

18. Regulator Valve of Air Supply for Smoke Generator. 45

19. Jig for Building Models and a Finished Model 47

20. Cardboard Models Tested. 47

21. Cardboard Models Tested. 48

22. Control Model with Normal Flow Pattern 52

23. Duct System. 54

24. Airfoil System 56

25. Airfoil System 58

26. Airfoil System (Top); Vent System (Bottom) 59

27. Deflector System 62

28. The Physical System. 67

29. Derived Quantities Dependent Upon the Basic Six Dimensions 70

30. Low Speed Wind Tunnel - Agricultural Engineering Laboratory - Viewed from the South 74

31. Exhaust Fan and Protective Screen. 75

32. Honeycomb Material Used in Anti-Turbulence Screen. 76

33. Honeycomb Screen Just Downwind from Contraction Section. . . 77

34. Experimental Equipment Location. 78

35. Disk, Floor Plate, Fixed End Walls with Cantilever Beams in Place for One Wall Panel. 79

36. Four Movable Panels and Removable End Wall Covers. 80

37. End Wall Covers and One Pair of Cantilever Beams with Wires Exiting Through Hollow Bolt. 81

38. Model with One of Four Movable Panels in Place 81

39. Designation of Beams and Gages 83

40. Full Bridge Strain Gage Circuit and Some Construction Details for One Beam - Al. 83

Figure Page

41. One Pair of Cantilever Beams Before Mounting 84

42. All the "B" Beams Mounted on One End Wall. 84

43. Block Diagram of the Complete Strain Gage Conditioning and Recording Circuit. 86

44. Equipment for Conditioning and Recording of the Strain Gages. 87

45. Wiring Diagram of Circuit Board, Bridge Unit, Balanching Unit and Power Supply. 88

46. Left to Right, Top to Bottom: Power Supply for Control Box Motor and Relays, Power Supply for Bridge Circuit, Control Box, Margin Marker Control Unit, Bridge Unit and Baldwin Balancing Unit 89

47. Control Box Showing, Left to Right, Motor and Clock Gears for Belt Drive of Cams - Between the Relays. 89

48. Control Circuitry for Strain Gages - One of Four Building Panel Circuits Located in Control Box Shown in Figures 40 and 42 90

49. Beckman Eight Channel Recorder Used to Document the Instantaneous and Average Strain Gage Readings 92

50. EAI Analog Computer Utilized to Condition the Instantaneous Readings of Strain Gages and Velocity to Obtain the Average Readings; Also Used to Obtain RMS Readings of Turbulence 93

51. Strain Gage Signal Conditioning and Recording Circuitry Using the Beckman Recorder and Analog Computer 94

52. Model in Tunnel with the Hot Wire Probe in Position a Little in Front of Large Window. Velocity Profile Screen is in Front of Second Window. View is up the Tunnel from Fan 95

53. Wind Recording System. 97

54. Four Channel Sanborn Recorder (Right), Hot Wire Signal Conditioning Unit (Top) and Two Channel Brush Recorder (Left). 98

55. Analog Circuit to Obtain the Average Velocity and Turbulence 99

Figure Page

56. Sample Signals of Analog Circuit for Velocity Average and Turbulence 101

57. Cantilever Beam Calibration. 103

58. Sample Cantilever Beam Calibration 106

59. Panel Calibration Using Loading Frame. 109

60. Calibration of Hotwire Apparatus 111

61. Modification of Tunnel Velocity Profile. 113

62. Velocity Discrepancy to the North and South of Center Line Measured at 9" Above Tunnel Floor. 115

63. Floor "Roughness" and Screens Producing Final Velocity Profile. 117

64. Low, Medium and Fast Velocity Log-Log Plots. 118

65. Low, Medium and Fast Velocity Profiles 118

66. Reynolds Number Tests - Unsealed Model. Horizontal Velocity, Single Hot Wire, in Volts Versus Reaction/Velocity^2 122

67. Reynolds Number Tests - Sealed Model. Horizontal Velocity, X-Wire, in Volts Versus Reaction/Velocity^2 . . . 123

68. Wind Force Reaction Number, N_F, as a Function of Reynolds Number, N_R, in Experiments with Building Models in a Wind Tunnel Testing Channel. 125

69. Joint Designation. 130

70. Deflector Configurations 135

71. Deflector Positions and Construction Details 136

72. Deflectors Tested and Their Controls 138

73. Tall Deflector (13/16") with No Gap at Position a_1 and 135° Orientation 138

74. Short Deflector (5/16") with Gap at Position a_3 and 45° Orientation. 139

75. Control in Place for Deflector Above 139

76. I-11 Versus I-1 Control. 142

Figure Page

77. Average Strain Readings on Panels 1 and 2, I-Series. 144

78. Average Strain Reading on Panels 3 and 4, I-Series 145

79. Panel Total Strain Readings, I-Series. 152

80. Total Inward and Algebraic Panel Total Strain Readings, I-Series 154

81. Absolute Panel Total Strain Readings and Total Outward Strain Readings, I-Series. 155

82. Modifications I-26 and I-28 Versus I-27 Control. 159

83. Modifications I-18 Versus I-24 Control 161

84. Modifications I-20 Versus I-21 Control 163

85. I-26(s) and I-28(s) Versus I-27(s) Control 172

86. I-12(s) and I-8(s) Versus I-14(s) Control. 172

87. I-18(s) and I-19(s) Versus I-24(s) Control 173

88. I-29(s) Versus I-30(s) Control 173

89. I-16(s) and I-17(s) Versus I-23(s) Control 174

90. Changes for Gages 1 and 2, I(s)-Series 179

91. Changes for Panel 1 Totals, I(s)-Series. 179

92. Changes for Gages 3 and 4, I(s)-Series 180

93. Changes of Panel 2 Absolute Totals, I(s)-Series. 180

94. Changes of Panel 2 Algebraic Totals, I(s)-Series 182

95. Changes for Gages 5 and 6, I(s)-Series 184

96. Changes for Panel 3 Totals, I(s)-Series. 184

97. Changes for Gage 7, I(s)-Series. 186

98. Changes for Gage 8, I(s)-Series. 186

99. Changes for Panel 4 Totals, I(s)-Series. 188

100. Changes in Outward and Inward Totals, I(s)-Series. 188

101. Changes for Panel Absolute Totals, I(s)-Series 190

Figure Page

102. Changes for Algebraic Panel Totals, I(s)-Series. 190

103. Airfoil Configurations Tested. 196

104. Airfoil Apparatus, $\beta = -6°$, $\beta = 6°$ 197

105. Airfoil e_2d_2 $(-\beta_3)$ on the Model. 198

106. Airfoil Equipment Disassembled 198

107. II-8 Versus II-7 Control 201

108. II-9(A) Versus II-7 Control. 203

109. Panel 2 Strain Readings Due to Alternative II Modifications. 204

110. Panel 3 Strain Readings Due to Alternative II Modifications. 205

111. II-9(s)(s), II-8(s)(s), II-9(a)(s)(s), II-9(a)(s) Versus Controls, II-(s) Series. 211

112. Average Strain Readings at Each Monitoring Point--Airfoils, Sealed 212

113. Panel Total Strain Readings--Airfoils, Sealed. 213

114. Total Building Strain Readings--Airfoils, Sealed 213

115. Duct Apparatus Med III, Left and Bottom; Big III, Right and Top. 221

116. Big III Versus Control--Strain in Chart Divisions. 224

117. Big III Versus Control--Force in Ounces. 224

118. Med III(s) Versus Control. 228

119. Big III(s) Versus Control. 228

120. Average Strain Readings--Ducts, Sealed 233

121. Panel Strain Readings--Ducts, Sealed 234

122. Building Total Strain Readings--Ducts, Sealed. 235

123. Eave Overhang Apparatus Installed on Model: Top, Bent Overhang--EOB(s); Bottom, Overhang with Holes--EOHi(s). 236

Figure Page

124. Eave Overhang Equipment. 237

125. EOi(s) Series--Average Strain Readings of Individual Monitoring Points. 240

126. EOi(s) Series--Panel Total Strain Readings 241

127. EOi(s) Series--Building Total Strain Readings. 241

128. EOHi(s) and EOB(s) Series--Averages of Individual Monitoring Points. 246

129. EOHi(s) and EOB(s) Series--Panel Totals. 247

130. EOHi(s) and EOB(s) Series--Building Totals 247

131. Unsealed Vented Model-Strain Changes with Respect to No Opening 256

132. Individual Strain Readings Registered at Monitoring Points and Total Strain Readings for Vent Tests. 257

133. Average Strain at Monitoring Points for Vent Tests 257

134. Panel Strain for Vent Tests. 262

135. Building Total Strain for Vent Tests 262

136. Spring Loaded Roof Vent Panels 268

137. Air Flow Visualization for Building with Duct. 270

138. Cardboard Duct with Flexible Plastic Section 271

139. Modified Wall Panels 271

140. Model Without Roof Showing Assembled Duct Mounted Inside Model 272

141. Completely Assembled Model with Ducts. 272

142. A1-B1, ROP1. 283

143. A2-B2, ROP1. 283

144. Panel 1, ROP1. 285

145. A3-B3, ROP1. 286

146. A4-B4, ROP1. 286

Figure Page

147. Panel 2 - Absolute, ROP1 287

148. Panel 2 - Algebraic, ROP1. 287

149. A5-B5, ROP1. 290

150. A6-B6, OP1 290

151. Panel 3, ROP1. 292

152. A7-B7, OP1 293

153. A8-B8, OP1 293

154. Panel 4, OP1 294

155. Outward, ROP1. 296

156. Inward, ROP1 296

157. Panel Totals - Algebraic, ROP1 298

158. Absolute Panel Totals, ROP1. 298

CHAPTER I

INTRODUCTION

Wind damage to single story, frame structures is a source of great financial loss each year. While it is not presently considered economically feasible to design such structures to withstand extreme conditions in the eye of a tornado, it should be possible to find means to minimize, and perhaps eliminate, damage due to high strain winds. Such damaging winds can occur during severe non-tornadic storms, and even along the peripheries of the eye path of a tornado.

Severe winds are known to create a pressure differential between inner and outer building surfaces--a pressure differential which is on some surfaces positive or inward, and on others negative or outward. In a tornado the sudden negative differential may even cause a structure to "explode". More often, however, wind damage results from an ordinary high wind in which fastenings are over-stressed to the point that the roof is displaced sideways and/or "lifted" from the walls. The walls may instead be separated and raised from the foundation. Even if all these fastenings and members are adequate to withstand high wind loads, the sheeting or "clading" may not sustain the forces induced.

Protection from Wind Damage

One obvious solution to wind damage is well designed buildings.

Proper wind design should be based upon Weather Bureau statistics as to the worst probable wind to occur during the design life of the structure at the given location. The well designed structure must then be properly constructed by conscientious laborers. This solution depends upon a "chain" of design and construction steps which results in no weak links--perhaps easier said than done, due to the many opportunities for human error and inadequacies.

Another approach to the problem could involve purposeful incorporation of a weak link into the chain--a link which might fail without endangering the whole structure. Such a method could utilize a pressure release device, reacting to a predetermined differential and set to activate under high stress, but before expensive structural damage ensued. Following release, the structure would become "vented". The "pop off" valve of a pressure cooker is an example.

The more familiar method of barrier protection from the wind has been studied by researchers and practiced by many who constructed, or more commonly planted, wind breaks. Nevertheless, wind breaks are either structures which must be designed and constructed at some expense, or grown with a long time delay. Also, wind breaks are susceptible to damage and the protection is then lost.

A further approach might be to incorporate into the original construction a system of deflectors, an airfoil, or ducts to alter wind flow over the structure and thereby attempt to achieve a more favorable pressure distribution.

Must of the past effort in wind research has been aimed toward the ability to accurately predict forces a building must sustain during its useful life--this for the obvious purpose of being able

to adequately design for these predicted loads. To date relatively little has been accomplished toward lessening wind loads a building must sustain other than changing the roof pitch and placing windbreaks.

This Investigation

The main objective of this investigation is to develop an integral protective system which will favorably alter the air flow over a modeled single story structure in order to alleviate damaging forces induced by a severe wind.

To accomplish this, both flow visualization techniques and tests on scaled models in a large low speed wind tunnel were planned for preliminary evaluation of several systems with potential to alleviate the usual wind force pattern.

Using the most promising system, more extensive study of the relationship between the system components and the resulting wind force was planned in order to obtain a method of predicting the force coefficients on a full sized structure equipped with the system.

CHAPTER II

LITERATURE REVIEW

Wind Description

The problem dealt with in this thesis concerns non-tornadic winds of high velocity but excludes the tornado. In a tornado, where a sudden pressure drop occurs, only the sturdiest of structures will survive. For most buildings the added expense of tornado proofing is not justified. The damages incurred in high velocity wind storms often occurring in the Great Plains area should be avoided, or at least alleviated, if at all possible. Sometimes this sort of wind occurs along the fringes of tornados and at other times these very high winds accompany weather fronts.

Any description of the wind must take into account its random occurrence. The description must consider the randomness of velocity, of turbulence and place of occurrence, all subject to the whims of mother nature. While trends are observable and predictions can be made, these are necessarily based upon analysis of a statistical nature of past weather data recorded in a number of locations over a period of years.

The major consideration in determining the wind forces a given shape of building will have to sustain, in a given region, is the velocity. The drag and lift forces are primarily dependent upon

wind velocity.

Velocity Magnitude

The measurement of wind velocity magnitude in the United States is based upon records of the Weather Bureau stations all across the nation. In the United States, the velocity observed is that of the "extreme - mile" wind, measured in miles per hour. The "extreme - mile" wind is the maximum velocity determined from the least time required for one mile of air to pass a fixed point (1a). It is customary to take the velocity observations at a distance of 30 feet (hereinafter referred to as "'") above the ground surface. Where this is not the case, the data is normalized to that height usually assuming a wind velocity profile of 1/7 (discussed later).

The storm recurrence frequency is statistically determined based upon the historical records of the United States Weather Bureau. If the 100 year period of time for which records had been kept for a given region, a storm of 90 miles per hour occurred only once, then the recurrence frequency expected would be once per 100 years. If no higher velocity storm occurred in the 100 year period, then 90 miles per hour would be considered the "100 year storm" for the region.

If a 60 miles per hour storm were the highest velocity storm which had occurred only 10 times in that same period, then its recurrence frequency would be 10 times per 100 years (or once per 10 years) and it would be the 10 year storm.

Since the 10 year storm occurred 10 times in 100 years the probability is that it can reoccur once each 10 years, however, it is possible to get two such storms only hours apart.

The United States Weather Bureau data is available for various storm mean recurrence intervals in the form of isotach maps showing the highest wind velocity which is expected to occur once, for example, over a 25 year period of time. The other recurrence intervals generally available are 10, 50, and 100 years (1b).

In designing a given structure, the useful life of the building is taken in consideration, as well as the potential loss of life and property in order to choose the design storm mean recurrence interval for the structure. The design storm for a temporary poultry structure would be less than for a commercial poultry processing plant where building failure could result in considerable loss of human life and property.

Velocity Variation with Height Above the Ground

The velocity of moving air ordinarily diminishes near the ground level due to retardation by objects on the earth's surface--trees, rocks, buildings, etc. Theoretically the velocity of the air at the surface of the ground is zero.

A number of fluid flow equations, both theoretical and empirical, exist for quantifying the variation of velocity with height above the surface. The most prominent of these are aptly discussed in detail by Nelson (2). Three of the more familiar forms are spiral, logarithmic and exponential profiles. Of these three, the most widely used is the exponential or power law profile.

The simplified method to describe the velocity pattern of surface winds is based upon turbulent fluid flow across a flat roughened surface. To further simplify, the roughened surface can be

considered smooth. The velocity distribution, or velocity profile of fluid flow over a flat smooth plate, is actually comparable to that in a closed smooth conduit or pipe where the radius of the pipe is equal to the thickness of the boundary layer over the flat plate.

Referring to Figure 1 (from reference 3), the boundary layer can be described as the layer of fluid flow adjacent to a surface upon which that surface has a retarding effect. Its thickness is δ; here it is the radius of the pipe, r_o. Beyond the boundary layer, theoretically, there exists uniform mean flow with velocity, U.

The nearer to the interior surface of the pipe a particular fluid element lies, the lower the horizontal velocity, u, of that element. Theoretically, there are fluid elements with zero velocity in contact with the pipe wall. Near to the surface of the pipe is a laminar sublayer within the otherwise turbulent boundary layer. It can be seen that the velocity distribution in the laminar sublayer is essentially linear. Though in fact, this laminar sublayer probably exists, it is often ignored since it causes very little change in the theoretical velocity distribution.

The equation used to characterize the velocity variation is known as Blasius' one-seventh-power law.

$$\frac{u}{U} = \left(\frac{y}{\delta}\right)^{1/7}$$

Knowing U at the extremity of the boundary layer δ, the velocity u can be found at any other height y. It is not necessary to know U and δ. If the velocity is known at any height, it can be found at any other height. Indeed, the equation is most often used to find the

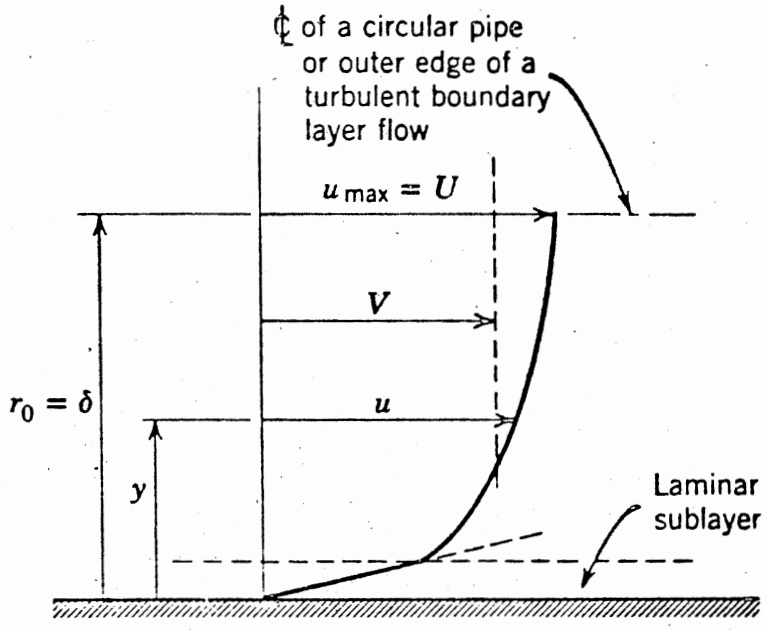

Figure 1. Turbulent Pipe Flow Used as a Model for Turbulent Boundary Layer Flow

velocity at some critical design height for a building, knowing the velocity at 30'.

For air flow across the earth's surface, the thickness of the boundary layer, δ, is open to debate, as is the value of 1/7--both mainly because there exists a multitude of different wind and surface combinations in which to apply the equation.

Davenport (4) suggests that the level above which the wind velocity ceases to vary due to ground surface friction is approximately 1,000-2,000'. In open countryside of Michigan, Sherlock (5) indicates that 900' is a good average, which fact agrees with Pagon (6).

Brunt (7) notes that either an increase in roughness or instability serves to increase the exponent above 33'. These two causes are generally acknowledged as the major causes of turbulent air. Stability refers to the lack of temperature variation with height. Storm winds of long duration are almost inevitably naturally stable near the ground because of the turbulent mixing of the air according to Sutton (8). Rudolf Geiger (9) stated that this condition is usually achieved with wind velocities of 13 miles per hour or greater. Severe local thunderstorms and frontal squalls are notably unstable where the air near the ground is warmer than the air aloft. Thermal interchange takes place between the lower air and the upper faster moving air which is unretarded by the earth's surface roughness. In extreme cases of instability, the value of the exponent in the power law can even approach zero as attested by Ali (10) who measured a value of 1/50 and O. G. Sutton (8) who suggests a value of 1/100. In such cases, the surface roughness has little effect on the velocity profile. Where, however, a large scale stable storm occurs, surface roughness

is the dominant influence on the variation of velocity with height.

The surface roughness does not refer to the mountainous terrain. Rather it is a function of the cumulative statistical drag effect on the wind of many obstructions determined by their size, density of location and height--i.e., trees, buildings, crops, rocks, etc., according to Davenport (4). Logic and experience show the surface roughness to be a minimum over the ocean and a maximum in a large city. Davenport further gathered data from all over the world and thoroughly analyzed it in a most extraordinary and extremely interesting fashion to arrive at the table in Figure 2 where $1/\alpha$ is the exponent to be used in the power law and Z_G is the thickness of the boundary layer.

Further, an effect of the magnitude of velocity itself upon the velocity profile is documented by G. F. Collins (11) wherein he finds that, after studying nine storms at Brookhaven Lab, Long Island, the exponent in the power law is increased by approximately 0.02 for every 10 miles per hour increase in the surface velocity of the wind.

However, it must be noted also that at least some feel the 1/7 power law or some version of it is of little interest below 30'--namely Thom (12) and Brunt (7)--mainly because at those heights the wind forces are of little interest to structural engineers.

Fluid Flow and the Building

Any body immersed in a moving fluid experiences force exerted upon it by the fluid. The component of the force which is perpendicular to the motion of the undisturbed fluid is lift. The component parallel to the motion of the undisturbed fluid is drag. The equations are:

$$F_D = C_D A \frac{\rho V^2}{2}$$

TYPES OF TERRAIN GROUPED ACCORDING TO THEIR AERODYNAMIC ROUGHNESS

Description	$\frac{1}{\alpha}$	z_G
Very smooth surfaces: e.g. large expanses of open water; low unsheltered islands; tidal flats; lowlands verging on the sea	$\frac{1}{8.5}$	800
Level surfaces with only low, surface obstructions: e.g. prairie grassland; desert; arctic tundra	$\frac{1}{7.5}$	900
Level, or slightly rolling surfaces, with slightly larger surface obstructions: e.g. farmland with very scattered trees and buildings, without hedgerows or other barriers; wasteland with low brush or surface vegetation; moorland	$\frac{1}{6.5}$	1,000
Gently rolling, or level country with low obstructions and barriers: e.g. open fields with walls and hedges scattered trees and buildings	$\frac{1}{5.5}$	1,100
Rolling or level surface broken by more numerous obstructions of various sizes: e.g. farmland, with small fields and dense hedges or barriers; scattered windbreaks of trees, scattered two-story buildings	$\frac{1}{4.5}$	1,200
Rolling or level surface, uniformly covered with numerous large obstructions: e.g. forest, scrub trees, parkland	$\frac{1}{3.5}$	1,350
Very broken surface with large obstructions: e.g. towns; suburbs; outskirts of large cities; farmland with numerous woods and copses and large windbreaks of tall trees	$\frac{1}{3}$	1,500
Surface broken by extremely large obstructions: e.g. center of large city	$\frac{1}{2.5} - \frac{1}{1.5}$	1,800

Figure 2. Wind Velocity Variation Data

and

$$F_L = C_L A \frac{\rho V^2}{2}$$

where C_D and C_L are dimensionless coefficients, A is the projected area perpendicular to the flow for F_D and the projected area parallel to the flow for F_L, ρ is the fluid density, and V is the uniform velocity of the fluid. The quantity $\frac{\rho V^2}{2}$ is the dynamic pressure of the moving fluid. Usually C_D and C_L are determined by experimental methods although it is possible to derive the quantities theoretically for some simple shapes.

The forces induced, either upon the object by the fluid or upon the fluid by the object, depend upon the fluid density, the fluid viscosity, the velocity of flow and the shape of the object. If the fluid is compressible, the elasticity (and the Mach Number) of the fluid is important. Air at lower velocities--less than sonic--is virtually incompressible. The fluid viscosity is important in laminar flow where the predominate retardation of air flow over or around an object is due to layers of air "sliding" over adjacent layers.

In such situations, the viscous forces are significant in relation to the inertia forces and must be considered. With turbulent flow, however, the viscosity and the viscous forces are no longer of any relative importance when compared to the magnitude of the inertial forces.

The drag and lift forces can again be divided into two components--one parallel to the <u>object surface</u> and one perpendicular to the <u>object surface</u>. For drag, the former is friction drag and the normal component is pressure drag.

The shape of the object determines whether the predominate

component of drag force induced is tangential or perpendicular to the object surface. For objects which are "streamlined" the pressure drag and the friction drag are small and of the same order of magnitude. For blunt or bluff objects (not streamlined) the friction drag is relatively unimportant and the pressure drag is quite significant.

A building on the earth's surface is blunt object and the predominate forces on the building are pressure forces. Surface or skin friction is relatively unimportant. A flat plate with wind moving across its surface is, on the other hand, subject to friction drag of relatively significant magnitude. Friction drag causes, in the case of air flow across the earth's surface, a considerable retardation effect near the surface as previously discussed.

The building offers an example of another flow phenomenon--that of flow separation and wakes. The flow lines of the fluid cannot conform to the building configuration due to the abrupt changes of geometry. The momentum of the air does not allow it to turn sharp corners. Flow separation occurs and the "separated region" is a wake area of turbulent rotational flow where lower pressure exists. Back flow and large scale eddies occur which indicate fully developed turbulent flow and an increase in energy dissipation (13). The size of the wake area can be used as a relative measure of energy dissipated under the same flow conditions (14).

The building protrudes into and disrupts the air flow, forcing it out around and up over the obstruction. A common misconception is that air forced up over the roof must speed up in order to keep up with the relatively undisturbed irrotational air at slightly higher levels. In reality, a given quantity of air is crowded into a smaller area as

the air above confines the disrupted flow below by resisting upward motion itself. The same sort of action takes place as in any pipe when the flow area is reduced. The velocity increases and the pressure decreases or perhaps more accurately, the forced separation downstream beyond the ridge is an area of decreased pressure so the fluid particles are accelerated in that direction. Lift is created on the surface in the separated region. If the roof surface of the building slopes steeply upward, the angle may be such that the upper portion of the windward roof incurs inward pressure forces due to the increased deflection of the air flow. The ridge area near the roof acts as a point of stagnation. This is reflected in the coefficients of the American Society of Agricultural Engineers standards (1b) in the table of coefficients, Figure 3.

For a gable type building the distinction of C_D or C_L is usually disregarded. The coefficient is designated inward or outward normal to the actual surface area considered rather than related to some projected area either perpendicular or parallel to the undisturbed flow.

Another air flow phenomenon can occur on the building's roof at the leading edge where turbulent air flow boundary layer is separated from the surface much as it does for flow around a blunt edged plate, only reattaching some distance further up the roof. The distance from the leading edge to the point of reattachment of the local boundary layer depends often upon slight changes in the angle of incidence with the impinging air flow, its turbulence and the surface roughness.

Potential for extreme local and total load exists when a building encounters air flow at some angle other than perpendicular to the long dimension. This was illustrated by Thomann (15) as shown in Figure 4.

TABLE 1—SHAPE COEFFICIENTS, *C*, FOR EXTERNAL WIND LOADS ON SINGLE SPAN GABLE-TYPE BUILDINGS—TOTALLY ENCLOSED

(For designing trusses, columns, rigid frames, and other main members)

H/W	Windward Wall Coef, C_3	Windward Roof Coef, C_2 — Roof Slope 1:12	2:12	3:12	4:12	5:12	6:12	7:12
0.10	0.70	—0.34	—0.24	—0.13	—0.03	0.05	0.12	0.19
0.15	0.70	—0.51	—0.35	—0.20	—0.05	0.05	0.12	0.19
0.20	0.70	—0.60	—0.47	—0.27	—0.06	0.05	0.12	0.19
0.25	0.70	—0.60	—0.59	—0.34	—0.08	0.05	0.12	0.19
0.30	0.70	—0.60	—0.60	—0.41	—0.18	0.01	0.08	0.16
0.35	0.70	—0.60	—0.60	—0.47	—0.26	—0.07	0.05	0.12
0.40	0.70	—0.60	—0.60	—0.53	—0.33	—0.15	0.01	0.09
0.45	0.70	—0.60	—0.60	—0.57	—0.39	—0.22	—0.06	0.05
0.50	0.70	—0.60	—0.60	—0.60	—0.44	—0.29	—0.14	0.00
0.60	0.72	—0.60	—0.60	—0.60	—0.49	—0.34	—0.20	—0.06
0.70	0.74	—0.60	—0.60	—0.60	—0.53	—0.39	—0.25	—0.13
0.80	0.76	—0.60	—0.60	—0.60	—0.57	—0.43	—0.30	—0.18
0.90	0.78	—0.60	—0.60	—0.60	—0.60	—0.47	—0.35	—0.23
1.00 or more	0.80	—0.60	—0.60	—0.60	—0.60	—0.51	—0.39	—0.28

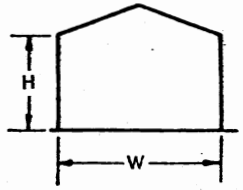

Leeward roof: $C_2 = -0.50$, for all values of H/W
Leeward wall: $C_4 = -0.40$, for all values of H/W
Negative values indicate external suction on building surface.

Figure 3. ASAE Standards - Shape Coefficients

Figure 8. *Left:* The flow field parallel to the diagonal of a flat roof is traced in a wind tunnel by applying dots of white paint to the roof surface of the model. When the tunnel is in operation, the airflow paints its own picture by stretching the dots to lines. *Right:* The pressure distribution resulting from the flow situation on the flat roof shown at the left is indicated in multiples of $(\rho/2)v^2$ below atmospheric pressure.

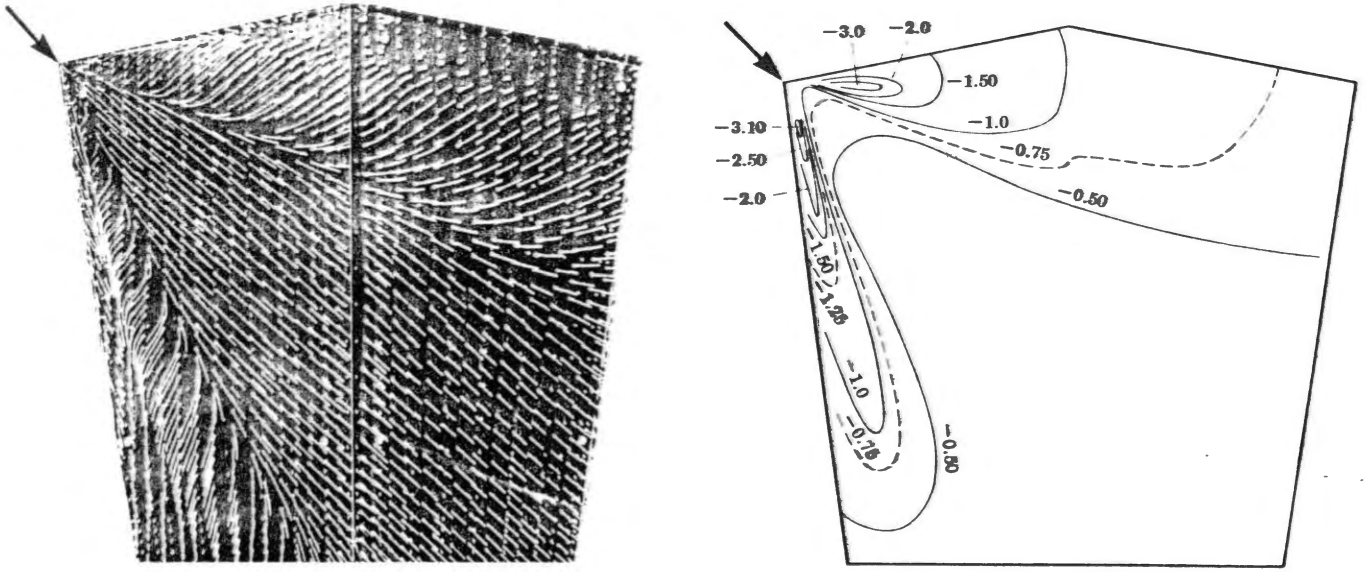

Figure 4. Effects of Angular Air Flow

The flow was parallel to the diagonal of a flat roofed structure. Streaks from white dots of paint reveal the resulting flow pattern and the multiples of $\rho V^2/2$ below atmospheric pressure show that locally, the negative pressure was immense.

Simulation and Modeling

The most practical method of studying wind effects on buildings has involved subjecting scaled models in a wind tunnel to controlled simulated natural winds. The pressure forces developed on the surfaces of the model are measured. The pressure forces are assumed to have a constant ratio to the kinetic energy of the wind in the tunnel measured at some appropriate place. The resulting ratio is a form of drag coefficient. This ratio can then be used to compute the wind forces on other buildings or models of proportionally the same shape by multiplying it times the kinetic energy of that wind flow even though the wind velocity is different.

The principles of similitude as explained by Murphy (16) are widely accepted as valid general modeling techniques. These principles indicate that similarity should exist in two ways for the study of wind forces on models of buildings; fluidic similarity and geometric similarity of the model to the prototype building.

Fluidic Similarity

Strict application of similarity of fluid flow would dictate that there are dimensionless parameters, called π (or pi) terms, which should be the same for both the model and the prototype in order for the modeling results to be applicable to prototype structures. One such

parameter that could be included is known as the Reynolds number or the ratio of viscous forces to the inertia forces ($L\ V/\nu$). L is a length characteristic, V is the mean velocity, and ν is the kinematic viscosity. If, indeed, the viscous forces are of significance in relation to the inertia forces, then similarity of Reynolds Number is essential.

In most experiments, the prototype fluid must be modeled by a fluid with a different viscosity in order to achieve the same Reynolds number since the geometric dimensions of the prototype are necessarily scaled down in modeling. In wind tunnel investigations it is not usually feasible to utilize a fluid other than air, the same fluid causing forces on the prototype structure. In order to utilize air and, for example, a 1:50 scale model, supersonic air velocities would be required in the tunnel. At those velocities, the Mach Number must be considered also.

This resulted in attempts to justify the disregard of the Reynolds Number by showing that in fully developed turbulent flow, the inertia forces are relatively much greater than the viscous forces. The overwhelming evidence seems to be that for "blunt objects" (not streamlined), it is reasonable <u>not</u> to require similarity of the Reynolds Number. The Reynolds Number is certainly important in laminar flow where viscous forces are not negligible.

The magnitude of the Reynolds Number involves a length term which should be significant in insuring the turbulent character of the fluid flow in the boundary layer. For some objects suspended in a uniform fluid flow, the length term is reasonably obvious, the diameter of the sphere, for example.

For a building in natural circumstances, the identification of the length term is not simple. Some have used the height of a building. If the smaller boundary layer near the roof's surface were to be considered, then one might consider the roughness of the surface (thickness of a shingle) or the distance from the leading edge. Nelson (2) suggested that to relate the dimensions of the building to the character of flow in the boundary layer, a ratio of some gross building dimension, such as the height, to a thickness parameter for the boundary layer (h/δ) seems appropriate.

Similarity of the Wind Profile

Wind profile similarity must include the horizontal velocity variation with vertical height above the ground. Irminger and Nkkentved (17) showed that differences in the roughness of the approach surface ahead of a building could cause large differences in the suction on the windward roof slope for gable roofed models with a roof slope of 20 degrees (hereinafter referred to as "°"). They suggested that a ratio of δ/h might be used as an indication of the Reynolds Number, where δ is the thickness of the boundary layer in the wind tunnel and h is the front height of the building.

This indicates that unless some method is used to accurately simulate to scale the wind's natural boundary layer, the tunnel boundary can distort the results obtained with the model. The ratio of forces on a freely exposed model to those on a model situated on a "ground plate" were greater on the former by 1.47 to 2.00.

Jensen (19) compared the results of wind tunnel studies of ground plane simulation and actual conditions with respect to vertical

variation of the horizontal velocity. He concluded that if care was used to scale the roughness conditions of the ground surface so that velocity gradients were similar, the wind tunnel studies were valid in predicting prototype behavior.

Similarity of Building and Its Surroundings

Murphy's application of the principles of similitude (16) calls for the use of scale factors for the pertinent length terms needed to describe the building. The length terms are reduced by the same scale factor unless the model is to be distorted in some direction. These length terms must be limited to those which are independent, and, if needed, can be further divided into L_x, L_y and L_z, according to Huntley (20), in order to better define the building by adding more identifiable pertinent quantities thus usually reducing the number of pi terms.

The size of the ground plane upon which the model is placed also can affect the results according to Leutheusser and Baines (21). They attribute discrepancies in results of some wind studies to an insufficient ground plane length--it should be long enough downwind to encompass the entire wake area of the building. (If the floor of the tunnel is used, this should not pose a problem unless the fan is too close to the model.)

Nelson (2) remarks that the end flow around buildings, especially those whose length is short in relation to width, may mask or confound the effect of other variables of building geometry on magnitude and distribution of wind pressures. He advises that the results of three dimensional flow experiments should not be applied to prototype

buildings unless it is established that end flow effects are inconsequential or that the end conditions are the same for the model and the prototype.

Of particular interest is the roof slope. Irminger and Nkkentved (17) and others have established that for the windward roof surface, there is a critical zone of roof slope in the range of 20° to 25°, where the suction forces on lesser slopes change to pressure forces. Beyond 25°, the forces are inward rather than outward.

Surprisingly, after reviewing many accounts (but by no means all) of wind force--model studies, no investigation found dealt with the effects of ignoring the eave overhang common for many gable roof structures. The overhang was simply omitted from the closed front studies--likely because of the complications it causes by adding to the analysis or because in some areas of Europe especially, eaves are not common.

Buckingham Pi Theorem

One important assumption underlies the experiment. The determination of what quantities are to be measured, how they are to be analyzed as well as the applicability of the results of the model studies to full scale building are all based upon the principles of similitude and ultimately the Buckingham Pi theorem.

Following a discussion of the principles of dimensional homogeneity, Buckingham (22, 376) says:

> "As a consequence, any equation which describes completely a relation subsisting among a number of physical quantities, of an equal or smaller number of different kinds, is reducible to the form
>
> $$\psi (\pi_1, \pi_2, \ldots, \text{etc.}) = 0,$$

where the π terms are all the independent dimensionless products of the form $Q_1^x, Q_2^y, \ldots$ etc., that can be made by using the symbols of all the quantities Q."

Buckingham has shown that the number of dimensionless and independent terms that it is possible to form is equal to the number of pertinent physical quantities needed to describe the system minus the number of fundamental dimensional units in which the physical quantities are expressed.

Murphy (16) is credited with the development of the theory of similitude with regard to the application of the Buckingham Pi theorem to the design and analysis of experiments in many fields of engineering and physical sciences.

Nelson (2) outlines the procedure of applying the Pi theorem to the planning and conduct of an experimental investigation as follows:

1. Decision as to the physical quantities or variables that are pertinent to the behavior of the system based on insight and knowledge of the physical system involved.
2. Combination of the pertinent variables into an appropriate set of dimensionless parameters (pi terms).
3. Determination of the functional relationship among the pi terms by conducting and analyzing the results of experiments wherein the values of certain pi terms are controlled or held constant so that the variation in others can be studied.

By combining the several pertinent variables into a smaller number of dimensionless pi terms, the number of tests to completely define a system's behavior should be reduced, subject to the limitation of the researcher to correctly select and combine the pertinent variables and

also subject to the limitations on the range of values of the pi terms through which tests can be made, according to Nelson.

Once a valid functional relationship is determined for one physical system, it is valid for all other systems which are physically similar, i.e., the essential variables needed to completely define the one, are the same needed to define the other and the functional relationship $\psi (\pi_1, \pi_2, \ldots . \pi_i) = 0$ has the same operator and the same value for each of the dimensionless pi terms. The individual variable values need not be the same but their ratio, as pi terms, will have the same value if the two systems are physically similar.

Force Measuring Methods

One early method of measuring forces on a model utilized a number of piezometer holes placed at the locations where pressure effects were needed. Wind pressure measurements were recorded using manometer techniques and pressure contours were plotted for the model's surfaces. From the evaluation of these pressure contours, the total force for a surface was obtained. This method was used by Irminger and Nkkentved (17) (18) and is documented by Ghaswala (23) in his historical development of wind tunnel tests.

Methods utilizing manometers have been refined by adding gang manometers and photographic means of recording the data. Others use double walled sections in the model and tape to cover all but one port, still recording essentially one point at a time.

At best, the method requires much work to collect and process the data. Many ports are needed to get an accurate picture. In addition, due to the weight the column of liquid in the manometers,

they are entirely insensitive to rapid pressure fluctuations and register only the mean pressure.

A similar method sometimes used employs pressure transducers at several places on each panel. As with gang manometers, some of the same problems are present with gang pressure transducers. Both the transducers and recording equipment are expensive to acquire in sufficient number but the electronic signals produced are easily recorded for interpretation by mapping techniques. Pressure fluctuations can be recorded and integrated electronically.

A third method, more suitable for this study, employs strain gage instrumented cantilever beams attached to each corner of movable building panels. The panels are actually suspended on the beams and as they react to the wind forces, strain in the beams produces signals which can be recorded. Nelson (2) was among the first to employ such a method, in the course of studying two dimensional wind effects on open front livestock shelters. He utilized three panels in a U-shaped trough suspended on 12 such "weighing bars". The trough was placed in a larger wind tunnel. The weighing bars were exposed to the wind in the tunnel as they were mounted on the outer sides of the trough. He found it necessary to shield them from the wind. His assessment of the beams was generally very favorable for open front buildings. This method can yield no information on localized pressures or forces but does give the corner reactions of the panels.

Flow Visualization Techniques

A number of methods to visually investigate flow phenomena have been used to gain insight on air flow patterns around buildings. Among

these are two dimensional techniques using oil or visual particles floated on a water surface, dye injected into a liquid, smoke and vapor introduced into a gas, tufts of yarn mounted on a solid surface (a grid board or aircraft wing), bubbles injected into an airstream, electromagnetic simulations, computer simulations, and schliern techniques. Some of these can also be used for three dimensional studies, permitting fluid flow investigations in any plane.

Irminger and Nkkentved (17) in the 1930's used powdered metals floated on water to investigate wind flow patterns over small shed buildings. They moved models through the floating particles and recorded two dimensional flow patterns using time delay photography.

Nelson (2) in the 1950's used a two dimensional smoke tunnel, manufactured by Aerodynamic Model Builders, Washington, D. C., in his investigations of wind flow over and through open front buildings. The apparatus (no longer available) utilized vaporized kerosene streams for tracing the flow.

Brown (24) in the 1960's developed a three dimensional high speed wind tunnel using coked straw to provide smoke tracers. By injecting the smoke into the slow moving air ahead of the contraction section he was able to achieve good results at wind speeds up to 220' per second.

Goddard (25) investigated three visual indicators for representation of supersonic air flow in a three dimensional wind tunnel; straw smoke, kerosene vapor and schlieren using nitrous oxide gas. Though all three tracing methods produced satisfactory results, kerosene was found to be the least expensive.

Theakston (26) developed a system to investigate three dimensional effects of wind and snow accumulations around buildings on a farmstead.

He mounted a model of a farmstead in a water flume and used sugar sand to simulate snow. The results were striking in both appearance and in reproduction of actual snow accumulation.

CHAPTER III

THE INVESTIGATION

In an attempt to discover some means of favorably altering air flow over a building to reduce wind forces, it was decided to develop and test several potential protective systems using modeling techniques. Two methods of investigation seemed appropriate; a qualitative investigation of flow patterns over models incorporating the proposed protective systems and further quantitative investigation of the most promising system. From the latter it was hoped there would result a means of predicting wind force coefficients on surfaces of a prototype structure thus altered.

Objectives

The following were the overall objectives of the investigation:

1. To develop several wind protective systems which could change the characteristic air flow over a structure.
2. To design and build a flow visualization chamber for qualitative evaluation of flow patterns resulting from the various alterations.
3. To evaluate the alterations by examining visual flow pattern changes and differences in dynamic force patterns exhibited by the models in simulated wind of an open countryside.

4. To formulate force coefficient prediction equations for the best system, if it favorably alters the characteristic pattern, in order to determine optimum size and arrangement of the system components (variables).

Scope of the Investigation

The investigation was limited to single story gable type structures with a roof slope of 4/12. The primary effort included investigation of 1/50 scale models placed normal to the mean flow of the wind. Some tests were run on models oriented at 0°, 15° and 30° from the normal in the final stages of the study.

Correlation of the results of the model study with prototype structures will be left for future study.

In the course of the study, a few unplanned structural variations were tested and results of these are briefly reported.

Method

The overall objectives of the investigation were met by the following steps:

1. Qualitative preliminary evaluations were conducted upon 1" cross-sections of models by flow visualization in a smoke chamber constructed for the investigation. The following four systems were evaluated:
   a. ducts venting the positive pressure on the windward wall into the suction area on the lee side (Figure 5a).
   b. an airfoil mounted above the roof ridge (Figure 5b).

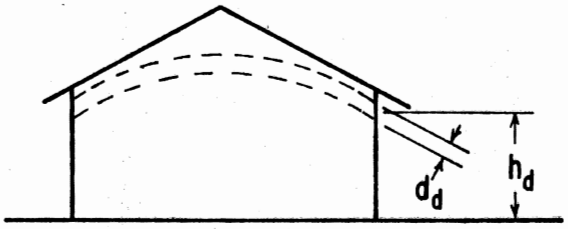

Figure (a)
Duct System

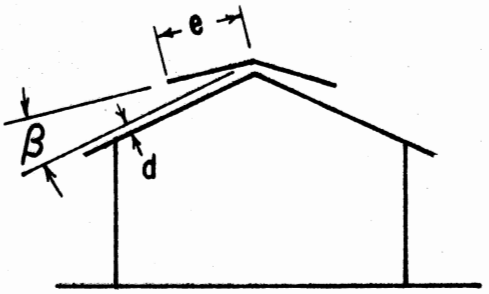

Figure (b)
Airfoil System

Air Flow ⇨

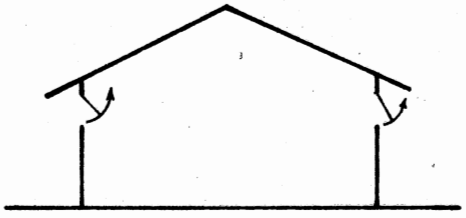

Figure (c)
Venting System

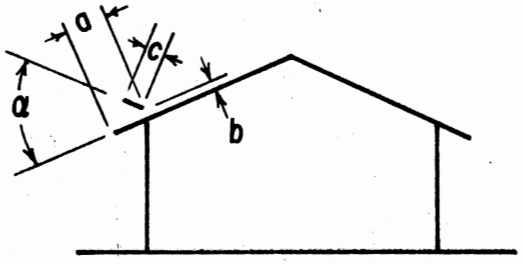

Figure (d)
Windward Deflector System

Figure 5. Four Systems Investigated

c. pressure releases venting the model (Figure 5c).

d. deflectors on the windward roof slope (Figure 5d).

2. Preliminary quantitative evaluations of the most promising systems were carried out in a low speed wind tunnel. To evaluate the systems, the dynamic reactive forces--induced by the altered air flow--were measured normal to four model surfaces; the windward wall, the windward roof, the lee roof and the lee wall. Four corner reactions for each surface were determined--16 in all. For comparison an appropriate control model was tested.

   The principles of similitude were utilized to analyze the systems. Tests were carried out in simulated severe turbulent winds (non-tornadic).

3. The best system was tested more extensively, quantitatively, in view of obtaining the necessary data for developing the prediction equations and determining the most favorable system characteristics.

   Pi terms, as elaborated in the Buckingham Pi Theorem, were derived, but usually only one variable was changed during the tests as indicated by the experimental design.

4. Analysis of the data (relationships of the variables changed to the 16 reactions) provided a basis for the force coefficient prediction equations and also the means of system optimization desired.

In presenting the stages of the study, as it developed, the qualitative phase is discussed, followed by the quantitative phase. The

quantitative phase is divided into a preliminary investigation and, finally, more extensive investigation of the one most promising system. The investigation, from start to finish, involved a progression of testing and rudimentary analysis as advantages and disadvantages of first one system, and then another, were evaluated in order to focus on the system which seemed to have the most merit.

Qualitative Investigation

Objectives

Flow visualization studies were conducted on models of various building modifications as well as upon the unmodified building.

It was hoped that resulting flow patterns would reveal which of the modifications in each system most altered the normal air pattern. In addition, it was hoped that it would be obvious some of the four systems did not favorably alter air flow and that these would thereby be eliminated. In reality neither objective proved quite so simple!

Method

The flow visualization method chosen utilized streams of kerosene vapor injected into an airstream ahead of scaled cardboard building models. The air flow patterns around the models could be easily detected by deflection of the white kerosene vapor streams against a dark background. These were photographed for recording purposes.

The length of the cardboard building model is distorted with respect to the height and width of the building. The scale of these latter two is 1/120 whereas the depth of the chamber limits the length

to 1". The air flow depicted is thus two dimensional and representative of that over a section of the central portion of the structure.

Equipment - Smoke Tunnel and Models

The qualitative studies planned were similar to those conducted several years earlier by Nelson (2) on models of open front buildings. Certain portions of the present apparatus were patterned after Nelson's written description of the no longer available commercial unit which he used.

The smoke tunnel, pictured in Figure 6, was constructed for the purposes of this study. It consists of three sections mounted on a plywood base:

1. The entrance section
2. The smoke visualization flow chamber
3. The exhaust chamber

These are detailed in Figures 7 and 8.

Of the three sections, only the exhaust section is permanently fixed to the plywood platform. The smoke chamber can be completely removed if necessary. For the purposes of changing models or cleaning the plexiglass, the thumbscrews, which clamp the three sections together to seal the units during operation, can be loosened. The smoke chamber and entrance section are moved 3/8" away from the exhaust section enabling the hinged back of the smoke chamber to clear the groove in the exhaust section and be opened without removing the smoke chamber. This can be seen in the back view of the tunnel shown in Figure 9.

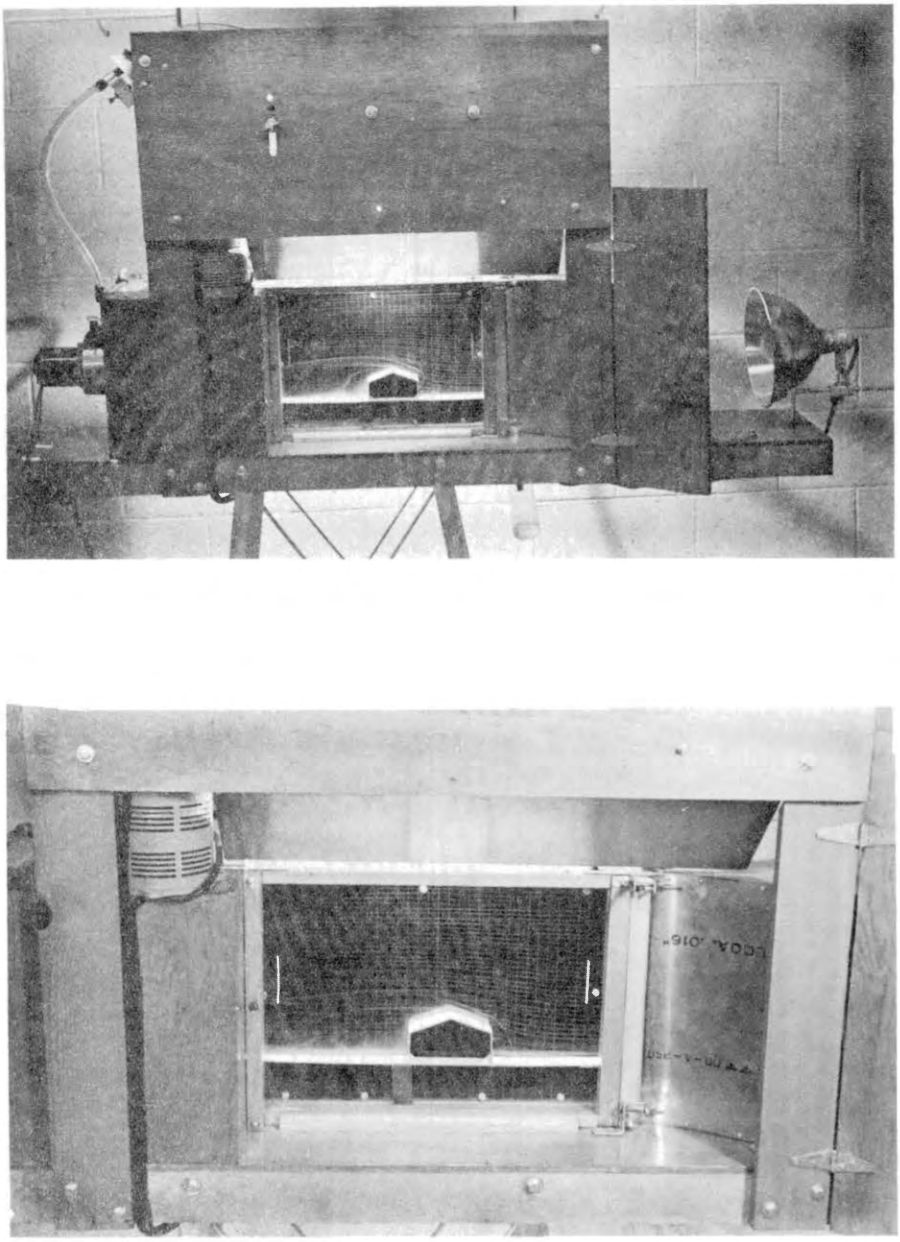

Figure 6. Front View of the Two Dimensional Smoke Tunnel Showing a Building Model in the Flow Viewing Chamber

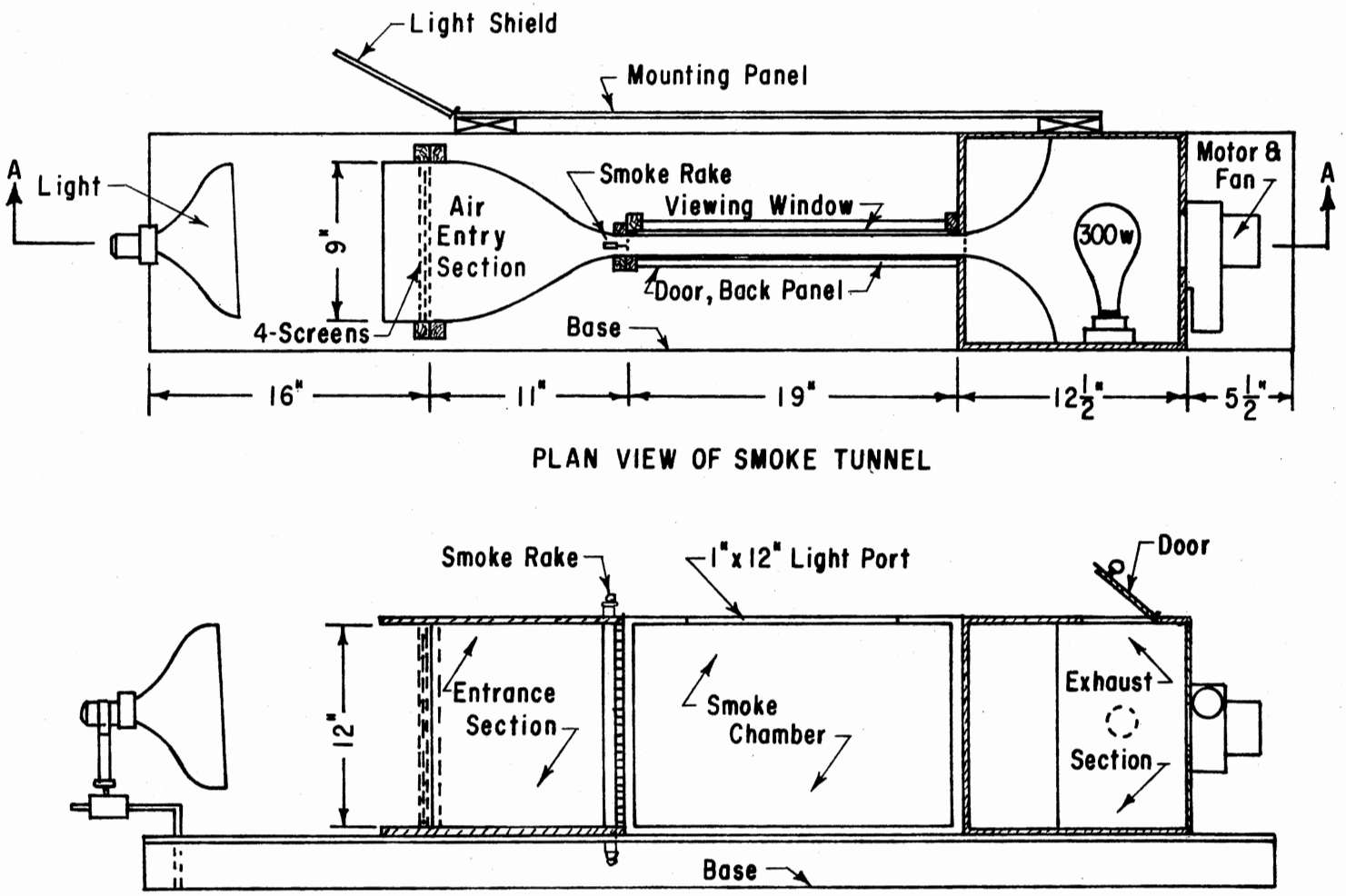

Figure 7. Detail Drawing of Smoke Tunnel

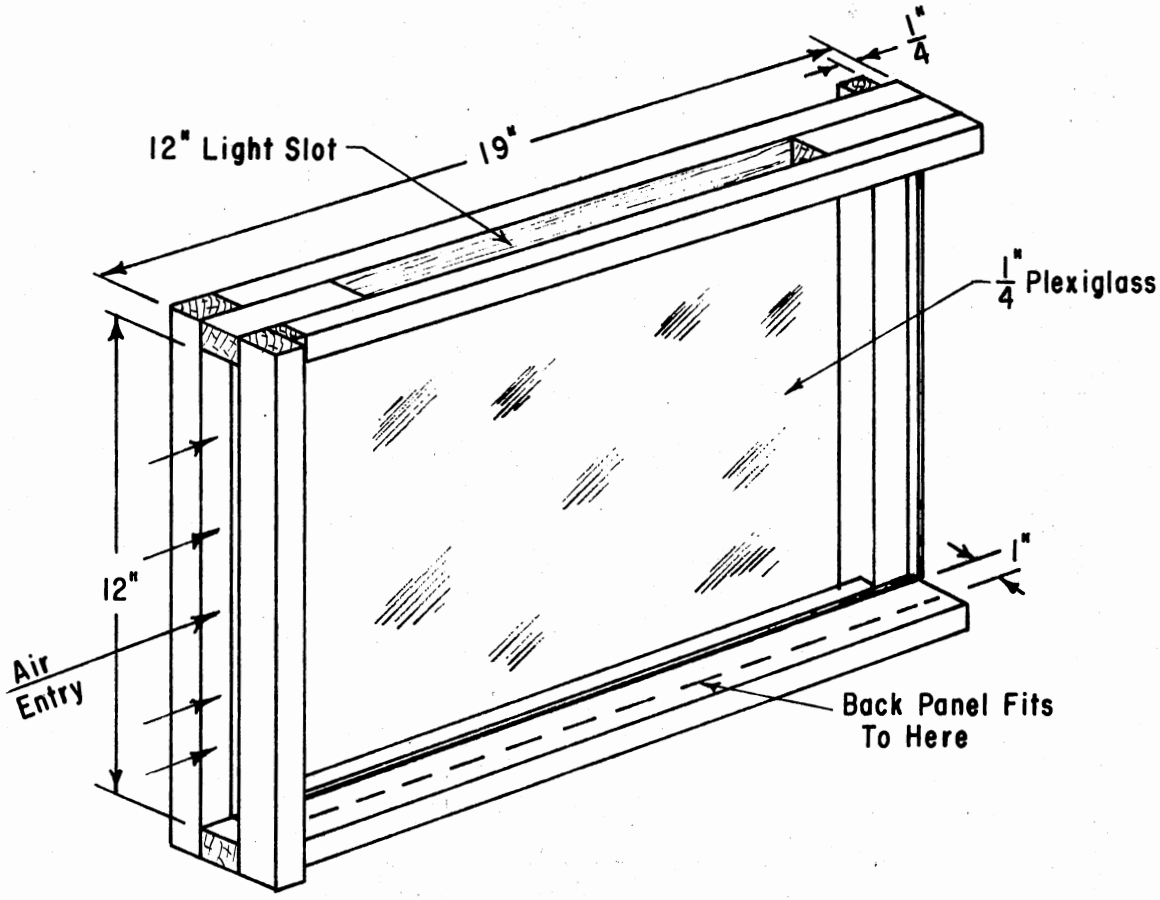

Figure 8. Perspective of Smoke Chamber, Without Door, Viewed From the Back

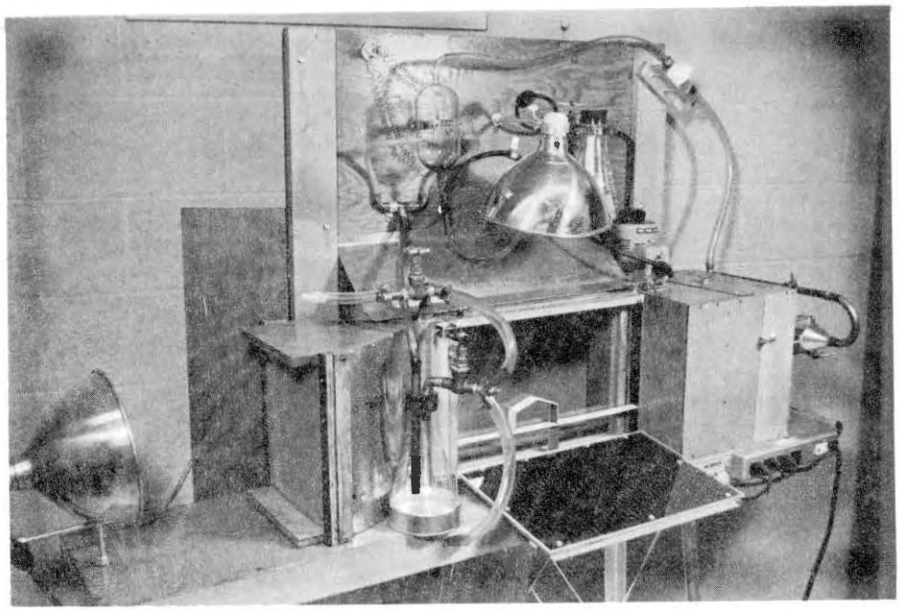

Figure 9. Back View of Smoke Tunnel

Entrance Section. This section's main function is gradual contraction of the incoming air permitting smooth entrance without generation of turbulence. The top and floor are plywood whereas the side walls are sheet metal. The entrance is covered with four layers of ordinary house screening, each separated by 1/8". These dampen the room turbulence of the entering air.

The entrance section also houses the smoke rake which forms and positions the streams of kerosene vapor. See Figure 10. The rake is located at the narrowest portion, or throat, of the entrance section, immediately ahead of the smoke chamber. The smoke rake is vertically positioned in the center of the 1" wide column of air moving from the entrance section and into the smoke chamber. The vapor is supplied to

both the top and the bottom of the smoke rake to insure adequate and even vapor flow to all the jets.

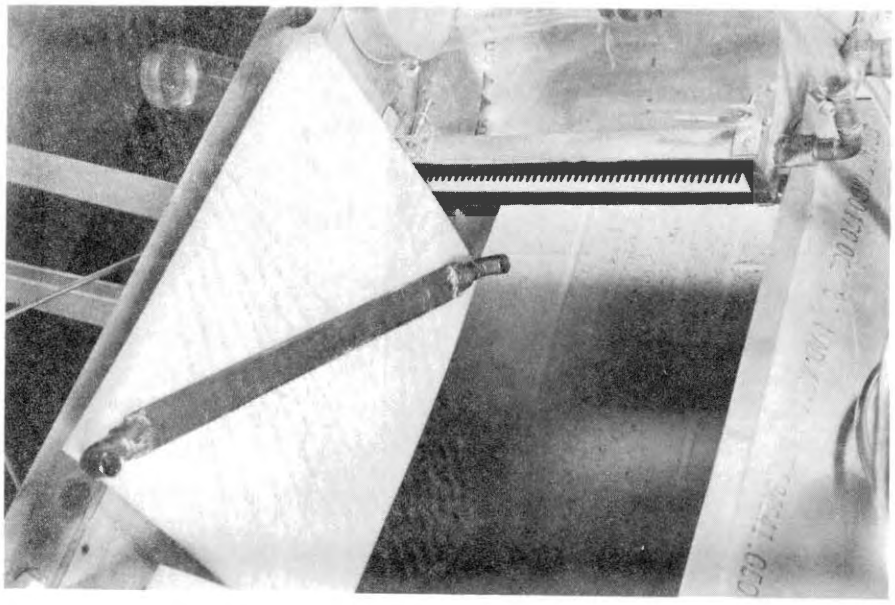

Figure 10. Smoke Rakes

The smoke rake consists of a section of 3/4" copper tubing, approximately 14" long, flattened to the shape of an air foil. The 46 smoke jets are 1/16" inside dimension copper tubing, and are

soldered in the trailing edge of the smoke rake at a vertical spacing of 1/4". The jets extend approximately 1/2" and are slightly tapered at the extremity to make them aerodynamically clean.

Figure 10 pictures two smoke rakes -- the final version installed, for which only the jets are visible in the throat of the entrance section, and an earlier version which utilized hypodermic needle tubing.

Smoke Chamber. Photos in Nelson's studies revealed only some details of the smoke chamber window of the apparatus. The size chosen for the window in this study was 18" long by 12" high. At 1/120 scale this size represents an area 180' by 120'. The 1" width simulates a 10' wide section along the prototype building length. Since the prototype is 40' wide, the 180' allows for adequate upstream room to encompass the point of separation, and downstream to see much of the leeward wake.

The smoke chamber, detailed in Figure 8 and pictured in Figure 11, is actually two plexiglass panels, the clear front window and the hinged back wall of the viewing chamber, mounted in a wood frame. The back is hinged the full length of the chamber at the bottom and the plexiglass is fixed to a hardboard door panel. Both pieces of plexiglass extend approximately 1/4" beyond the frame at the exit end and fit into the grooved entry of the exhaust chamber (Figure 12). This necessitates sliding the smoke chamber away from the exhaust chamber in order to open the door as explained earlier. The top of the chamber includes a 1" wide slot 12" long, covered top and bottom with plexiglass, to allow top lighting of the smoke viewing chamber.

The grid pattern (1/2" by 1/4") seen on the rear plexiglass panel of the viewing chamber was made by scratching its back surface

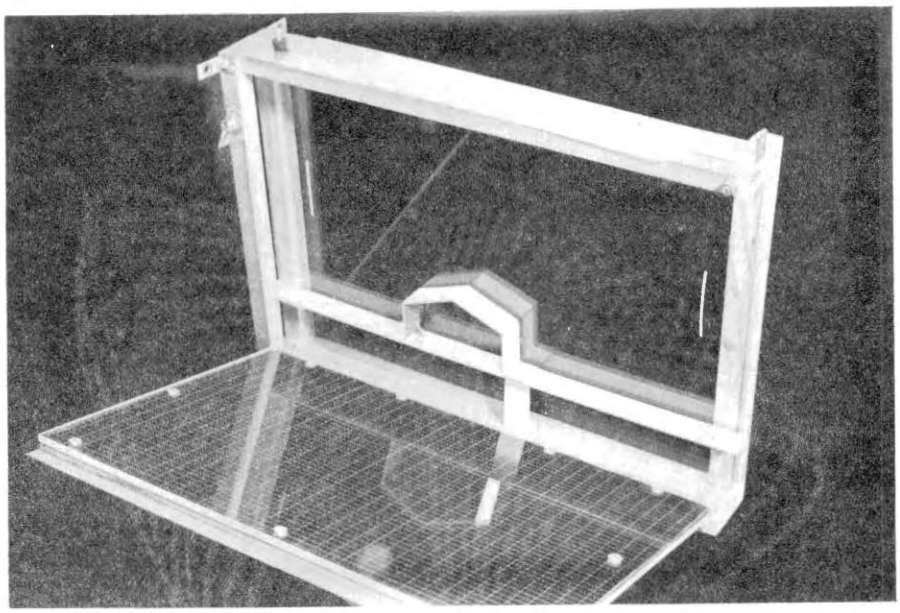

Figure 11. Smoke Chamber with Door Open and Model in Place

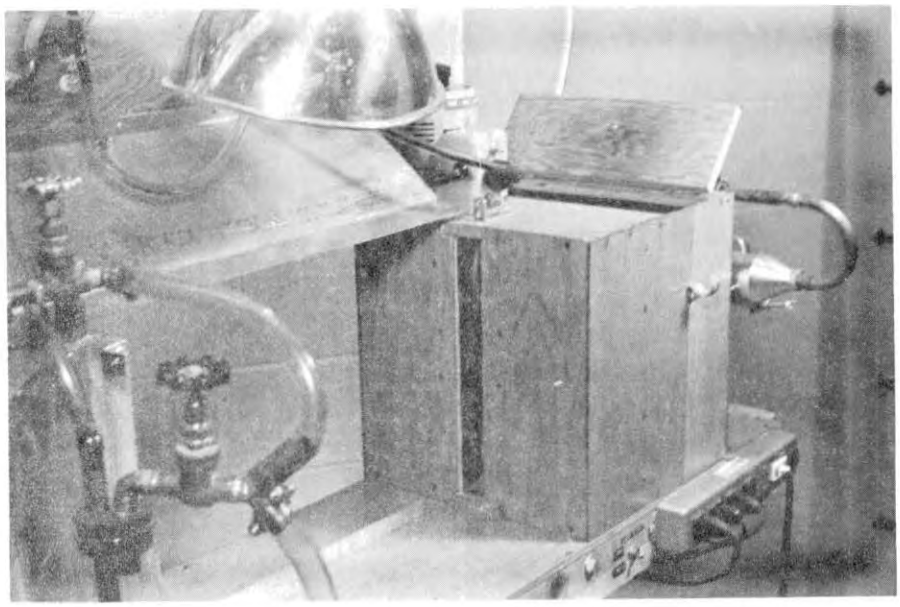

Figure 12. Exhaust Chamber Showing Access Door Open and Entrance Groove for Smoke Chamber

with a grooving tool. The plexiglass is mounted on 1/4" hardboard covered with black velvet cloth. Small spacer washers were placed between the velvet and the plexiglass at each fastener to avoid crushing the velvet. The velvet gives high contrast with the white vapor streamlines and the grid furnishes orientation and dimension to show the divergence of the streamlines and the length or spacing of vortices or other phenomena.

Exhaust Section. The exhaust section is a 12" (inside dimension) plywood cube with the divergence portion formed of sheet aluminum, as shown in Figures 7 and 12. A 40 cfm fan is mounted on the rear of the exhaust section and pulls the air through the smoke chamber (Figure 13). A damper provided on the exhaust part of the fan regulates air flow rate through the smoke chamber within the range of 75 to 375' per minute.

Smoke Generating Equipment. The most important part of the apparatus is the smoke generating equipment diagrammed in Figure 15. This equipment is mounted on the back of the plywood panel over the smoke chamber, as pictured in Figures 9 and 14.

The mounting board for the smoke generating equipment is a 16" by 36" plywood panel mounted on 1" by 4" supports and located 8" above the smoke tunnel. Relative positions of the equipment are shown on the flow diagram (Figure 15).

The vapor generator is the critical component of the smoke tunnel. The unit, shown on the left in Figure 14, was constructed by a skilled glassblower. The generator consists of a flask formed from 3" glass tubing necked down to fit 10 mm O.D. glass tubing at the bottom, 12 mm

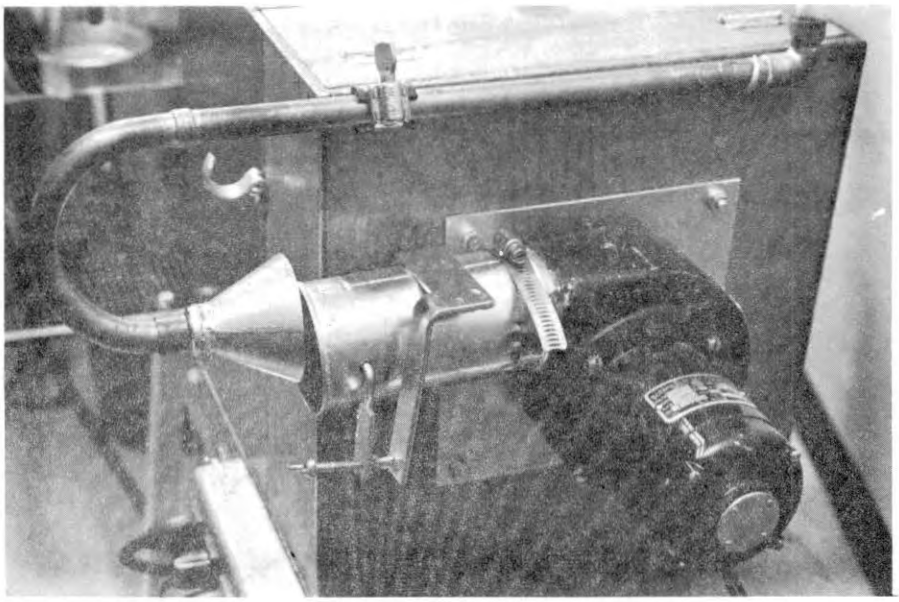

Figure 13. Exhaust Fan with Butterfly Control and Early Version of Air Supply for Smoke Generator.

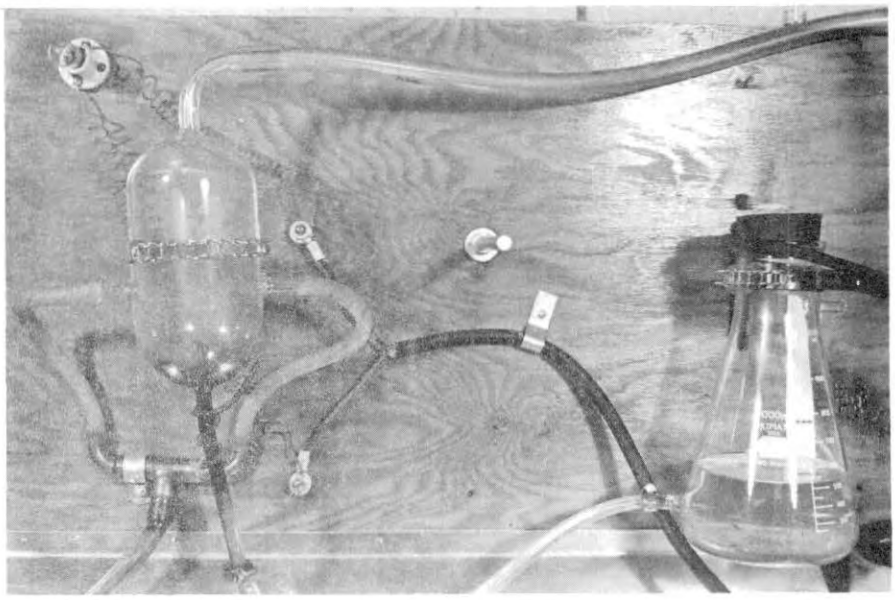

Figure 14. Vapor Generation Equipment

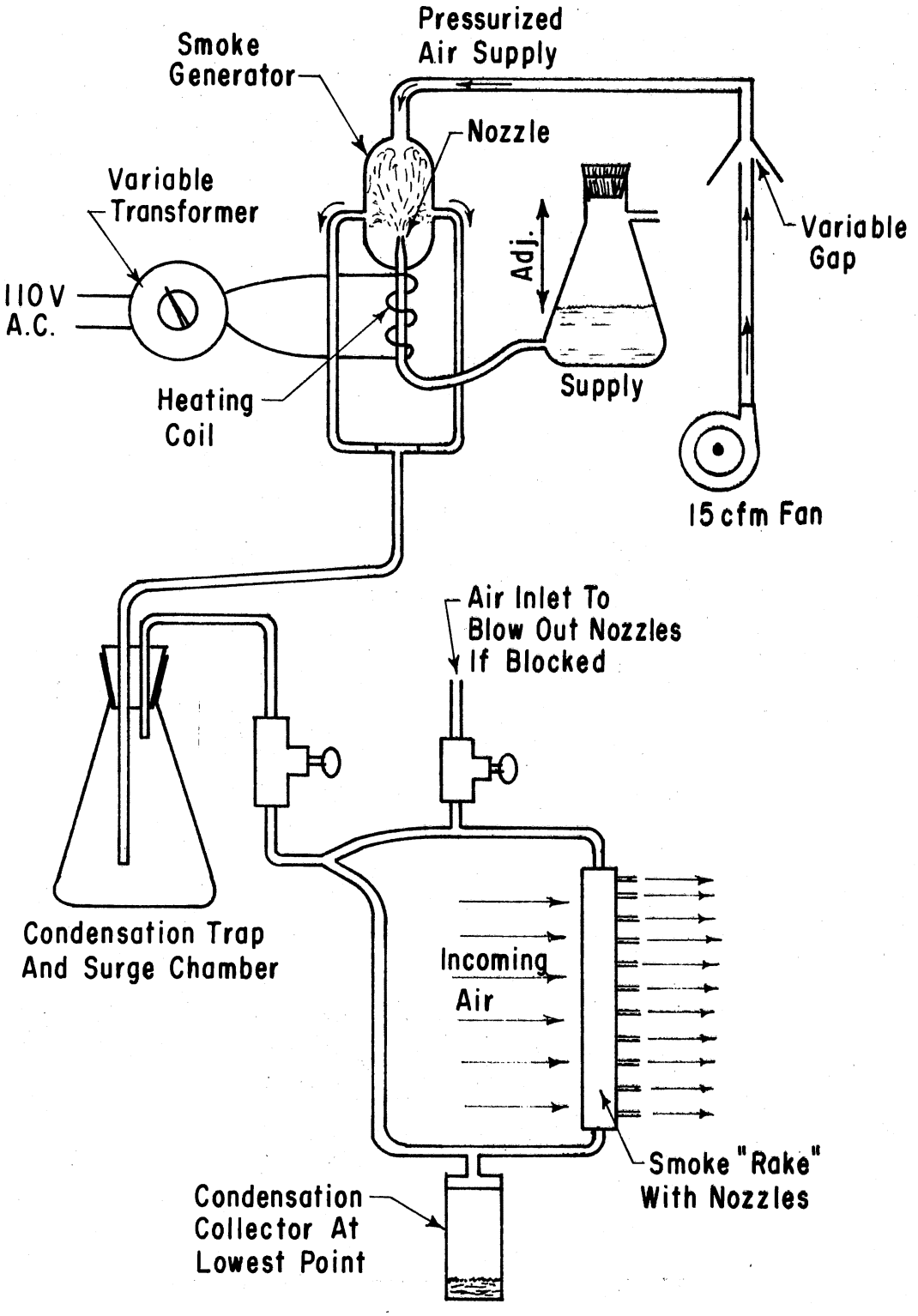

Figure 15. Flow Chart for Vapor Generator

glass tubing at the top, with discharge ports of 10 mm glass tubing attached to each side. The glass tube at the bottom is 8" long and is inserted approximately 1" into the generator flask. This 1" long section is necked down to form a 1/16" I.D. nozzle at its upper extremity. The supply tube is connected to the kerosene reservoir with Tygon tubing and the glass section immediately below the flask is wrapped with three turns of nichrome wire 8" long. This wire heating element vaporizes the kerosene in the glass tube and the vapor is discharged into the flask through the nozzle or jet. The incoming air at the top is mixed with the kerosene vapor and exits through the side ports of the flask. Most uniform vapor generation is obtained when the kerosene level is kept at the elevation of the bottom heating coil.

The kerosene reservoir, shown on the right in Figure 14, is adjustable vertically to maintain optimum level in the generator tube. Heat control is obtained by regulating voltage with the Variac shown in Figures 9 and 15. Optimum voltage for the heating unit shown is 34 volts. An indicator light is wired in parallel with the heating element.

Earlier, part of the discharge from the smoke chamber main fan was recirculated to pressurize the generator flask and force the vapor through the flask and the smoke rake. This earlier equipment can be seen in Figures 9, 12 and 13. A separate smaller blower has been added since these pictures were made, a 15 cfm fan as detailed on the vapor flow chart (Figure 15). It was mounted underneath the base. The arrangement is shown in Figures 16 and 17. This has proved superior in providing a steady stream of vapor.

A mixing valve, a small funnel with the air from the blower

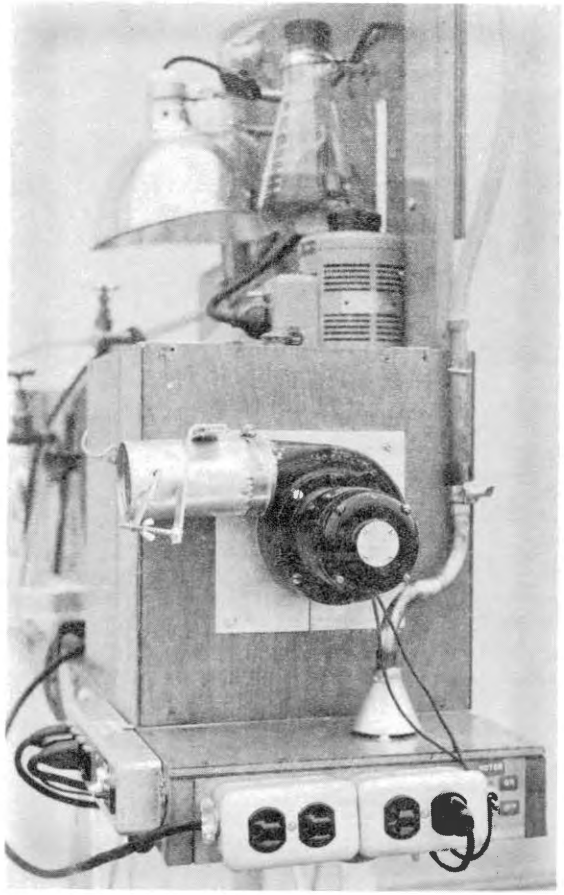

Figure 16. Exhaust Section, Exhaust Fan and Butterfly Control. Also Shows Variac Unit and Final Version of Air Supply for Smoke Generator.

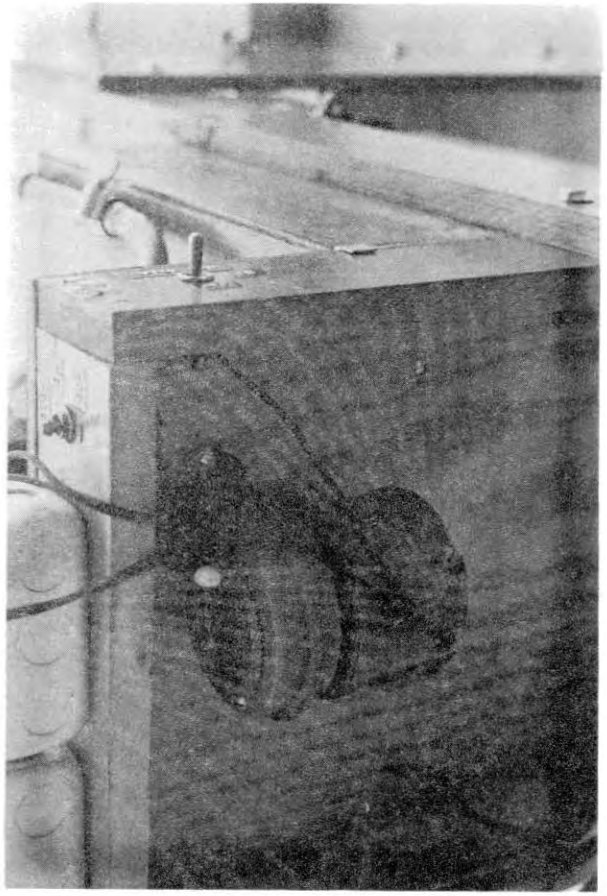

Figure 17. 15 cfm Fan for Final Version of Air Supply for Smoke Generator.

directed into it across an adjustable gap, is used to control the air flow rate to the smoke generator and, subsequently, the intensity of the vapor streamlines. This valve is located in the line between the blower and the generator flask. It is pictured in Figures 9 and 18.

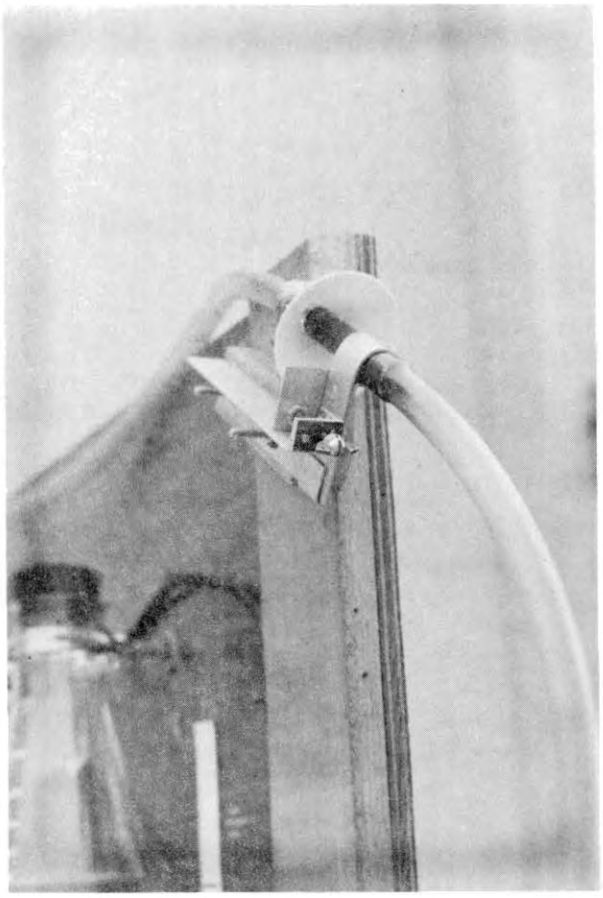

Figure 18. Regulator Valve of Air Supply for Smoke Generator

Lighting. Three lights to illuminate the vapor streamlines are positioned at the entrance section, over the smoke chamber, and inside the exhaust section. The top of the smoke chamber contains a transparent window to enable passage of light.

A 100 watt light is mounted inside the exhaust chamber to provide illumination of the back side of the model. However, this light should be used sparingly, only while photographing, because the heat buildup in the exhaust chamber from the light can cause depression of the smoke streamlines in the smoke chamber. A door in the top of the exhaust chamber provides access to change or clean the light. A sheet metal shield is used between the mounting panel and the smoke tunnel, to shield the viewer and camera lens from the glare of the top light illuminating the smoke chamber. A hinged piece of plywood is also used near the entrance section to eliminate glare from the light.

Jig for Models. The building models, made of white posterboard, were all fabricated by use of a wooden jig to insure uniformity. The jig is shown in Figure 19. All the cardboard pieces were cut to a uniform width of 1" and to length as marked on the jig. A cardboard "ground plate" was utilized for each model. The basic shape of the building was marked on a wooden block which was cut in two pieces, one of which was placed inside the building and one on top of the building during gluing. The upper wooden strip on the jig is slightly inclined with respect to the bottom strip so that the pieces when slid into place for gluing were wedged in position. After the basic building and ground plate were fabricated the various modifications were added. The resulting 20 models are pictured in Figures 20 and 21.

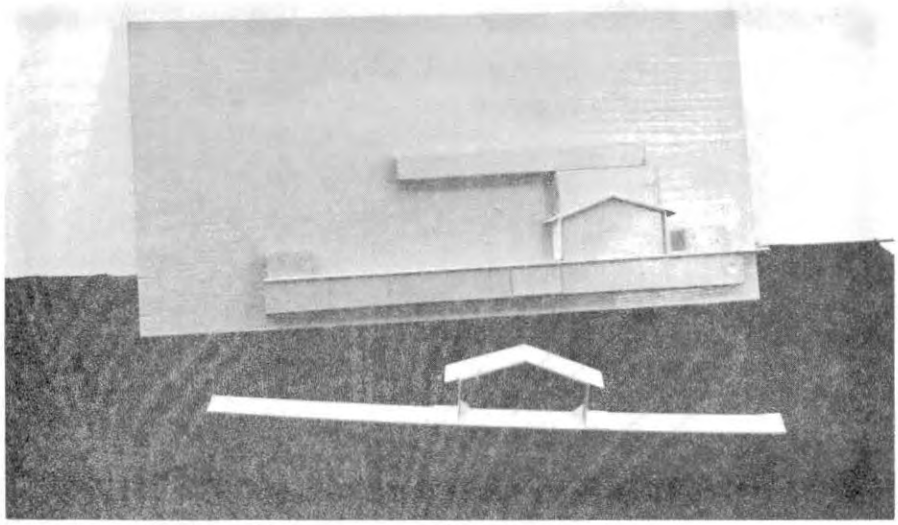

Figure 19. Jig for Building Models and a Finished Model

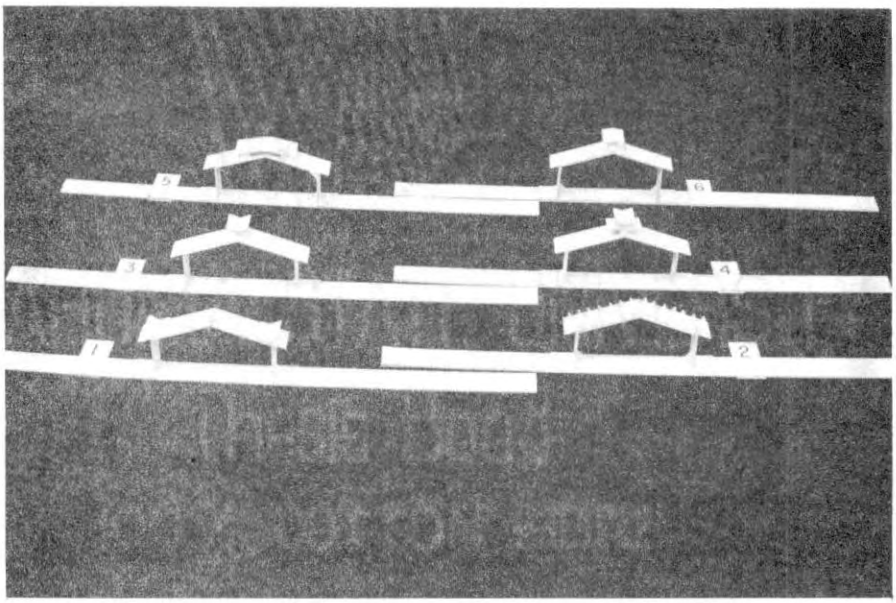

Figure 20. Cardboard Models Tested

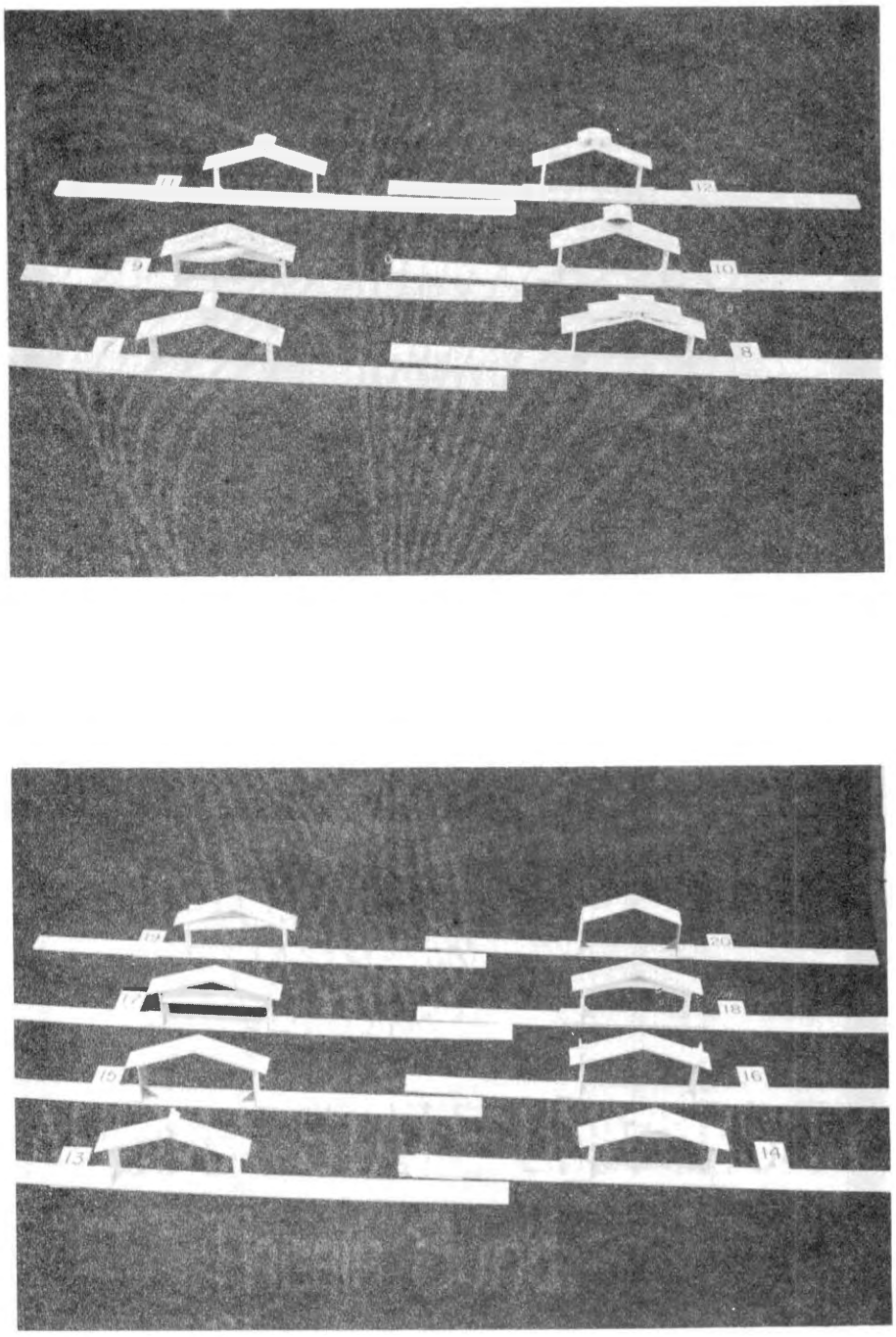

Figure 21. Cardboard Models Tested

Procedure

The procedures for use of the smoke tunnel developed are in Appendix A.

Each of the models was placed in the smoke tunnel and tested at an approximate air flow of 100 fpm as determined by a portable hot wire anemometer. There was no attempt made to obtain exactly the same flow rates for each test but rather photos were taken when well defined streamlines were obtained.

It was soon discovered that the models had to be placed in the smoke chamber at exactly the same distance from the floor of the smoke chamber in order to obtain good comparisons upstream of the building. A prop underneath the ground plate and marks inside the chamber helped to assure uniform placement.

Discussion of Results

The apparatus designed was tested employing a number of conventional shapes, both suspended and mounted on ground plates. These included 1" sections of square and rectangular boxes, aircraft wings, cylinders and a half cylinder. The resulting flow patterns were comparable to those shown in many of the standard fluid textbooks. The apparatus also performed well for the building models and the intended pictures were obtained. At times the vapor stream, upon reaching the model, broke up into secondary streams and eddies which would flow in the boundary layer along the faces of the plexiglass panels. Too, if the models were not placed the same vertical distance from the floor of the chamber, the vapor stream closest to the ground

plate tended to become mixed with the slower air in the ground plate boundary layer. The air flow did not differ appreciably from picture to picture. If this precaution was not observed, however, the vapor stream path portrayed a slightly different element of air flow and the photographic results do differ somewhat.

One factor tends to make the recorded "photographic data" non-representative of the real situation. The high velocity wind flows encountered in a natural wind storm, even in a high, straight, non-tornadic storm, are certainly not laminar flow. The flow conditions in the smoke tunnel, however, were of necessity laminar flow. When turbulent flow was achieved at higher velocities, the vapor streams broke up completely making distinct flow patterns indistinguishable. Later, after the original photos were made, the apparatus furnishing pressure into the vapor bottle was altered by adding a separate 15 cfm fan in place of capturing and recirculating a part of the exhaust air from the tunnel. This change enabled much higher air velocity through the tunnel without the diffusion of the vapor streams. Velocities of 300 fpm could be maintained without stream breakup. Still this must be considered essentially laminar flow.

In spite of the laminar flow conditions, much was learned about the nature of the flow around the models through use of the smoke tunnel.

Conclusions

The flow visualization studies were undertaken originally in order to ascertain which of the modifications in each system showed the most promise and which system seemed most worthy of further testing,

quantitatively, in the large wind tunnel.

Actually, however, even with the flow visualization studies, it was virtually impossible to draw conclusions that would eliminate any of the systems and permit quantitative evaluations to be carried out on only one or two of those remaining. The flow studies did indicate that significant differences in air flow patterns would exist with certain of the modifications, but the exact nature and the quantity of the differences was still a mystery. It appeared that some of the modifications were apt to relieve the building wind stresses on one portion of the structure and increase them on another.

Consequently the smoke tunnel studies were used in a different way than originally intended. The flow photos were studied to determine which modification within each system seemed to produce the most extreme departure from the standard pattern.

The photos labeled in Figure 22 represent the normal, unmodified or control structure. The two at first appear to be different, but a closer look will reveal unmistakable similarity of the air pattern. In test 15 the camera was closer than for test 1, but the main difference is in the placement of the model with respect to the jets. In test 1 a nozzle was at floor level and the vapor stream mixed with the boundary layer as mentioned earlier. In addition, the velocity of air was slower in test 1 than test 15 so that the two lower streams are actually turned down under the eave. They eddy and are diffused. This diffusion is apparent in the wake area also. Test 15, on the other hand, has no tracer stream close to the ground plate and the velocity is such that no stream intercepts the eave.

Apart from the above differences, the air flow pattern is

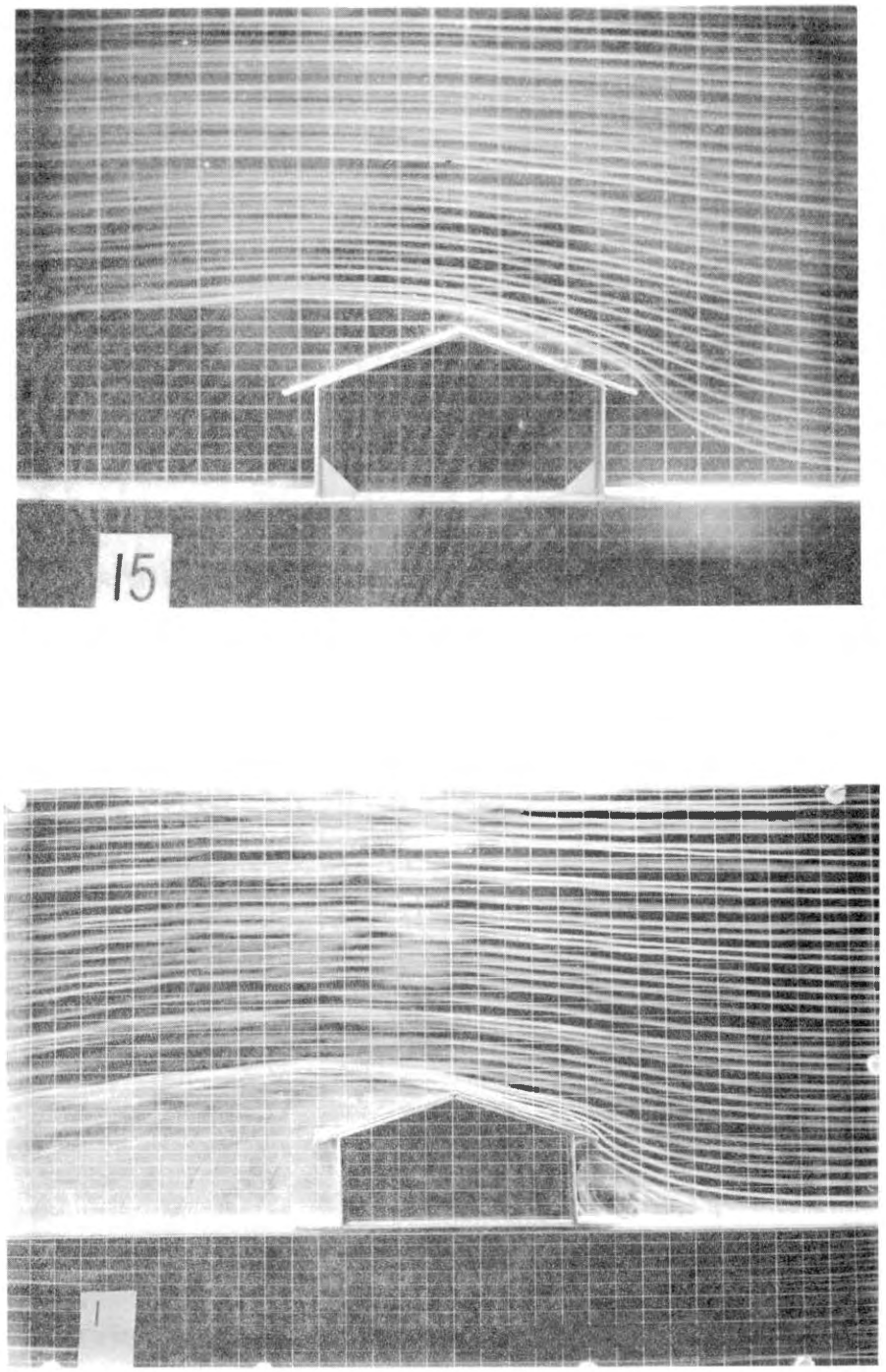

Figure 22. Control Model with Normal Flow Pattern

essentially the same.

Duct Systems. Figure 23 shows four types of ducts tested. All four show definite signs of air passage. This system was tested to attempt to "bleed off" or vent some of the positive pressure upstream into the wake or suction regions beyond. It is evident that all the modifications considered would have some effect.

The choice of the "best" one to test was admittedly influenced by practicality of being able to incorporate such a system into a real structure and into the larger wind tunnel model which utilized four movable panels, independently able to react to the wind forces.

It appeared difficult to include either 9, 14A or 19 in either a real building or the wind tunnel model. Number 18, on the other hand, had the best possibilities for both since a duct system could be utilized on a large building and, using an extremely flexible section between two rigid tubes, the wind tunnel model could at least be attempted.

Unexpected results occurred. Test 9 was expected to vent from the upwind wall to the downwind roof and the other tube was used primarily because of symmetry. It also spanned a pressure differential as shown by the exiting air in the downwind wall. Of the four, the main air stream over the roof on test 9 also bends back down the most. One and one-half inches behind the building, the main stream is only 2" high (8 divisions) in place of the usual 2-3/4" (10 - 12 divisions) for the control model.

For none of the three (9, 14A, 18) does the mainstream beyond the ridge rise 1-1/2 - 1-3/4 divisions as does the control. Only in 19,

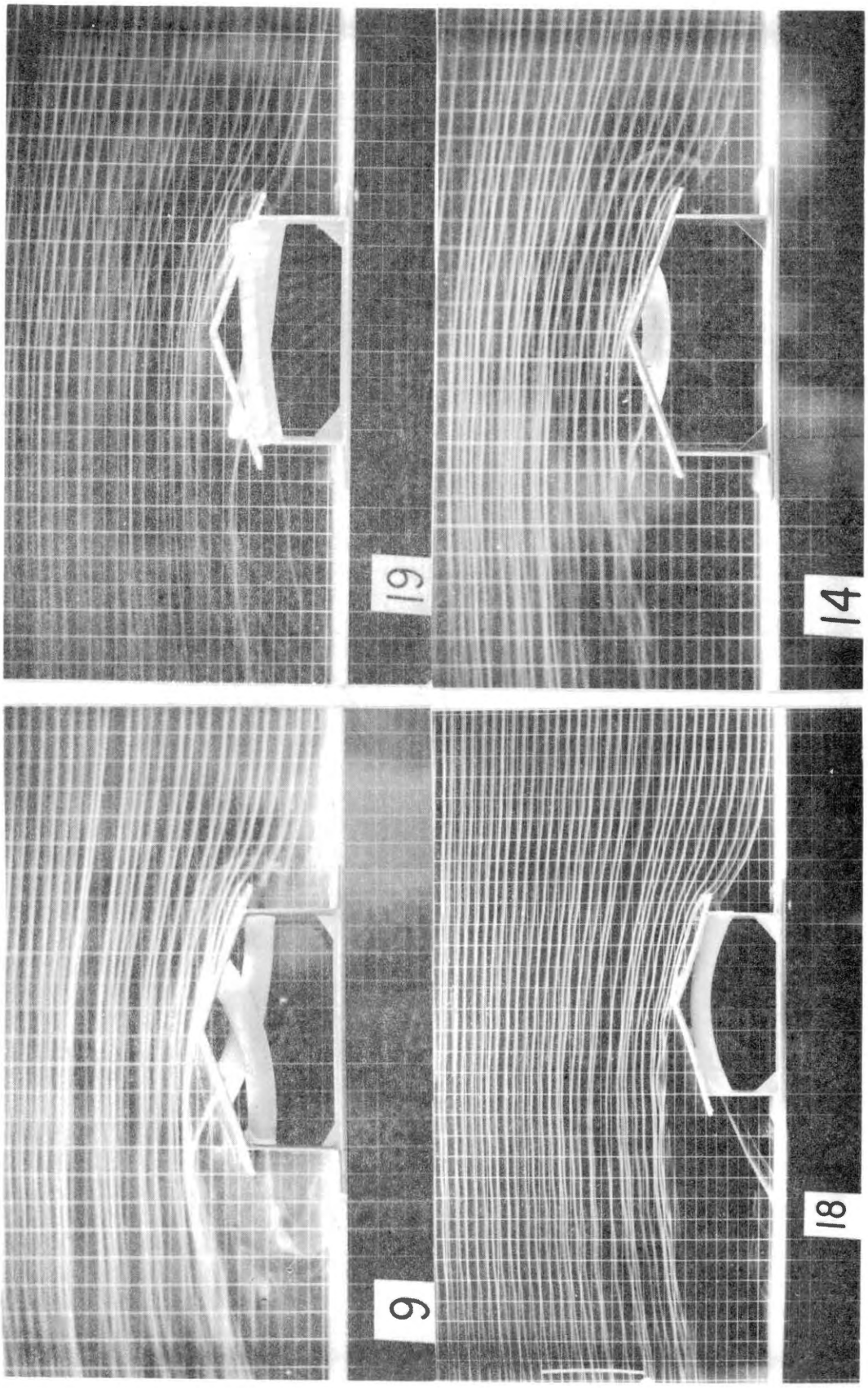

Figure 23. Duct System

where the protruding entrance of one duct breaks up and forces the streams further aloft, does the deflected mainstream appear to be higher.

Airfoil Systems. The "Airfoil System" contains all the modifications which were mounted above the roof ridge of the building.

Figures 24, 25 and 26 show the 10 configurations tested in the smoke tunnel - they are numbers 6, 11, 12, 13; 7, 4, 8, 5; 3 and 10.

Several seemingly absurd configurations were tested in the smoke tunnel. Though some of them had little chance to be practical or effective, they were nevertheless tested to obtain an understanding of how the air pattern could be altered.

Some interesting patterns are exhibited and again surprising results can be noted. In Figure 24, number 6, the air flow was definitely deflected into the wake region though some air was forced aloft by the airfoil. The air deflected downward shows an oscillating effect. Some secondary flow, along the surface of the glass, is seen in this photo. Number 11 is the same deflector mounted lower or closer to the roof. It can be seen that it is more effective in deflecting the air flow down the back roof surface.

Number 12 has a rounded deflector and shows a similar pattern to 6 and 11 but it would appear that the entire front roof surface is in a wake. After the initial separation at the leading edge of the roof it seems that the airstream does not reattach itself to the surface. The airfoil does force more air aloft but effectively turns a significant part of the flow (4 streams) down the back roof.

Number 13, though not tested quantitatively in the study, might

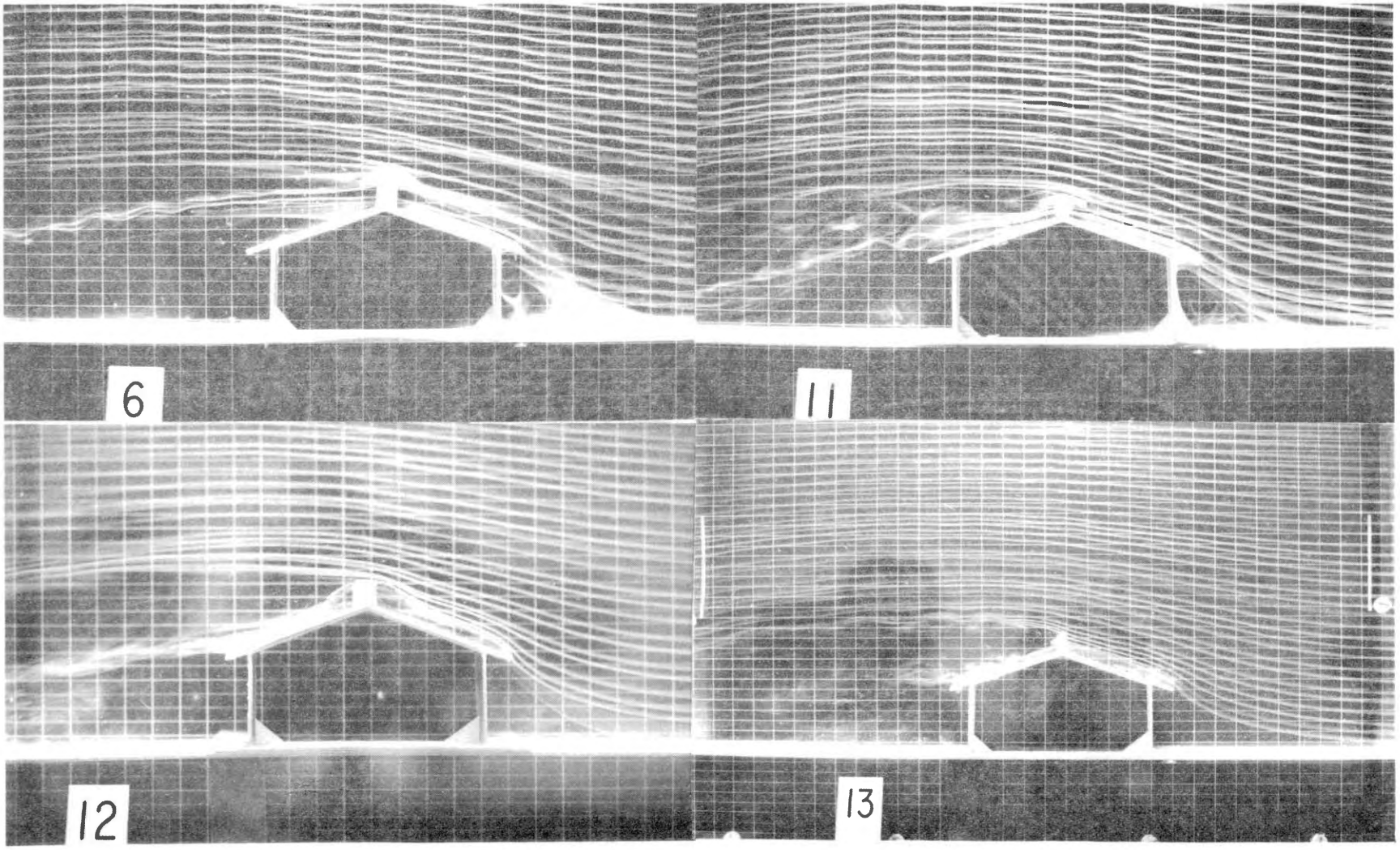

Figure 24. Airfoil System

be further investigated in the future. It is a swinging deflector to function for winds in either direction and appears very effective in diverting at least some of the flow down the back roof. It is very simple and a series of tests would not be difficult to design - altering the size, the weight, the gap between the deflector and the roof and perhaps even vents in the deflector.

Numbers 7 and 4 in Figure 25 and 3 and 10 in Figure 26 are interesting but show no promise in the opinion of the investigator. Evidences of secondary flow can be seen in 10.

Perhaps the most interesting of all the models tested in the smoke tunnel are numbers 8 and 5 in Figure 25.

Number 8 is fascinating. The air literally tumbled down the back roof slope like a waterfall. Equally unusual is the oscillating flow from the higher horizontal piece spanning the gap between the inclined deflectors. This flow stays in the pattern until beyond the building it is drawn down.

Number 5 was selected for further quantitative testing due to its simplicity and effectiveness of turning the flow down the back roof. Though not so dramatic as 8 it was much more practical. The possibility of simulating several conditions with the same equipment on the large wind tunnel model indicated that number 11 could also be investigated.

Venting System. The venting system was based upon the concept that the pressure differential causing forces on the building surface could perhaps be relieved by opening certain portions of the structure's cladding in an attempt to equalize the inner and outer pressure.

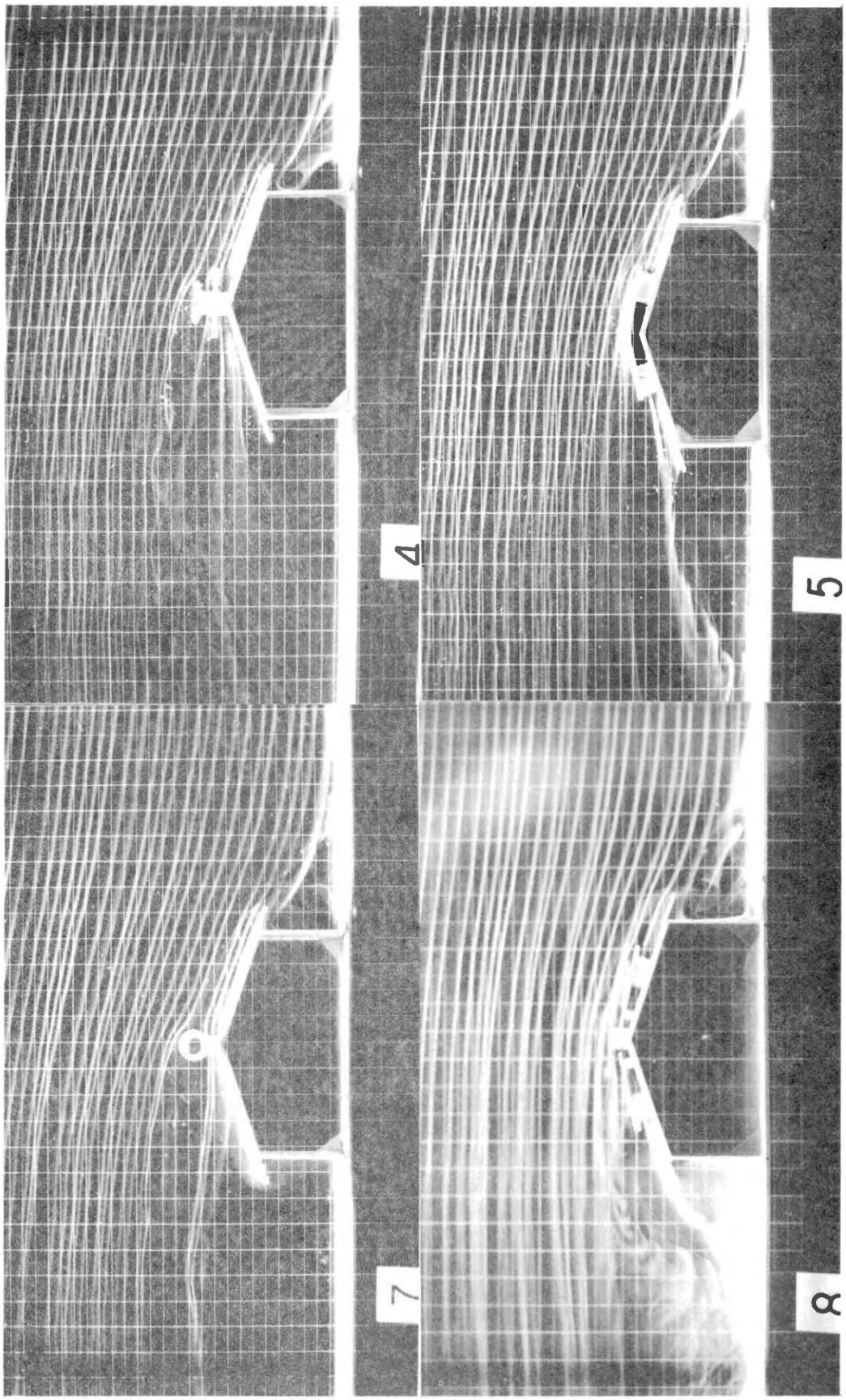

Figure 25. Airfoil System

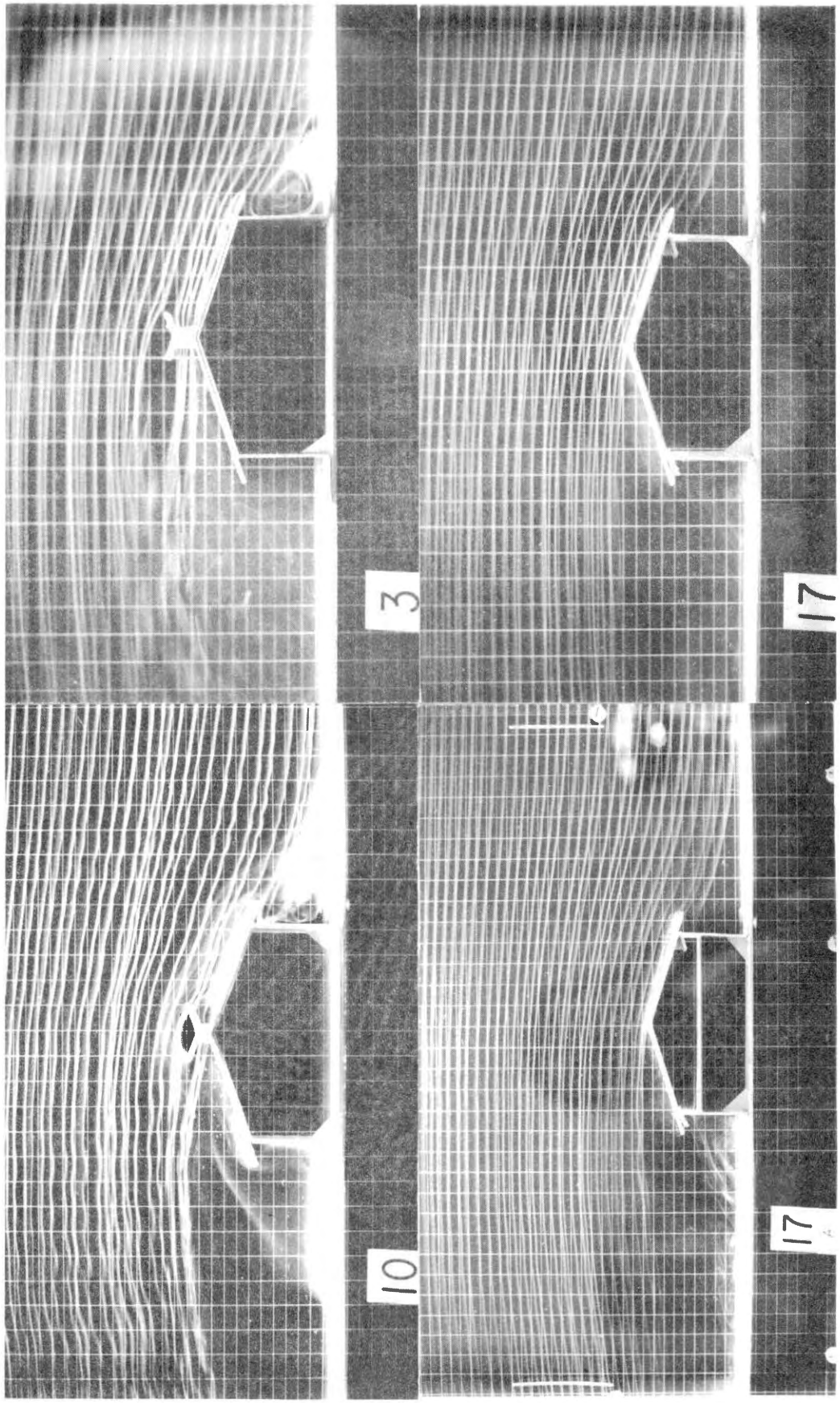

Figure 26. Airfoil System (Top), Vent System (Bottom)

Some buildings in areas struck by tornados have been observed to survive if the openings in the cladding were sufficiently large. One notable example is an airplane hanger where the doors were open.

First thoughts were of metal sheeting with weaker fasteners which would pop off before the stresses in the framework of the structure became severe enough to destroy the building. Later ideas focused upon spring loaded panels which might open inward in response to a positive pressure buildup on the windward side. The speculation was that upon opening, the air would rush inside the building and open a second panel on the leeward side to enable the air to flow through the building.

Models 17 and 17A in Figure 26 were tested in the smoke tunnel to simulate the above mentioned effects. Model 17 showed that the circulation inside the building diffused the vapor streams to such an extent that they were no longer very distinguishable. Figure 17A, which limited interior circulation to the "attic", was the result of attempting to overcome the diffusion of 17 in order to make the effects more visible.

The dark blotches on 17A are reflections of the photographer due to mirror effect on the plexiglass. These were later avoided by photographing behind a cardboard screen with only a hole for the camera lens.

It is, of course, impossible to determine from the smoke tunnel photos to what extent the modifications affect the magnitudes and directions of the forces. For this reason, the modification shown in Test 17 was included in the tests carried out in the large wind tunnel.

Deflector System. All modifications utilize air deflectors placed above the eaves of the roof -- usually near the leading edge (Figure 27).

The intended purpose of these modifications was to cause early separation of air flow. This normally occurs at the ridge where the abrupt change in building geometry makes it impossible for flow lines to follow the building shape.

The major difference between 1 and 16 is the angle of deflection with respect to the roof. In both, the windward roof slope is in a wake region.

Modification 2 consists of a series of delfectors distributed across the roof surface. The resulting air flow pattern seems to be the same as the normal pattern, only shifted a little higher. Undoubtedly the deflectors would cause large horizontal forces on the roof. It seems that the main effect would be similar to greatly increasing the roof surface friction without any significant possibility to beneficially change the normal pattern of forces. It was eliminated from further testing.

Modifications 1 and 16 were retained for the purposes of testing in the wind tunnel. The two were actually combined into one test which incorporated a deflector used at varying angles to the roof surface.

Summary

As a result of the flow visualization studies, it was decided to conduct preliminary quantitative evaluations on building models

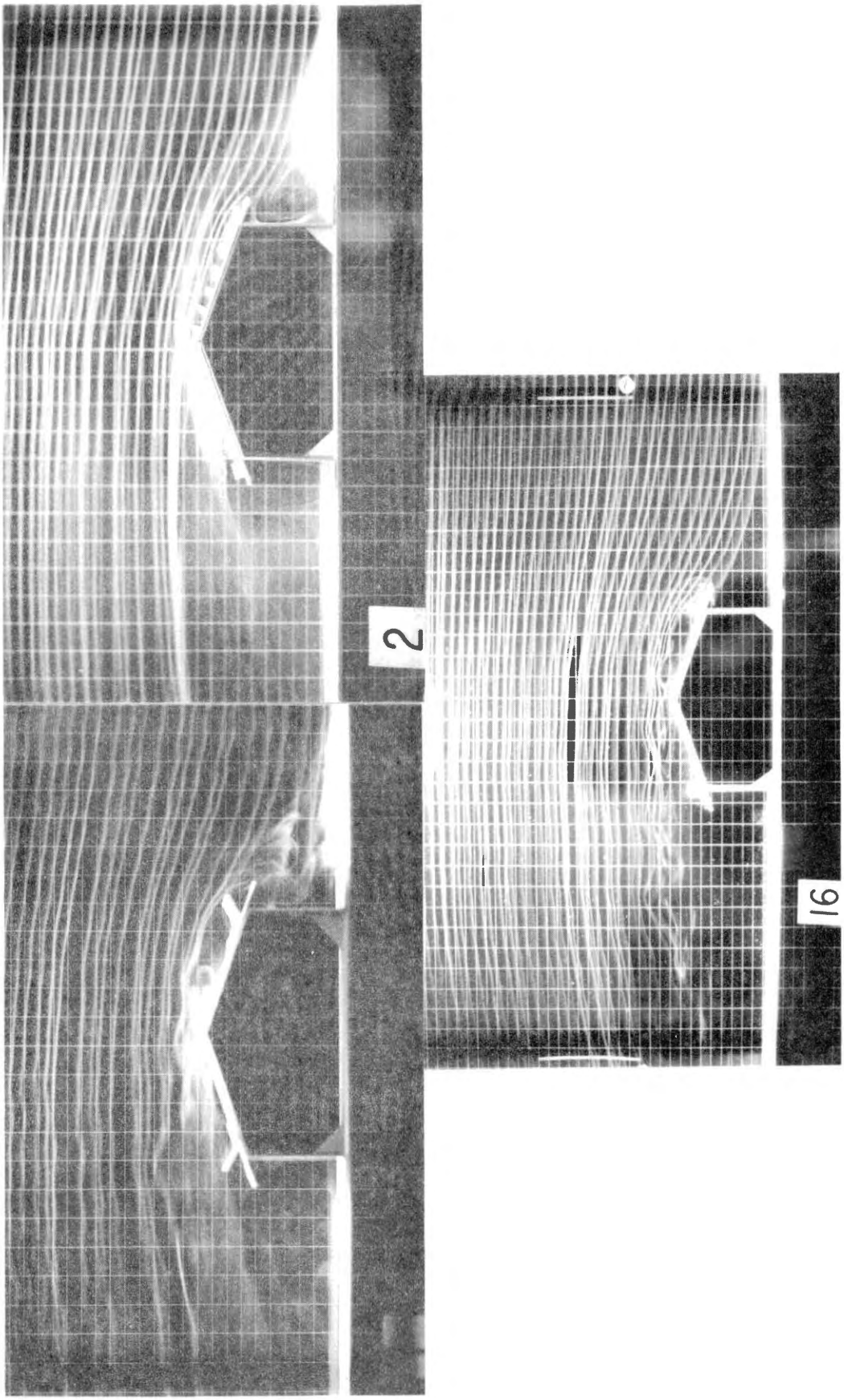

Figure 27. Deflector System

including:

No. 18 of Figure 23 (duct system)

No. 5 and 11 of Figure 25 (airfoil system)

No. 17 of Figure 26 (venting system)

No. 1 and 16 of Figure 27 (deflector system)

These were selected both because of their alteration (hopefully favorable) of the normal air flow pattern and because of their possibility of being incorporated into the model to be tested in the wind tunnel and into an actual prototype building.

Quantitative Investigation

Objectives

After the qualitative investigation it became even more evident that it was necessary by some means to quantitatively evaluate the changes in forces occasioned by the various building modifications.

Specifically, the objectives of the quantitative studies were:

1. To examine the differences in the force patterns exhibited by the models in the simulated wind of an open countryside.
2. To formulate force coefficient prediction equations for the best system, if it favorably alters the characteristic air pattern, in order to determine the optimum size and arrangement of the system components.

Method

An investigation of scaled building models in a large, low speed

wind tunnel was selected as the most feasible way to quantitatively study the effects of the modifications upon the typical wind force pattern.

A velocity profile near to that of open countryside was simulated in the wind tunnel by trial and error methods. Next, wind forces on the appropriate control model were recorded for comparison with the forces on the same model with various modifications.

The scaled models incorporating the various modifications were subjected to limited preliminary testing and evaluation in order to select the one most promising modification. All preliminary testing took place at top wind tunnel velocity of approximately 40 miles per hour with the model perpendicular to the wind. The "best" was then subjected to more extensive testing which included several wind velocities and the building oriented also at 15° and 30° to the wind.

The scaled model building represented a prototype 40' by 100' rectangular building with walls 16' high and eave overhang of 3'. The roof slope of the gable type building was 4/12. The windward wall, the windward roof, the leeward roof and the leeward wall all contained movable panels suspended at all four panel corners on small cantilever beams -- 16 in all. The 16 cantilever beams were instrumented, each with a pair of strain gages mounted so as to respond only to bending forces and not axial forces. The beams, thus instrumented, translated even the slightest movement into an electronic signal which could be recorded. The beams were calibrated, before and after the tests, by suspending known weights from each of them and recording the resulting signals from the strain gages.

During the actual tests as the panels responded to the wind

pressures (either outward or inward), the slight, rapidly fluctuating movement was recorded continuously for a brief period of time. The same signals were simultaneously input into the analog computer where they were "averaged" and reinput to the recorder alongside the corresponding "instantaneous" signals.

Simultaneously, the horizontal and vertical wind velocities, their averages from the analog computer and the horizontal and vertical turbulences were documented on two other recorders.

Experimental Design

In planning the experiment a prior effort was made to define the systems' behavior using the anticipated pertinent quantities and appropriate pi terms.

Pertinent Quantities. The pertinent quantities for the definition of the physical system are listed in Table I. Certain of them are illustrated in Figure 28. These pertinent quantities, all in the force-length-time (FLT) system of dimensions, are the components of the pi terms listed in Table II. Analysis of the 16 pertinent quantities for Alternative I shows 13 pi terms are required to define the system since they are expressed by three dimensions. The pi terms were evolved by inspection and tested for dependence. The pi terms must be independent. Independence does not, however, insure relevance.

Many of the pi terms thus established for the system were not varied during the experiment - the pi terms to describe the basic building and the air flow are examples. One exception is to be noted; π_5 was varied in one phase of the experiment - specifically L_S was

TABLE I

LIST OF PERTINENT QUANTITIES

No.	Symbol	Quantity	Units	Dimensions
		Basic Shape of Building (Constant for This Experiment)		
1	h_f	height of building at eaves	ft	L
2	W	width of building across end walls	ft	L
3	Θ	angle between roof and horizontal, expressed as tangent or slope	--	--
4	L	length of building along side wall	ft	L
5	L_r	length of roof ridge	ft	L
6	L_s	length of roof slope	ft	L
		Wind Description		
7	ϕ	orientation of mean flow w.r.t. length of building	--	--
8	V_H	horizontal velocity at eave height, above ground plane	ft/sec	LT^{-1}
9	n	exponent which describes the velocity profile or distribution of V_H with elevation above ground	--	--
10	ρ	air density - including variables of temperature, pressure and relative humidity	$\frac{lb\text{-}sec^2}{ft^4}$	FT^2L^{-4}
11	x	distance ahead of front wall to where horizontal velocity is measured	ft	L
		Description of Alternative I - Deflector		
12	a	position, relative to the leading edge of roof, of pivot point on deflector	ft	L
13	b	open distance of deflector pivot pt from roof slope - zero indicates no gap whereas positive value indicates the amount of gap	ft	L
14	c	deflector width	ft	L
15	α	angle of deflector with roof slope (L_s)	--	--
		Description of Alternative II - Airfoil		
16	β	angle of airfoil with roof slope (L_s)	--	--
17	d	shortest distance between roof and airfoil	ft	L
18	e	width of airfoil - measured parallel to L_s	ft	L
		Description of Alternative III - Duct		
19	h_d	distance from ground to center of duct	ft	L
20	d_d	diameter of ducts	ft	L
21	N	number of ducts	--	--
		Force Description		
22	R_i, $i = 1\text{-}8$	reactions at corners of panels (normal to its surface), lbs/ft of panel (measured along its length)	lbs/ft	FL^{-1}

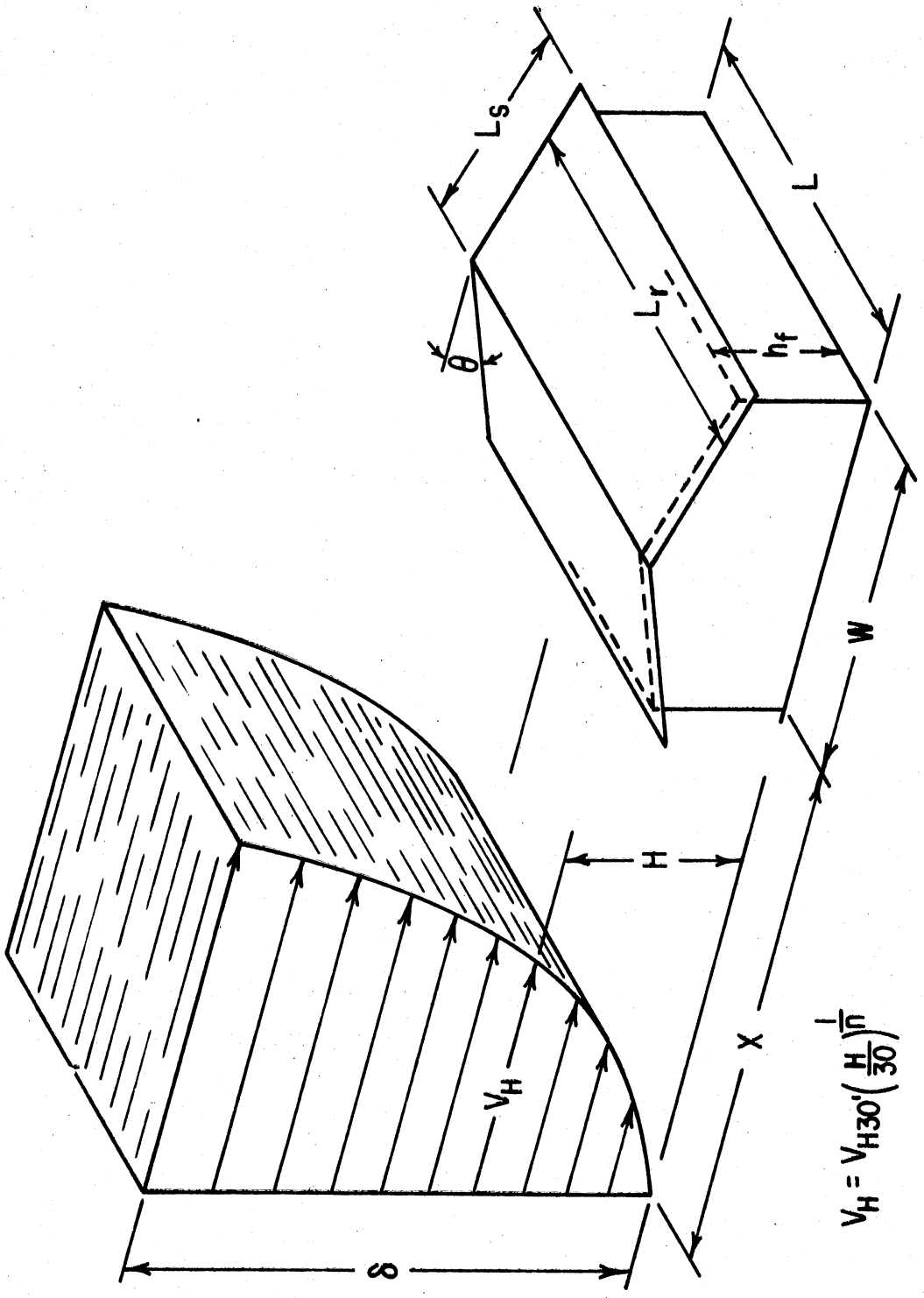

Figure 28. The Physical System

TABLE II

PI TERMS

No.	Quantities	Description
π_1	$\frac{2R_f}{\rho(V_H)^2 L_s}$	dependent Pi term which is a form of lift coefficient for roof surfaces
	or	or
	$\frac{2R_i}{\rho(V_H)^2 h_f}$	drag coefficient for wall surfaces
		General for All Alternatives
π_2	h_f/W	an aspect ratio
π_3	Θ	roof slope parameter
π_4	L/L_r	ratio of the length of the sidewall to the roof ridge length
π_5	$L_r L_s$	ratio of roof ridge length to roof slope length
π_6	L/W	an aspect ratio
π_7	ϕ	wind orientation w.r.t. to building
π_8	n	characterizes wind velocity profile
π_9	x/w	ratio of distance to where velocity is measured to the end wall
		For Alternative I - Deflectors
π_{10}	a/L_s	position factor for deflector
π_{11}	b/h_f	gap index
π_{12}	c/h_f	deflector height index
π_{13}	α	angle of deflector with the roof slope
		For Alternative II - Airfoils
π_{14}	β	airfoil angle
π_{15}	d/h_f	airfoil elevation index
π_{16}	e/L_s	airfoil coverage index
		For Alternative III - Ducts (Tubes)
π_{17}	h_d/h_f	duct height index
π_{18}	$d_d^2/h_f L$	duct area index (when multiplied by $N\pi/4$ gives percent of total wall area in ducts)
π_{19}	N	number of ducts
		For Alternative IV - Venting
		Only the height of opening will be varied and its physical location will be documented

varied in a minor eave overhang test.

Quantities 1-6 in Table I describe the basic building shape. These are the only quantities needed. Other useful quantities can be derived from these six, if necessary. (See Figure 29). Some examples are:

$h_r = h_f + \frac{W}{2} \tan \Theta$ — Ridge height

$O_W = L_S \cos\Theta - \frac{W}{2}$ — Horizontal projection of eave overhang along the side walls

$L_O = L_S - \frac{W}{2 \cos\Theta}$ — Roof overhang along side walls

$O_L = \frac{L_r - L}{2}$ — End overhang

Quantities 7-11 define the wind effects at the eave height of the building with respect to a known velocity at a relative position ahead of the building. With the velocity known at 30' (7-1/4" for the model) above the ground, the n value is all that is required to specify the velocity profile. The air density, which includes variables of temperature, barometric pressure and relative humidity, can change and must be included. The final quantity, angle of orientation (ϕ) of the wind to building, refers to the deviation of the wind from right angle impingement on the upwind side wall.

Pi Terms. The general functional relationship for the pi terms is;

$$\pi_{22} = \Psi (\pi_2, \ldots, \pi i)$$

where the operator Ψ is to be determined by the analysis of the data from the investigation. Since in this case several of the general pi

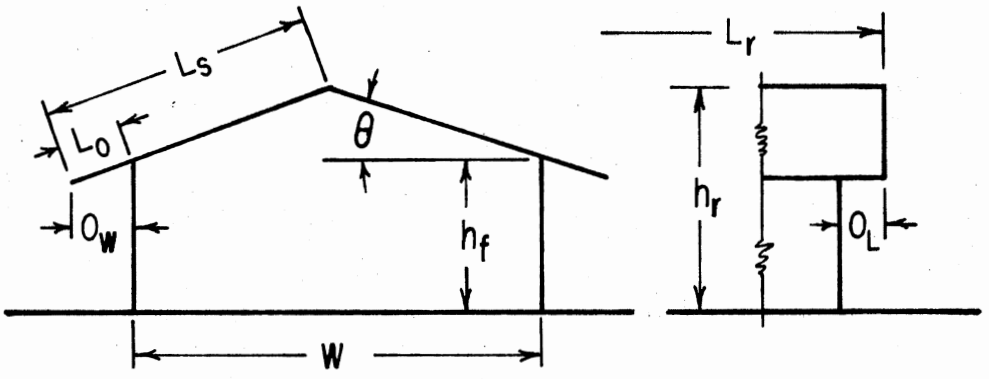

Figure 29. Derived Quantities Dependent Upon the Basic Six Dimensions

terms are not to be varied, they have to be treated as potential constraints in the ability to categorically apply the experimentally derived information to buildings of all shapes and sizes. Rather the information is strictly applicable only to structures with

$h_f/W = 16'/40' = 0.4$

$\Theta = \text{Arc tan } 4/12 = 18.44°$

$x/W = 125.83'/40' = 3.14575$

$L_r/L_s = 106'/24.244' = 4.372$

$L/W = 100'/40' = 2.5$

$L_r/L = 106'/100' = 1.06$

found in a wind velocity profile, which when measured at a height of 30' is characterized by an exponent of $\frac{1}{n} = 0.17445$ in equation $V_H = V_{H30'} \left(\frac{H}{30'} \right) \frac{1}{n}$. This gives N a value of 5.732. H here has the value of h_f or 16'. The (H/30') ratio is, of course, the same if the scaled values of the model are used. During the planned preliminary tests, π_2, π_3, π_4, π_5, π_6, π_7, π_8, and π_9 are held constant.

For Alternative I then

$\pi_1 = \Psi (\pi_{10}, \pi_{11}, \pi_{12}, \pi_{13})$ and $\pi_{14\text{-}19}$ are zero.

For Alternative II

$\pi_1 = \Psi (\pi_{14}, \pi_{15}, \pi_{16})$ and $\pi_{10\text{-}13}$ and $\pi_{17\text{-}19}$ are zero.

For Alternative III

$\pi_1 = \Psi (\pi_{17}, \pi_{18})$ and $\pi_{10\text{-}16}$ are zero while $\pi_{19} = 20$

During Alternative IV (Venting)

$\pi_1 = \Psi$ (opening), its location will be documented.

The range of values tested for each pi term (variable) is

documented for each alternative separately.

The results of this experiment may be applicable to other similar systems, as defined by these pi terms, but it cannot be proved solely by the results of the tests to be carried out.

The advantage of reducing the number of experimental quantities to be varied during experimentation to define the system's behavior is not the goal of forming the pi terms in this investigation since, in all but one case only one term in each will be varied. Rather, the goal was to better understand the system by analyzing the relationship of its components. It is hoped, of course, that the system is sufficiently defined and that the results will be generally applicable.

Pi Terms Not Included.

1. The pi term δ/h_f is often considered. δ is the thickness of the boundary layer. Where the profile is to be changed by various treatments of the tunnel floor and the resulting thickness of the boundary layer might not be representative of a scaled condition of natural wind, this would be an important variable. It represents the degree of boundary layer immersion. This is not the case in this investigation as the boundary layer is simulated to scale and δ/h has not been included as such.
2. The ratio of the surface roughness of the roof to some characteristic length. It is recognized that the roughness of an object in air flow influences the point of separation of the local boundary layer -- along the roof surface, for example. It is quite likely that the air flow separates at

the leading edge of the roof eave and reattaches somewhere before reaching the ridge. The surface roughness could affect the reactions to be measured but it was felt this would have but little effect in comparison to the alterations to be tested and has therefore been ignored.

3. Reynold's Number. The viscious forces were not considered to be pertinent in this experiment because a preliminary effort was made to insure the establishment of fully developed turbulent flow in which the ratio of viscous forces to inertia forces would be insignificant. The assumption is that the force coefficients (π_1) would not be affected to any great extent by the velocity of the air.

Equipment

The quantitative investigation required an extensive system of electronic and mechanical equipment. The major components included the wind tunnel, the model, the cantilever beam sensors, and the circuitries for the strain gages, for recording the wind characteristics and for partially analyzing the data with the analog computer.

Wind Tunnel. The large wind tunnel, permanently installed in the Agricultural Engineering Laboratory, includes a 50' length, 4' by 4' in cross-section. (Figure 30). The 16 blade fan, located in the exhaust diffuser (Figure 31) has variable pitch blades and is driven by a 15 horsepower electrical motor. For a given blade pitch, fan speed can be regulated by a control which changes the effective diameter of one of the drive pulleys.

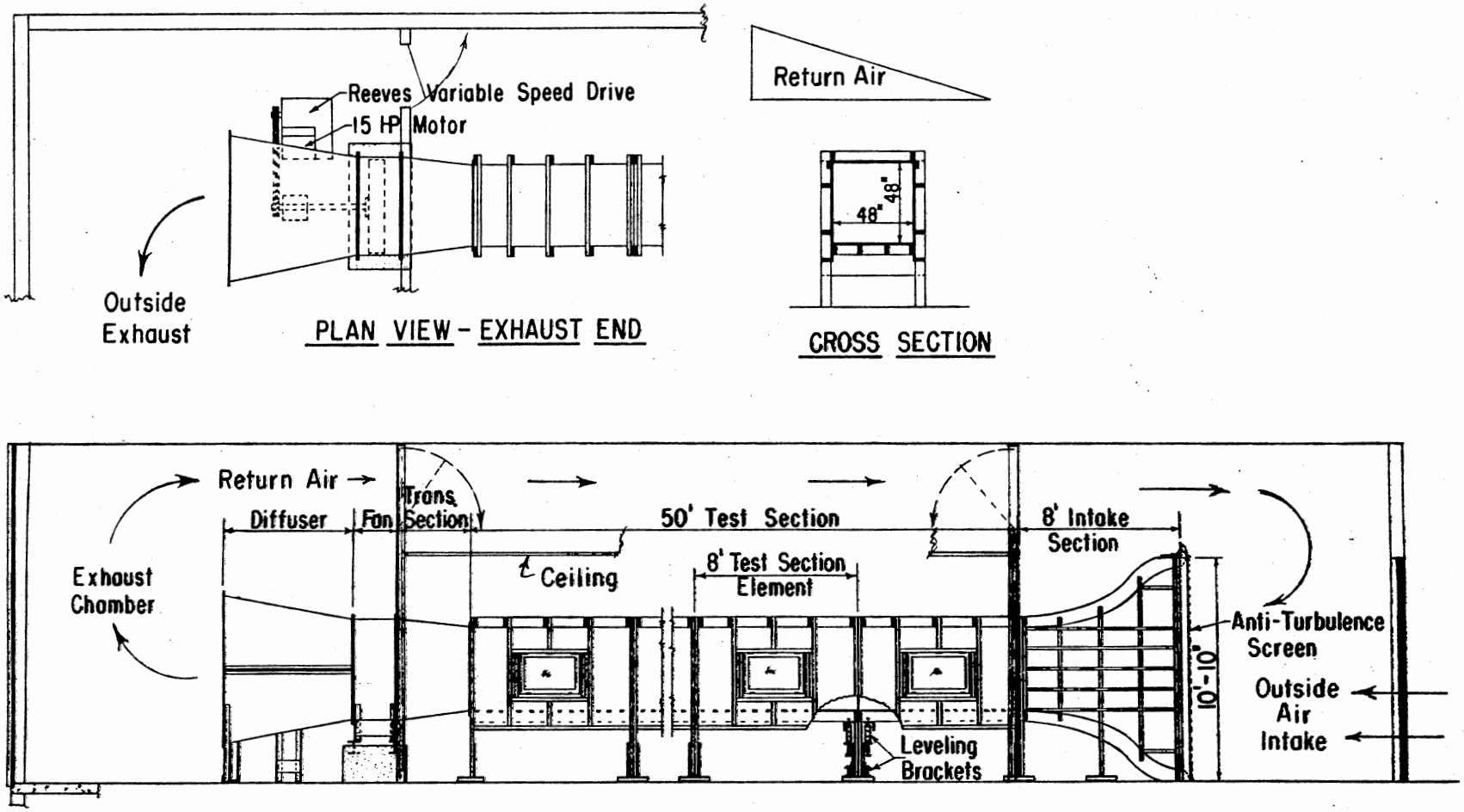

Figure 30. Low Speed Wind Tunnel - Agricultural Engineering Laboratory - Viewed From the South

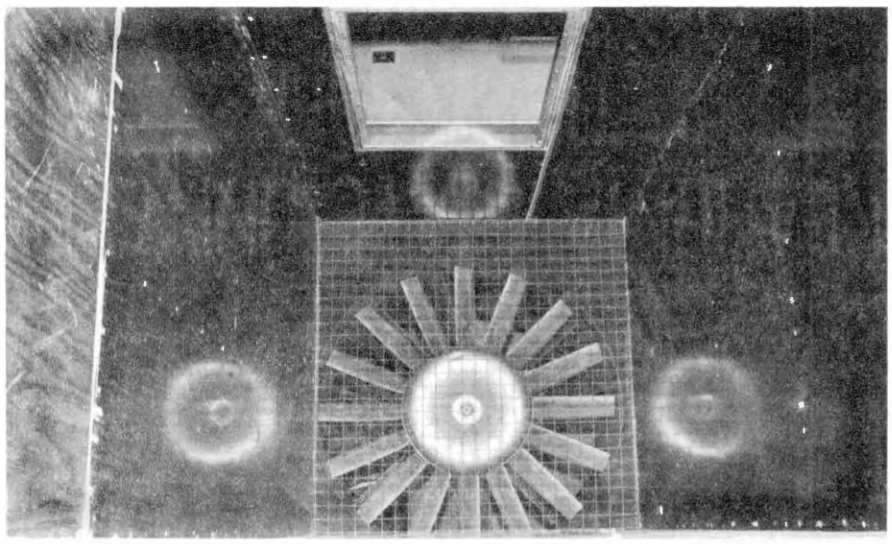

Figure 31. Exhaust Fan and Protective Screen.

For the tests the propeller blades were set to maximize the air speed. This resulted in attainable wind velocities of 25 to 40 mph.

To eliminate unusually high tunnel turbulence detected by the sensitive hot wire, it was necessary to further dampen the air flow. A series of tests were performed, as a part of another study, with a variety of screens in different sections of the tunnel. Rectangular meshes of several sizes were tried in front of the fan and at several places along the length of the 4' by 4' portion of the tunnel. Two

sizes of honeycomb screen were fabricated by utilizing tin cans 4-1/4" and 6-1/4" in diameter with both ends cut out. Due to the size of screen which would be necessary at the entrance of the contraction section, where the screen should be most effective, the tests were restricted to the smaller 4' by 4' section. Final choice of screens utilized a honeycomb material (Figure 32) used in aircraft construction at the position shown in Figures 33 and 34 in addition to the regular anti-turbulence screen.

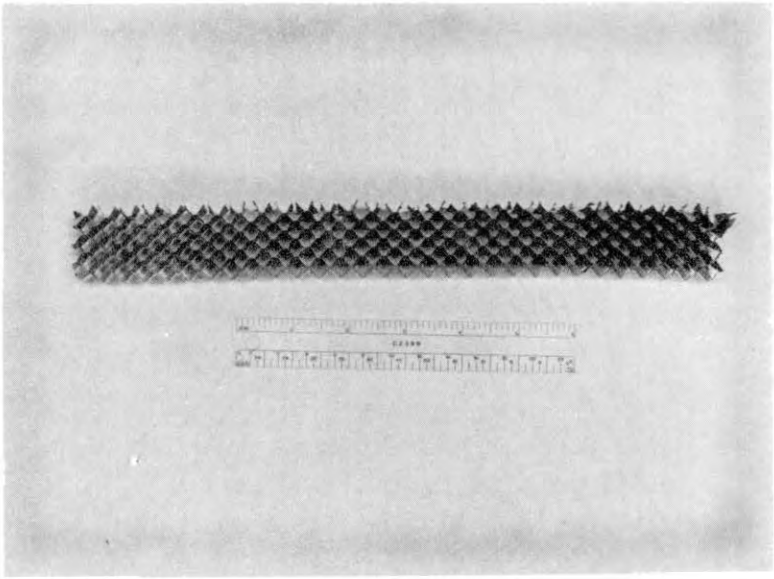

Figure 32. Honeycomb Material Used in Anti-Turbulence Screen.

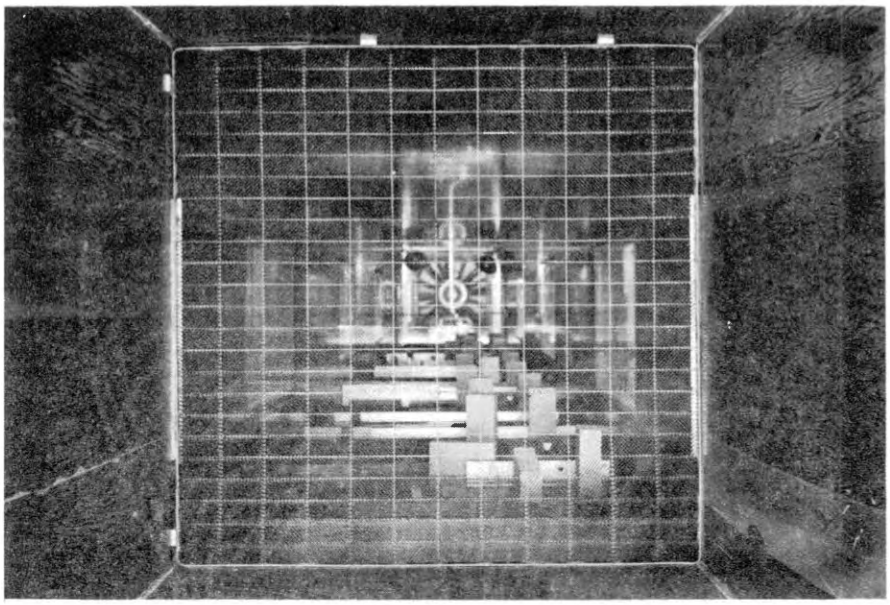

Figure 33. Honeycomb Screen Just Downwind from Contraction Section.

In addition to these precautions the wooden portion of the tunnel and the metallic diffusion section of the fan shroud were isolated from each other. Previously the protective screen for the fan (Figure 31) was bolted between the shroud and the wooden tunnel, fastening the latter two rigidly together. The screen was removed and fastened inside the metal shroud leaving a 1/4" gap between the tunnel and the shroud. It was then sealed with duct tape. The effect was to eliminate mechanical vibrations of the fan from the wooden walls of the tunnel.

One further alteration of the tunnel was necessary. To facilitate entry into the tunnel the window at the model installation site was considerably enlarged by lowering the bottom sill to the level of the tunnel floor (Figure 34).

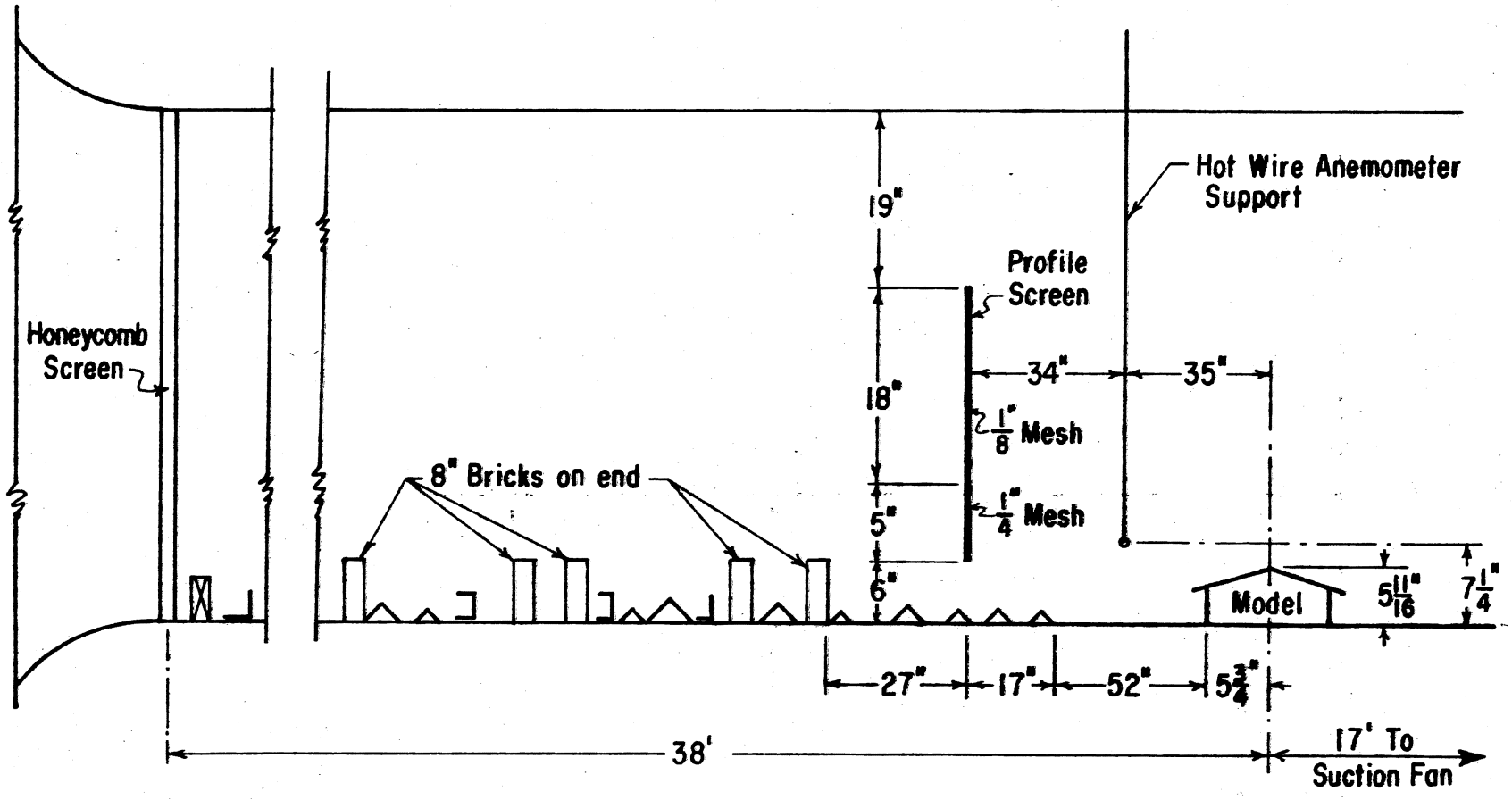

Figure 34. Experimental Equipment Location

The Model. The plexiglass model was installed on the floor of the tunnel ≈ 20' upstream of the suction fan. Refer to Figures 34 and 52. The building model was attached to an aluminum baseplate which was inlet into a 27" diameter plywood disk cut from a special floor section of the tunnel (Figure 35). A center pivot enabled rotation of the whole disk to attain orientations of 0-45° with respect to the wind flow. The 1/50 scale model represented a gable single story building of the type often used in agricultural and industrial service. The prototype selected was 40' by 100' with 16' high walls, 4/12 roof slope and 36" overhang all around.

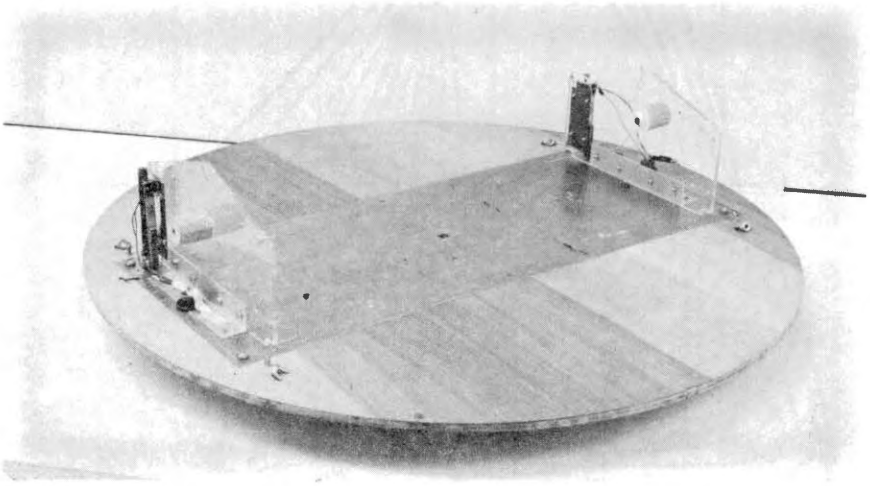

Figure 35. Disk, Floor Plate, Fixed End Walls with Cantilever Beams in Place for One Wall Panel

The building model was comprised of eight plexiglass parts in addition to the aluminum floorplate (Figure 36). Four movable panels, suspended on 16 cantilever beams, constituted the surfaces reacting to the tunnel wind forces -- one beam for each of the four corners of each panel (Figures 37 and 38). Each beam was instrumented with a pair of strain gages. (See Figure 40). The four panels were the front or upwind wall, the upwind roof, the downwind roof and the downwind wall. Two of the remaining building model parts were the fixed end walls upon which the cantilever beams were mounted (Figures 35 and 42). The final two model parts were the removable end wall covers which enclose and protect the cantilever beam mechanisms and wires from the wind and extraneous vibrations (Figures 36 and 37).

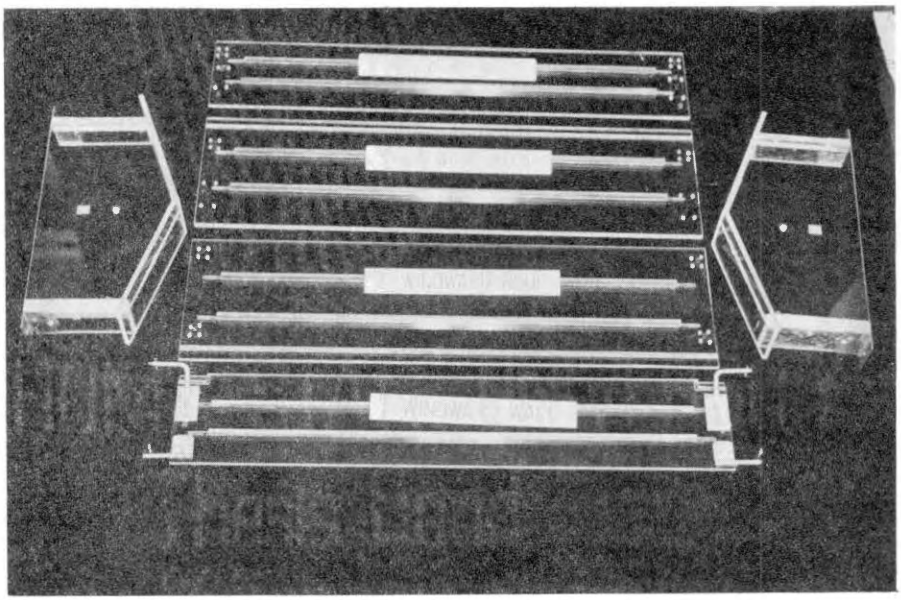

Figure 36. Four Movable Panels and Removable End Wall Covers

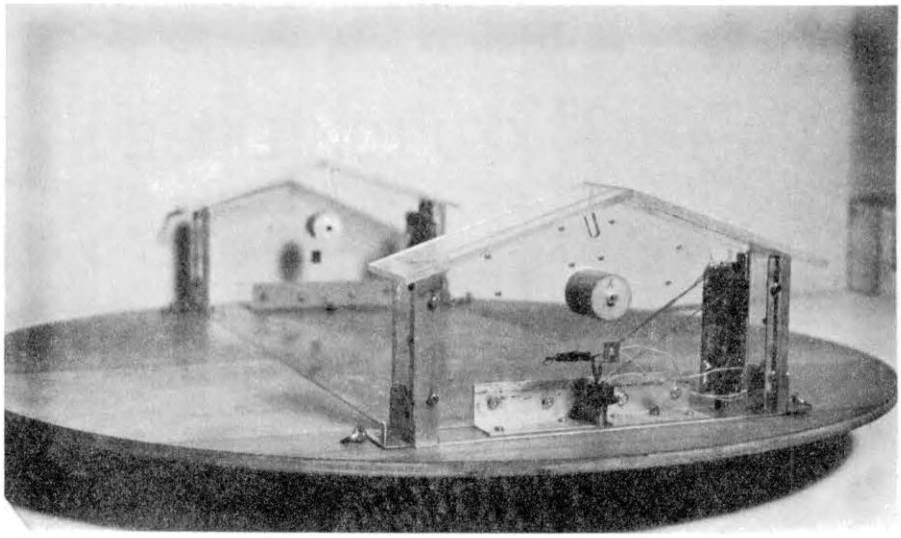

Figure 37. End Wall Covers and One Pair of Cantilever Beams with Wires Exiting Through Hollow Bolt.

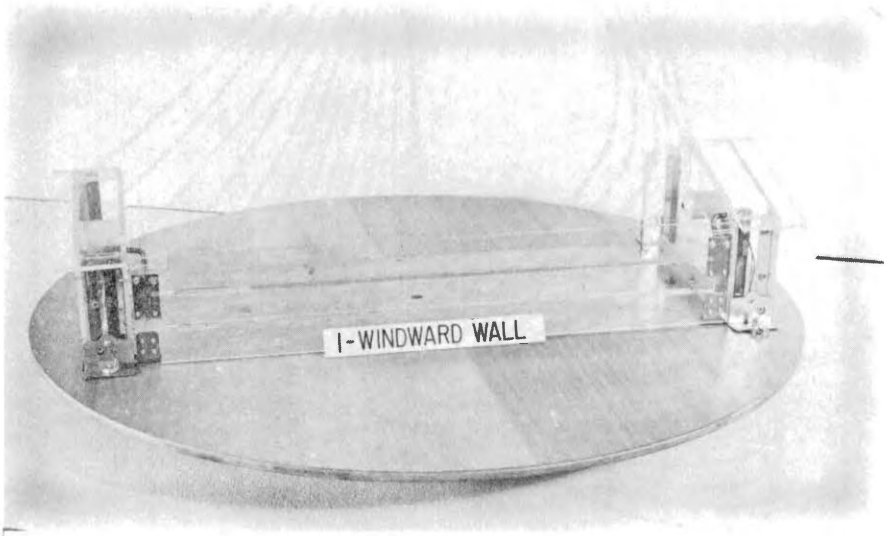

Figure 38. Model with One of Four Movable Panels in Place.

Plexiglass (3/16" thick) was chosen as the material for the model in order to allow easy visual inspection of the cantilever beams and linkages. Each of the plexiglass panels (20 19/32" long) had to be stiffened lengthwise. Eighteen inch aluminum strips 1/8" wide, 1/4" and 5/16" deep for the walls and roof panels respectively, were inlet 1/16" into the plexiglass and securely cemented. Two strips per panel were used. These can be seen in Figure 36. The 20 19/32" length of the movable panels represents 85' 10" of the 100' length of the prototype.

The Cantilever Beams. The 16 cantilever beams are divided, for the purposes of identification, into two groups, A and B. Each group contains eight beams, two corner beams for each of the four panels at one end of the model. The designations of the eight are shown in Figure 39. A5 is on the "A end" (south) of the model at the leading corner of the back roof panel. For example, the beams supporting that back roof panel are, on the south end of the model, A5 and A6 while at the north end they are B5 and B6.

Some of the construction details of the cantilever beam assemblies can be seen in Figure 40. They are assembled in pairs on a small plate used to mount them on the fixed end wall of the model (Figure 42). One such assembly is pictured in Figure 41. The actual beam is galvanized sheet steel while the mounting portion of the assembly is brass. Regular solder was used.

Since the actions of some of the beams would necessarily overlap, certain beams were mounted at different distances from the mounting plates. This is denoted in Figure 39 by "hi" and "Lo". "Hi" signifies

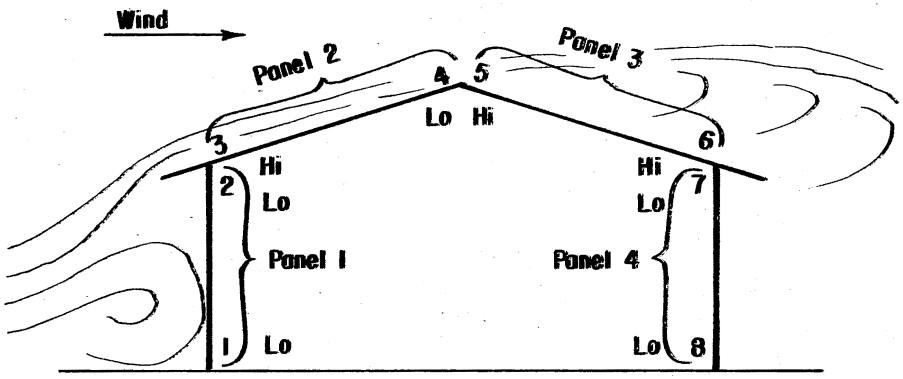

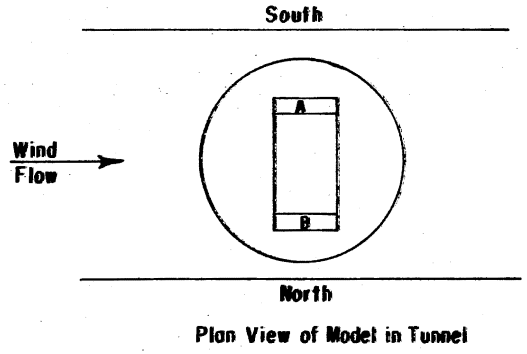

Figure 39. Designation of Beams and Gages

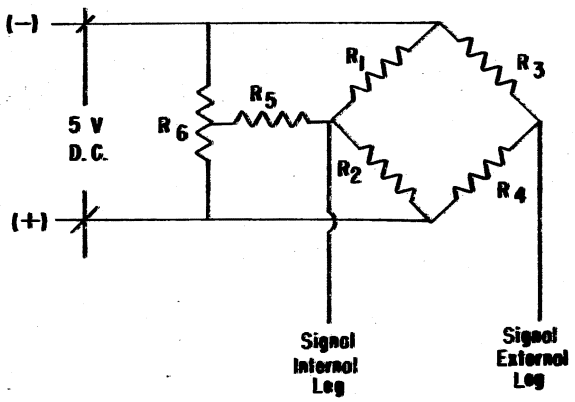

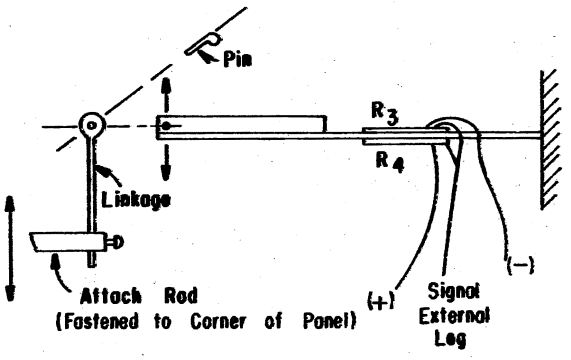

Figure 40. Full Bridge Strain Gage Circuit and Some Construction Details for One Beam - A1

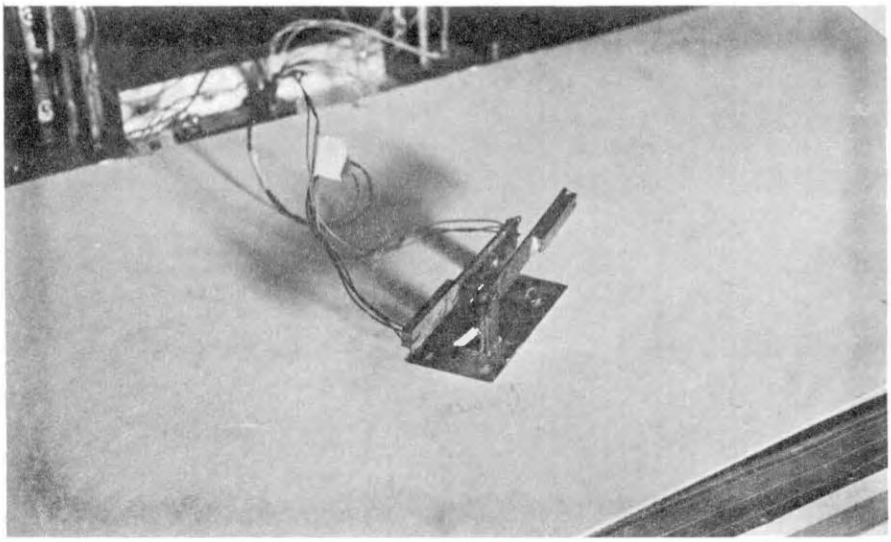

Figure 41. One Pair of Cantilever Beams Before Mounting

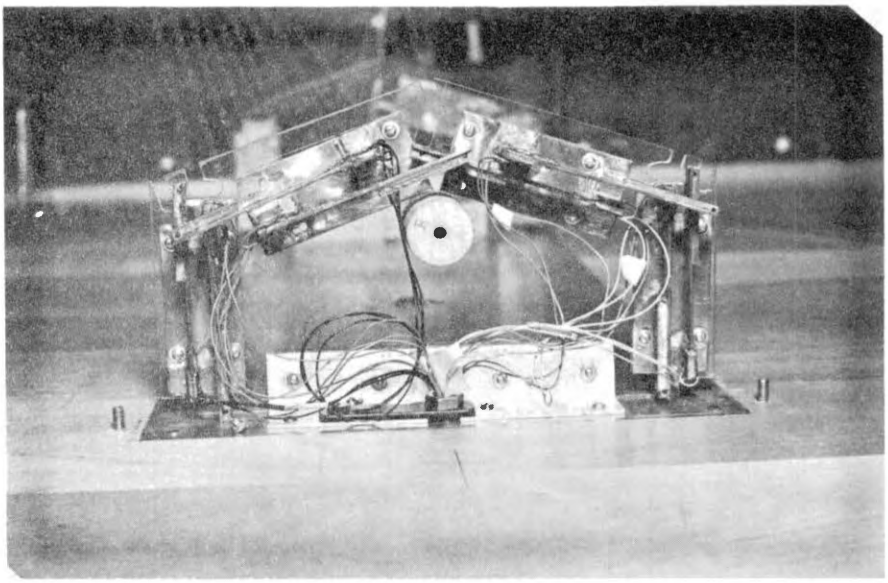

Figure 42. All the "B" Beams Mounted on One End Wall

that the distance between the mounting plate and the edge of the beams is 11/16". "Lo" indicates a 3/16" distance. The mounting plate holes are elongated for placement adjustment on the building end walls. On one end the linkages are pin connected to the slotted beams and the other end fits through a hole in the attach rods. The linkage distance is adjusted by means of a set screw tapped into the end of the attach rods. (See Figures 36 and 40).

Strain Gage Circuitry. On each cantilever beam a pair of strain gages was mounted so as to null out any axial forces and at the same time double the bending forces. Refer to the wiring diagram in Figure 40. All the small wires for the strain gages on one end of the model exited through a hollow bolt in the floor of the mechanism cubicle. This can be seen in Figure 42. Figure 43 shows the complete block diagram of the strain gage conditioning and recording circuit. Figure 44 illustrates the equipment used.

A full bridge circuit was set up by constructing the circuit board, the bridge unit and rewiring a Baldwin balancing unit as depicted in Figure 45. Resistance values are listed in Table III. For the sake of simplicity only the wires for one (A1) of 16 pairs of gages are shown. Actually all 16 are fed into the control box (Figures 46, 47 and 48) where, by means of cams, micro-switches and relays, the gages for one of the four building panels were connected to the Beckman recorder and EAI Analog Computer at any one time.

The control box was constructed to record the forces on a given panel for approximately 13 seconds. This was followed by a null period of three seconds. Automatically the next panels were recorded

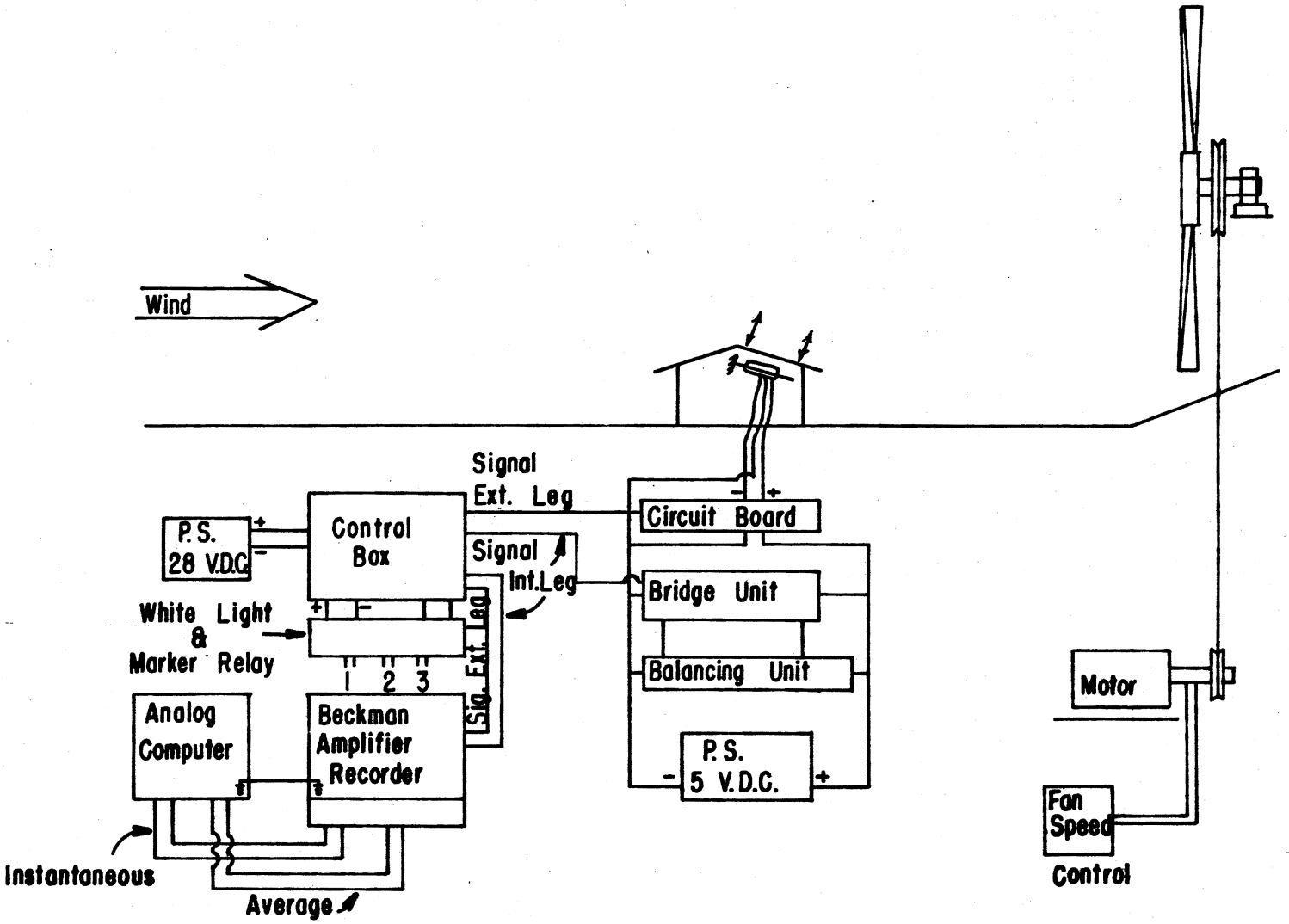

Figure 43. Block Diagram of the Complete Strain Gage Conditioning and Recording Circuit.

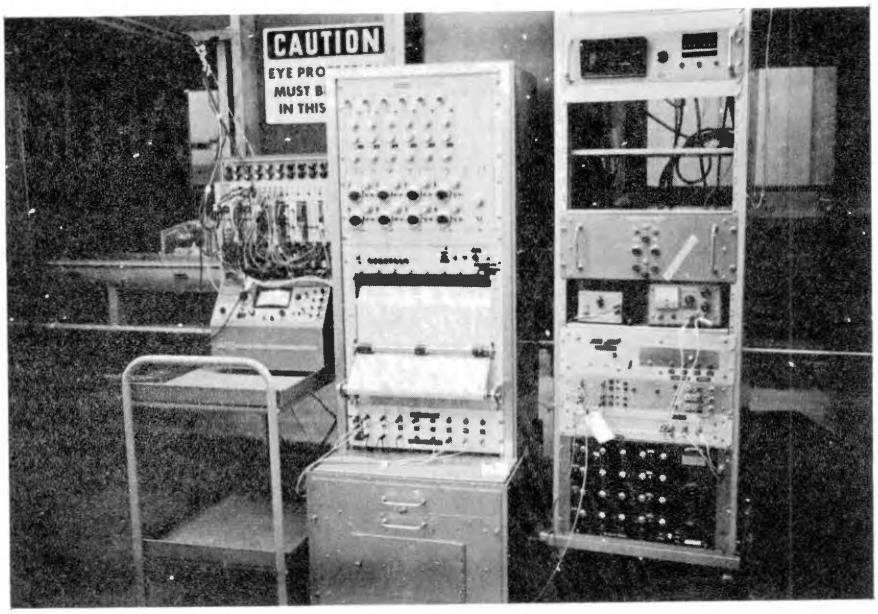

Figure 44. Equipment for Conditioning and Recording of the Strain Gages

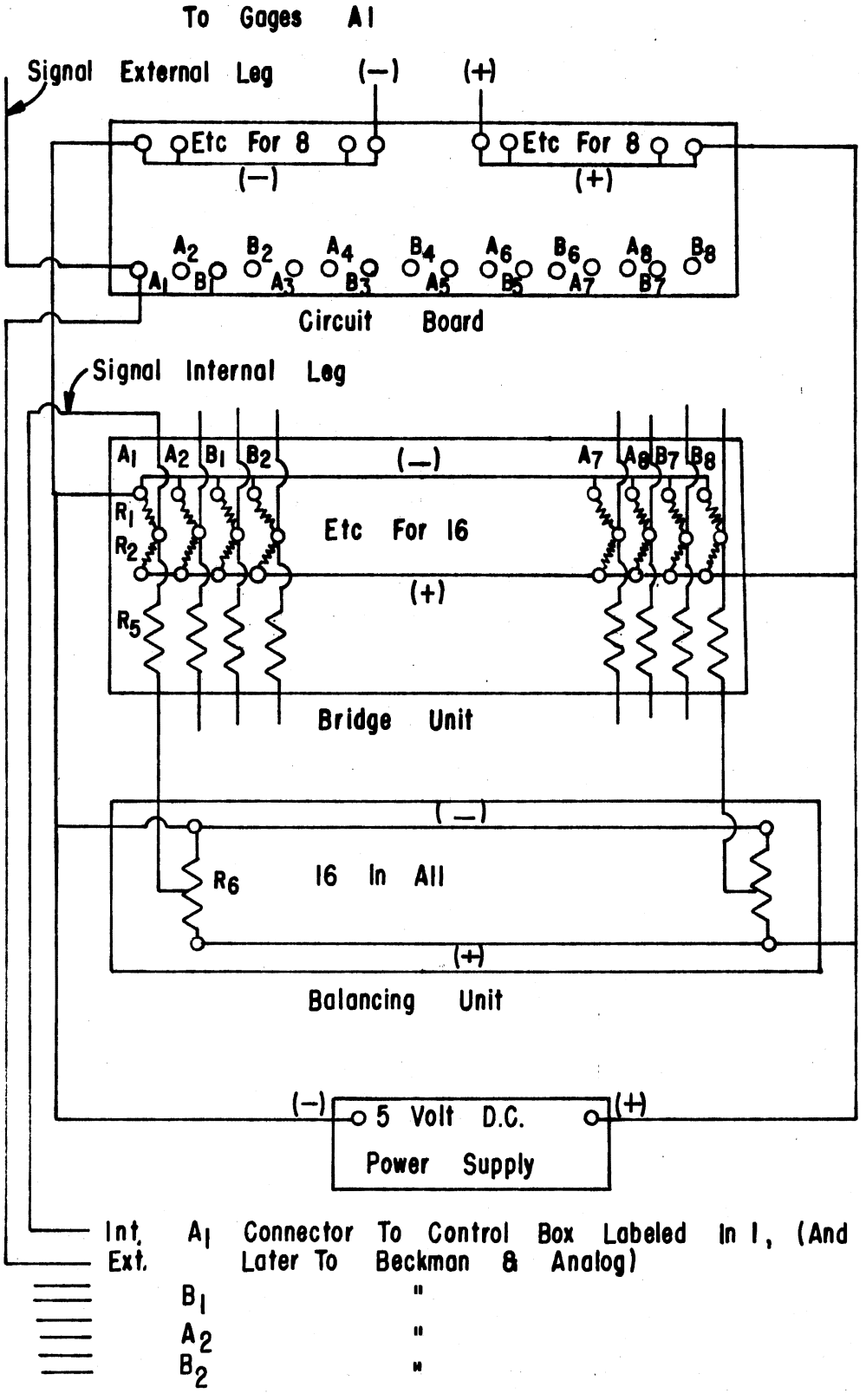

Figure 45. Wiring Diagram of Circuit Board, Bridge Unit, Balancing Unit and Power Supply

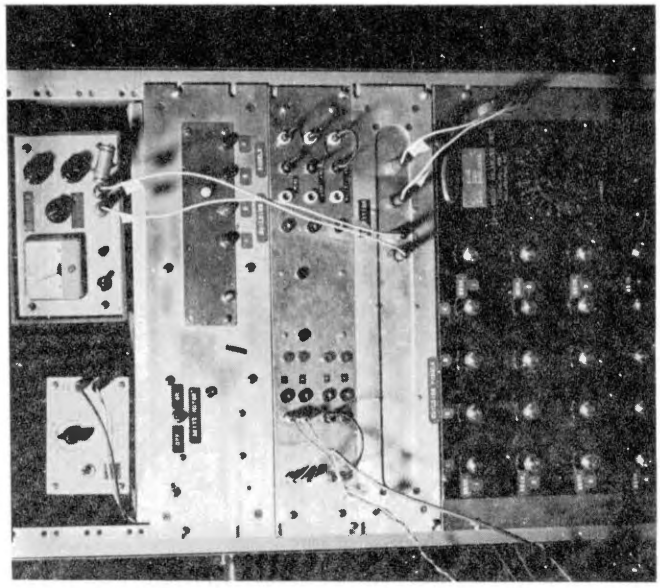

Figure 46. Left to Right, Top to Bottom: Power Supply for Control Box Motor and Relays, Power Supply for Bridge Circuit, Control Box, Margin Marker Control Unit, Bridge Unit and Baldwin Balancing Unit

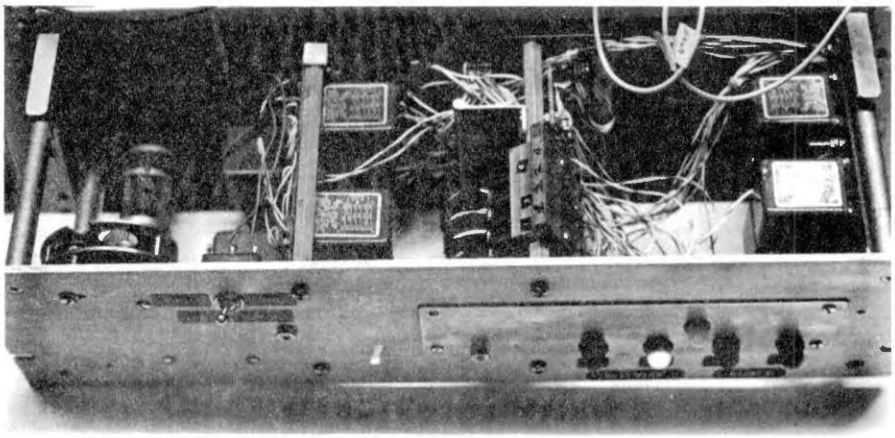

Figure 47. Control Box Showing, Left to Right, Motor and Clock Gears for Belt Drive of Cams - Between the Relays

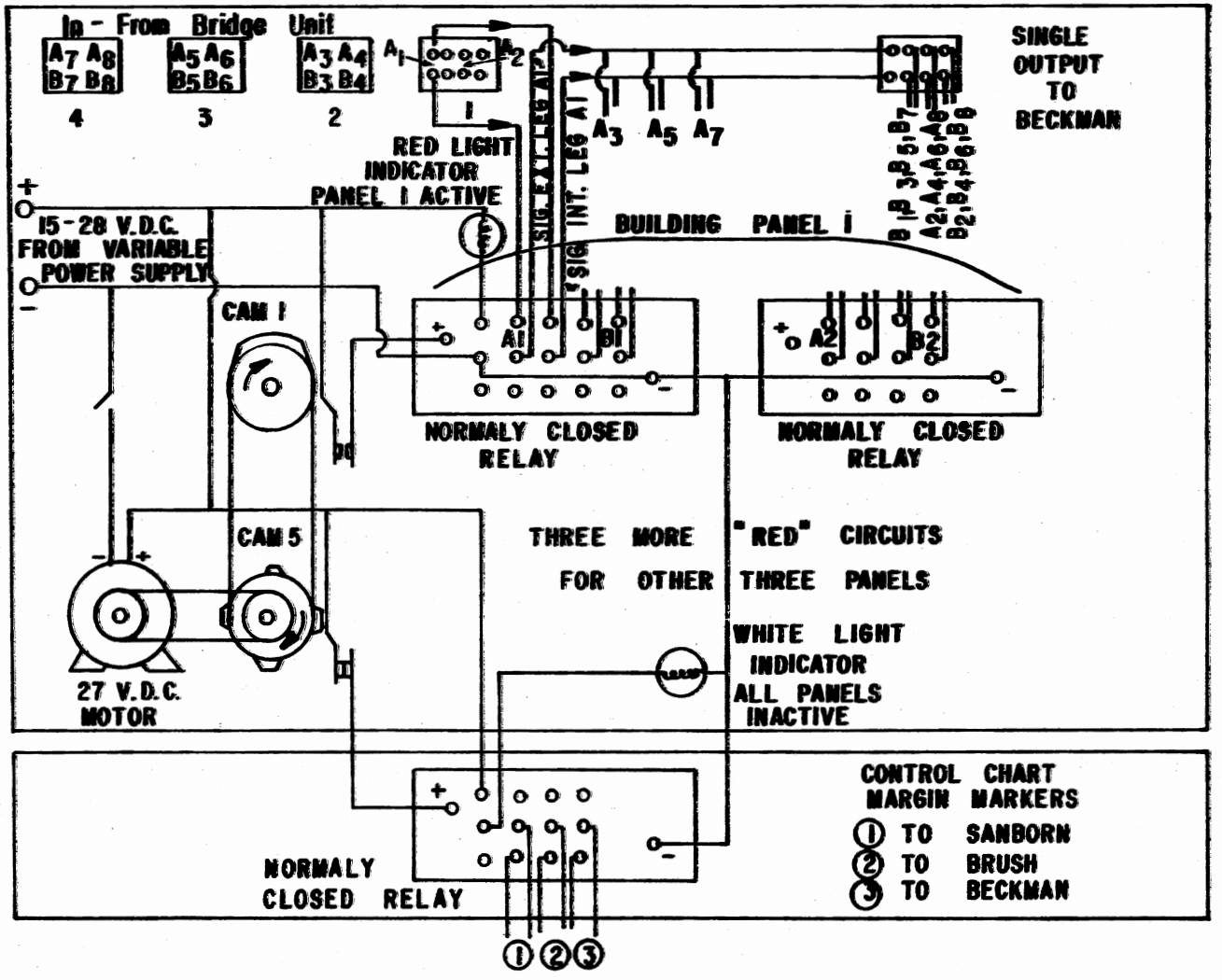

Figure 48. Control Circuitry for Strain Gages - One of Four Building Panel Circuits Located in Control Box Shown in Figures 40 and 42

successively in the same fashion until power for the drive motor in the control box was interrupted. The same relays controlled the chart margin markers for the three recorders so as to synchronize the recordings of velocity, turbulence and forces. The control box also contained red indicator lights for each of the panel relays and a white light for the null period between to show which panel, if any, was being recorded. The white light indicated when no panel was connected to the recorders.

TABLE III

STRAIN GAGE CIRCUITRY RESISTANCE VALUES

R_1	1000Ω (5%)	Fixed Value
R_2	1000Ω (5%)	Fixed Value
R_3	120Ω	Strain Gage
R_4	120Ω	Strain Gage
R_5	56Ω (5%)	Fixed Value
R_6	2000Ω	Variable Resistor for Balancing

On the Beckman eight channel recorder (Figure 49 and 51) the first four channels were utilized to register the instantaneous forces (actually strains which by means of the calibration could be interpreted as forces) of the given panel on the model. The second four

channels registered the averages of these forces. The latter were outputs from the EAI Analog Computer (Figure 50). The "EMP" averaging concept was used and is explained further in Appendix B and Analog Circuitry which follows.

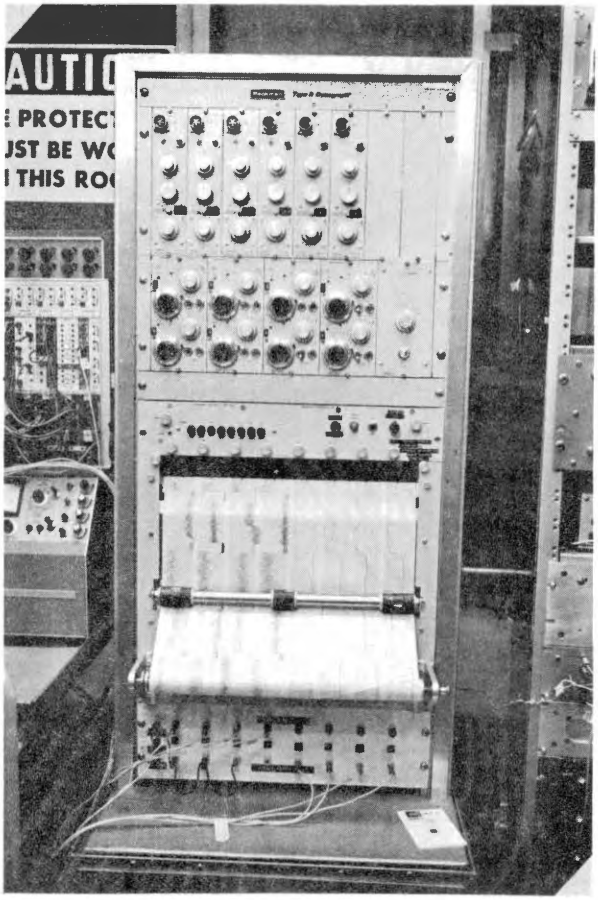

Figure 49. Beckman Eight Channel Recorder Used to Document the Instantaneous and Average Strain Gage Readings

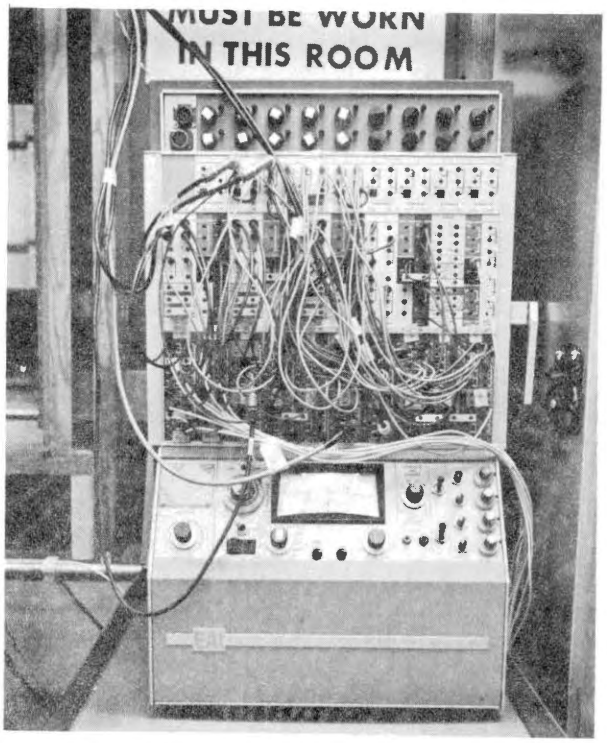

Figure 50. EAI Analog Computer Utilized to Condition the Instantaneous Readings of Strain Gages and Velocity to Obtain the Average Readings; Also Used to Obtain RMS Readings of Turbulence

Equipment and Circuitry for the Wind Characteristics. An x-wire probe (Figure 52) for a hot wire anemometer (Datametric) provided the signals used to characterize the air flow in the tunnel. The telescoping support mechanism for the hot wire probe extended down from the roof into the tunnel. The cable for the probe passed down through the tube. The device was rotatable and marked above the roof of the tunnel denoting location of the probe in inches above the floor of the tunnel. An indicator showed when the probe was perpendicular to the tunnel air flow. The device was 35" ahead of the model, as

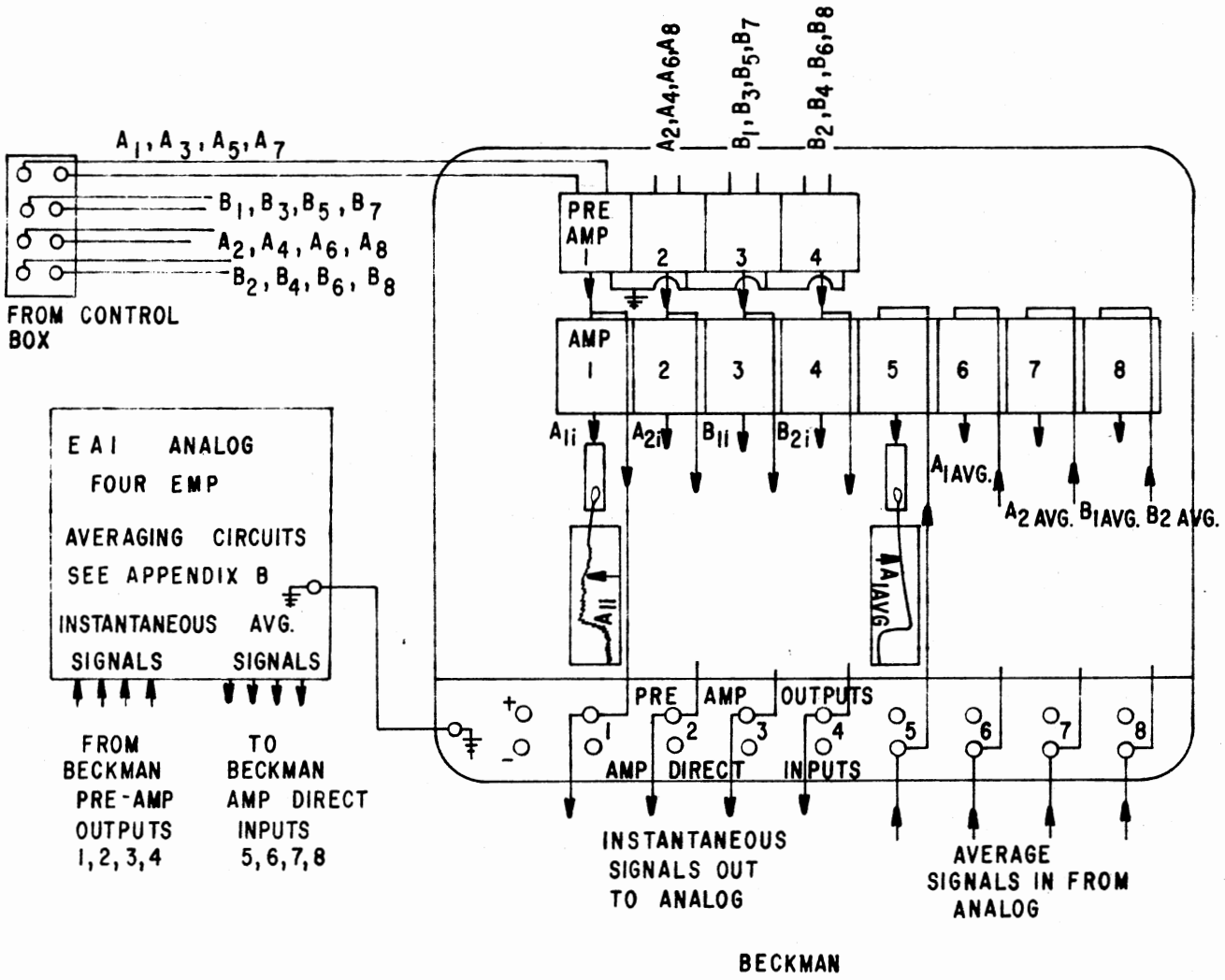

Figure 51. Strain Gage Signal Conditioning and Recording Circuitry Using the Beckman Recorder and Analog Computer

shown in Figure 34, and included a clamping feature which enabled the hot wire to be fixed at any height above the tunnel floor up to 33".

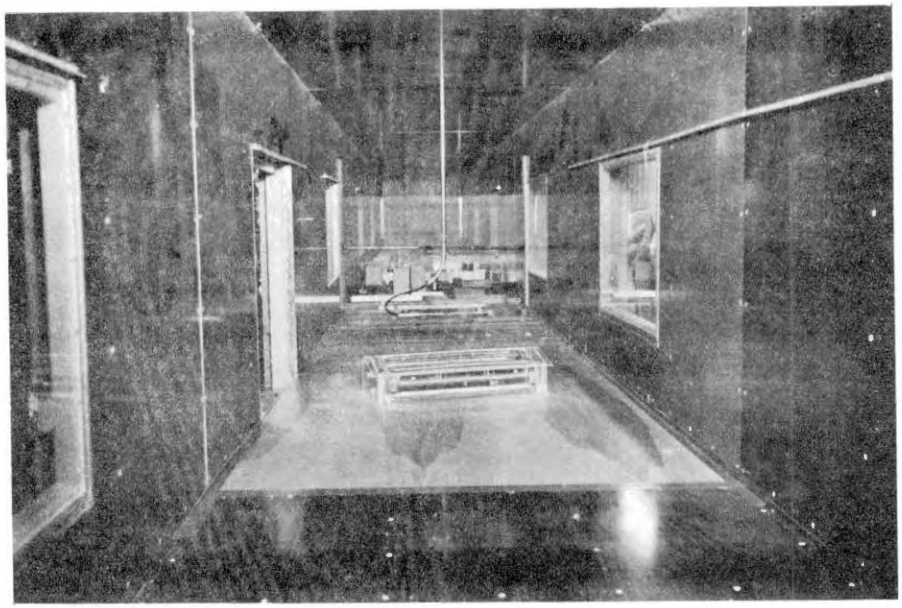

Figure 52. Model in Tunnel with the Hot Wire Probe in Position a Little in Front of Large Window. Velocity Profile Screen is in Front of Second Window. View is Up the Tunnel from Fan

The hot wire was employed first to establish the vertical wind profile characteristics of the tunnel for several air velocities by taking readings in vertical increments. It was then set at the height of 7-1/4" (30' full scale) above the floor of the tunnel, again 35" (145' 10") upstream from the centerline of the building model, for the

actual tests of the various modifications.

The x-wire circuitry is illustrated in Figure 53. The signals produced (one from each of the two wires on the probe) are, when properly conditioned, a measure of the horizontal and vertical velocities. From each of these two velocities, additional signal conditioning yields the turbulence in that particular direction. The hot wire unit (706A) produces a nonlinear signal which must be linearized in order to be conditioned by the Sum-Difference unit (900-6). This unit outputs the sum and the difference of the instantaneous signals from the two wires. These resulting signals are linearly proportional to the horizontal and vertical velocities respectively. These two velocities were recorded on two of the four channels on the Sanborn Recorder and also input to the EAI Analog Computer. The EAI further conditioned the two instantaneous velocities to produce the average velocities and the turbulences. The two average velocities were fed back to the remaining two channels of the Sanborn Recorder.

In Figure 53, the gains at each step are also noted. It was necessary to reduce the signal strength between the linearizer and the Sum-Difference unit by use of two operational amplifiers for each of the signals. The horizontal and vertical turbulence were documented on a two-channel Brush Recorder.

All the above mentioned equipment is shown in Figure 54. From top to bottom on the right are the operational amplifiers, the Datametrics anemometer controls, and the Sanborn Recorder. The Brush Recorder is on the left.

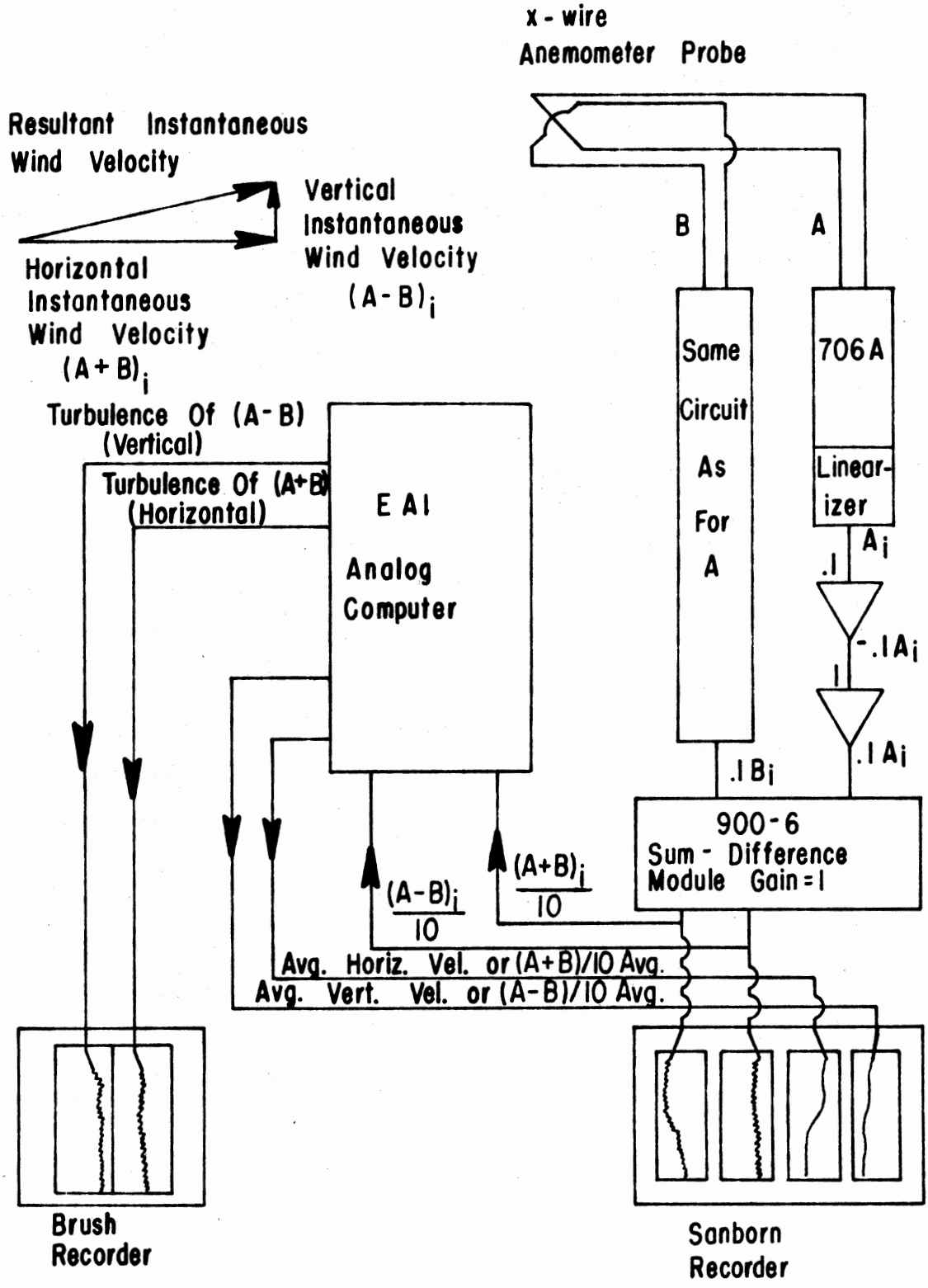

Figure 53. Wind Recording System

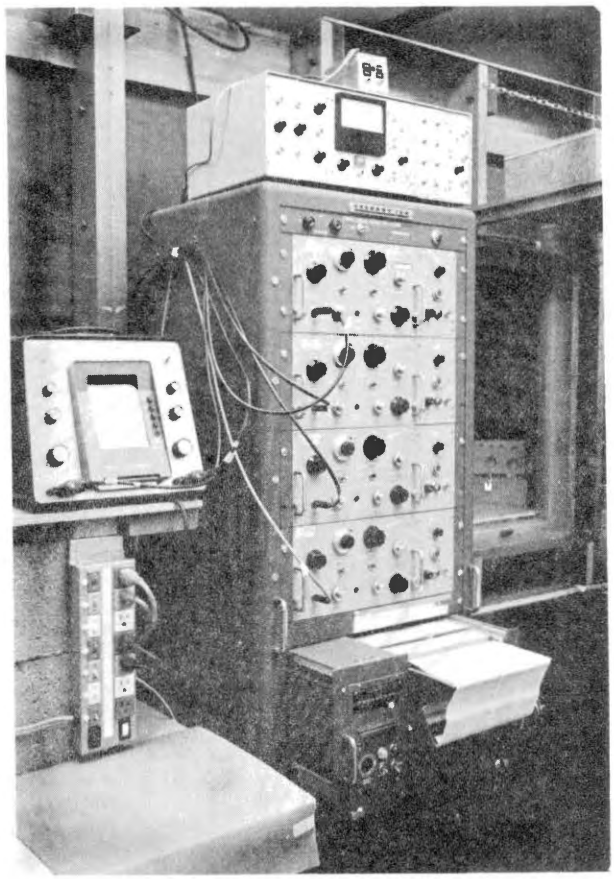

Figure 54. Four Channel Sanborn Recorder (Right), Hot Wire Signal Conditioning Unit (Top) and Two Channel Brush Recorder (Left).

Analog Circuitry. The mean or the "arithmetic average" of the instantaneous signals were determined electronically by use of the "Exponentially Mapped Past" concept described in Appendix B. Figure 55 illustrates the analog circuits necessary to determine the average velocity and the turbulence of an instantaneous velocity input. It can be seen that two such "EMP" circuits are employed to

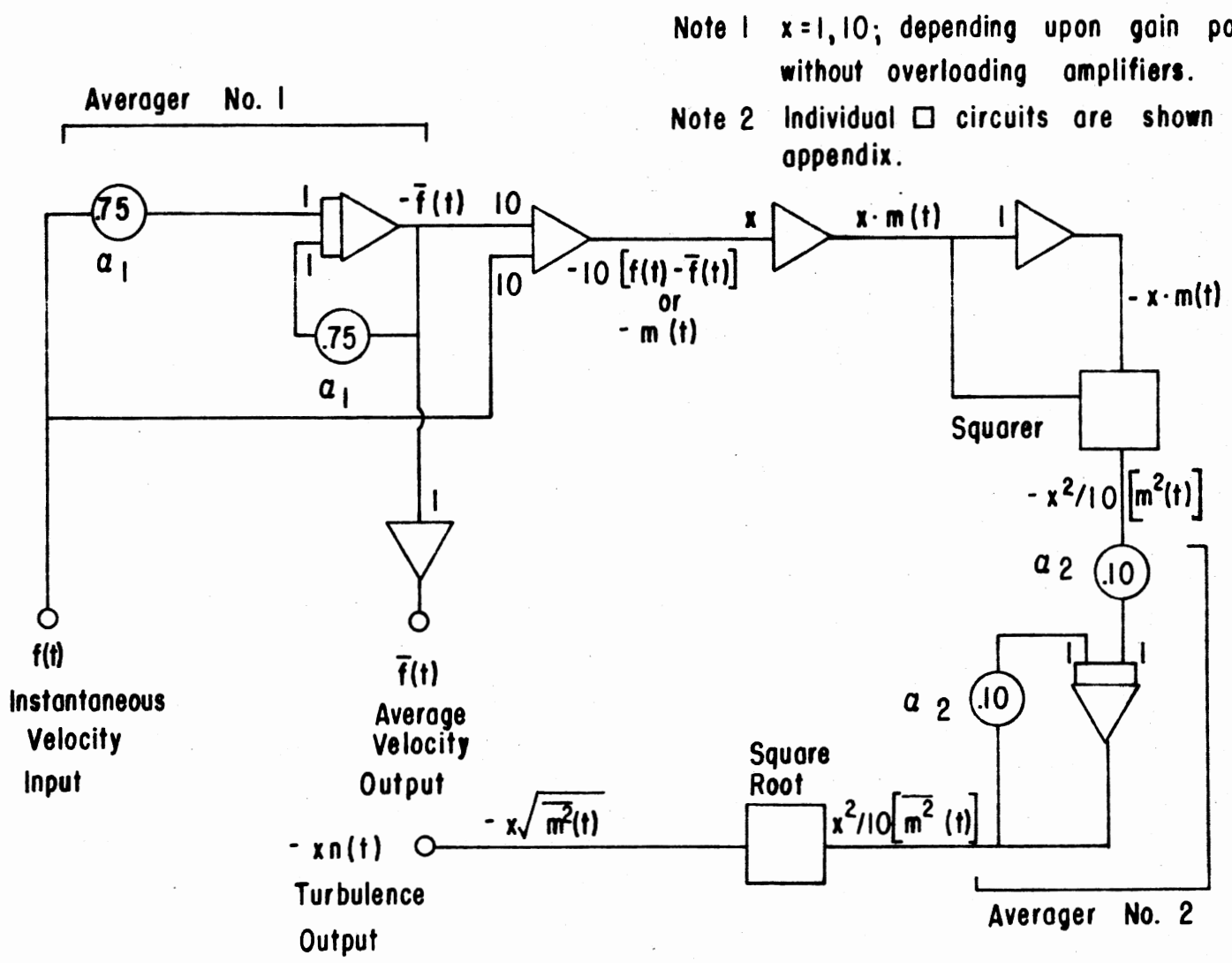

Figure 55. Analog Circuit to Obtain the Average Velocity and Turbulence

obtain the turbulence, i.e., averager no. 1 and averager no. 2. The average velocity is monitored at the output of the first averager.

Examples of the type of signals one might expect to monitor at each step along the circuit in Figure 55 are illustrated in Figure 56.

The constantly varying instantaneous input is shown in Figure 56a. The same signal, averaged using the "EMP" circuit, is pictured in 56b. The curve or trace of the signal is no longer wildly fluctuating but still responds to changes in the general level of the instantaneous signal. With a time delay dependent upon the values of α_1, the average magnitude responds to the instantaneous magnitude. In the actual circuit of Figure 55, the average signal produced by the averager is negative due to inversion by the integrator.

The summer combines the original signal and the negative average signal to obtain a signal matching the original, but now displaced by the negative average to fluctuate about the zero voltage line. This can be seen in 56c. A gain of 10 and inversion result in 56d. In the actual circuit it is 56d and not 56c which would be monitored. The latter is included to clarify the meaning or significance of 56d.

Next in Figure 55 is an operational amplifier which increases the signal. For a great many of the tests the gain of this amplifier (marked x) was one. Otherwise overload of the analog occurred. An inverter is next in the circuit and furnishes the negative input required for the squarer. The squarer requires both positive and negative values of a given signal in order to square that signal. In the process the squared signal is actually divided by a factor of 10.

Still referring to Figures 55 and 56, the "EMP" circuit is

a) $f(t)$ or Instantaneous Velocity

b) $\bar{f}(t)$ or Average Velocity

c) $\left[f(t)-\bar{f}(t)\right]$ or Velocity Fluctuations

d) $-10\left[f(t)-\bar{f}(t)\right]$ or $-m(t)$, The Mirror Image of (c) Times 10

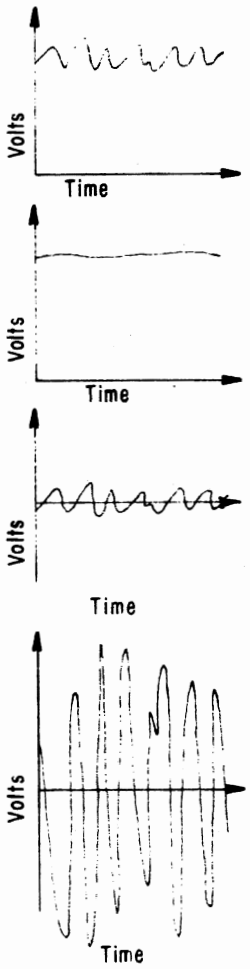

e) $m(t)$ Rapidly Flucuating Peaks All Above Zero Due To Squaring

f) $\overline{m^2}(t)$ Steady Line Representing Mean Square

g) $\sqrt{\overline{m^2}(t)}$ or $n(t)$, The Square Root of (f) Above. Known As Root Mean Square, $n(t)$ Is A Measure of The Turbulence.

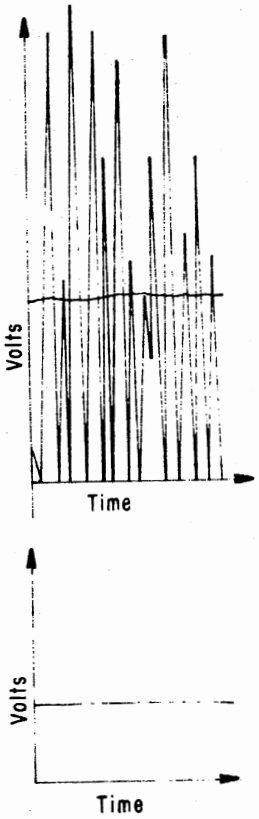

Figure 56. Sample Signals of Analog Circuit for Velocity Average and Turbulence

utilized a second time to obtain the mean square. Figure 56e and f represent this step.

The remaining step requires taking the square root of the resulting signal in order to find the Root Mean Square, or RMS, which is the universally accepted measure of turbulence.

Signal inversion, or sign change, takes place each time the signal passes an integrator or operational amplifier. Also the analog circuit, which squares the signal, results in a 0.1 gain, whereas the circuit which takes the square root of the signal multiples the signal by 10.

The alpha values in the two averaging circuits determine two characteristics of the resulting averaged signal. First, the greater the alpha value, the longer the time period of averaging for the signal. Therefore, a highly fluctuating signal would be smoothed moreso by a longer averaging time. The resulting signal would be less susceptible to the individual fluctuations of the original signal. Second, a longer averaging time causes a greater lag time before the average signal responds to large changes in the level of magnitude of the original signal. In general, one may have to compromise in order to get an average signal which is smooth enough to be useful and yet does not lag too much in response to large changes in the general level of the original signal.

Calibrations

Several pre-investigation calibrations and documentations were necessary to establish the operation standards for the equipment and conditions of air flow.

Cantilever Beam Calibration. Each of the 16 cantilever beams instrumented with strain gages were calibrated before and after the tests. The calibration consisted of fixing the beam mounting plate in a small vise and inserting a series of known weights in a small tin can hung from the link point of the beams (Figure 57). The resulting strain signals were recorded. The normal range of weights for the initial calibration was 1-16 ounces. These were placed on the beams in one ounce increments. A3 and B3 were stronger beams and required approximately 20 ounces for full chart deflection with the Beckman recorder sensitivity set at 5 and X.1.

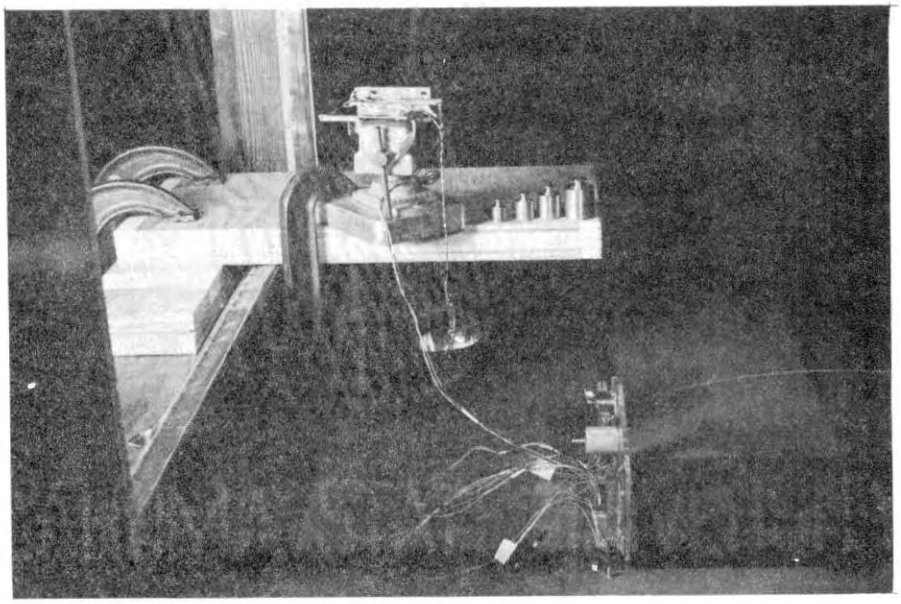

Figure 57. Cantilever Beam Calibration

Calibration initially included loading and unloading of the beams in both directions from the no load position. To accomplish this the weights were successively added and then removed. The beam was then turned over in the vise and the process repeated. This was necessary because initially it was not certain that some of the beams would always be loaded in only one direction.

Several months later, for the final calibration, observations had proved that beams at some of the locations were always loaded in the same sense. For example, the windward wall was, without exception, pushed inward. Therefore, the final calibration of these beams was checked in only that one direction. In addition, final calibration was carried out at a different recorder sensitivity (2 and X.1); again, because experience had shown the wind forces on the model did not approach the magnitude of the earlier calibration. The maximum final calibration weight used was eight ounces for A3 and B3 -- most of the other beams required six ounces.

The calibrations were done under static load conditions since, upon changing the weights, any vibration was quickly dampened and a steady line resulted on the recorder.

Comparisons of Initial and Final Calibrations

The initial calibration, the final calibrations, and the majority of the tests run were all recorded in a slightly different manner. This made conversion to a common basis necessary for comparison.

Most of the model tests were run at recorder amplifier settings of X.1 and 2 with full chart deflection interpreted as a value of 200. The initial calibrations used X.1 and 5 and were interpreted on the

basis of 200. The final calibrations were taken using amplifier settings of X.1 and 2, but with full chart deflection being considered at a value of 40.

The calibration data in its original form, was analyzed using linear regression on a desk top Hewlett-Packard computer-plotter. The main object was to determine the slope of the curve representing the linear relationship of force applied at the link point to the resulting electronic strain readings in volts as recorded on the Beckman. Secondarily, the regression correlation coefficients gave indication of the "fit" of the straight line to the data points.

As a result of the earlier mentioned inconsistencies of amplifier settings and the differences of value attributed to full chart width, the slopes from the "initial" regression were adjusted by using the ratio of initial sensitivity to the final sensitivity, i.e., 5/2. The slopes resulting from the analysis of the final calibration need only be multiplied by five to convert 40 full scale to the basis of 200.

Initial and final calibrations of all the beams are included in the Appendix in tabulated form.

All the correlation coefficients prove to be very near to unity. The initial calibration contained only two curves with less than .9994 as a correlation coefficient. These were A7-IN (.9973) and A5-OUT (.9989). Final calibration showed no fit worse than .9995. The cantilever beams and the strain gage equipment produced signals which were very linear.

A sample final calibration plot (that of B1-IN) is shown in Figure 58.

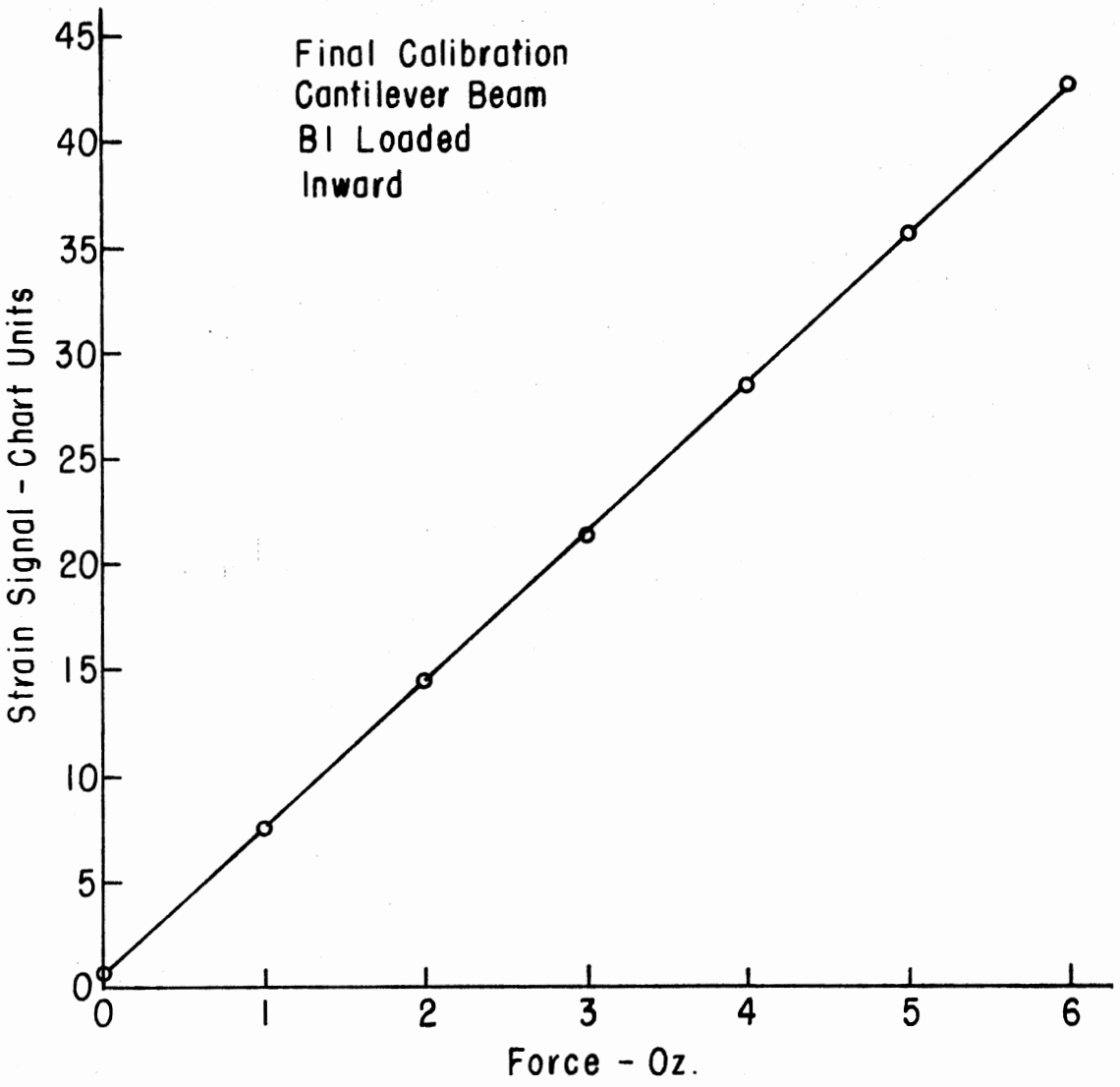

Figure 58. Sample Cantilever Beam Calibration

The equation for the line is:

Strain = 7.0079 X Force + 0.561

where Strain is in chart units and Force is in ounces. The coefficient 7.0079 represents the slope of the line in terms of chart units of strain per ounce of force.

The curve for the same beam-direction combination for the initial calibration has the equation:

Strain = 13.9479 X Force - 1.06

Slope Comparison

Initial	Final
5/2 X 13.9479 = 34.8698	5 X 7.0079 = 35.0395

The difference between the B1-IN slopes for initial and final calibrations is only 0.5%. However, the range of differences for the other beam-direction possibilities was from 0.1 - 7.6% (Table IV).

Half of the 24 beam-direction possibilities had differences of less than 3% between the initial and final calibration slopes. The other half, however, was between 3-8%. Eighteen of the 24 had differences of less than 5%. Refer to Table IV.

The larger differences are disturbing. There are reasonable explanations, however. The initial calibrations were accomplished immediately following installation of the strain gages on the beams. The beams had been flexed only a few times manually. They had not yet been attached to the model nor functioned dynamically. In the succeeding months they were flexed continually during numerous tests. In retrospect it would have been advisable to subject the beams to some dynamic loading as "break-in" before initial calibration.

TABLE IV

CALIBRATION DIFFERENCES

Differences Between Initial and Final Calibration Slopes	Number (Out of 24)
> 1%	5
1-2%	5
2-3%	2
3-4%	1
4-5%	5
5-6%	3
6-7%	1
7-8%	2

In addition, the calibrations include the effects of the equipment used to condition and record the signals. Initially it was not realized that an hour or two was necessary for warmup before taking readings in order to stabilize the equipment.

For these reasons, it is felt that the final calibrations are more reliable. The most important tests were close (in time) to the final calibrations; their values will be used in quantitative evaluations of the data. The initial calibrations were certainly not without value as they corroborated the linearity of the beams at the outset and provide proof that no major changes in calibration could have occurred.

As a further check, for the tests with the model at 0° orientation to the wind, the panels were subject to a "frame calibration procedure". An eyelet was placed in the center of each panel to which a line was attached. The line passed over a pully placed in an appropriate position on the frame. Any weight attached to the other end of the line loaded the panel from its center point and normal to the panel plane. (Figure 59). Any gage malfunction or significant change in the calibration could thus be detected.

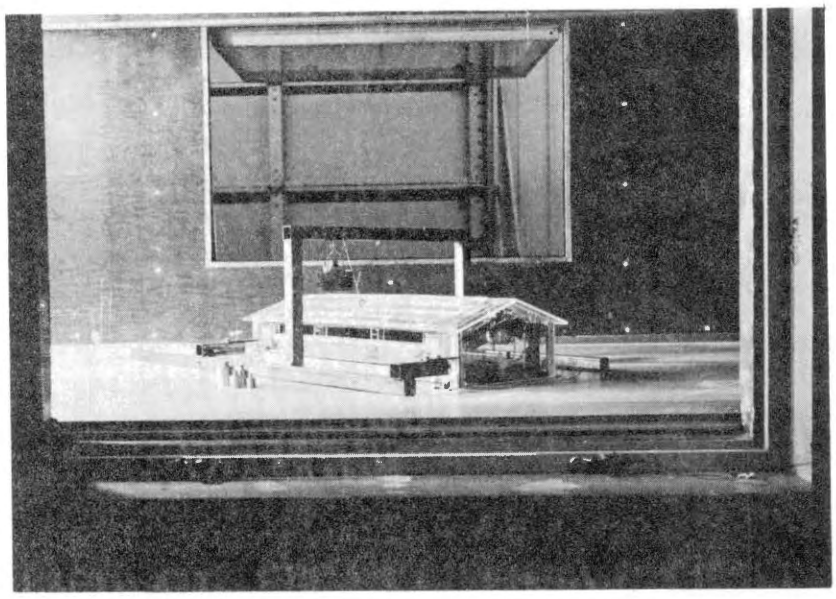

Figure 59. Panel Calibration Using Loading Frame.

This same "frame calibration" procedure was used in the final series of tests (discussed more later) in order to standardize the

results as it was discovered when loosening the disk center bolt and reorienting the building, the gages were so sensitive that they reacted to the tension in the center bolt.

Calibration of the Hot Wire Anemometer. The hot wire anemometer was calibrated with the apparatus shown in Figure 60. The pitot tube and the hot wire were both placed in the same constant air velocity from the fan-tube arrangement shown. The unknown reading of the hot wire could then be related to the known velocity reading of the pitot tube.

The Establishment of the Velocity Profile. The goal was to achieve a vertical wind velocity distribution, which would simulate that of open countryside - i.e., with an n value of $\simeq 7$ in the equation $V_H = V_{H1} \left(\frac{H}{H1} \right)^{1/n}$ previously discussed in the literature review.

While the main effort was to establish this vertical distribution (of the horizontal wind movement), the vertical velocity and the turbulences of the two directions were also documented - until one of the two hot wires in the probe became defective.

For the 12 initial trials, readings were taken 8" to the south of the tunnel centerline (32" from the north wall). The probe was 35" (representing 145' 10" full scale) ahead of the center of the model. Starting at 1" above the floor the wind characteristics were recorded in 1" increments up to 9". After that, 3" increments were used up to 33". This represented a range of 4.167 to 137.5' full scale.

The horizontal and vertical velocities and their averages from the analog were all recorded on the Sanborn 4 channel recorder. Simultaneously, the turbulences, also from the analog, were documented

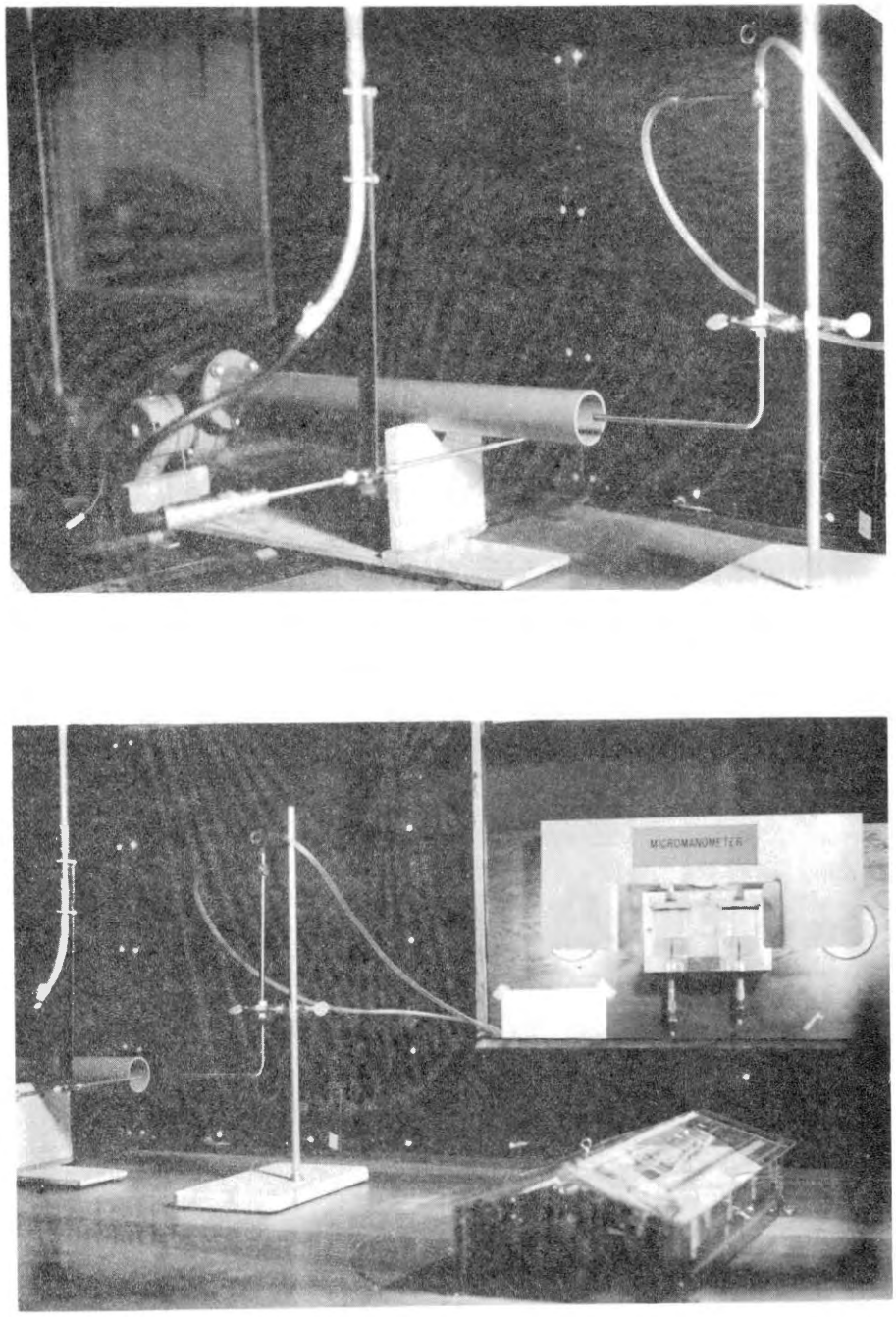

Figure 60. Calibration of Hot Wire Apparatus

on the 2 channel Brush recorder.

Beginning with only the bare tunnel floor, the stainless steel screen over the entrance of the convergence section and the honeycomb screen at the entrance of the 4' by 4' portion of the tunnel (Figures 30 and 33), a series of trial and error tests were employed to finally establish the velocity distribution accepted ($n \simeq 6$). The following steps were the most important:

1. Bare tunnel floor with no modification. The resulting velocity pattern (Figure 61:1) showed the lower 4" to correspond roughly to the desired 1/7 slope. Uniform velocity existed in the upper portion beyond, however. Since there was no way to further increase the upper levels of velocity, the lower levels of air had to be further retarded.
2. A trip was installed immediately behind the honeycomb screen and spanned the entire 4' width of the tunnel. This metal rectangular bar, 4" high, initiated the ground plane effect by retarding the air near the floor.

   Also installed was an assortment of angle irons, both short and long pieces -- fastened with duct tape, along the full length of the tunnel floor up to 10" ahead of the probe. Figure 61:2 shows the result. The effect was satisfactory but the velocity in the portion 9-18" above the floor was too high still. Above 18" the velocity was slightly slow.
3. Utilizing supplemental screens of varying meshes, sizes

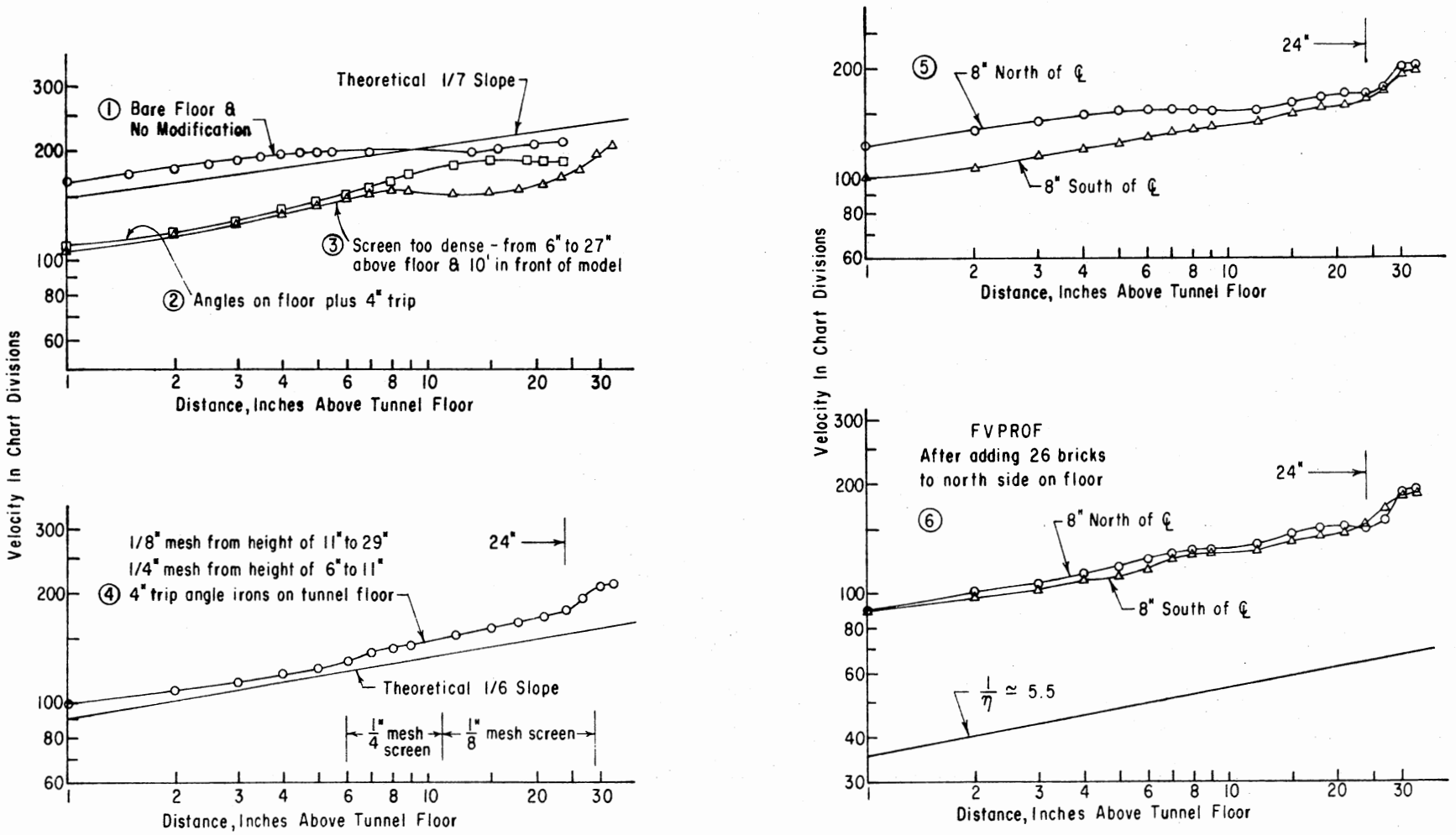

Figure 61. Modification of Tunnel Velocity Profile

and combinations, an attempt was made to further retard the air in the 9-18" portion. The ends of the screens were stapled to two pieces of 1/4" plywood and the plywood pieces were pressed outward by an "expanding jack" made from a Volkswagen tie rod bar. The jack was placed horizontally across the tunnel, its ends pressing the plywood end pieces against the tunnel side walls thereby stretching the screening across the tunnel (Figure 34, Figure 54 just beyond the window ahead of the model and in the foreground of Figure 63). Results of an early attempt are shown in Figure 61:3. The screen was too dense and over correction occurred.

4. The combination shown in Figure 61:4 produced acceptable results; ≈ 1/6 slope. Having finally achieved a reasonable result in this fashion, a series of readings were taken rotating the hot wire probe as well as going through the previous height pattern. Readings were taken 8" either side of the centerline, ascending and then decending, rotating the hot wire probe at each height to get a "south" and a "north" reading with respect to the centerline of the tunnel.

The severe difference (Figure 61:5) between these lateral readings (i.e., north and south) led to a check with the pitot tube at the height of 9" traversing the tunnel. The differences were confirmed (Figure 62) and an exhaustive attempt was made to discover the cause - to no avail.

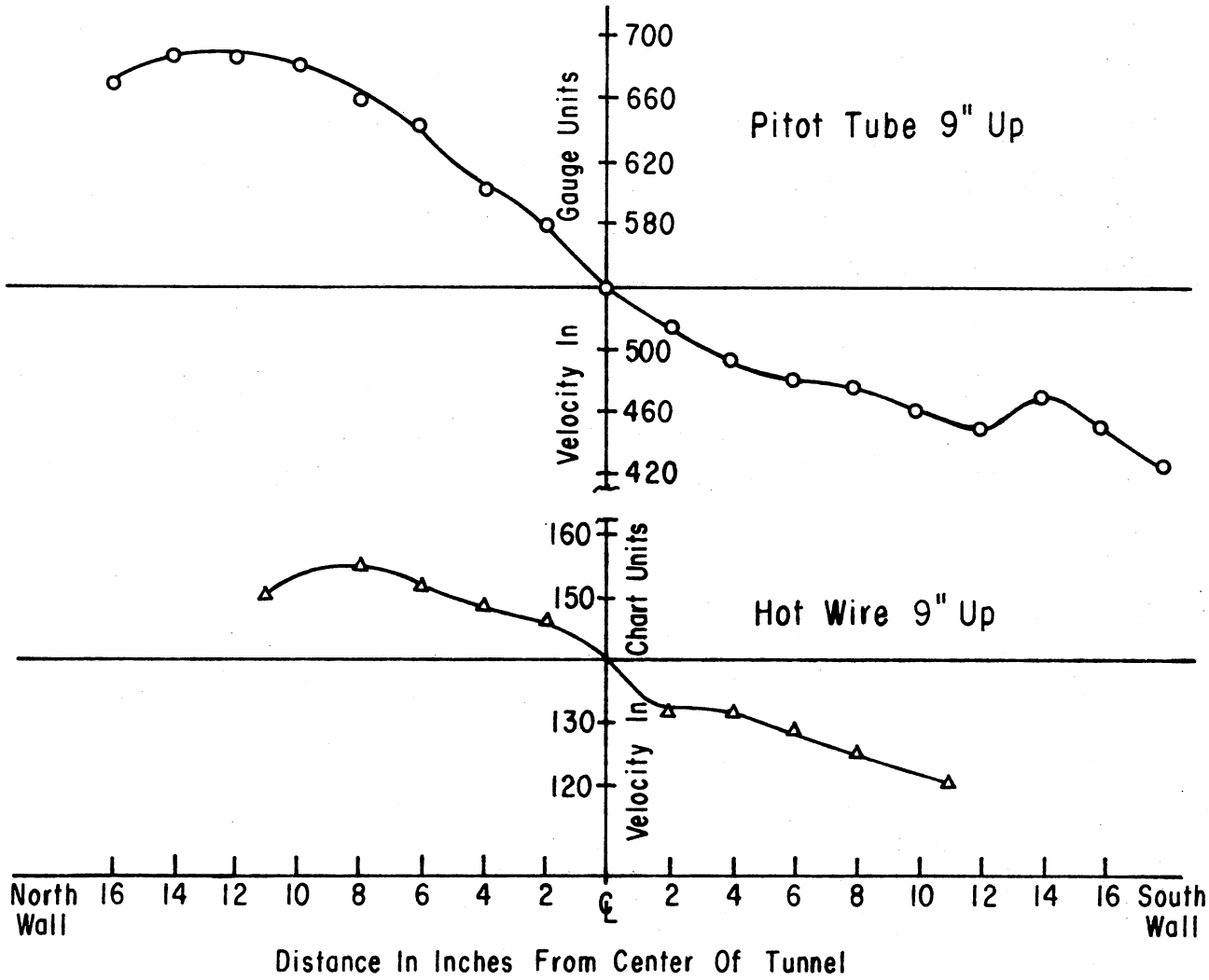

Figure 62. Velocity Discrepancy to the North and South of Center Line Measured at 9" Above Tunnel Floor

The triangular shaped loft, between the sloping roof and the ceiling of the room housing the tunnel, was suspect since it served as an air return. It was proved not to be the cause by opening the large outside doors at either end of the tunnel and closing the loft return. It is possible that, even with the outside doors open, the 90° bend of the air flow through the room and out the door at the exhaust end caused the same effect as the triangular shaped loft. It would seem, however, that the bend (Figure 30) might cause the slowing of the air flow rather than its higher velocity on the north.

Lacking any reasonable explanation that could be verified, an expedient solution was chosen. Adding more ground effect material on the floor along the north wall slowed the air and evened out the previous discrepancy. Twenty-six bricks in an upright position were used (Figure 63). This undoubtedly altered the homogeniety of the turbulence but subsequent difficulty with one of the hot wires prevented verification.

The result of the bricks was to eliminate much of the original difference (as great as 20%), though some remained (≃ 5%). (See Figure 61:6).

The final velocity distribution accepted is shown on log-log paper in Figure 64 for three velocities and the profiles are plotted in Figure 65. They reflect the average readings of the horizontal velocity at each height for three fan speeds within the range of the tunnel's operation; low (430 rpm) labeled LVPROF, medium (510 rpm) labeled MVPROF and fast (610 rpm) called FVPROF.

Stepwise linear regression of the horizontal wind velocity data collected during the final test for establishing the profile was

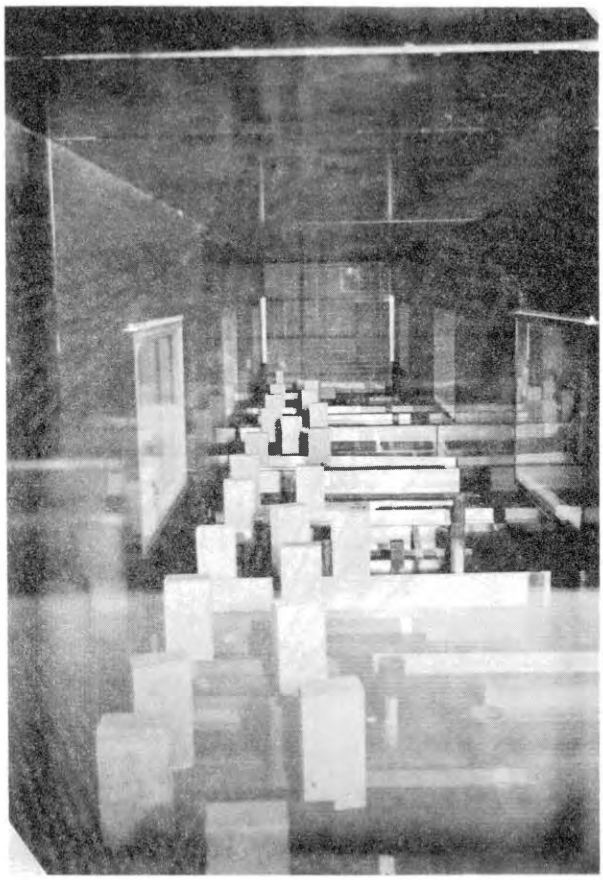

Figure 63. Floor "Roughness" and Screens Producing Final Velocity Profile

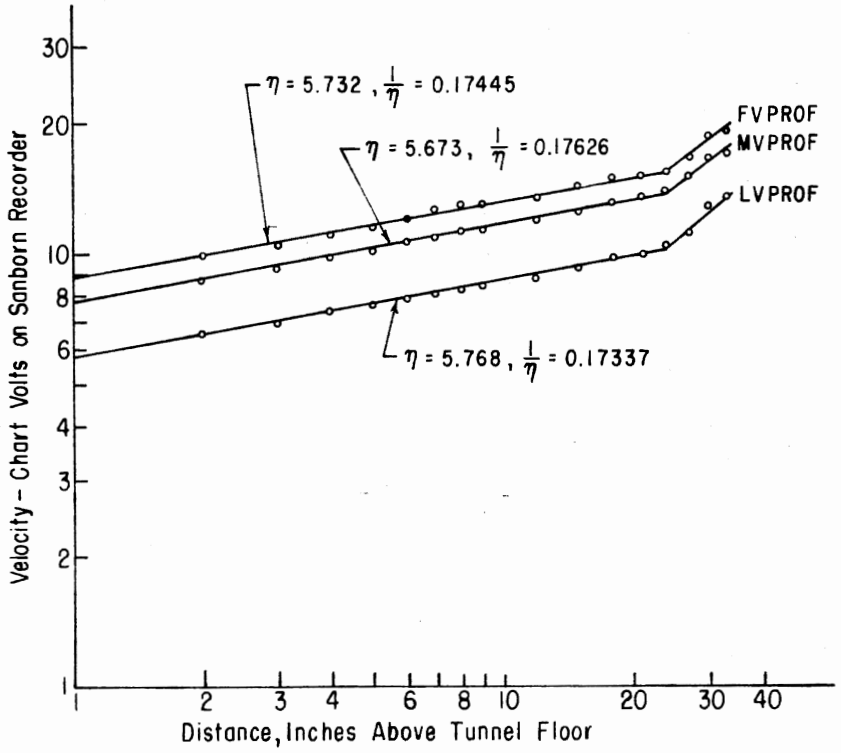

Figure 64. Low, Medium and Fast Velocity Log-Log Plots

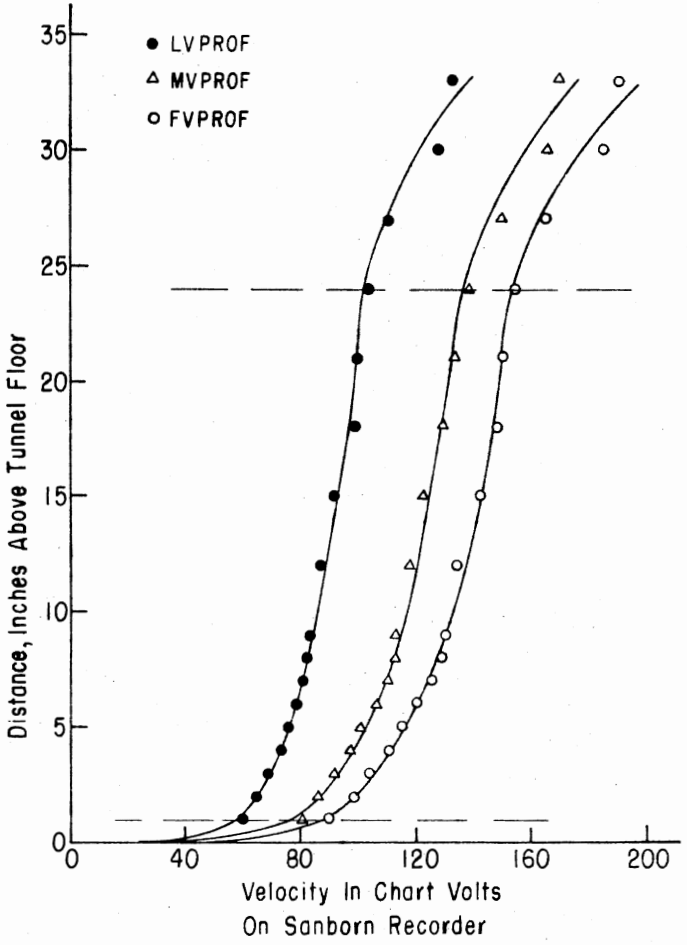

Figure 65. Low, Medium and Fast Velocity Profiles

analyzed by use of the IBM 370 Scientific Subroutine Package. A programmed logarithmic conversion of the data was necessary.

The general form of the wind equation selected to describe the profile is:

$$V_H = V_{H1} \left(\frac{H}{H1} \right)^{1/n} \quad [1]$$

or in logarithmic form,

$$\log V_H = \log V_{H1} + 1/n \, (\log H - \log H1). \quad [2]$$

If H1 = 1, then,

$\log H1 = 0$,

and the equation becomes:

$$\log V_H = \log V_{H1} + 1/n \, (\log H). \quad [3]$$

The $\log V_{H1}$ is the intercept of the curve with the line H1 = 1 when plotted on log-log paper.

And 1/n is the slope of the curve when measured in non-logarithmic or linear units.

From the computer analysis of the data plotted in Figure 64 the values in Table V were obtained for Log V_{H1} and 1/n in Equation 3.

Only the data between 1 and 24" (equivalent of 100' above the ground) was included in the analysis. Above 24", the screen (highest point, 29"), was not effective in simulating the desired horizontal velocity profile. The shapes of the three velocity profiles in rectangular coordinates, shown in Figure 65, also illustrate the departure from the desired profile after the height of 24" above the tunnel floor is exceeded. The desired profile did exist in the bottom half of the tunnel and was considered sufficient when compared to model height of 5.84".

TABLE V

VELOCITY PROFILE DATA

Inches from Centerline	FVPROF		MVPROF		LVPROF	
	Log V_{H1}	1/n	Log V_{H1}	1/n	Log V_{H1}	1/n
8" South	1.93706	0.17464	1.87867	0.18173	1.74913	0.18000
8" North	1.95399	0.17316	1.89642	0.17152	1.77574	0.16688
Avg	1.94476	0.17445	1.88812	0.17626	1.76258	0.17337

The consistent small differences still remaining between the North and South curves in Figure 61:6 show the previously discussed problem was not completely overcome.

Reynolds Number Investigations. A preliminary examination of the reaction values at various velocities was made to determine if fully developed turbulent flow did exist over the test range.

Early portions of the experiment were carried out with "unsealed" models; "unsealed" signifying that the joints around the four panels were open ≈ 1/32" to allow movement. This procedure was continued on through preliminary elemination tests in searching for some modification which would effectively reduce the wind forces on the model.

At one point, the discovery was made that taping 2 mil plastic material over the roof ridge joint caused considerable alteration of the force pattern recorded by the gages. The tape was placed so as to

allow freedom of movement and yet seal the joint in a fashion similar to roof ridging, some air being able to escape out small gaps at the very ends. Subsequently it was learned that leakage of air through the 1/32" joints was anything but negligible, and the same sort of sealing was attempted for the remaining joints (to be described later). As a consequence of this later discovery, the Reynold's Number tests for independence from viscous effects were repeated for the sealed model.

Both tests are presented -- the first (unsealed) is the only one that clearly shows any dependence of the reactions upon the viscous forces. Both unsealed A8 and B8 exhibit a marked variation with respect to velocity. All the others, by contrast, show some variation which might seem very significant if it were not for the much more pronounced dependence of unsealed A8 and B8.

The two figures (66 and 67) show 16 terms of the form $R_i/(V_{H30})^2$ plotted against V_{H30}. In reality, the terms expected would be $R_i/\rho L_S V_H^2$ versus, say, $h_r V_H \rho/\mu$. For these tests, however, all the quantities other than those actually plotted were constant and would not relatively change the plots. Since h_r would be an arbitrary choice of a length term, the plots would have no more meaning than those shown. Further, the plots are simply in chart divisions per volt^2 for the reactions and in volts for velocity. The relationship between velocity in volts and velocity in feet per second is linear. Again using the unrefined data in this fashion changes only the scale -- not the relationship.

One further difference between the unsealed and sealed plots will be noted. The velocity readings on the "unsealed tests" were obtained

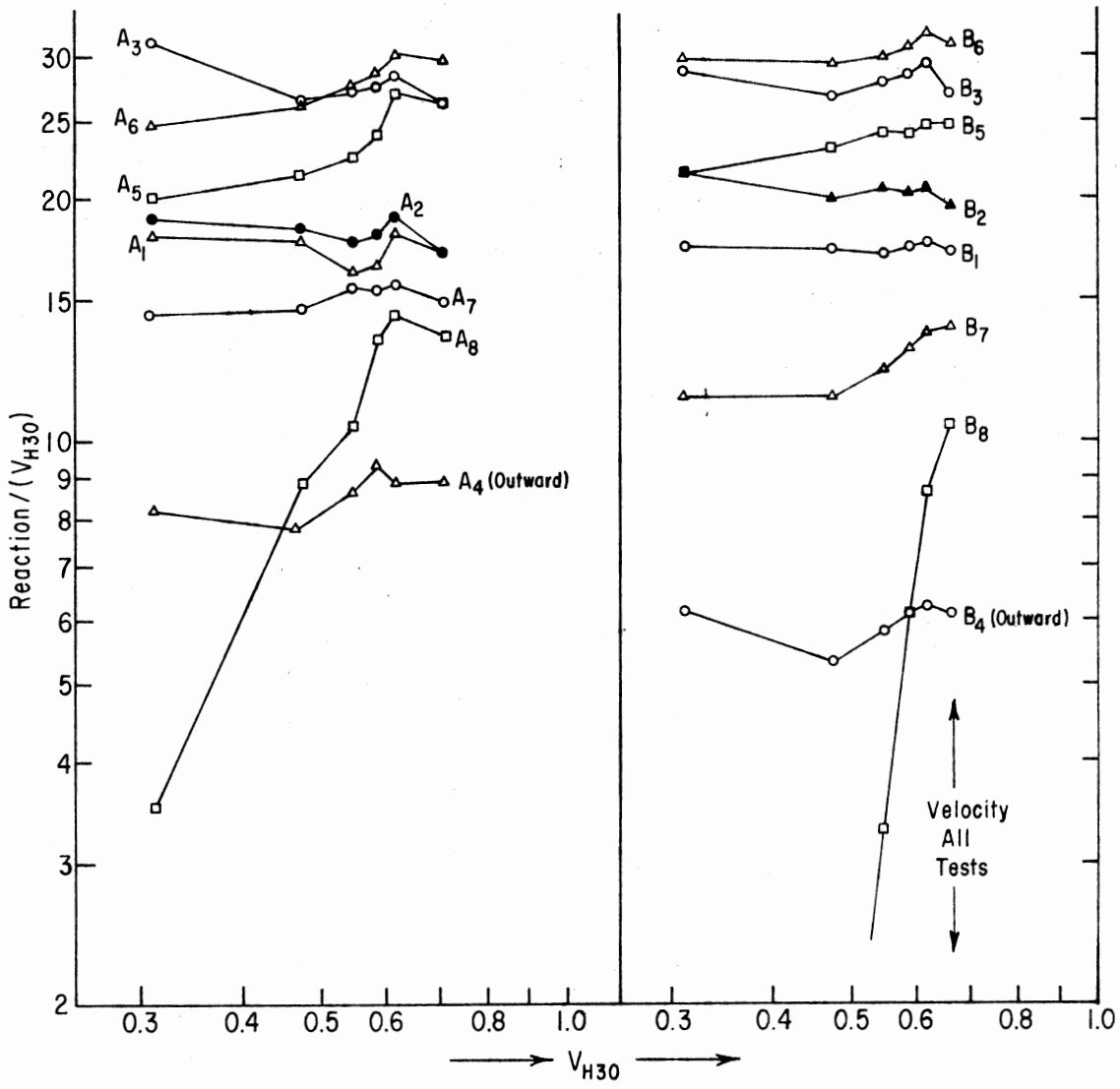

Figure 66. Reynold's Number Tests - Unsealed Model. Horizontal Velocity, Single Hot Wire, in Volts Versus Reaction/Velocity^2.

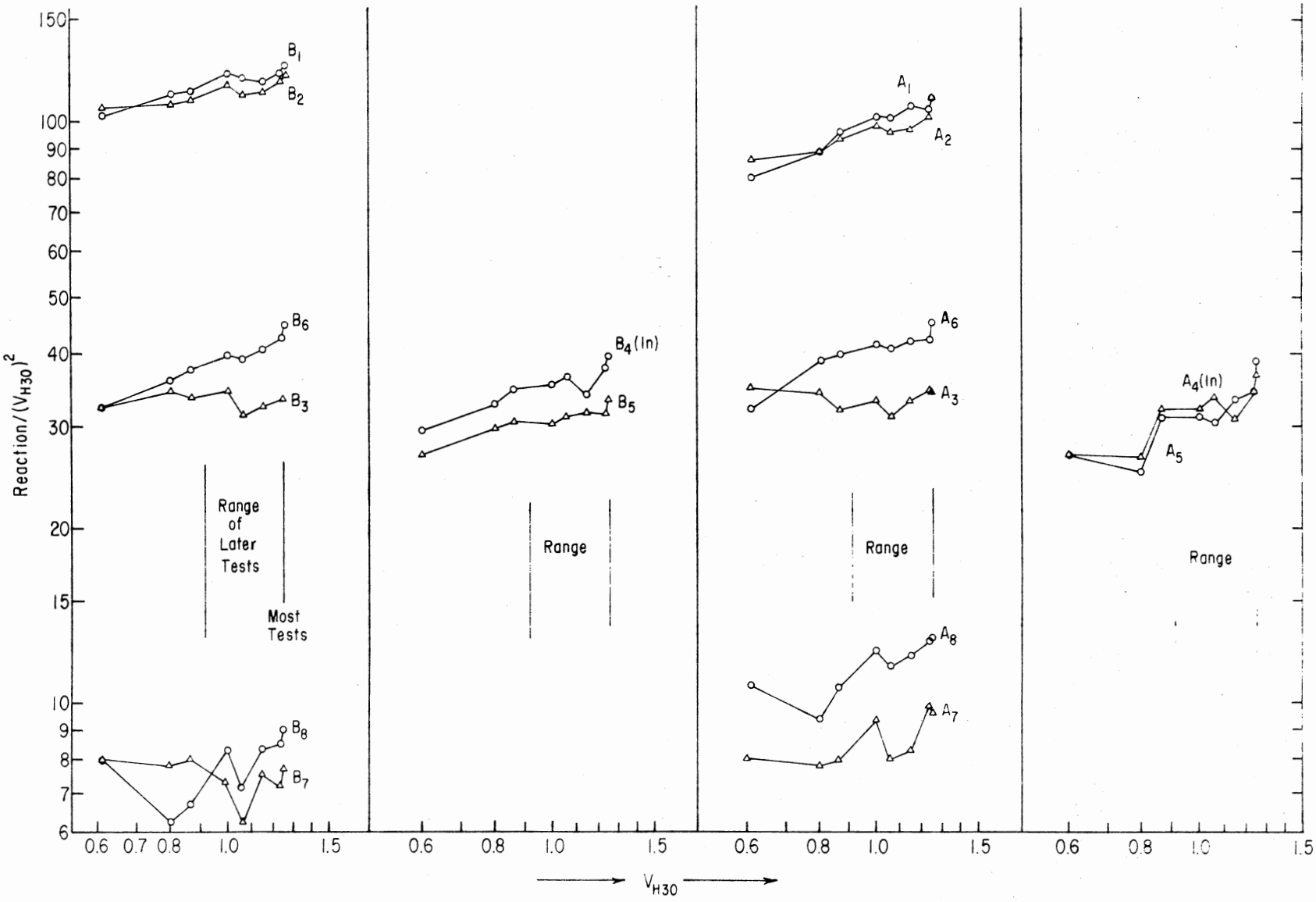

Figure 67. Reynolds Number Tests - Sealed Model. Horizontal Velocity, X-Wire, in Volts Versus Reaction/Velocity^2.

after one circuit of the x-wire probe had been malfunctioning. The hot wire for the remaining intact circuit was used in the ordinary single wire fashion. The "sealed tests" were obtained during normal operation of the x-wire probe. This makes comparison of the absolute magnitudes of the unreduced data futile. The relative magnitudes are interesting, however.

The Reynold's Number tests cover the entire velocity range available without changing the pitch of the tunnel fan blades -- i.e., from approximately 20-45 mph. The upper end of the range (.92 - 1.25v) was used in the later testing. It would have been desirable to run the fan at much slower speeds than the actual range of later tests in order to clearly establish for each reaction the same transition through the critical velocity that can be seen for A8 and B8 (unsealed). Were this to have been possible all the reactions would exhibit more typical behavior shown in Figure 68 ( ).

Conclusions

Most of the tests run later were at top speed (≃ 1.25v). However, it seems a safe assumption that fully developed turbulent flow did exist for the entire range of velocities tested and for all the reactions except for A8 and B8 unsealed. These two reactions are the lower corners of the back wall where fully developed turbulent flow apparently did not exist at the lower velocity for the unsealed model.

Attention has been called to the interesting differences in the relative magnitude of the unsealed versus the sealed reactions. In retrospect, it can be easily observed that even with minor leakage,

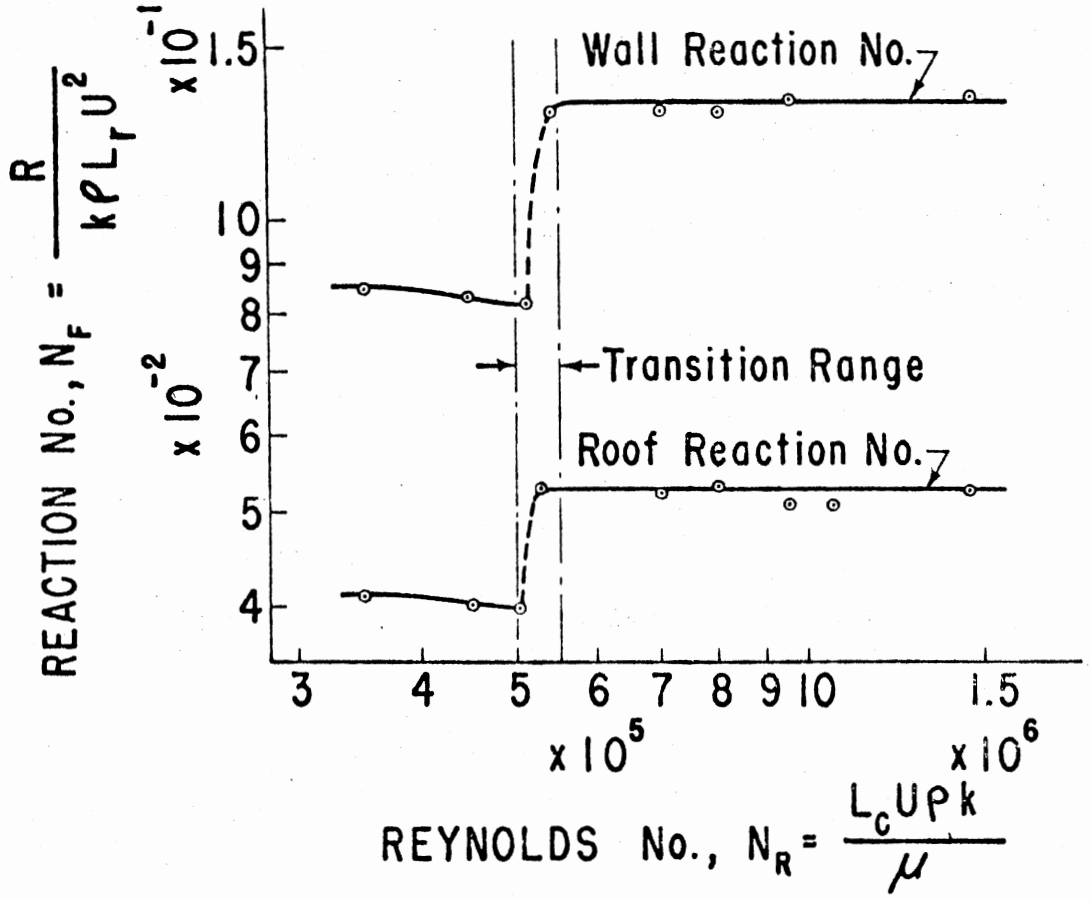

NOTATION:

R = Wind force reaction, $lb._F$/ft. of building length

ρ = Air mass density, $lb._M$/cu. ft. of air

k = Newtonian constant, 1/32.2, $lb._F$-$sec.^2/lb._M$-ft.

L_r = Roof slope length or wall height, ft.

U = Wind velocity, ft./sec.

L_c = Channel length, ft.

μ = Air viscosity, $lb._F$ $ft.^{-2}$ sec.

Figure 68. Wind Force Reaction Number, N_F, as a Function of Reynolds Number, N_R, in Experiments with Building Models in a Wind Tunnel Testing Channel

the forces to be dealt with in design are vastly different. Early conclusions from the unsealed tests were that B3 and A3 (leading edge of roof) were by far the greatest forces. As a result stiffer beams were employed at A3 and B3. The highest unsealed forces are A3, B3; A6, B6; A5, B5 (all roof forces), whereas for the sealed model A1, B1 and A2, B2 (front wall) are higher forces than the 3's, even after allowing for the beams of greater stiffness (≃ 150%). B4 and A4 forces even changed directions since with the unsealed model they were outward, but are inward for the sealed model.

Procedure.

1. The electronic equipment was subjected to a two hour warmup period prior to running of tests. This avoided "drift" of the strain gages.
2. The Beckman recorder required a calibration check with an internal signal meant to result in 20 mm deflection on each channel.
3. The model to be tested was outfitted as necessary.
4. A "shake down" run up was performed before each test by vibrating the model panels, with modification completed, in the tunnel wind for a short time at the highest velocity. This accomplished two things:
   a. The first run after each major change determined the Beckman recorder scale which could be used and in which direction the loading would cause the recorder pens to move.
   b. Overcoming handling of the model, such as frame

calibration or changing from one modification to another when the panels might not come back to rest in their normal no load static positions.

5. Frame calibration as described earlier was next performed if needed.
6. When frame calibration was used a second run up was needed afterward.
7. The velocity and turbulence recorders were zeroed.
8. The strain gages were electronically balanced to set the recording pens for the channels at the chart position desired (usually near zero). This was done under no wind load conditions using the Baldwin Balancing unit as modified, and using the control box to connect the panels one at a time to the Beckman. The panel being balanced was identified by illumination of its red light on the control box.
9. Initial static readings were taken before the first replication by running the control box through one complete cycle of four red lights while recording on the Beckman the zero load readings.
10. Wind tunnel velocity was advanced (never decreased) to the desired level.
11. Data collection for one replication was completed with the control box automatically determining the length of each panel run and switching to the next panel until all four had been recorded. Simultaneously the wind data was recorded. The control box motor was manually switched off when the white light came on.

12. The fan was slowed to minimum speed and its power interrupted.
13. When the fan came to rest, the static readings were again taken under no wind conditions to determine the "tare" readings for the run just finished.
14. Second and third replications were taken in the same fashion with no run up or initial static readings.
15. Installation of the next building modification then followed.

Steps 4 to 15 were repeated; 5, 6 and 8 being done only when necessary.

Modification identification and atmospheric conditions were recorded directly on charts along with the recorder scales employed.

Variations in the Standard Procedure. For the preliminary tests only the top velocity attainable in the tunnel was used, but for the final tests the three velocities shown in Figure 65 were utilized. During the latter, a shim with three notches was inserted in the position cut off switch controlling the variable diameter of the fan drive. This insured use of the same velocities each time. The three different velocity settings were achieved during the same run always, in the same sequence; slow, medium, fast. This was necessary as randomizing the order often produced different velocities depending upon whether the fan speed was rising or descending to the desired value.

Due to the time involved in changing the modifications on the model, it was decided to take three replications in the fashion

described above instead of randomizing the replications as well. This would have been unbiased, and preferable, but not practical.

Sealing Tests. After completing the first series of preliminary tests on the Deflectors, the Airfoils and the Ducts, several attempts were made to discover the effects on the unaltered building model of sealing the 1/64-1/32" gaps or joints between the movable panels.

The force changes which resulted from these attempts drove the front wall strain readings completely off the charts, so that a recorder scale change from the setting of X.1 and 2 to X.1 and 5 became necessary. At the same time the forces on the front roof were greatly reduced.

The initial discovery of the importance of leakage for even these small panel gaps was made while experimenting with sealing the roof ridge. It was sealed by taping a single strip of 2 mil plastic over the crack between the upper edges of the two roof panels while a metal welding rod lay under the plastic in the actual crack. Upon withdrawing the rod, the configuration of the sealing strip resembled the roof ridging normally used on corrugated metal roofs since it was open at the ends. The flexibility of the plastic and the "play" left when the rod was removed enabled each roof panel to move independently of the other. Sealing was therefore along the length of the roof panel.

By progressively adding similar sealing at each of the horizontal joints, the force pattern which evolved became entirely different than that for the unsealed model. Referring to Figure 69, the effects observed are listed in Table VI.

The sealing of joint 1 was accomplished by taping a piece of

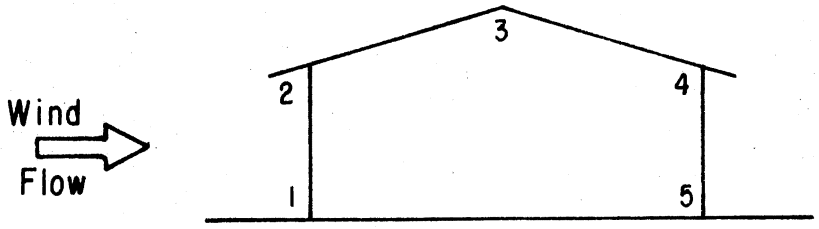

Figure 69. Joint Designation

TABLE VI

CHANGE IN STRAIN DUE TO SEALING JOINTS
(RECORDED STRAIN IN CHART DIVISIONS)

Test	Joints Sealed	(Inward) Panel 1	Panel 2** ALG Total	ABS Total	Panel 3	Panel 4	ABS Total	ALG Total	IN	OUT
VI-13	none	318	569	569	724	393	1994	1368	318	1686
VI-12	#1	353	483	483	642	331	1809	1103	353	1456
VI-11	#1, 2	586	187*	255	289	69	1199	41(IN)	620	579
VI-10	#1, 2, 3	526	82*	245	304	64	1139	49(IN)	594	545
VI-9	#1, 2, 4, 5	731	149*	283	215	3(IN)	1232	370(IN)	801	431
VI-8	#1, 2, 3, 4, 5	708	240*	302	282	8(IN)	1300	194(IN)	747	553

*A4 and B4 were inward but net still outward
**A3 and B3 multiplied by 1.5

plastic on the floor of the tunnel and letting it lay loosely against the building. Later the panel was pushed in a bit and the plastic was spot taped to panel 1. Joint 4 was sealed by hanging a piece of plastic inside the model taped to the underside of panel 3 near the top of the back wall. Suction outside the building pulled it up against joint 4. Joint 5 was taped similar to joint 1, except inside the building.

Vertical cracks on the ends of the roof and wall panels were not sealed with the exception of those on the front wall. The plastic was taped only to the wall panel. The positive pressure on the front wall and air flow around the ends of the model held the plastic across the two vertical joints.

The model was then considered to be "sealed". Frame calibration, as explained earlier, showed no interaction due to sealing the joints in this fashion. Once sealed, all tests for one alternative were run without changing the sealing conditions.

Although sealing the building model in this fashion certainly did not make it completely air tight, the sealing drastically altered the reactions. Where previously the highest forces were on the two roof panels, and the forces were high on the back wall, the most serious force after sealing was seen to be on the front wall. The two back panels underwent a reduction of 400 recorded strain units. This drastic change can only be accounted for by the near complete closing off of the leakage which previously was adding internal outward pressure to the suction existing outside the model even though all the cracks were the same size.

The most severe change was due to closing joint 2 at the top of

the front wall. The other joints assuredly had a pronounced effect, also.

The net forces on the model were altered from predominantly outward on the leaky model to predomanantly inward on the sealed model. The steady increase of the inward forces is accompanied by a steady decline in the outward forces.

The conclusion of this aspect of the investigation was that leakage through the small gaps around the panels could not be ignored. Air leaked both into the model and out again through these small joints. When air flow velocity was increased, the width of the gaps increased to a certain extent, also. This was especially true for the joint at the top of the front wall where even a microscopic raising of the roof opened the gap and allowed air to be scooped into the model by the eave overhang. This introduced a variable into the investigation which was neither accounted for nor controllable except by sealing the joints. All remaining tests were run with efforts to seal the building model except where noted later.

The data suggests that controlling the sealing, or lack of it, at the five locations, might be the most effective way of controlling both the magnitude and distribution of the forces sustained by the structure. Some type of controlled leakage could well be a topic for future study.

Deflectors

Objective. The objective of this portion of the preliminary quantitative investigation was to determine the beneficial effects, if any, of forcing early separation of the roof surface's boundary layer

by disruption of the flow near the leading edge of the upper surface of the windward roof panel. This would, it was theorized, cause the front roof surface to be in a "wake" region, in addition to that wake normally existing for the two panels beyond the roof ridge. Normal boundary layer separation for moderate roof slopes first occurs at the leading edge but quickly reattaches until the abrupt change of geometry at the roof ridge makes it impossible for the air flow to continue to follow building configuration.

Method. Utilization of a series of different sized deflectors in several positions and orientations mounted along the full length of the upwind movable roof panel, provided the means of disruption of the usual flow. The downwind roof panel was not modified, though in natural circumstances the wind can blow from any direction. This was judged unnecessary as, in the wind tunnel, the lower portion of the roof on the backside would be in a wake area of non-direct flow.

The preliminary study encompassed limited evaluation of a portion of tests foreseen for a comprehensive investigation should the modification look promising.

Equipment Unique to the Deflector Investigation. The particular deflectors tested were based upon the flow visualization results showing the most disruption.

The deflector configurations tested are shown in Figure 70. The symbols used are as follows:

a - denotes position on the roof up from the lower edge of the roof. Three series of holes were tapped into the upwind roof panel (No. 2). The sets of holes could be

used to place the deflector at any of four positions without overhanging the edge of the roof. A fifth position, with some overhang, was also possible. These positions are shown in Figure 71. Proceeding from higher to lower positions on the roof, the diatances from the edge of the roof to the deflector rotation point are:

a_0 = 2-7/16", 121-7/8" full scale
a_1 = 1-13/16", 90-5/8" full scale
a_2 = 1-3/16", 59-3/8" full scale
a_3 = 9/16", 28-1/8" full scale
a_4 = -1/16", -3-1/8" full scale

b - denotes the gap between the bottom deflector and the base plate mounted on the roof.

b_1 = 0.0"
b_2 = 0.125", 6-1/4" full scale

c - denotes the height of the piece making up the deflector.

c_1 = 5/16", 15-5/8" full scale
c_2 = 7/16", 21-7/8" full scale (not tested)
c_3 = 13/16", 40-5/8" full scale

α - measures the angle between the deflector and the roof surface.

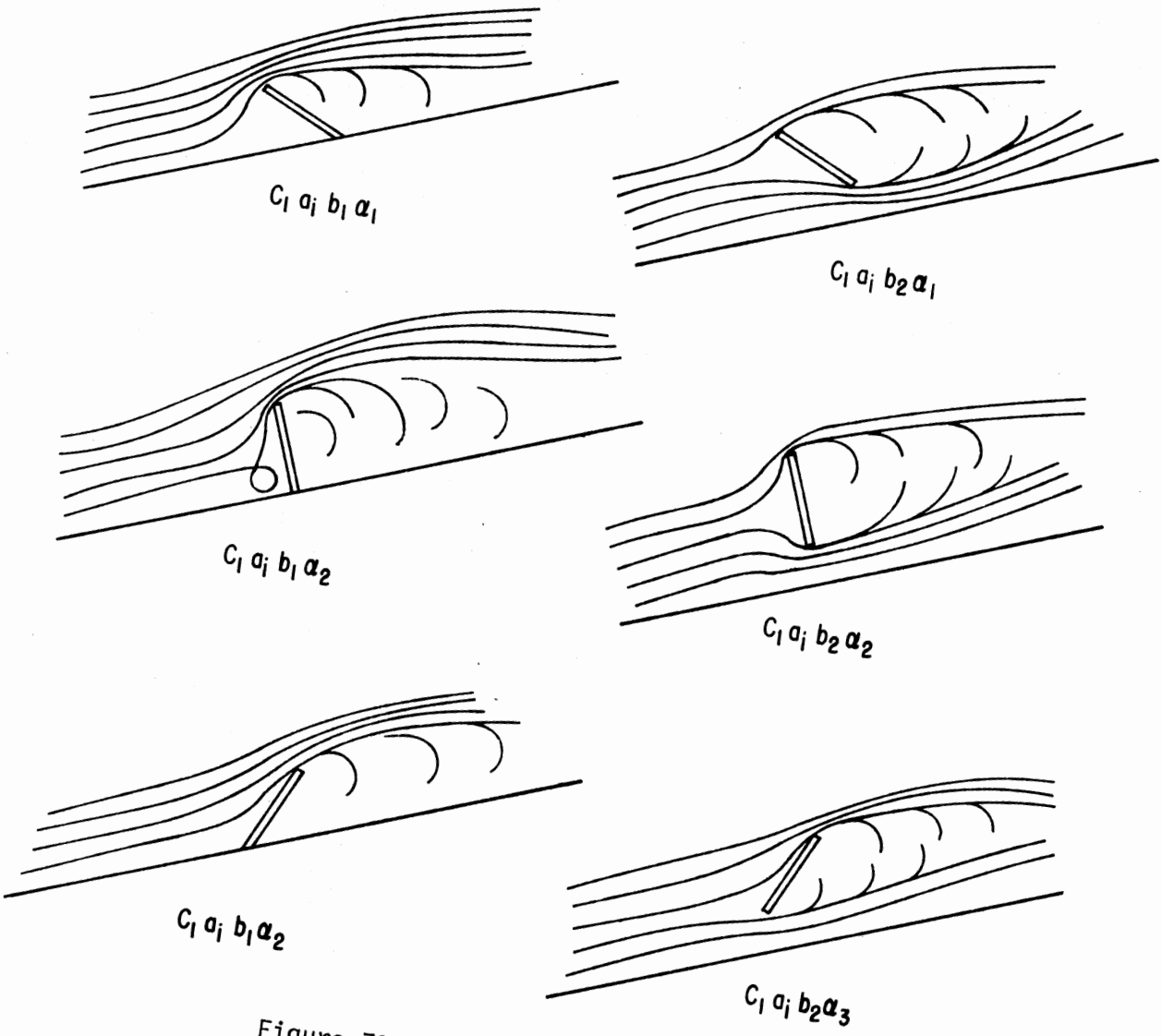

Figure 70. Deflector Configurations

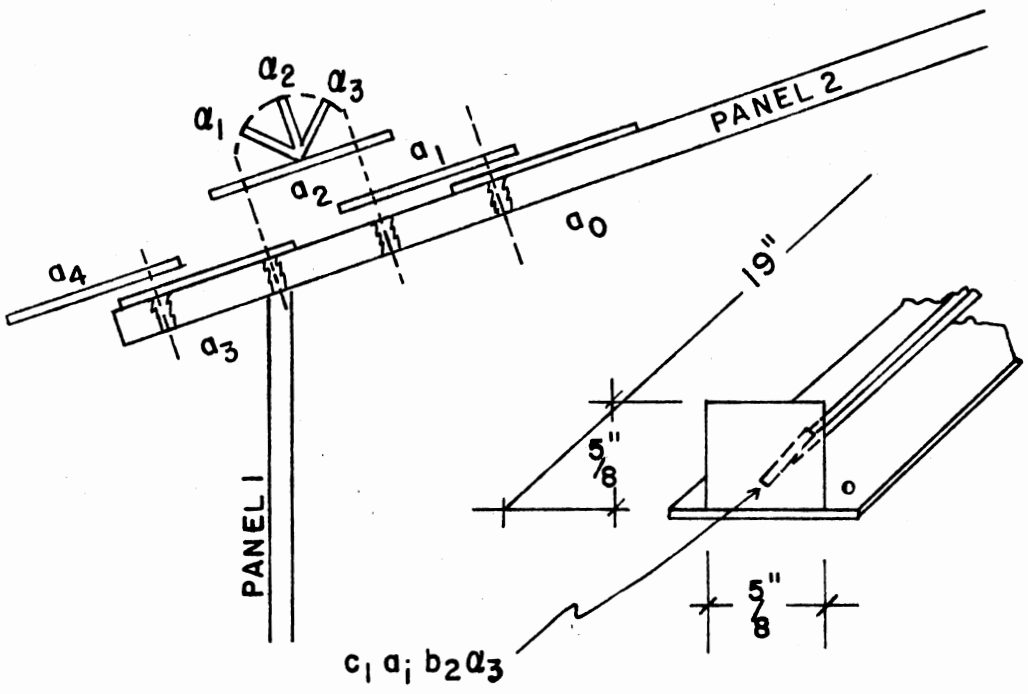

Figure 71. Deflector Positions and Construction Details

$\alpha_1 = 45°$

$\alpha_2 = 90°$

$\alpha_3 = 135°$

$\alpha_4 = 0°$

α_4, or 0°, signifies the control - i.e., no deflector, but rather a flat metal strip, of equivalent weight fastened in the same "a" position as the deflector. In Figure 72, from left to right, are pictured $c_{3}a_{i}b_{1}\alpha_{4}$, $c_{3}a_{i}b_{1}\alpha_{3}$, $c_{1}a_{i}b_{1}\alpha_{4}$, $c_{1}a_{i}b_{2}\alpha_{3}$, $c_{1}a_{i}b_{2}\alpha_{2}$ and $c_{1}a_{i}b_{1}\alpha_{2}$ -- i being determined by location on the roof. Figure 73 shows the model with $c_{3}a_{1}b_{1}\alpha_{3}$ in place. Figure 74 illustrates $c_{1}a_{3}b_{2}\alpha_{1}$ while its control is pictured in Figure 75.

Procedure. Utilizing the series listed in Table VII, the initial tests were run under "unsealed" conditions. No effort was made to seal either the clearance needed between the movable panel and the fixed portion of the model or the clearance between the panels themselves. This clearance varied from 1/64" to 1/32". Later, after discovering the importance of leakage, certain of the tests were repeated under "sealed" conditions to ascertain the value of the modification under those circumstances.

The tests were conducted in the normal manner described earlier for all the quantitative tests. Only top speed was used. The order resulted from random selection.

Both α_1 and α_3 (45° and 135°) were achieved with the same deflector reversed.

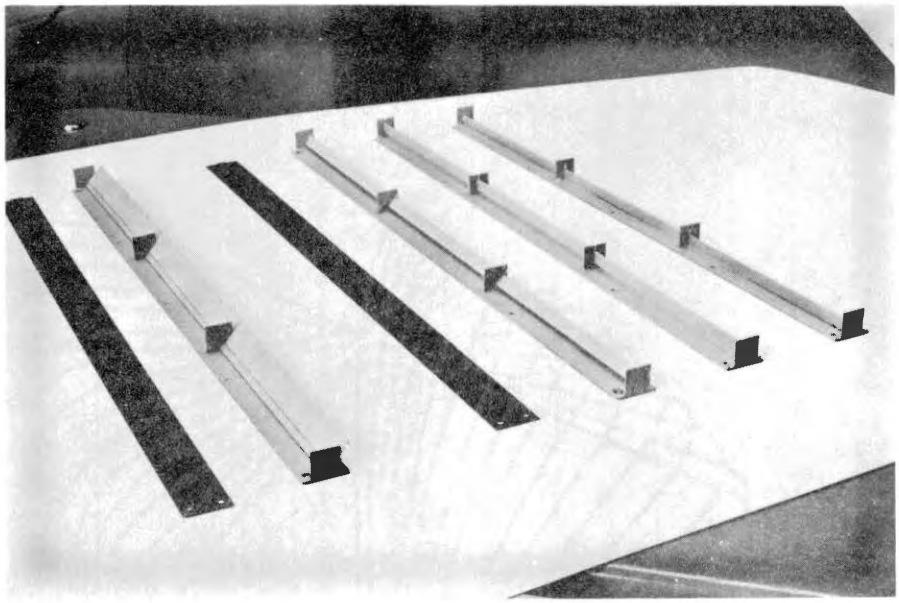

Figure 72. Deflectors Tested and Their Controls

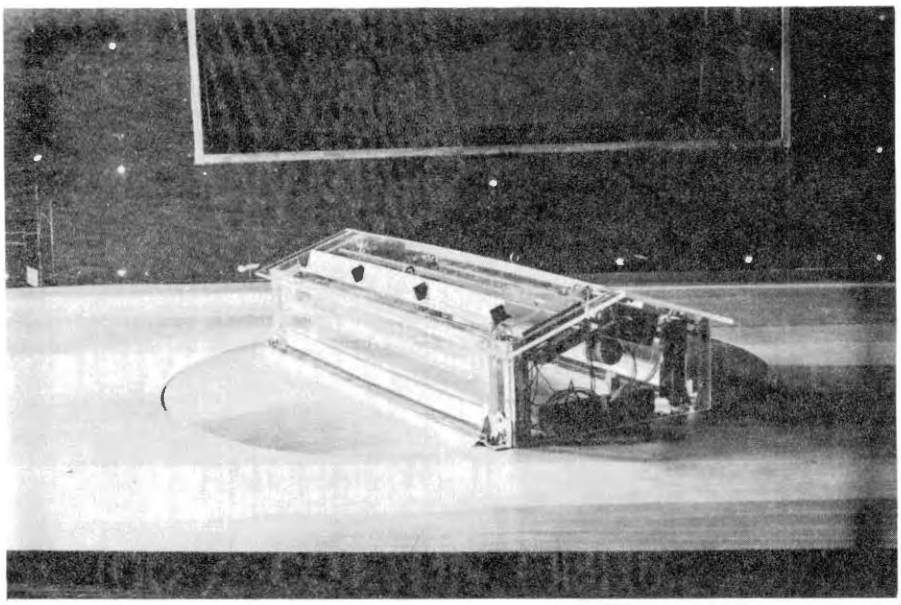

Figure 73. Tall Deflector (13/16") with No Gap at Position a_1 and 135° Orientation

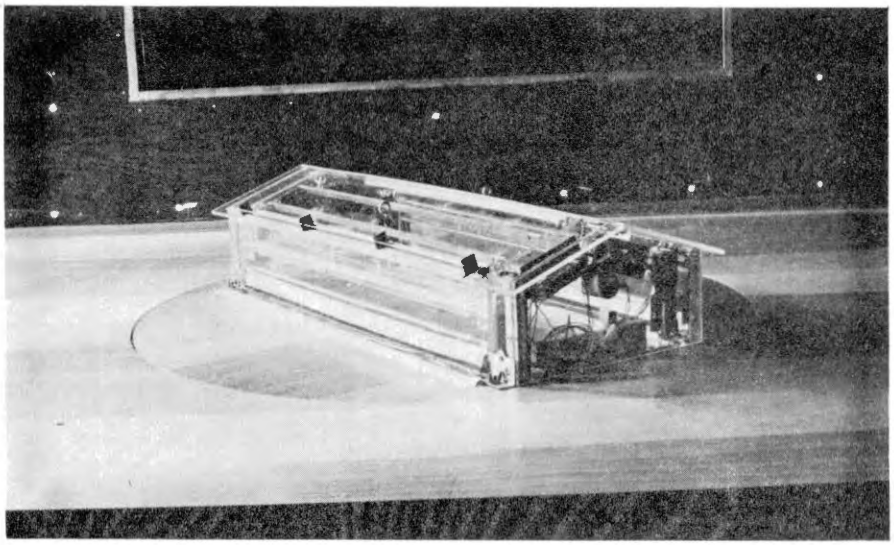

Figure 74. Short Deflector (5/16") with Gap at Position a_3 and 45° Orientation

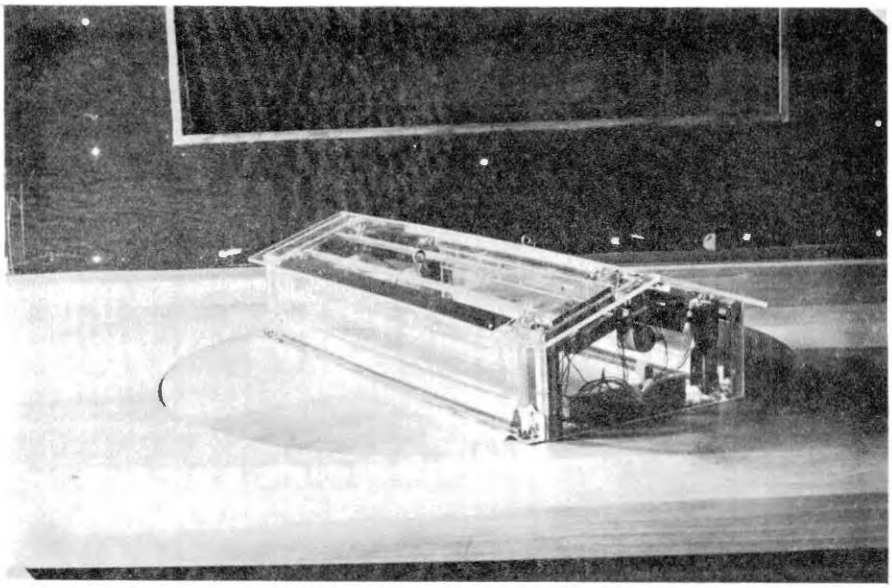

Figure 75. Control in Place for Deflector Above

TABLE VII

UNSEALED TEST SERIES FOR
ALTERNATIVE I

c	a	b	α	Order
c_1	a_1	b_2	α_1	11
			α_2	3
			α_3	7
		b_1	α_1	4
			α_2	13
			α_3	2
			α_4	1*
	a_3	b_2	α_1	12
			α_2	9
			α_3	8
		b_1	α_1	10
			α_2	5
			α_3	6
			α_4	14*

* Control

Results-First Deflector Series, Unsealed Model. The series listed in Table VII was carried out over a period of two days without de-energizing the electrical circuits.

The data was analyzed and plotted without precise correction for calibrations and minor changes in velocity in order to quickly ascertain the size of effect due to the deflector modifications. One such plot (I-11, c_1 a_1 b_2 α_1) is shown in Figure 76. The lines connect the two recorded voltages in chart divisions, due to strain, for similar gage locations on the two ends of the building model, i.e., A and B. The dashed line is the control whereas the solid line is the modification. The sign indicates the modification raised the forces (+) or lowered the forces (-). Here it can be readily detected that all the wind force induced strains decreased except those at A1 and B1, A2 and B2.

The plot shown is one of the better results. The general pattern of all the tests showed sizable increases in all cases for panel 1 (A1, B1, A2, B2), often increases for panel 2 (A3, B3, A4, B4), always decreases in panel 3 (A5, B5, A6, B6) and usually decreases for panel 4 (A7, B7, A8, B8).

The relationship of the control forces[1] is typical for all the tests on the unsealed models. The forces on the front wall are inward while all the other panels experience outward forces. The highest outward forces by far are those at the leading edge of the roof (the 3's) followed closely by the forces on the back roof panel. The 4's at the

[1]The results of the tests are commonly referred to hereafter in terms of how the forces were affected. More properly, the results should be discussed in terms of the effects on the strain readings caused by the wind induced forces on the model surfaces.

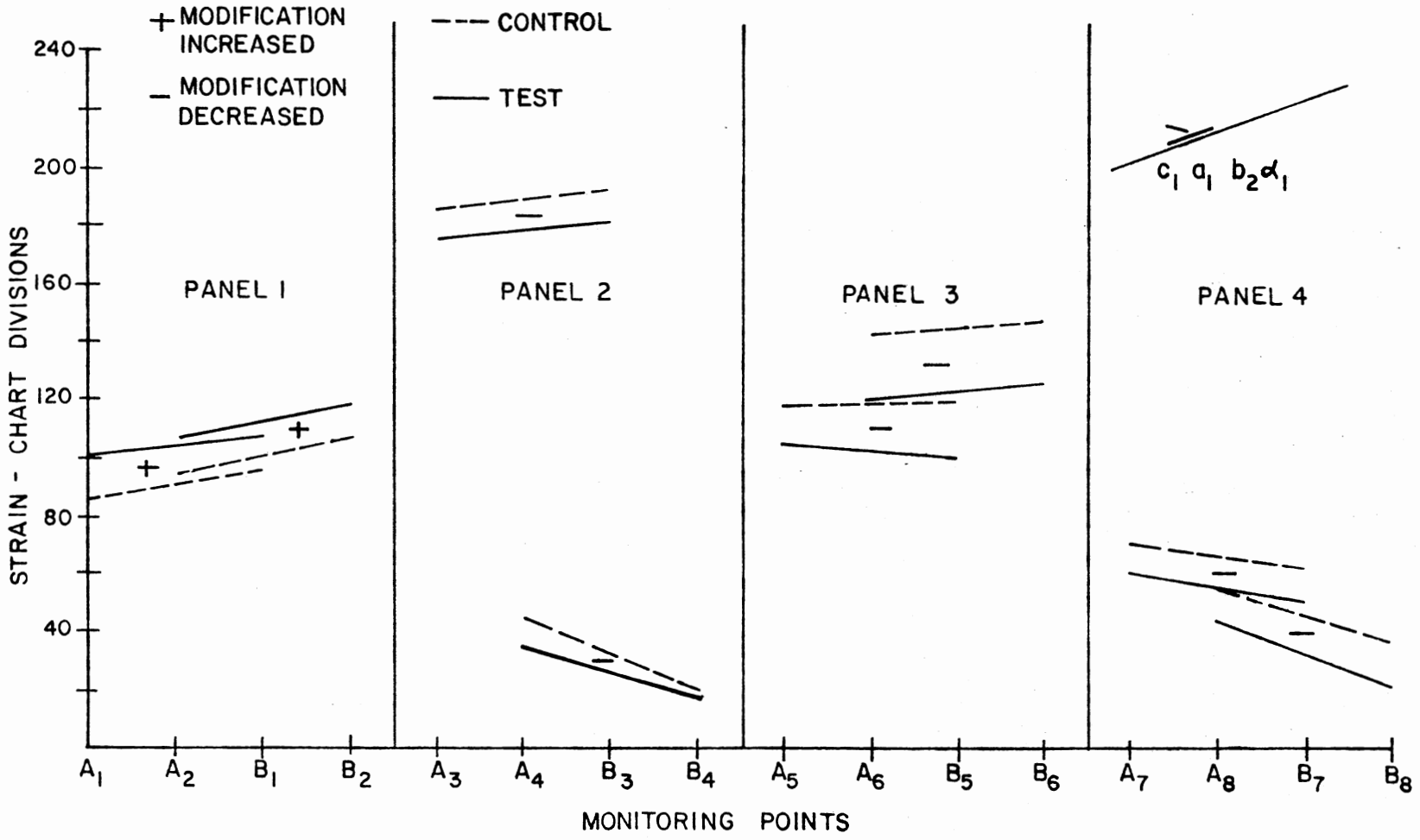

Figure 76. I-11 Versus I-1 Control

top of the leading roof panel are low as are the forces on the back wall.

It will be noted that the slopes of the line between two comparable gages can be partially accounted for by differences in stiffness of the beams. Exact comparison between the 1's, for example, could be obtained only by eliminating the difference due to the calibration factors, etc., Table XXIV. The beams for the 3's are approximately one and one-half times as stiff as the others so their readings have been multiplied by 1.5 to give a better quick indication of the relative magnitudes of the forces without going to the effort of completely reducing all the data.

It appears there is potential to reduce certain of the forces at the expense of increasing others. In order to assess the effect of deflector orientation, position on the roof and the presence of a gap between the deflector and the roof, the plots shown in Figures 77 and 78 were prepared.

For these tests, c is constant at value c_1, using the 5/16" deflector strip. The plotted X's are b_2's, or 1/8" gap. The plotted dots are the b_1's, or no gap. Three angles are plotted between α_4, or 0°, which is plotted at either extremity of one axis. The angle sequence is then 0°, 45°, 90°, 135° and 180°, with the control represented on either end. The scales do <u>not</u> start at zero so only the top of the three dimensional "force column" is shown. On the figures, each of the vertical axes are labeled with the test identification.

Panel 1 - Some interesting results are noticeable. In Figure 77 where panel 1 forces AV1 (average of A1 and B1) and AV2 are represented

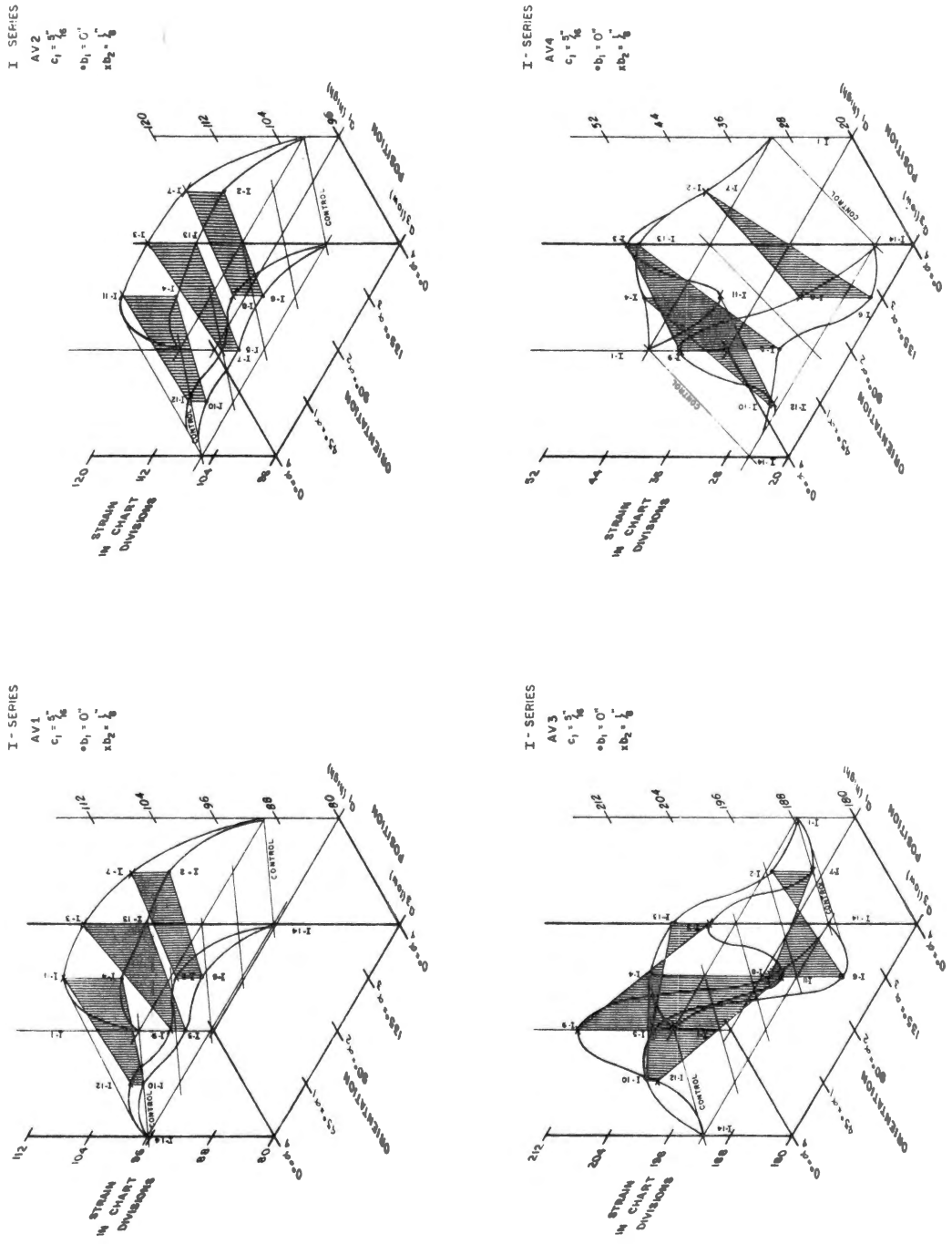

Figure 77. Average Strain Readings on Panels 1 and 2, I-Series

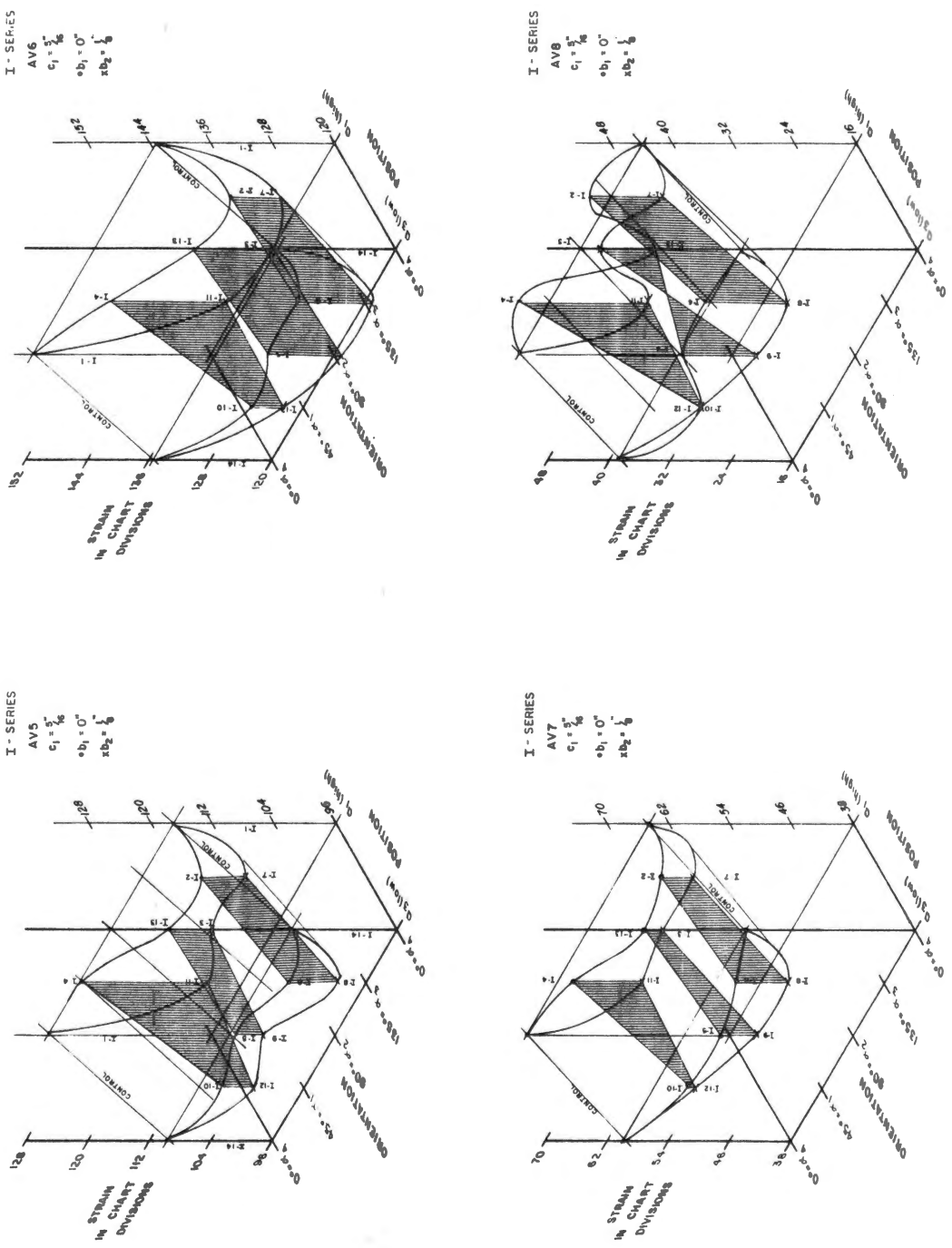

Figure 78. Average Strain Readings on Panels 3 and 4, I-Series

very similar effects are seen.

1. All the forces are increased for all tests but surprisingly the 90° modification forces are lower than for either 45° or 135° modification except at a_3.
2. The deflectors with gaps cause higher force changes, both increases and decreases.
3. The controls vary due to position with the a_1 position, higher on the roof, resulting in lower control forces on the front wall.
4. Similarity exists between the force patterns at deflector positions a_1 and a_3.
5. The forces with the deflector at position a_1, high on the roof, are more often greater than those with the deflector at a_3.

Panel 2 - In Figure 77, showing AV3 and AV4 forces, the following can be observed. The forces on the 3's are highly dependent upon the modification, displaying very unusual behavior. That A3 and B3 are the most affected is not really surprising, as they are the roof reaction most directly under the deflector. The A3 and B3 forces were multiplied by a factor of 1.5 to give an approximate comparison with the other gages since the 3's are less flexible beams.

For AV3:

1. With some effort, a pattern showing "sine" wavelike response can be detected. The curve for the no gap modification in the a_3 (low on roof) position resembles a distorted sine wave going full cycle. The curve for the modification with a gap (X's) for position a_1 resembles 1-1/2 cycles of a sine wave.

The gap curve at a_3 looks like a normal distribution curve.

2. The gap curves and no gap reverse their relative positions between a_1 and a_3 at both 90° and 135° orientation.
3. The forces for position a_3 (low on roof) are higher in general.
4. The forces are only reduced below the control values for α_3 (135°) at positions a_1 and a_3 and for modification $a_1\ b_2\ \alpha_1$ (I-11 shown in another form, earlier, Figure 76).
5. α_2, or 90° orientation looks unfavorable in that the forces are increased considerably.

For AV4:

1. The 4's, at first glance, look to differ from the 3's, but upon further inspection very definite similarities exist.
2. The slope of the control plane is reversed.
3. The form of $a_1\ b_1\ \alpha_i$'s looks very much like a "normal distribution" curve.
4. The same tendency for forces to be lower at $a_3 b_1 \alpha_3$ and $a_1 b_2 \alpha_2$ is exhibited here, also.
5. Again α_2 (90° orientation) causes high increases in the forces.
6. The modifications with gaps (X's) cause higher forces than the no gap modifications (dots) except for I-11.

Panel 3 - The behavior of panel 3, Figure 78, offers more interesting insight into th system behavior pattern. The tendencies of panel 3 are largely the inverse or mirror patterns of panel 1. However, the forces are all reductions.

1. The lowest forces are generally associated with α_3 for AV5

TABLE VIII

SUMMARY OF PARTIALLY REDUCED DATA, DEFLECTORS--UNSEALED MODEL (RECORDED STRAIN IN CHART DIVISIONS)

		Position α_3, 1/8" Gap						Position α_3, 0 Gap					
	I-14 Control	I-12	% Change	I-9	% Change	I-8	% Change	I-10	% Change	I-5	% Change	I-6	% Change
AV1*	96.33	102.67	+ 6.6	101.84	+ 5.7	105.00	+ 9.0	101.00	+ 4.9	99.67	+ 3.5	101.67	+ 5.5
AV2*	105.67	111.50	+ 5.5	111.17	+ 5.2	113.67	+ 7.6	109.17	+ 3.3	108.67	+ 2.8	109.67	+ 3.8
AV3**	191.50	201.50	+ 5.2	215.75	+12.7	194.75	+ 1.7	202.75	+ 5.9	206.00	+ 7.6	185.50	- 3.1
AV4	24.67	25.83	+ 4.7	42.33	+71.6	30.50	+23.6	26.33	+ 6.8	29.17	+18.2	21.33	-13.5
AV5	109.67	102.50	- 6.5	105.33	- 4.0	99.50	- 9.3	106.50	- 2.9	109.17	- 0.5	106.00	- 3.3
AV6	135.33	122.50	- 9.5	118.83	-12.2	119.17	-11.9	126.50	- 6.5	128.50	- 5.1	128.83	- 4.8
AV7	59.67	54.34	- 8.9	50.17	-15.9	50.34	-15.6	55.17	- 7.6	55.17	- 7.6	57.33	- 3.9
AV8	38.84	32.00	-17.6	28.84	-25.8	29.17	-24.9	32.00	-17.6	38.33	- 1.3	39.84	- 2.6
Panel 1*	404.00	428.33	+ 6.0	426.00	+ 5.5	437.33	+ 8.3	420.33	+ 4.1	416.67	+ 3.1	422.67	+ 4.6
Panel 2	432.33	454.67	+ 5.2	516.17	+19.4	450.50	+ 4.2	458.17	+ 6.0	470.33	+ 8.8	413.67	- 4.3
Panel 3	490.00	450.00	- 8.2	448.00	- 8.5	437.34	-10.8	466.00	- 4.9	475.33	- 3.0	469.67	- 4.2
Panel 4	197.00	172.67	-12.4	158.00	-19.8	159.00	-19.3	174.33	-11.5	187.00	- 5.1	194.34	- 1.4
Inward*	404.00	428.33	+ 6.0	426.00	+ 5.5	437.33	+ 8.3	420.33	+ 4.0	416.67	+ 3.1	422.67	+ 4.6
Outward	1119.33	1077.33	- 3.8	1122.17	+ 0.3	1046.84	- 6.5	1098.50	- 1.9	1132.67	+ 1.2	1077.67	- 3.7
Panel Total Abs.	1523.33	1505.67	- 1.2	1548.17	+ 1.6	1484.17	- 2.6	1518.83	- 0.3	1549.33	+ 1.7	1500.33	- 1.5
Panel Total Alg.	715.33	649.00	- 9.3	696.17	- 2.7	609.51	-14.8	678.17	- 5.2	716.00	+ 0.1	655.00	- 8.4
	0° & 180°	45°		90°		135°		45°		90°		135°	

*Inward
** now multiplied by 1.5

TABLE VIII (Continued)

	Position α_1, Gap = 1/8"							Position α_1, Gap = 0					
	I-1 Control	I-11	% Change	I-3	% Change	I-7	% Change	I-4	% Change	I-13	% Change	I-2	% Change
AV1*	89.75	103.83	+15.7	105.17	+17.2	102.67	+14.4	96.00	+ 7.0	96.67	+ 7.7	98.00	+ 9.2
AV2*	100.25	112.17	+11.9	112.67	+12.4	111.83	+11.6	105.17	+ 4.9	106.33	+ 6.1	106.84	+ 6.6
AV3**	187.50	177.50	- 5.3	190.50	+ 1.6	181.25	- 3.3	194.50	+ 3.7	195.75	+ 4.4	186.75	- 0.4
AV4	30.25	24.59	-18.7	41.17	+36.1	34.67	+14.6	34.67	+14.6	39.67	+31.2	34.83	+15.2
AV5	117.25	100.50	-14.3	104.00	-11.3	103.67	-11.6	116.83	- 0.4	109.67	- 6.5	109.33	- 6.8
AV6	143.25	122.00	-14.8	119.67	-16.5	123.17	-14.0	137.17	- 4.3	130.17	- 9.1	129.67	- 9.5
AV7	64.50	53.50	-17.0	54.67	-15.3	54.83	-15.0	62.50	- 3.1	57.00	-11.6	58.67	- 9.0
AV8	44.00	31.00	-29.5	41.59	- 5.5	37.33	-15.1	48.33	+ 9.8	34.17	-22.4	46.83	+ 6.4
Panel 1*	380.00	432.00	+13.7	435.67	+14.7	429.00	+12.9	402.33	+ 5.9	406.00	+ 6.8	409.67	+ 7.8
Panel 2	435.50	404.17	- 7.2	463.33	+ 6.4	431.83	- 0.9	458.33	+ 5.2	470.84	+ 8.1	443.17	+ 1.8
Panel 3	521.00	445.00	-14.6	447.33	-14.1	453.67	-12.9	508.00	- 2.5	479.67	- 7.9	478.00	- 8.2
Panel 4	217.00	169.00	-22.1	192.50	-11.3	184.33	-15.0	221.67	+ 2.2	182.33	-16.0	211.00	- 2.8
Inward*	380.00	432.00	+13.7	435.67	+14.7	429.00	+12.9	402.33	+ 5.9	406.00	+ 6.8	409.67	+ 7.8
Outward	1173.50	1018.17	-13.2	1103.17	- 6.0	1069.83	- 8.8	1188.00	+ 1.2	1132.83	- 3.5	1132.17	- 3.5
Panel Total Abs.	1553.50	1450.17	- 6.7	1538.83	- 0.9	1498.83	- 3.5	1590.33	+ 2.4	1538.83	- 0.9	1541.83	- 0.8
Panel Total Alg.	793.50	586.17	-26.1	667.50	-15.9	640.83	-19.2	785.67	- 1.0	726.83	- 8.4	722.50	- 9.0

*Inward
** now multiplied by 1.5

though for AV6 the α_2 orientation results in the lowest forces in two instances.

2. The gap modifications' (b_2) forces are lower than the b_1's (no gap).
3. The 5's show the α_2 orientation to cause lesser reductions than α_1 or α_3 in general.
4. For α_1 and $a_1 b_2$ the forces are lowest for the 5's, I-11.
5. For α_3 and $a_3 b_2$ the forces are lowest for the 6's, I-8.

Panel 4 - Panel 4 forces (Figure 78) are somewhat erratic and the forces are lower than the other gages with the exception of the 4's on panel 2.

1. All forces represent reductions over the controls with some exceptions for AV8.
2. Cyclic trends are seen in AV8 at a_1, and opposite tendencies exist for the gap modifications than those exhibited for those with no gap under the deflector. Gap modification forces show to be highest at α_2 (90°) for the α_1 position with the forces for α_1 (45°) being the lowest.
3. In general gap curves are lower for all -- exception is noted for AV8 at a_1 and 90° orientation.
4. Some evidence can be seen at $a_3 \alpha_1$ of greater reduction for the no gap curves, I-11.
5. Similarity exists to considerable extent between AV7 as the inverse of panel 1.

Table VIII summarizes the partial reduction of the data showing the average strain readings in chart divisions for each of the monitoring

monitoring points and a tabulation of the percentage of change for each modification compared to its control for either position a_3 (I-14) or a_1 (I-1). The highest inward control forces, all on panel 1, are AV2 and AV1 in order of severity. The highest outward control forces are AV3, AV6, AV5, AV7, AV8 and AV4, again in the order of severity of magnitude.

Summary of Panel Forces - Panel 1, inward forces, Figure 79, show the effects of the three variables. All the modifications caused the control forces to increase. The 1/8" gap caused higher increases to result on the front wall at both the high and low position on the roof.

The magnitude of the increases (13% to 15%) is greater with the modification itself at the higher position on the roof, a_1. The effect of α, the orientation of the deflector, is slight. At a_3 the increases (5.5% to 8.5%) are in an order from low to high of 90°-45°-135°, though the differences are small. The modification causing the smallest force increases on panel 1 is I-5 (0.0" and 90°).

Panel 2, all outward forces, show erratic effects as a combination of the 3's and the 4's. Here the panel on which the deflectors were mounted is the one most directly affected, largely by the angle α. There is no consistent pattern. At a_3 the gap caused the higher increases. At a_1 the opposite is true. There is some similarity in the no gap pattern at a_3 and a_1 though I-6 caused a reduction where I-2 did not. The only other reductions are found for I-11 and I-7, both with a gap at a_1 (high on the roof). The extreme difference between I-11 (gap) and I-4 (no gap) is noted but remains unexplained. The I-4 result resembles that of I-10 at a_3 but the result of I-11 does not

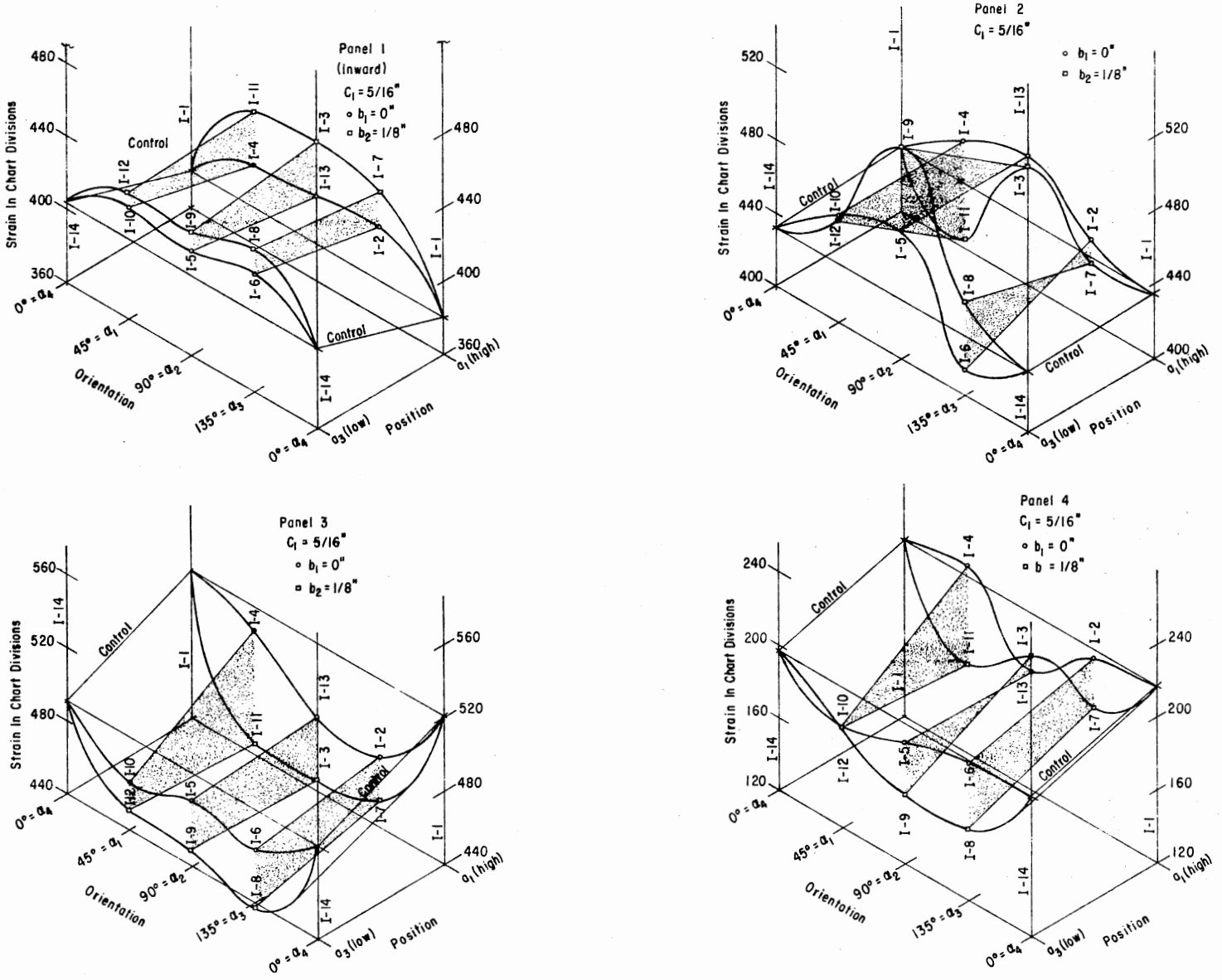

Figure 79. Panel Total Strain Readings, I-Series

resemble that of I-12, also at a_3. Perhaps the differences involve the reattachment of the boundary layer as affected by the location of the modification. The most favorable modification on panel 2 is I-11 at a_1 (high) with 1/8" gap and orientation of 45°. It reduces the outward forces on the panel.

Panel 3 outward forces show a surprising similarity to the inward forces on panel 1. Nearly every comment made for panel 1 is true of panel 3, except the force pattern there represents a universal reduction with respect to the control forces. Where an increase was indicated for panel 1 the same pattern of decrease holds for panel 3, I-4 being the only significant deviation. The range of decrease for position a_3 (low) is 3% to 10.8% or ≃8% average. The most favorable modification at a_3 is I-8 (1/8" and 135°). The range of reduction for the high position on the roof (a_1) is 2.5% to 14.6% or ≃12%. The most favorable modifications are I-11 (1/8" and 45°) and I-3 (1/8" and 90°).

Panel 4 forces are outward and generally reduced. Only I-4 (0.0" gap and 45°) at a_3 represents an increase. Though the percentage of reduction is high (20%) in some instances, all the panel 4 forces are the lowest on the building. The gap results in higher reductions with the exception of I-3 at a_1.

The inward forces (Figure 80) are all on panel 1 so the same remarks apply to both. It is not possible to reduce these forces. To the contrary, they increase.

The outward forces (Figure 81) are reduced with the exceptions of I-4, in the high position with no gap and 45° orientation, and the two 90° modifications at the low position. The highest outward panel forces, on panel 3, are reduced whereas those on panel 2 most often

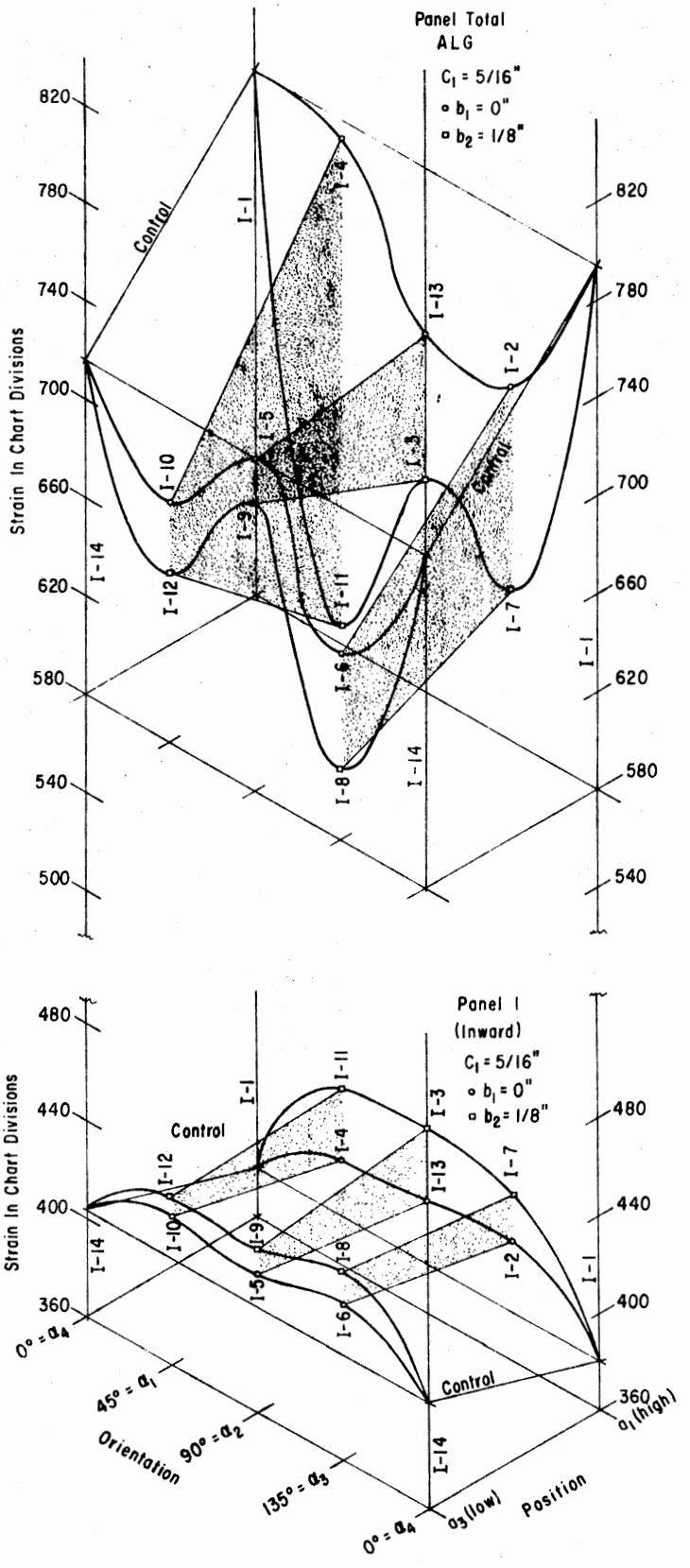

Figure 80. Total Inward and Algebraic Panel Total Strain Readings, I-Series

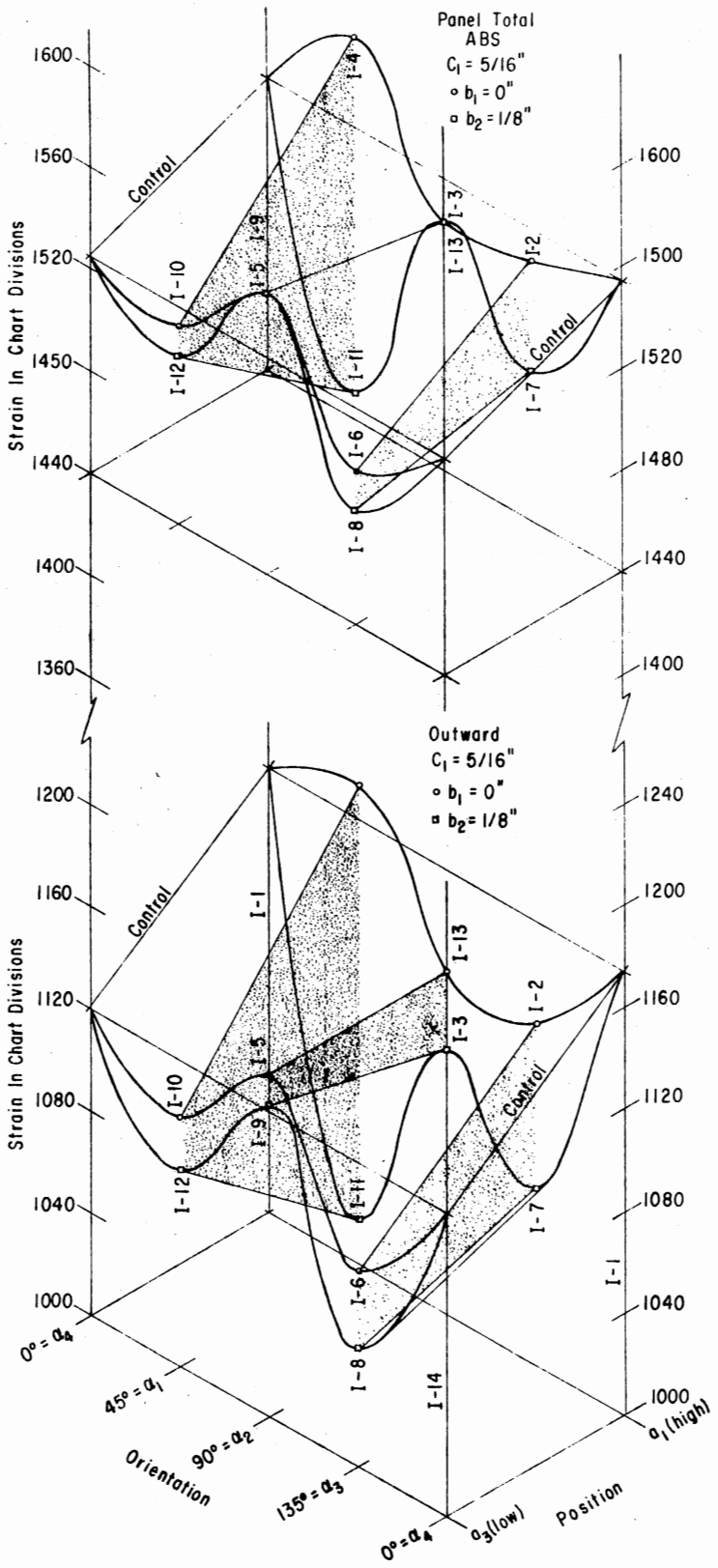

Figure 81. Absolute Panel Total Strain Readings and Total Outward Strain Readings, I-Series

are increased. I-11 results in the largest decrease, 13.2%, I-7 in 8.8% and I-8 in 6.5%. α_3 of 135°, in general, is best for all situations, except for the II-11 (45°) improvement which is better than I-7 (135°).

The relative pattern of the absolute total forces, the outward forces (Figure 81) and the algebraic or net forces (Figure 80) is essentially the same since they are mathematically derived. The sum of the outward forces plus the inward forces results in the absolute total forces. Their difference results in the algebraic or net total forces. Since the inward forces show little variation, the pattern of the outward forces dominates both the algebraic and absolute totals. The inward forces serve to accent the extremes of the outward force pattern in the case of the algebraic or net force and diminish the totals with respect to the controls. From the standpoint of the net forces, (which are outward in nature) all the modification forces are less outward than those of the controls. This results from the control net forces being predominantly outward initially, from the outward forces being reduced by the modifications and from the increase in inward forces. While the extremes of the outward pattern are diminished for the absolute totals, their position with respect to the controls is shifted down and they are the largest overall numbers considered. Again, only I-4 and the two 90° modifications at a_3 actually increase the absolute totals beyond the control level.

Supplemental Tests - Deflectors, Unsealed Model. During later supplemental tests, attempts were made to verify previous findings for I-11 and I-8 with the results shown in Table IX.

TABLE IX

SUPPLEMENTAL TESTS - I-11 AND I-8
PERCENT CHANGE WITH RESPECT TO
CONTROL MODEL

I-11	Original Series	Later Fast Velocity	Later Medium Velocity	Without Analog
Panel 1	+13.7%	+3.1%	+2.7%	+10.4%
Panel 2	-7.2%	+2.7%*	+4.0%*	-4.8%
Panel 3	-14.6%	-6.9%	-10.6%	-13.5%
Panel 4	-22.1%	-9.2%	-8.3%	-11.0%
Panel Totals (Absolute)	-6.7%	-2.7%	-3.0%	-5.5%
I-8				
Panel 1	+8.3%	+10.4%	+6.2%	
Panel 2	+4.2%	+4.1%	+6.2%	
Panel 3	-10.8%	-11.7%	-13.7%	
Panel 4	-19.3%	-14.6%	-16.0%	
Panel Totals (Absolute)	-2.6%	-2.9%	-3.9%	

The results for I-11 are both disturbing and at the same time reinforce previous conclusions. The lack of reduction on panel 2 in the two cases (*) resulted from increases in the 3's (toward leading edge of roof). Still other later tests confirmed the earlier results. Obvious inability to reproduce the exact same results is unexplained except for minor changes in equipment due to numerous dismantlings.

Nevertheless the general pattern of the same kind of redistribution of forces is confirmed by the later tests.

I-8 shows much more consistency than does I-11, reinforcing the

earlier results.

Small Deflector at Highest Position - The 5/16" deflector with a 1/8" gap was tested at the highest roof position, a_0, with deflector orientations of 45° and 135°.

The tests were I-28 and I-26, respectively. The results are shown in Figure 82 and Table X. Both produced similar results, but, of the two, I-26 (orientation of 135°) proved to be superior as it is the lower line in all instances except for the 1, 2, and 4 gages where it is the highest. It caused the greatest decreases and the greatest increases. The increases are slight but the decreases are significant.

TABLE X

I-26 - I-28 - I-27
PERCENT DIFFERENCE

	I-27 Control	I-26		I-28	
Panel 1	381	411.7	+8.0%	406.7	+6.7%
Panel 2	419.6	411.5	-1.9%	427.8	+2.0%
Panel 3	547.7	485.3	-11.3%	508	-7.2%
Panel 4	292.7	252	-13.9%	264.3	-9.7%
Total	1641	1560	-4.9%	1606.7	-2.0%

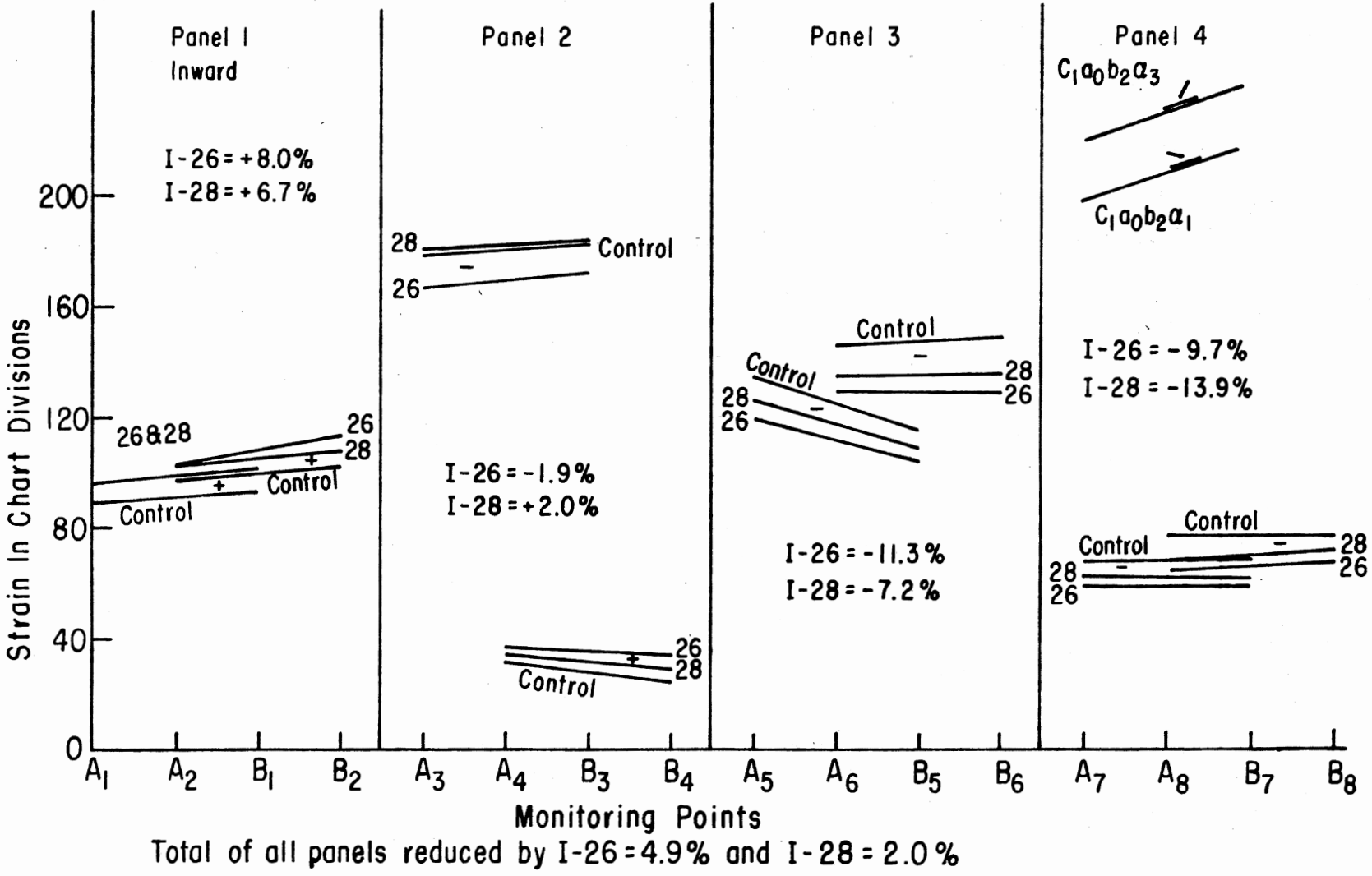

Figure 82. Modifications I-26 and I-28 Versus I-27 Control

Especially important to note is the redistribution of forces from locations of highest values to the locations of lower values. The increase in the 4's is acceptable in view of the decreases of the 3's, the 5's, and 6's. The control forces are maldistributed whereas the modification forces show better distribution except perhaps on the front wall. It, however, is better able to sustain inward forces than is the roof to resist outward forces.

The percentages of change on panel 2 mask the real benefit of relieving A3 and B3 by adding in a similar increase at A4 and B4 on the same panel.

The increase in A4 and B4 is likely due to the deflector forcing the air aloft and creating more suction over the area most directly sensed by the 4's.

Large Deflector at Highest Position - With the 13/16" deflector at angle 135° and no gap at position a_0, $c_{3\,0}$ a_1 b_3 produced the results shown in Figure 83.

The overall reduction 3.5% is not high (though respectable) when compared to some other modifications. The most apparent fact is that tremendous redistribution took place. Front wall forces were increased as usual, though moreso due to the exaggerated height of the deflector. Reductions (sizable) took place for all other gages except the 4's where negative pressures increased 200%.

This later phenomenon could be expected since previously the flow had apparently reattached before the ridge and held the roof down. Now a strong wake area is created behind the high deflector (no gap) which is placed higher on the roof (nearer A4 and B4) than for previous tests.

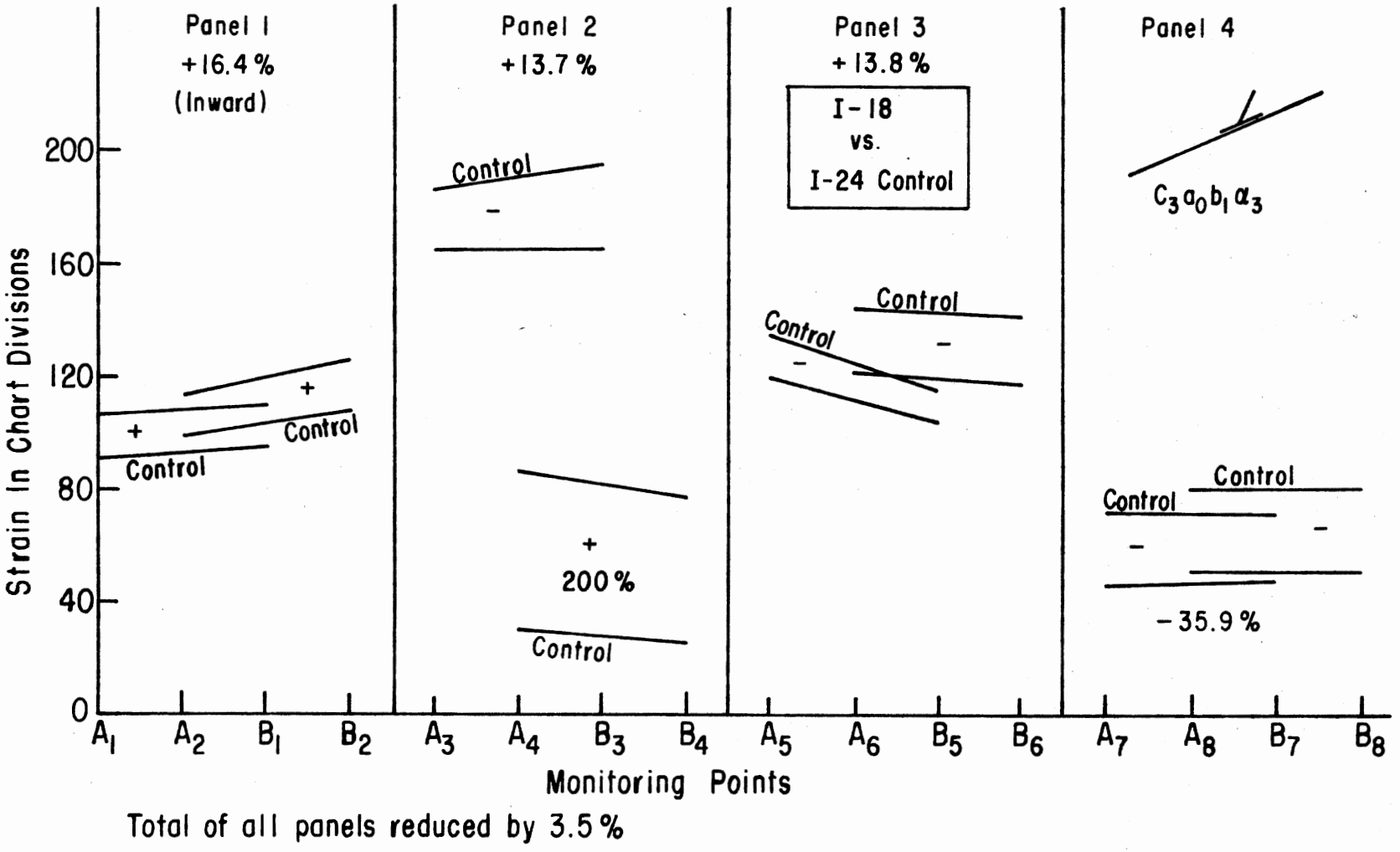

Figure 83. Modification I-18 Versus I-24 Control

One effect was greater reduction of the highest forces at A3 and B3, by 13.3%, and for the back panels. The 200% increase in the 4's overshadows the 3's decrease and the panel shows a net increase of 13.7%.

The 4's were already the lowest forces and this change results in a better distribution. More inward force is transferred to the front wall, but the front wall is better able to withstand it. The high increase in the 4's still results in forces there lower than the other roof forces.

The result is impressive. More study of position a_0 is merited. In the long series of I tests first run, a_1 usually resulted in greater force reductions than a_3. Disadvantages would be encountered with such a high deflector. Shear forces would not be negligible and the lack of the deflector's mate on the downwind roof could distort the results, but more study would be worthwhile to determine if comparable or better results could be obtained with shorter deflectors and gaps.

Deflector Mounting Plate Extended Beyond Normal Eave Overhang - With the 5/16" deflector at angle 45°, with 1/8" gap and located at position a_4, overhanging the end of the roof, $c_1 a_4 b_2 \alpha_1$ produced the results shown in Figure 84. The percentages marked are changes from the control.

The overall advantages are equal or better than several of the other modifications. The main disadvantage is that the highest forces (on panel 2) increased. The increase is very slight (2.8%). Other force reductions for the same modification are much greater (13% for panel 3). The A3-B3 forces for both the control and the modification on panel 3 are quite high because the upwind eave overhang was

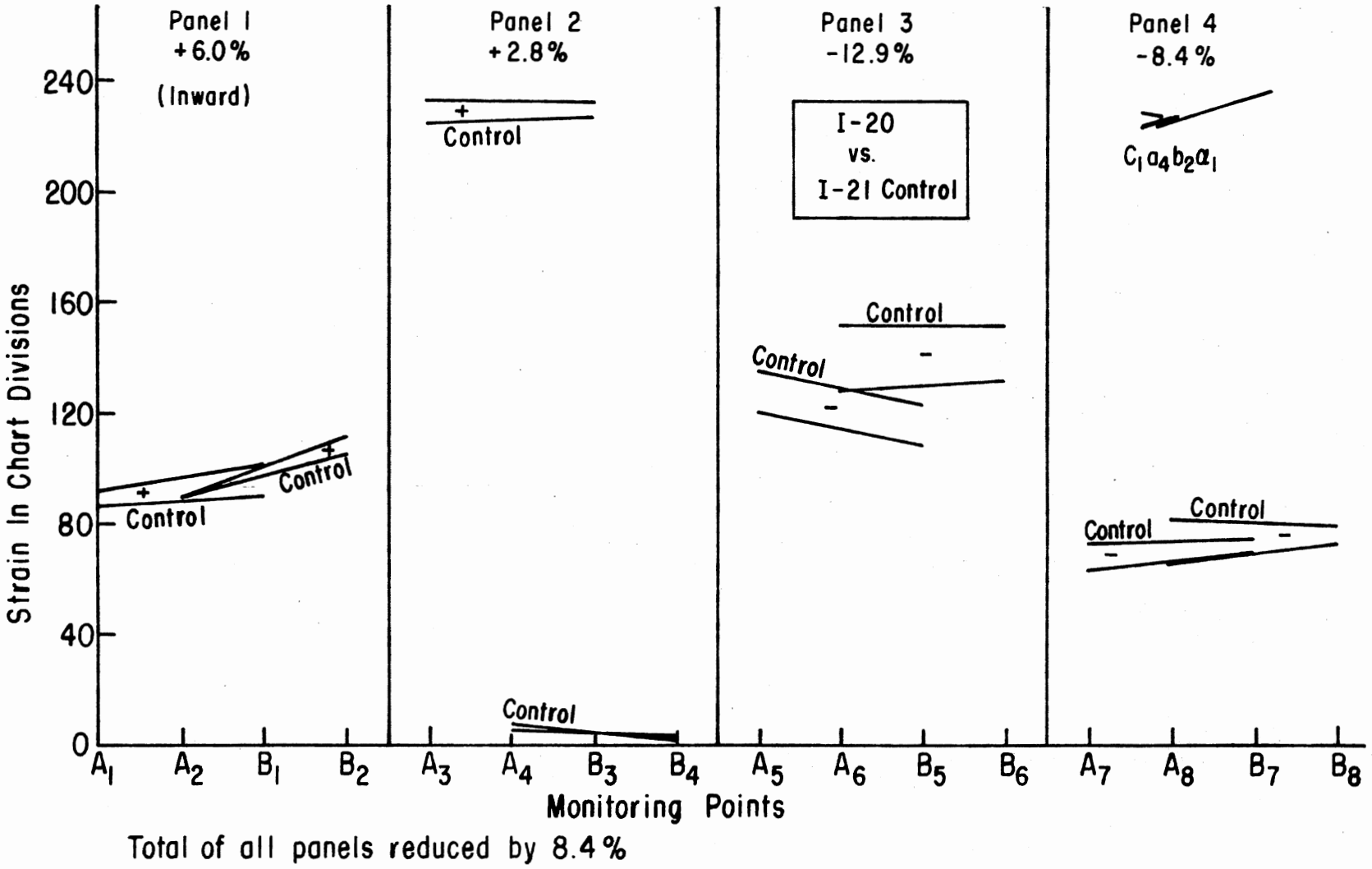

Figure 84. Modification I-20 Versus I-21 Control

increased by the position of the deflector mounting plate.

Conclusions - This configuration resulted in 8-1/2% reduction of the total forces on the model. It should be investigated in a future study to determine the effect of deflectors suspended directly over the leading edge of the roof without the interference of the mounting plate. In this way only the deflector would affect the air flow and not the mounting plate as was the case for this test. Then the forces at A3 and B3 would not be higher simply due to increased eave overhang. The deflectors should be tried at various angles and positions with respect to the edge to determine if it is possible to destroy the lift on the leading edge of the front roof without increasing the force on the front walls, yet maintaining the gains now present for the back surfaces.

Conclusions--Deflectors, Unsealed Model. The evidence points to a definite relationship between the deflectors tested in the first series and the resulting forces. There are several arguments both against and in favor of such a definitive conclusion.

In general, the deflectors increase forces on the upwind surfaces and decrease forces on the downwind surfaces. A similar pattern of change exists for panels 1, 3 and 4, though panel 1 forces are inward and the third and fourth panel forces are outward.

Redistribution of forces does take place as reflected by the small changes in the absolute totals but larger decreases in the algebraic or net totals. Panel 3, which initially sustained the highest total forces, and panel 4 are reduced at the expense of increases on panel 1 and 2. The panel 2 forces do not in general rise to the former high

level of panel 3.

At several points in the results a pattern can be observed. This would appear to be related to the orientation (α) of the deflector with respect to the roof surface. The sine wave sometimes represents the pattern and the normal distribution curve better fits others. The α_2 (90°) position seems to cause the extremes for these curves.

On the other hand, the plotting of α_4 (control) on each end tends to make the data appear "pattern-like". Actually, with three points (here at α_1, α_2, and α_3), a pattern will evolve no matter how they are arranged, i.e., $^{\circ}{}_{o}{}^{o}{}_{o}$, $_{o}{}^{o}{}_{o}{}^{o}$, $^{\circ}{}_{o}{}^{\circ}$, etc. Though this is true for any arrangement of three points, the apparent pattern must be due to more than this because the deflector tests were performed in random order. Too, the six points taken at the two positions in random order tend to show the same pattern at both the high and low deflector positions for several gages.

The individual modifications most successful in the first series are those at 135° orientation, I-7, I-8, I-6, I-2. I-11 at 45° looks promising. However, the general favorability of the 45° orientation is jeopardized by the puzzling results of I-4 with no gap, the counterpart to I-11 at position a_1. The tests for I-4 may have been faulty in some aspect but if so, the fault is not apparent. It may be that with no gap underneath, the forces are simply that different, especially since the interaction of the deflector with the separation and reattachment of the air flow at the leading edge of the roof remains a mystery.

The orientation effects are not the only ones to show a decided influence. The position of the deflector on the roof surface (a_i) also

indicates a marked influence. In general, this series indicates higher force changes for deflectors mounted at a_1 than for a_3, the latter being at the low position on the roof. At a_1, even the 90° orientation is advantageous; I-3 and I-13.

Further, the presence of a gap under the deflector shows a definite relationship to the resulting force pattern. In a number of instances the modifications with an 1/8" gap show more severe changes (favorable and unfavorable) in the force pattern.

Nevertheless, there was difficulty in repeating any one test later and obtaining quantitatively exactly the same results. I-11 ($c_1 a_1 b_2 \alpha_1$), one of the best tests, for example, later showed increase for panel 2 similar to its no gap counterpart, I-4, whereas earlier it had shown decreases. The tests were made over a period of two days when weather conditions were almost constant. Attempts to repeat the controls showed the same general pattern but the exact quantities varied somewhat. For this reason, on following tests, the control was run immediately after or before the test on the modification.

Also, the percent of change in the first series is not drastic which could account for the difficulty in attempting to repeat the tests accurately. These smaller differences make doubtful any authoritative conclusions.

The fact that the two controls gave different levels of forces raised some concern.

In spite of this, the pattern of the modifications compared to the controls at a_1 and a_3 are often similar, reinforcing the existence of a definite relationship. Almost without exception the modifications increase forces on panel 1 and 2 and decrease forces on panels 3 and 4.

Later tests on sealing the joints gave reason to suspect that shifting the control weight from one position to another might change slightly the gap at the top of the front wall thus causing differences in leakage.

Leakage which did prove to be a dominant influence, could account for the similarity of the patterns on the upwind wall and the downwind roof and wall, though the former are increases and the latter are reductions.

In summary, it seems a definite relationship exists in the first series between all the variables tested, i.e., α, b, and a. The differences do not result in universal relief for the structure. None of the changes are as dramatic as hoped. More comprehensive investigation is indicated wherein wider ranges and smaller increments of the variables should be tested. Each of the variables may prove influencial, especially in view of the deflector's position with regard to the bubble of separation at the leading edge and the resulting air flow pattern.

Further study should include a consideration of where a building is best able to sustain forces without damage. The front wall where the cladding is pushed into a strong framework is likely better able to withstand higher forces than can a roof which is ordinarily highly vulnerable to uplift. It may <u>not</u> be necessary to find a modification which reduces all the wind forces on a structure or even the total forces, if the force pattern can be easily redistributed to portions of the building more able to resist.

It is possible to redistribute the forces on the building using the deflectors tested. It is not possible to reduce panel 1 forces,

though the use of certain deflectors do minimize the increase (I-5, for example), that same deflector causes the least reductions on the other panels.

The key, it seems, is the ability to reduce panel 2 forces with some type of deflector since almost all configurations tested resulted in reduction on panels 3 and 4. Obviously certain deflectors resulted in larger increases on panel 1 and that should be considered along with the above.

The evidence of the first series leads to the conclusion that some combination of gap deflectors near a_1 probably at 135° orientation is most capable of producing the desired effects. If 45° is used it should also be tested with the gap.

It would, in retrospect, seem more appropriate to investigate deflectors in the 7/16" to 9/16" range. A few supplemental tests were run at a_0 (higher than a_1) and at a_4 (lower than a_3). They were run using the c_1 (5/16") and c_3 (13/16") deflectors, the latter with no gap. The supplemental tests were further random attempts at higher and lower positions on the roof to discover a combination which might be more effective. Indications are that both positions do indeed have merit. Again, the panel 1 forces increased, but the modification at the high position caused reduction of the forces for AV3, the highest of the outward forces. At the high position AV4's outward force was increased, but even then the forces are not high when compared to the other roof forces. Even the deflector in position a_4 shows the ability to reduce the forces on all but the front wall. The slight increase for AV3 must be attributed to the extension of the normal overhang from the mounting plate for the deflector assembly.

Even a subtle change in the deflector might result in a relationship with the boundary layer separation and reattachment which could be effective in reducing the lift on the front roof and still reduce the forces for panels 3 and 4 while incurring only small increases on panel 1.

The fact that net increases were small and other alternatives existed led to the abandonment of this alternative for, hopefully, bigger and better results.

Deflectors, Sealed Model. After discovery of the dramatic significance of sealing the small cracks between the movable panels, a select group of the deflectors were further subjected to experimentation using the "sealed" model.

Still utilizing the same nomenclature listed earlier the following tests diagrammed in Table XI were run:

	Controls
I-16 ($c_{3}\ a\ b_{3}\ \alpha_{1}$)	I-23 ($c_{3}\ a\ b_{4}\ \alpha_{1}$)
I-17 ($c_{3}\ a\ b_{1}\ \alpha_{1}$)	
I-8 ($c_{1}\ a\ b_{3}\ \alpha_{2}$)	I-14 ($c_{1}\ a\ b_{4}\ \alpha_{1}$)
I-12 ($c_{1}\ a\ b_{1}\ \alpha_{2}$)	
I-18 ($c_{3}\ a\ b_{3}\ \alpha_{0}$)	I-24 ($c_{3}\ a\ b_{4}\ \alpha_{0}$)
I-19 ($c_{3}\ a\ b_{1}\ \alpha_{0}$)	
I-29 ($c_{3}\ a\ b_{3}\ \alpha_{2}$)	I-30 ($c_{3}\ a\ b_{4}\ \alpha_{2}$)

I-26 ($c_1 a_0 b_2 \alpha_3$)

I-27 ($c_1 a_0 b_1 \alpha_4$)

I-28 ($c_1 a_0 b_2 \alpha_1$)

TABLE XI

TEST SERIES - ALTERNATIVE I, SEALED MODEL

Description			Tests	Controls
c_3 b_1	a_0	α_1	I-19(s)	I-24(s)
		α_3	I-18(s)	
	a_2	α_3	I-29(s)	I-30(s)
	a_3	α_1	I-17(s)	I-23(s)
		α_3	I-16(s)	
c_1 b_2	a_0	α_1	I-28(s)	I-27(s)
		α_3	I-26(s)	
	a_3	α_1	I-12(s)	I-14(s)
		α_3	I-8(s)	

Results - Deflectors, Sealed Model

Complete analysis of the results is futile because the tests run do not include the needed variations of all the deflectors which would permit total isolation of the various effects. Only one test was run

at the a_2 position on the roof and none at a_1. The 13/16" deflector was not tested with the 1/8" gap nor was the 5/16" deflector tested without the gap. The main comparison intended was between the two deflectors either at a_3 or a_0 with 45° and 135° deflector orientation.

The results of each test are plotted against the appropriate controls in Figures 85 through 89.

A common control for all was not possible since the weight of the two deflectors differed and the location of the weight on the roof registered some minor differences in the control model readings. However, all the sealed controls varied but little among themselves. I-27(s) at A3-B3 is the monitoring point which shows the greatest departure within all the control forces. All the control patterns reveal the worst inward forces to be on the front wall; top and bottom, about equal. Gages A3 and B3 no longer experience the highest forces, but are now nearly equal those of A5, B5, A6 and B6, all about half the magnitude of the front wall forces. All the A3 and B3 readings have been increased by 1.5, the approximate relative difference due to increased stiffness of these two heavier beams. A4 and B4 are no longer outward, but are inward and about of the same severity as the 3's, 5's, and 6's. The back wall forces are very much reduced over the unsealed tests, now being near zero but slightly outward.

Figures 85 through 89 indicate that tentative observations could be made, other than simple better or worse judgments, even on the basis of the incomplete information.

Table XII shows a summary of the strains on the unmodified model, the results of the various deflectors and the percentage of change. The two readings, on either end of the model, for a common monitoring

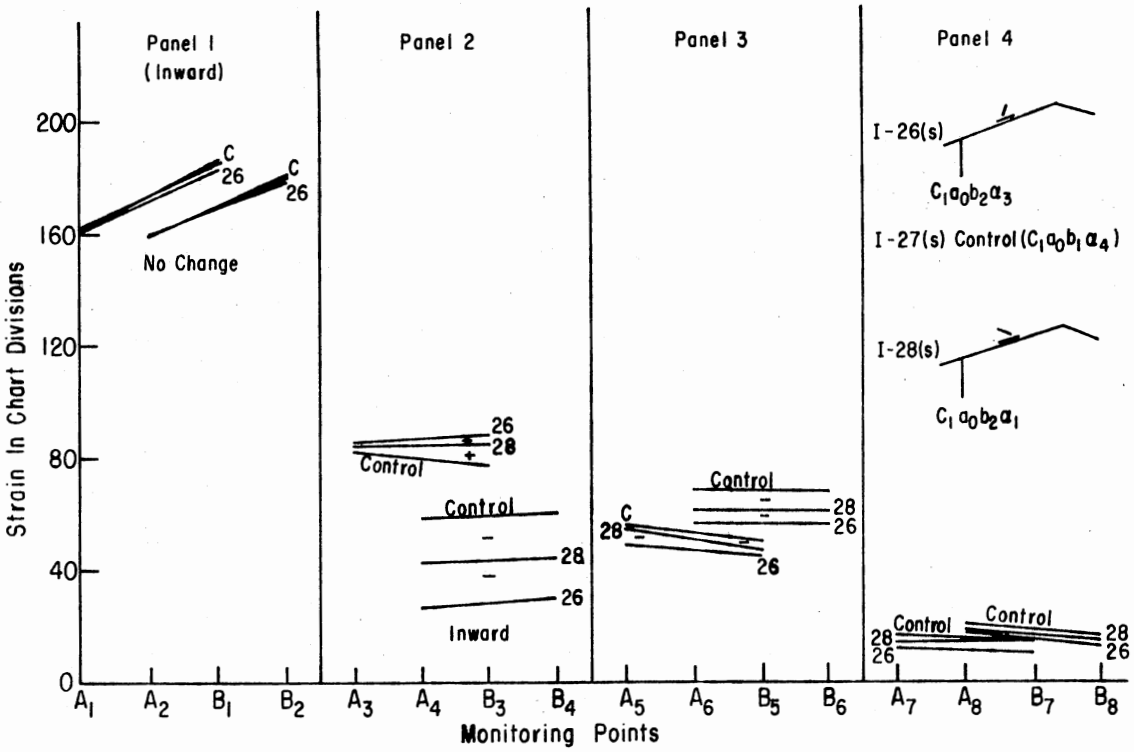

Figure 85. I-26(s) and I-28(s) Versus I-27(s) Control

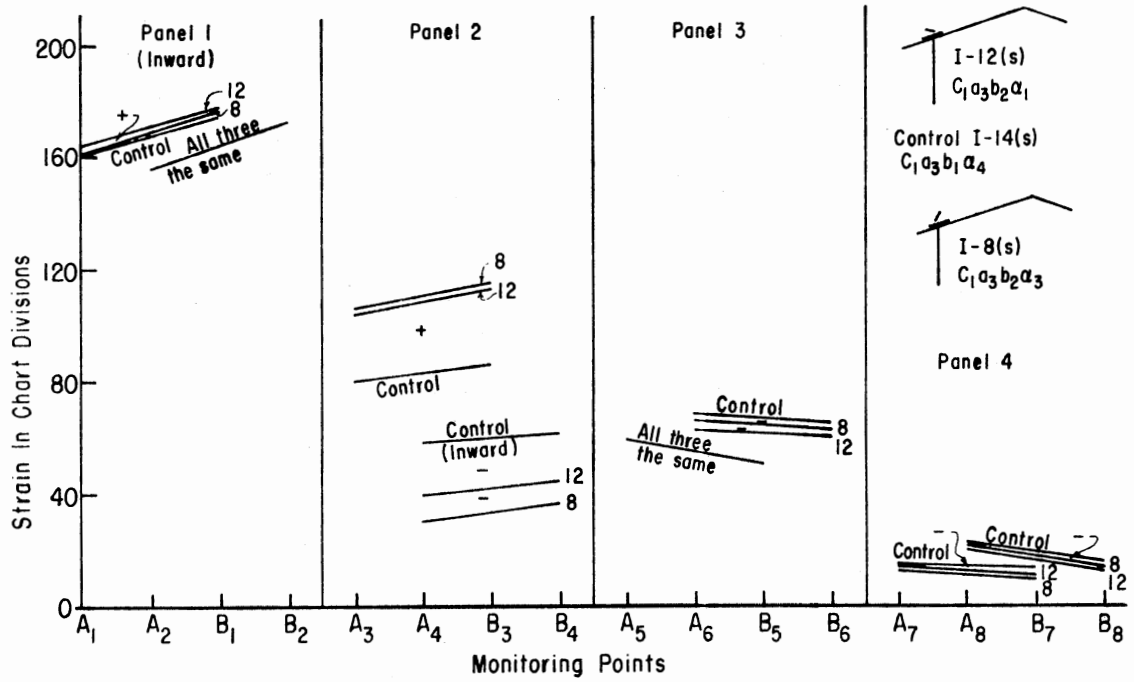

Figure 86. I-12(s) and I-8(s) Versus I-14(s) Control

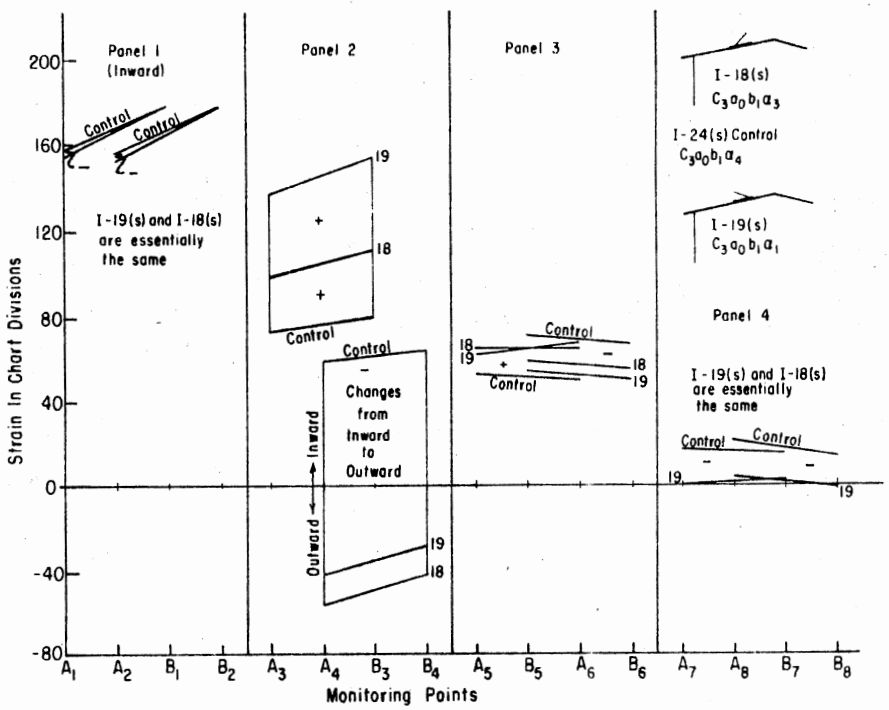

Figure 87. I-18(s) and I-19(s) Versus I-24(s) Control

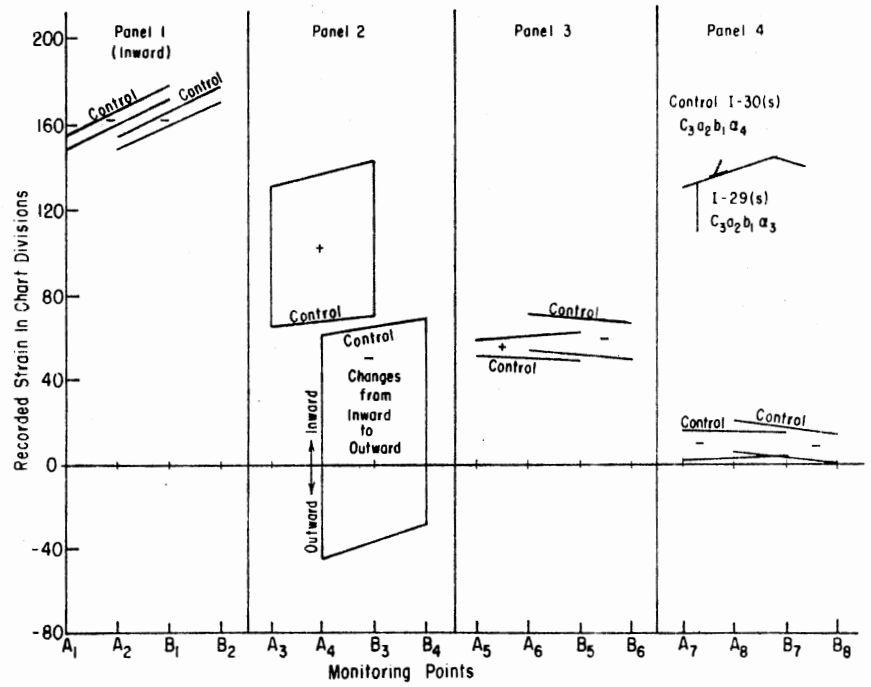

Figure 88. I-29(s) Versus I-30(s) Control

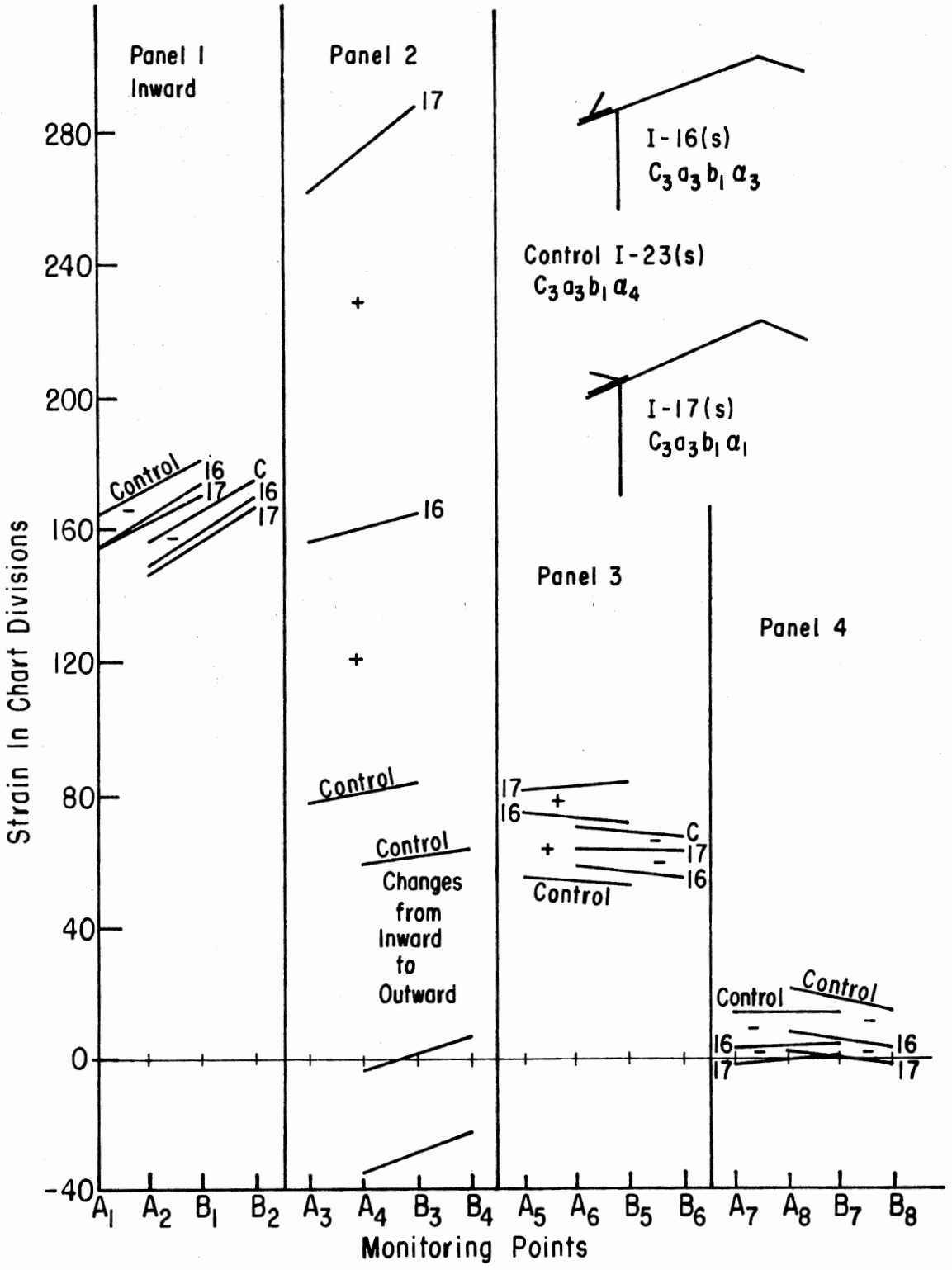

Figure 89. I-16(s) and I-17(s) Versus I-23(s) Control

TABLE XII

SUMMARY OF PARTIALLY REDUCED DATA, DEFLECTORS--SEALED MODEL (RECORDED STRAIN IN CHART DIVISIONS)

	I-27(s) Control	I-28(s) 45°	% Change	I-26(s) 135°	% Change	I-14(s) Control	I-12(s) 45°	% Change	I-8(s) 135°	% Change
AV1*	172.67	172.83	----	171.67	- 0.6	167.15	170.15	+ 1.8	167.67	+ 0.3
AV2*	169.33	168.33	- 0.6	167.83	- 1.0	164.00	165.00	+ 0.6	164.83	+ 0.5
AV3**	79.00	84.25	+ 6.7	85.75	+ 8.5	83.25	108.25	+30.0	109.75	+31.8
AV4*	58.83	43.00	-26.9	27.83	-52.7	59.33	41.50	-30.0	32.67	-45.0
AV5	53.00	50.50	- 4.7	46.83	-11.6	54.33	53.70	- 1.2	54.17	- 0.3
AV6	67.67	60.50	-10.6	55.00	-17.3	66.33	61.20	- 7.8	63.83	- 3.8
AV7	15.00	14.17	- 5.5	11.33	-24.5	13.50	11.50	-14.8	11.50	-14.8
AV8	18.17	16.00	-11.9	15.17	-16.5	18.33	15.50	-15.5	15.50	-15.5
Panel 1*	684.00	682.33	- 0.2	679.00	- 0.7	662.30	670.33	+ 1.2	665.00	+ 0.4
Panel 2	275.67	254.50	- 7.7	227.17	-17.6	285.20	299.50	+ 5.0	284.80	- 0.1
Alg. Panel 2	40.33	82.50	+104.5	115.83	+187.2	47.83	133.50	+179.0	154.17	+222.2
Panel 3	241.33	222.00	- 8.0	205.67	-14.8	241.40	229.80	- 4.8	236.10	- 2.2
Panel 4	66.33	60.33	- 9.0	53.00	-20.1	63.70	54.00	-15.3	54.00	-15.3
Inward*	801.67	768.33	- 4.2	734.67	- 8.4	781.00	753.33	- 3.5	730.33	- 6.5
Outward	465.67	450.83	- 3.2	430.17	- 7.6	471.60	500.33	+ 6.1	509.50	+ 8.1
Panel Total Abs.	1267.33	1219.16	- 3.8	1164.83	- 8.1	1252.60	1253.67	+ 0.1	1239.83	- 1.0
Panel Total Alg.*	336.00	317.50	- 5.5	304.50	- 9.4	309.40	253.00	-18.2	220.83	-28.7

*Inward

** now multiplied by 1.5

TABLE XII (Continued)

	I-24(s) Control	I-18(s) 135°	% Change	I-19(s) 45°	% Change	I-30(s) Control	I-29(s) 135°	% Change
AV1*	167.85	165.85	- 1.2	165.50	- 1.4	166.75	160.83	- 3.5
AV2*	166.00	163.35	- 1.6	164.70	- 0.8	166.00	159.17	- 4.1
AV3**	75.75	103.50	+36.6	144.75	+91.1	67.83	136.50	+101.2
AV4	62.00*	49.50	-179.8	35.35	-157.0	64.75*	36.17	-155.9
AV5	50.80	63.85	+25.7	63.50	+25.0	49.75	60.33	+21.2
AV6	67.65	55.85	-17.4	50.85	-24.8	68.50	51.00	-25.6
AV7	15.15	1.15	-92.4	0.70	-95.4	15.50	3.2	-79.4
AV8	17.15	2.35	-86.3	1.30	-92.4	17.50	3.8	-78.3
Panel 1*	667.70	658.40	- 1.4	660.40	- 1.1	665.00	640.00	- 3.8
Panel 2	275.50	306.00	+11.1	360.20	+30.7	265.17	345.33	+30.2
Alg. Panel 2	27.50	306.00	+1012.7	360.20	+1209.8	6.17	345.33	+5496.9
Panel 3	236.90	239.40	+ 1.1	228.70	- 3.5	236.50	222.67	- 5.9
Panel 4	64.60	9.00	-86.1	4.00	-93.8	66.00	14.00	-78.9
Inward*	791.70	658.40	-16.8	660.40	-16.6	794.50	640.00	-19.5
Outward	453.00	552.40	+21.9	592.90	+30.9	438.17	582.00	+32.8
Panel Total Abs.	1244.70	1210.80	- 2.7	1253.30	+ 0.7	1232.67	1222.00	- 0.9
Panel Total* Alg.	338.70	106.00	-68.7	67.50	-80.1	356.33	58.00	-83.7

*Inward

** now multiplied by 1.5

TABLE XII (Continued)

	I-23(s) Control	I-16(s) 135°	% Change	I-17(s) 45°	% Change
AV1*	172.17	163.50	- 5.0	162.00	- 5.9
AV2*	165.67	159.00	- 4.0	155.75	- 6.0
AV3**	79.75	160.50	+101.2	275.25	+245.1
AV4	60.50*	29.17	-148.2	1.75*	-97.1
AV5	52.67	71.50	+35.8	82.00	+55.7
AV6	67.83	56.17	-17.2	62.00	- 8.6
AV7	13.50	3.20	-76.3	0.5	-96.3
AV8	17.00	5.50	-67.7	0.5	-97.1
Panel 1*	675.67	645.00	- 4.5	635.50	- 6.0
Panel 2	280.50	379.33	+35.2	554.00	+97.5
Alg. Panel 2	38.50	379.33	+885.8	547.00	+1320.8
Panel 3	241.00	255.33	+ 6.0	288.00	+19.5
Panel 4	61.00	17.40	-71.5	2.00	-96.7
Inward*	796.67	645.00	-19.0	639.00	-19.8
Outward	461.50	652.07	+41.3	840.50	+82.1
Total Panel Abs.	1258.17	1297.07	+ 3.1	1479.50	+17.6
Total Panel Alg.	335.17*	7.07	-102.1	201.50	-160.1

*Inward

** now multiplied by 1.5

point have been averaged. The two averages were then added together and doubled to obtain each of the four panel totals. Where outward forces and inward forces exist on a single panel, the absolute total and the net or algebraic total has been tallied. The building totals include the sum of all the outward forces and the sum of the inward forces. The total algebraic force for the building is their difference and the absolute total is the sum of inward and outward forces.

In order to better compare the modifications and their five different controls, Figures 90 through 102 show the percent of change of each with respect to its own control.

The predominate unmodified building forces are inward and consist of high forces on the front wall as well as lesser forces at the top of the leading roof panel--about 33% of the former. Reductions in the total inward forces are in the 4% to 8% range for the short deflector and 16% to 20% range for the large deflector, as seen in Figure 100.

Changes in inward force do occur, small increases or reductions, on the front wall. Behavior of AV1 and AV2 are nearly identical (Figure 90) and panel 1 (Figure 91) reflects the same pattern. For the small deflector (5/16") with a 1/8" gap underneath, the maximum changes on the front wall are 1% to 2% increases with the deflector near to the leading edge of the roof. The larger deflector (13/16") results in a maximum of 4% to 6% decreases, again near the roof's leading edge. Both tend to lose their influence as they are positioned nearer to the ridge of the roof. As might be expected, the deflector leaning into the flow of wind (45°) causes the greatest changes.

Outward forces existing on panel 2 (Figure 92) at AV3 are greatly affected by the modifications--moreso with positions nearer the

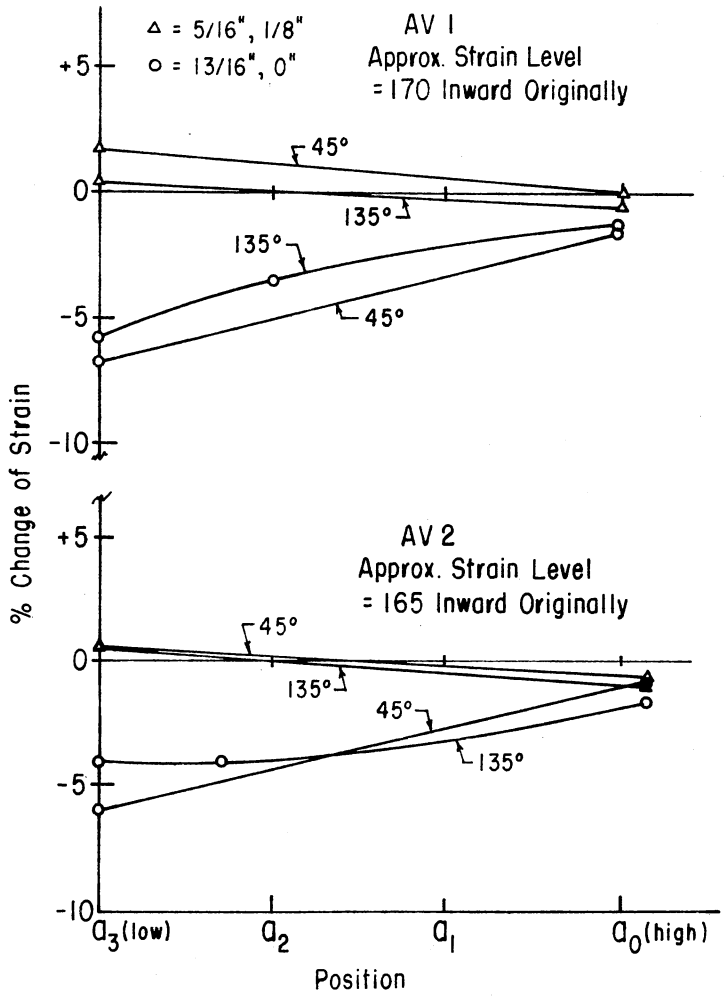

Figure 90. Changes for Gages 1 and 2, I(s)-Series

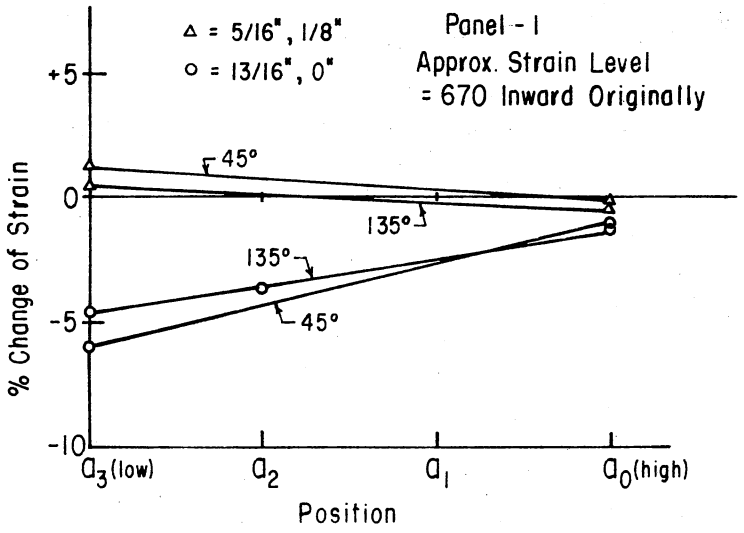

Figure 91. Changes for Panel 1 Totals, I(s)-Series

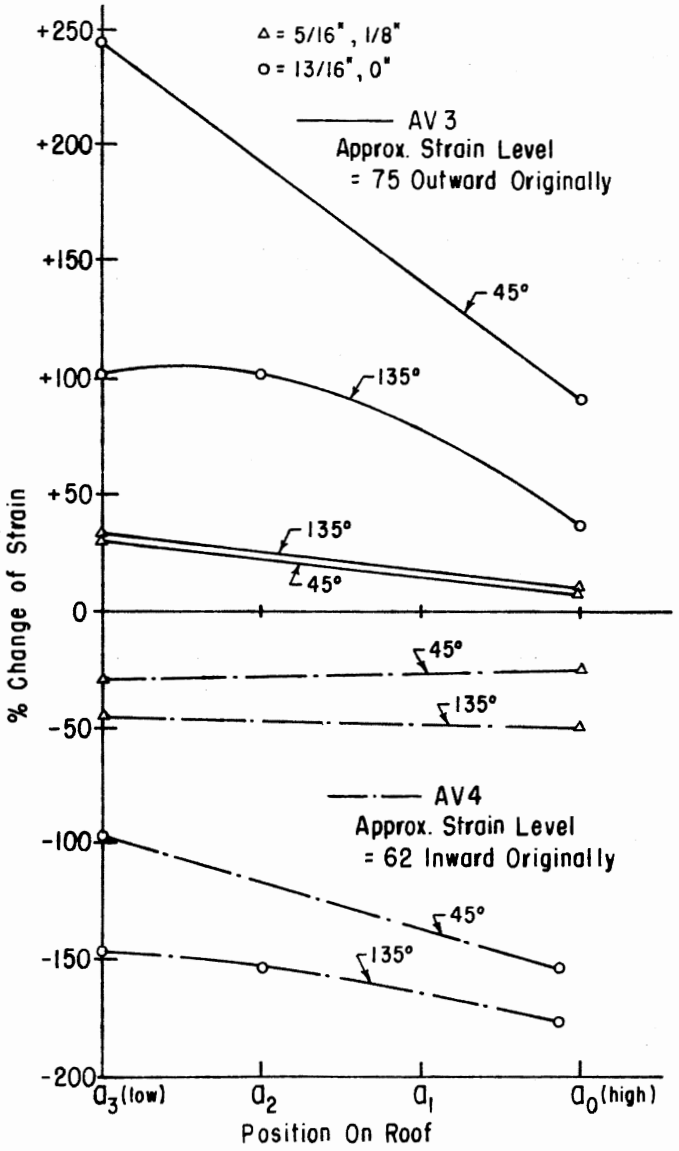

Figure 92. Changes for Gages 3 and 4, I(s)-Series

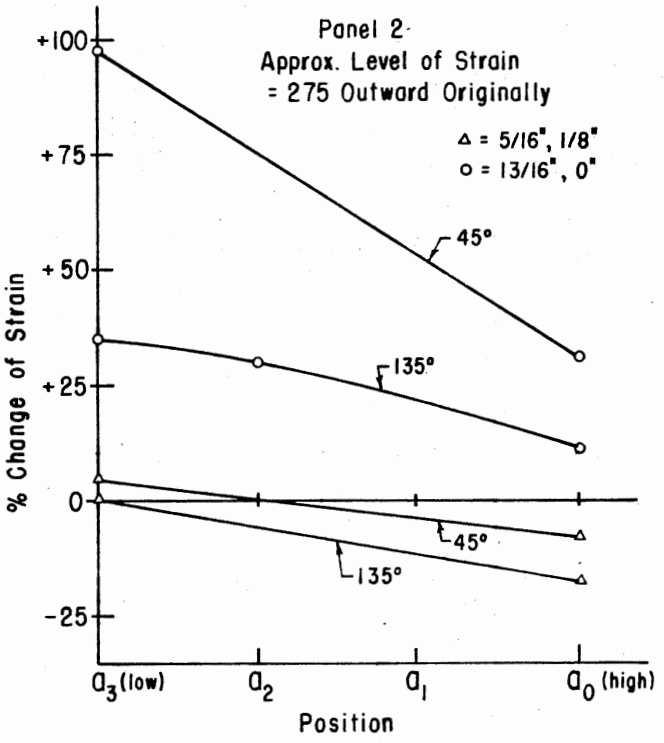

Figure 93. Changes of Panel 2 Absolute Totals, I(s)-Series

leading edge of the roof and the greater changes are associated with the higher deflector. All the changes are increases in outward forces ranging from 7% to 245%. From the one test at position a_2, it seems a_2 may be the more critical position but, with only one such observation, it is difficult to be certain. Except in the case of the short deflector, 135° causes less increase than 45°.

At AV4 the original inward forces are reduced even beyond 100% with the large deflector for any combination of orientation and position. This actually represents a change from inward to outward force. Except in the case of the short deflector oriented into the wind, the effect is greater for positions nearer the top of the roof and the point where AV4 is measured. The reductions range from 27% to 180%. The deflectors oriented at 135°, or with the flow of the wind, create the largest changes. The changes at AV3 and AV4 combine (Figure 93) to decrease the absolute force on panel 2 for the 135°, 5/16" deflector at all positions on the roof. The same is true for the 45°, 5/16" deflector above position a_2. The tall deflector always resulted in increases of the absolute force on panel 2. The changes caused by the 135° orientation are more advantageous than those of 45°--135° causes less increase or greater decrease.

From the standpoint of net forces on panel 2 (Figure 94) immense changes took place. This is not surprising since the net forces on panel 2 for the control nearly balance. Again, the drastic combinations are those of the tall deflector. Its ability to increase the absolute total and even change the direction of the forces at the top of the front roof panel from inward to outward are reflected by the net forces. Since only one test was run at position a_2, and since it caused a large

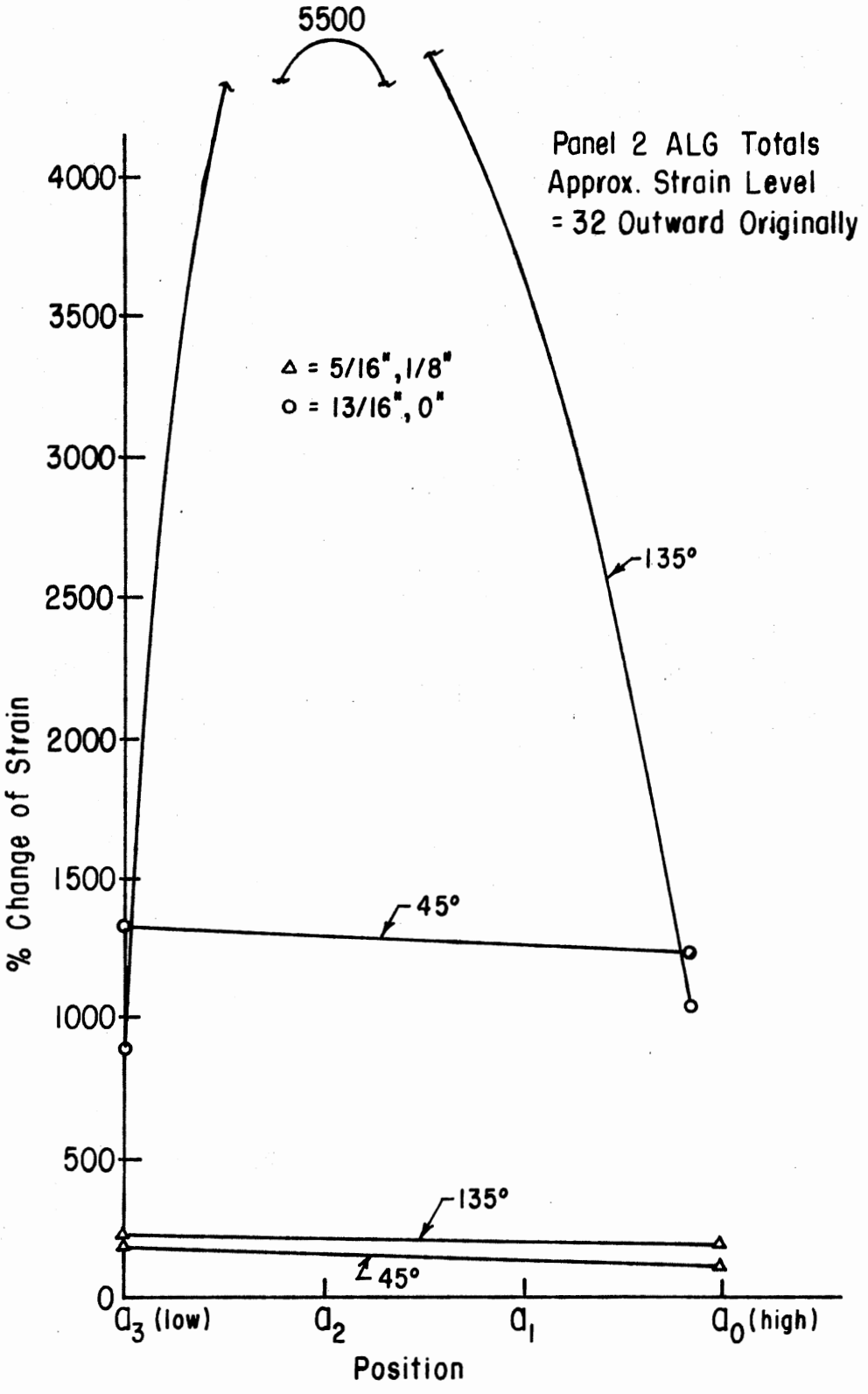

Figure 94. Changes of Panel 2 Algebraic Totals, I(s)-Series

imbalance in the net forces on panel 2 as shown in Figure 94, one can only speculate as to the validity of connecting by straight lines all the other points on this graph.

AV5 and AV6, Figure 95, pose an interesting situation. All the modifications on the leading roof panel resulted in reductions (from 4% to 26%) at 6 on the back panel. It appears that for the short deflector, 135° is best--i.e., produces the greatest reductions--above position a_2. The tall deflector seems to favor positions below a_1 when oriented at 135°. AV5 on the other hand shows increases (21% to 56%) for all combinations of the tall deflector. 45° orientation causes the greatest increase. The increases are also greater for the deflector position nearer to the front of the structure. The short deflector causes universal reduction (0% to 12%) for AV5. 135° causes the greatest declines. The points for both AV5 and AV6 at a_2 again arouse the suspicion that the straight lines may be questionable. The reductions are greater for deflector positions higher on the roof. The manner in which the changes in outward force on panel 3 combine leaves much to speculation (Figure 96). First impressions cause one to surmise that the high increases for the 45° tall deflector with no gap make it an unfortunate choice at all but the highest position on the other roof panel. Were its behavior defined at deflector positions a_1 and a_2, however, that might not be true, since, for 135° orientation, a_2 shows reduction of the outward forces--the increase in the 5's being cancelled by the decrease in the 6's. It would be very interesting, also, to know the actual behavior resulting from use of the short deflector at positions a_2 and a_1. On the basis of what is known, the best choice is 135° orientation for the short

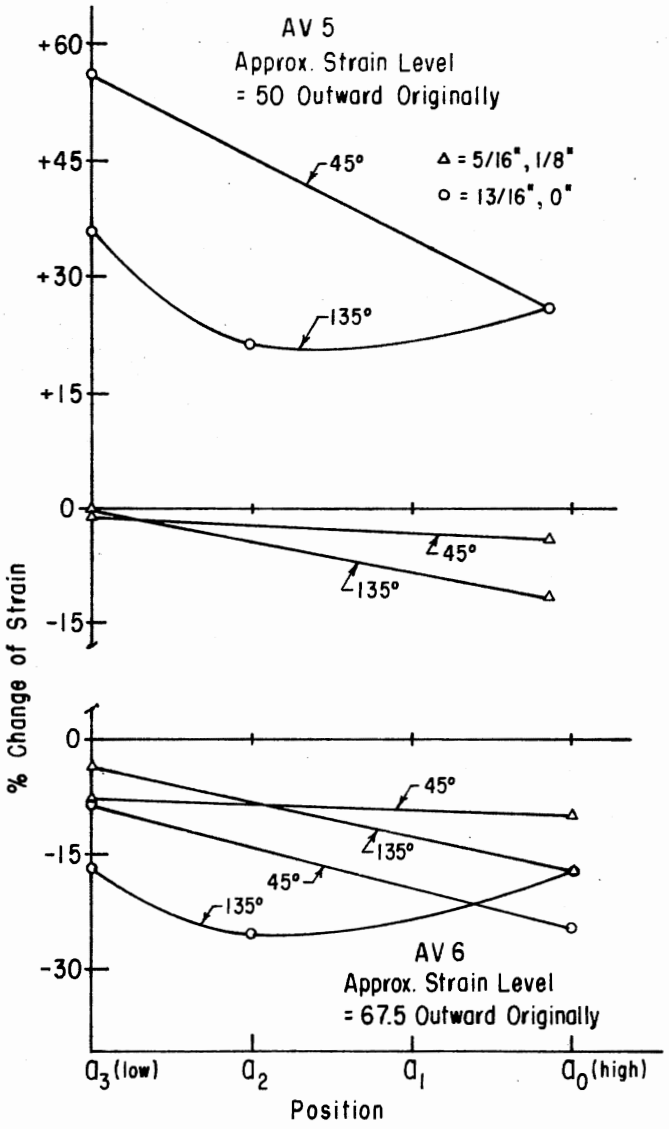

Figure 95. Changes for Gages 5 and 6, I(s)-Series

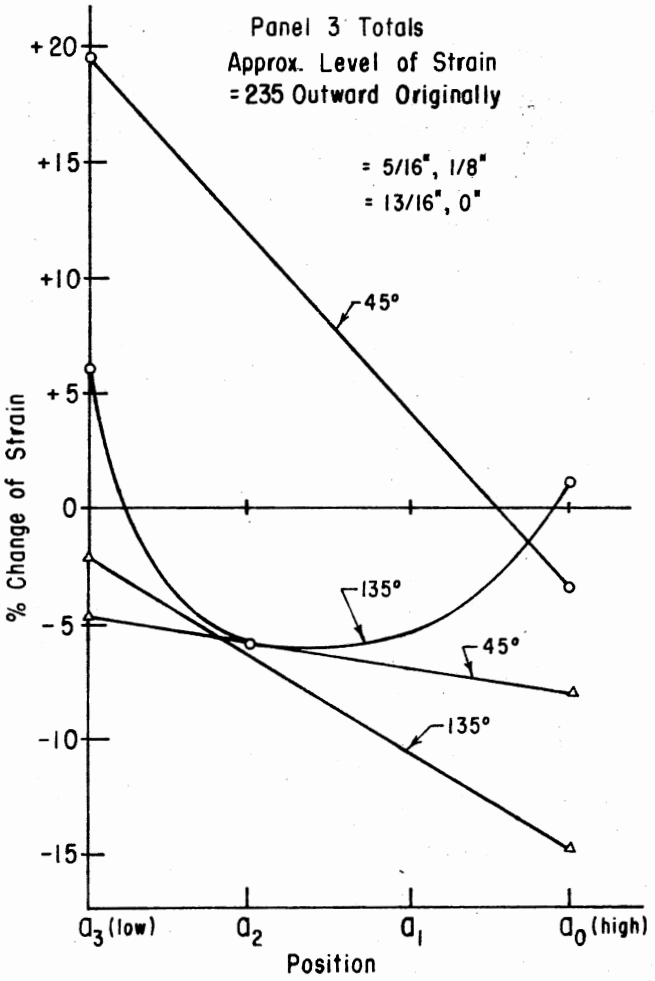

Figure 96. Changes for Panel 3 Totals, I(s)-Series

deflector with the 1/8" gap on the model at the high position on the roof where 15% reduction is noted in the total outward forces of panel 3.

On panel 4, the changes are always reductions, sometimes nearly 100%--meaning forces drop to near zero. Both AV7 and AV8 display similar behavior as seen in Figures 97 and 98. The large deflector, with no gap causes the greater reductions. Apparently the greater the deflection of flow on the front portion of the building, the greater the reduction on the back surfaces. Exception is noted at AV5 where the greater disruption caused higher increases. Similarity is noted for the behavior of the 45° orientation for both the tall and short deflectors. With the deflector at a_3 position on the front roof, a reduction occurs on the back wall but as the position is varied, the reduction is diminished. The 135° orientation, however, causes increasing reduction on the back wall as position changes from a_3 to a_1. Quite a difference in the patterns of the tall deflector with no gap and the short one with a gap are noticed. Whereas for the latter, the 45° and 135° curves show the same reduction at the low position (α_3), they diverge as the deflector was moved up the roof; the 45° curve gradually shows less reduction while the 135° shows more. The tall deflector with no gap shows quite different results for the two orientations at the low position, but the results gradually converge as the deflector was moved up. The 135° orientation curve drops to meet the rising 45° orientation curve. The main difference is actually the relative positions of the 135° and 45° curves for the large deflector. Whether this difference is due to the height of the deflector or the presence of the gap, it is impossible to know.

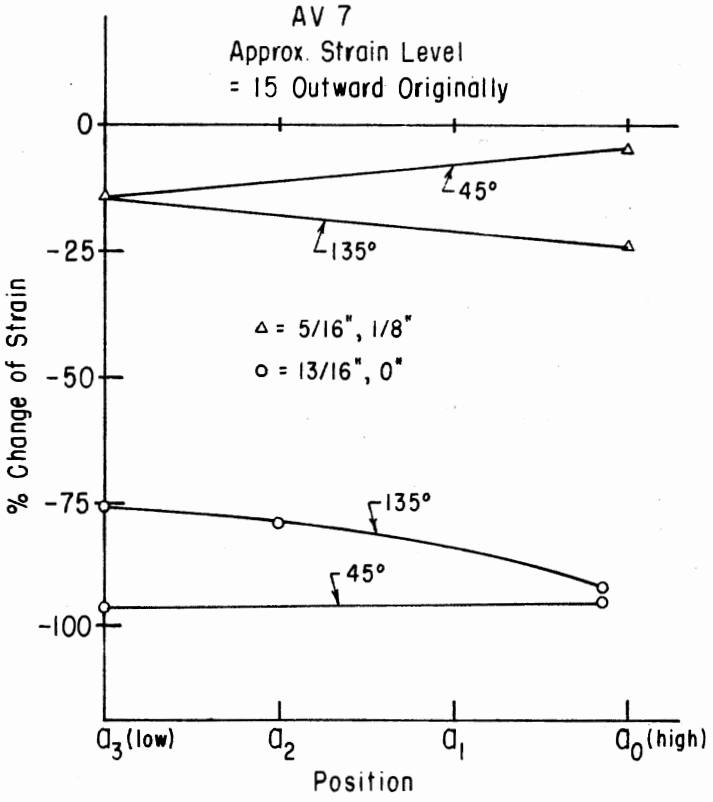

Figure 97. Changes for Gage 7, I(s)-Series

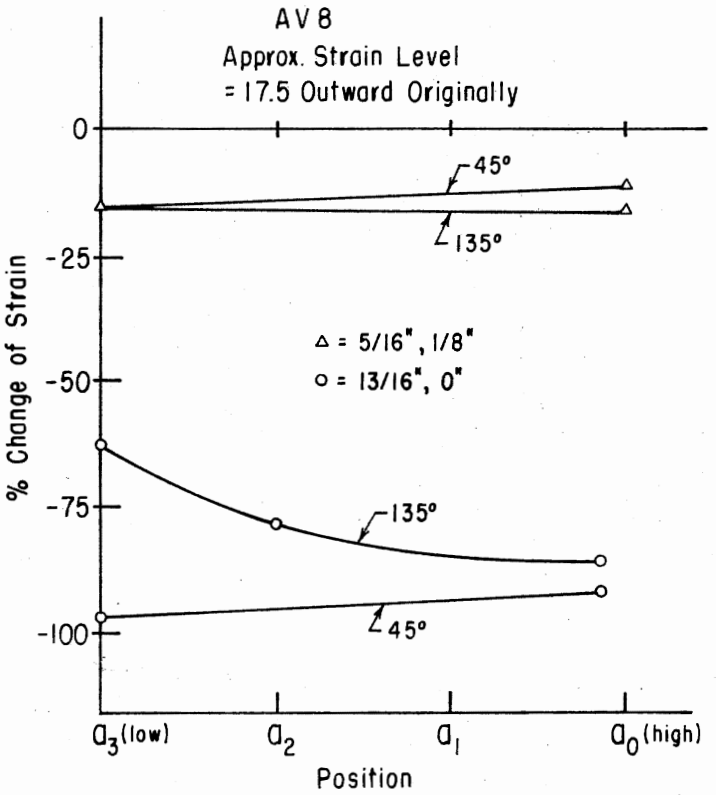

Figure 98. Changes for Gage 8, I(s)-Series

However, it is easy to suspect that the difference in magnitude of the changes plotted is due to the height of the deflector whereas the difference in relative position of the 45° and 135° changes is due to the gap.

Panel 4 forces, in Figure 99, which are all outward, are reduced the most by the large deflector with no gap and 45° orientation. Almost 100% reduction is noted for the low position. All the positions and orientations of this deflector result in reductions of 70 to 100% . However, the forces are low and rather insignificant in magnitude. Reductions of 10 to 20% are noted for the short deflector with a gap. The same behavior pattern of AV7 and AV8 is reflected here since the two were nearly identical to each other in magnitude and changes.

The inward forces on the structure can always be reduced by both modifications as seen in Figure 100. Small changes in panel 1 inward forces and the complete reversal of AV4 from inward to outward have both been previously discussed and are the causes.

The outward forces initially at AV3, AV5, AV6, AV7 and AV8 individually undergo great changes but combine in a surprising way (Figure 100). The large deflector advantages at AV6, AV7 and AV8 are outweighted by the tremendous increases for AV3 and the inward to outward tendency of AV4. The 45° orientation causes the greatest increases. The short deflector with a gap caused less drastic changes at all the monitoring points, yet the <u>only</u> reductions in total outward forces are shown for it--high on the roof, at least beyond a point between a_2 and a_1. The 135° orientation is best where 8% reduction is possible at a_0 and 3% at a_1. It appears that tests with the deflector at position a_2 would alter but little this conclusion.

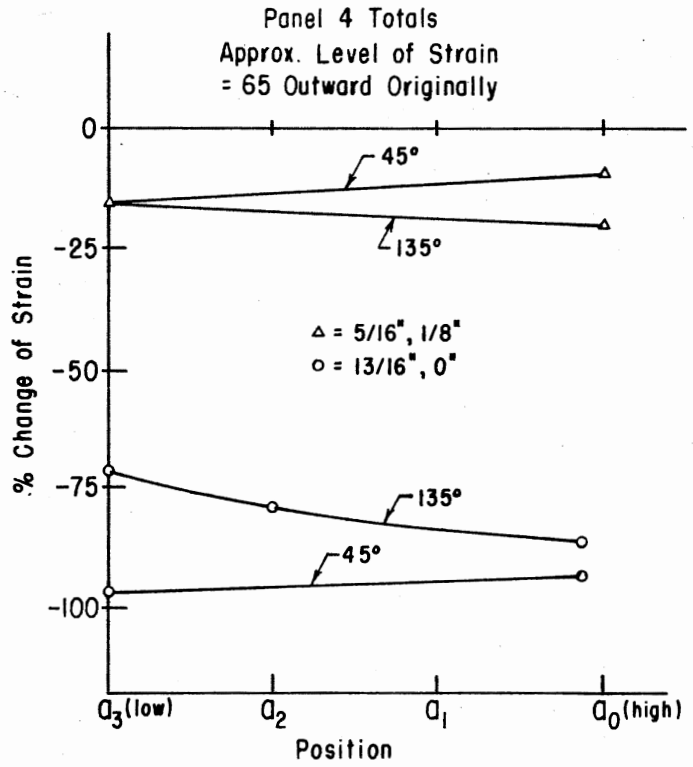

Figure 99. Changes for Panel 4 Totals, I(s)-Series

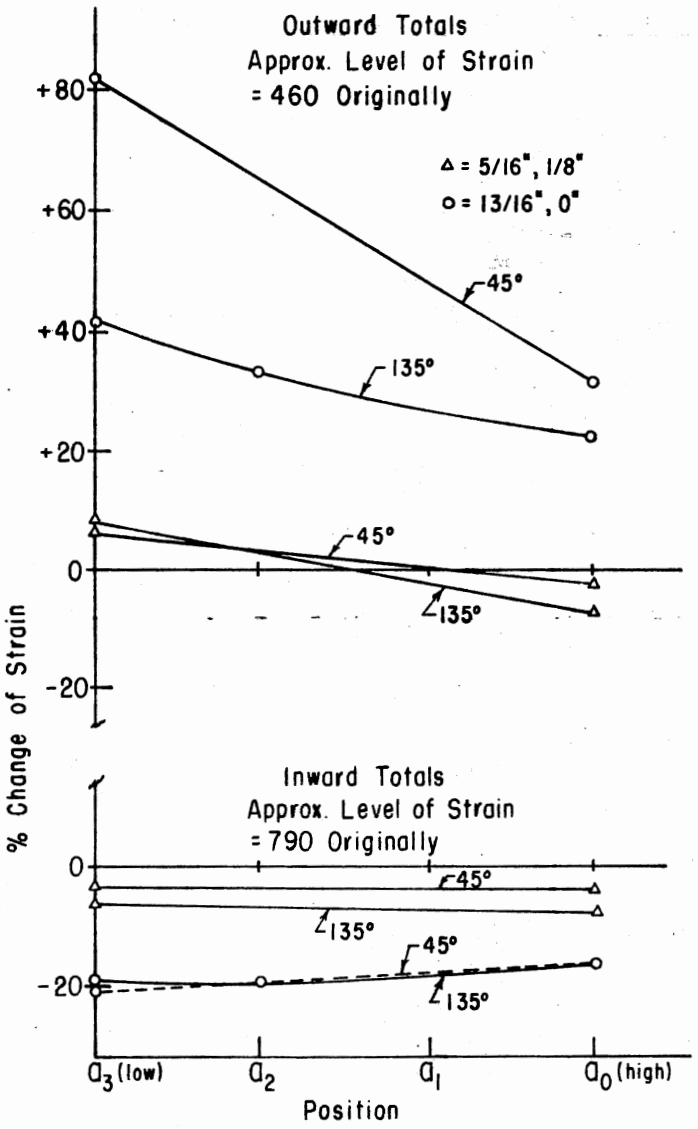

Figure 100. Changes in Outward and Inward Totals, I(s)-Series

Total absolute forces, in Figure 101, show reductions for all the modifications except for the 45° orientation of the large deflector with no gap. The 135° orientation of the small deflector with a gap is universally the best, and moreso at the higher position on the roof, a_3, where an 8% reduction is possible.

Total algebraic or net forces show reduction for all modifications. Some show changes of over 100%, meaning that the net forces are changed from being initially inward to outward with the modifications. Figure 102 shows the changes that do occur. The next to the lowest curve, I-16(s), will serve as a base to understand the others. With the large deflector, no gap, oriented at 135°, low on the roof, the inward and outward forces are nearly balanced. In fact, in that situation, the 100%+ change has made the balance on the outward side, instead of inward as with the controls. The way this has occurred, however, is by a large increase in outward forces 40% (mainly on panel 2) along with a 20% decrease in inward forces (again, mainly on panel 2 at AV4). This resulted in a better overall balance of forces for the building but an increase in the overall absolute force level of 3% and a drastic imbalance on panel 2. The 45° orientation is worse yet. Verification of this is also apparent in Figure 89 comparing I-16(s), I-17(s) and the control I-23(s).

The real significance of the algebraic or net totals lies in its indication of redistribution of the forces. The absolute total may even remain constant for some modifications as forces change from outward to inward, but the presence of those changes will be reflected in the change of the algebraic total. I-12(s) is an example where the total absolute forces as indicated by the strain readings remain

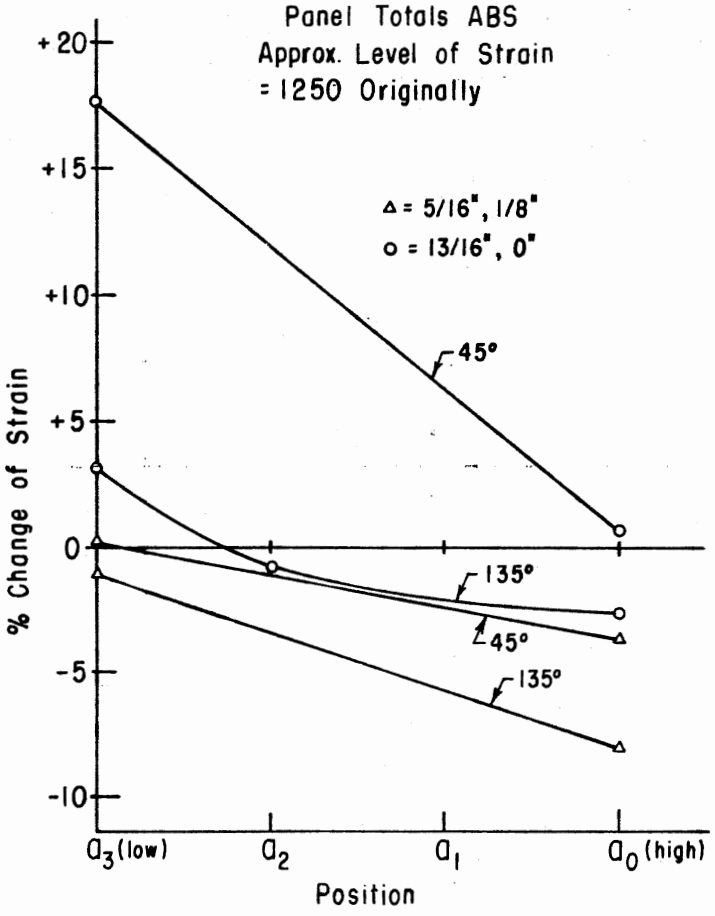

Figure 101. Changes for Panel Absolute Totals, I(s)-Series

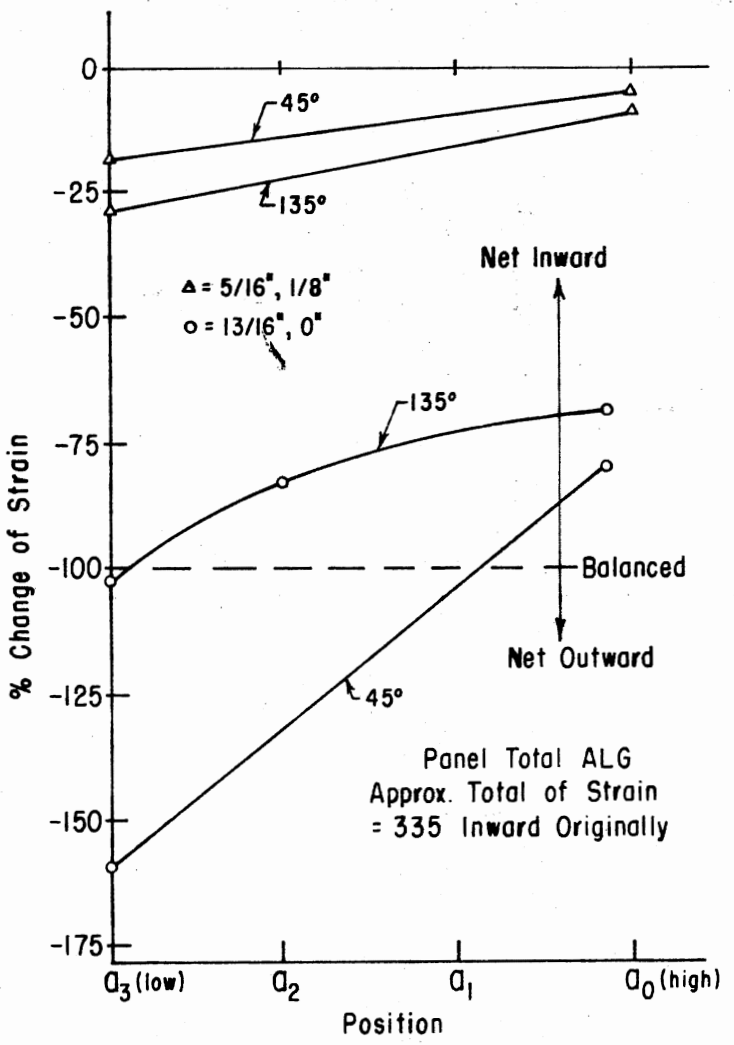

Figure 102. Changes for Algebraic Panel Totals, I(s)-Series

1253.67 for the modification as compared to 1252.6 for the control. The initially very high inward forces drop from 781 to 753.3 (-3.5%) and the total outward forces change from 471.6 to 500.3 (+6.1%). The algebraic total reflects this immediately by a -18% change, a better balance. Still the location of these changes may be a detriment if critical forces were increased as was the case here where the worst outward force, AV3, increased some 25 units (30%).

The algebraic totals reflect extreme redistribution of forces is possible with the deflectors. Only the 135° orientations are desirable. More extreme redistributions take place at lower positions on the roof and with the larger deflector. 45° causes the most extreme changes (-160%) for the large deflector--even complete reversal of the inward predominance. 135° orientation results in complete reversal only at a_3 (-102%). Since only the small deflector achieves reduction of the algebraic total forces by reducing the outward and inward forces, the large deflector cannot be considered beneficial.

Conclusions - Deflectors, Sealed Model. It is regrettable that the increase universally caused at AV3 occur since they are often quite large and overshadow the gains elsewhere. AV3 is also originally the point of highest outward force. More complete testing is desirable at positions a_1 and a_2. The large deflector, 13/16" tall, differs radically in size from the small one, 5/16" tall. At least one size in between, and possibly three (7/16", 9/16" and 11/16") would have documented the changes more completely. The presence or lack of a gap, with even the two sizes of deflector, would have been helpful. It is unlikely that discovery of what is actually occurring could be

determined without testing all the options, at each position with its own control, since the evidence indicates all the variables are not adequately defined by the similitude analysis--and would, indeed, be difficult to define. It is likely that the separated air flow at the leading edge of the roof reattaches itself back to the roof surface in a myriad of different ways as affected by the deflector. Even the most subtle change in position on the roof or orientation of the deflector could cause radical differences in the flow pattern. The effect of a gap under the deflector could have the same effect. A different shape of deflector or a vented deflector might cause discovery of a method to favorably alter the air flow also.

The data, incomplete as it may be, shows evidence of certain trends which can guide any future effort.

The 45° orientation (at least with no gap) is not beneficial in that it leans into the wind without being able to direct any air flow underneath it. That might aid its alteration of the air flow to be more favorable.

The earlier the air flow is disrupted and the more it is disrupted, the greater are the inward reductions for AV1 and AV2 and the greater are the outward increases for AV3. Beyond the deflector--i.e., at AV4, AV6, AV7 and AV8, the greater disruption of the taller deflector causes greater changes. Deflector positions nearer the ridge cause higher changes in general. AV5 is puzzling as the 13/16" deflector behavior falls into the "before" category of AV3 but the 5/16" deflector with the gap behaves like the other "beyond" situations.

The most promising of the deflectors tested is the 5/16" height with a 1/8" underneath and oriented at 135°--I-26(s). Its most

effective position is nearest to the ridge of the roof where it changed the levels of recorded strain as follows:

AV1*	-0.6%
AV2*	-1.0%
AV3	+8.5%
AV4	-52.7%
AV5	-116.%
AV6	-17.3%
AV7	-24.5%
AV8	-16.5%
Panel 1*	-0.7%
Panel 2	-17.6%
Alg. Panel 2	+187.2%
Panel 3	-14.8%
Panel 4	-20.1%
Inward*	-8.4%
Outward	-7.6%
Panel Total Abs.	-8.1%
Panel Total Alg.	-9.4%

* Inward forces

The only increase, that of AV3 (8.5%), was overcome by the reductions elsewhere--still it remains the critical outward force. The high increase for panel 2 algebraic forces results from being predominantely outward initially and the above mentioned outward increases at AV3 combined with a greater drop in inward forces at AV4. This results in the net being more outward than initially.

Much more needs to be known about this option. Tests in the vicinity of AV4 itself would seem very appropriate in addition to the previous suggestions. The deflector concept certainly has merit but was dropped from the final study because of the AV3 increases and the hope of a more promising alternative.

Airfoils

Objective. The primary objective of this group of modifications was to determine the potential beneficial effects of attempting to turn the air flow down the back side of the building. For an unmodified building of the same shape, the abrupt boundary change at the ridge of the roof makes it impossible for the air flow to follow the building geometry and separation occurs. It was hypothesized that perhaps the concentrated air flow at the ridge, upon diversion down the back roof into the normal wake area, might cause redistribution of forces which would result in reduction of all the forces or at least those most critical.

Method. Limited trials of one type of airfoil showing the most effects in the smoke studies were undertaken as a preliminary investigation to see if the concept had merit. The roof ridge modifications were mounted along the upper edges of both roof panels. The tests were carried out at top velocity for the wind tunnel and only with the building model perpendicular to the main flow of the wind. The tests run were part of a larger series to be run should the modification look promising. The airfoil could be assembled several ways in order to incorporate different options.

Initial tests were run on the unsealed model as the dramatic importance of even a little leakage had not yet been discovered. Later select options were rerun under "sealed conditions".

Equipment Unique to the Airfoil Investigation. The airfoil configurations tested are shown in Figure 103. The symbols used are:

e - denotes the width of the airfoil down the roof slope. Two widths were used:

e_1 = 1-1/2", 6.25' full scale

e_2 = 2-1/4", 9.375' full scale

d - is the least distance of the airfoil from the roof's surface, measured perpendicular to the surface of the roof.

d_1 = 7/16", 21-7/8" full scale

d_2 = 5/16", 15-5/8" full scale

d_3 = 0"

β - indicates the angle of inclination of the airfoil with respect to the roof's surface.

β_1 = 0°

β_2 = 3°

β_3 = 6°

A fourth angle was utilized in supplemental tests, that of -6°, again maintaining the same values for d. It is designated $-\beta_3$, or simply -6°.

In Figure 104 half of $e_2 d_2 (-\beta_3)$ is shown on the left, whereas half of $e_2 d_2 \beta_3$ is shown on the right. During actual use, the modification was symetrical on both sides of the ridge. Figure 105 shows

II ALTERNATIVE - AIRFOILS

e	d	β	ORDER
e_1	d_1	β_1	8
		β_2	10
		β_3	9
	d_2	β_1	4
		β_2	6
		β_3	5
	d_3	β_1	7
e_2		β_1	14
	d_2	β_1	1
		β_2	3
		β_3	2
	d_1	β_1	11
		β_2	13
		β_3	12
e_1	d_1	$-\beta_3$	9(A)
e_2	d_1	$-\beta_3$	13(A)

$\beta_{1,2,3} = 0°; 3°, 6°; -\beta_3 = -6°$

$d_{1,2,3} = \frac{7}{16}", \frac{5}{16}", 0$

$e_{1,2} = 1\frac{1}{2}", 2\frac{1}{4}"$

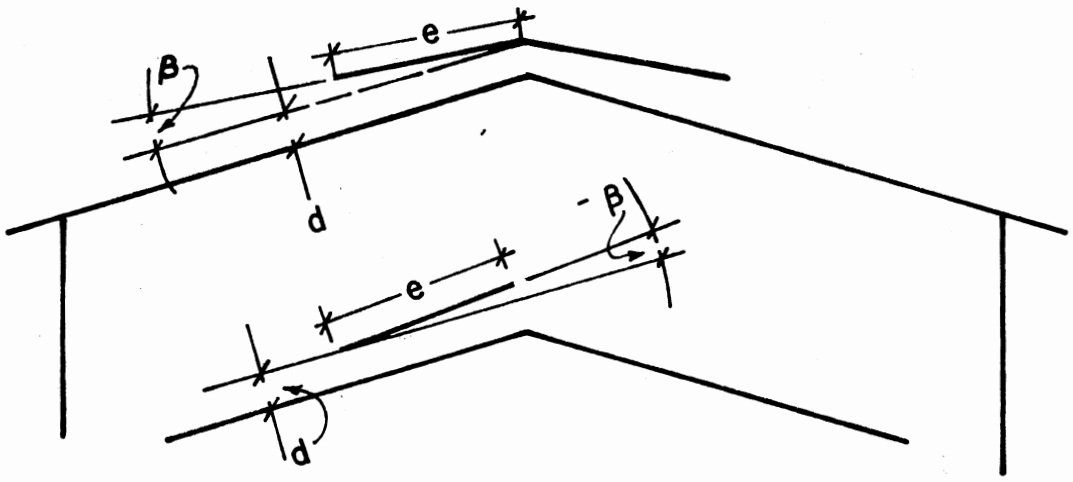

Figure 103. Airfoil Configurations Tested

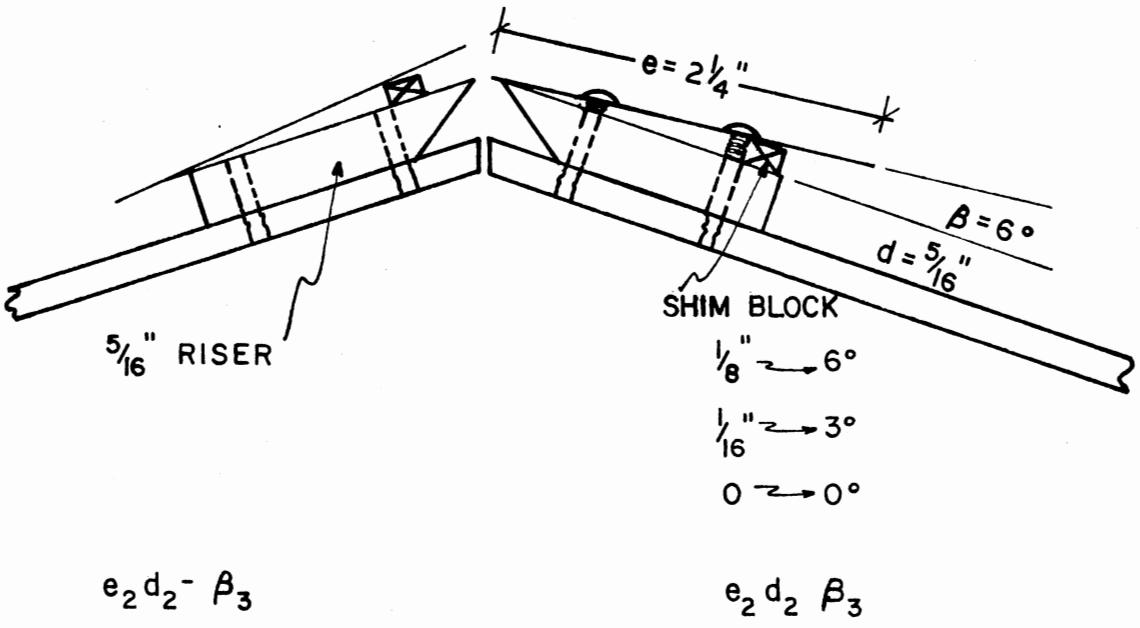

Figure 104. Airfoil Apparatus, β = -6°, β = 6°

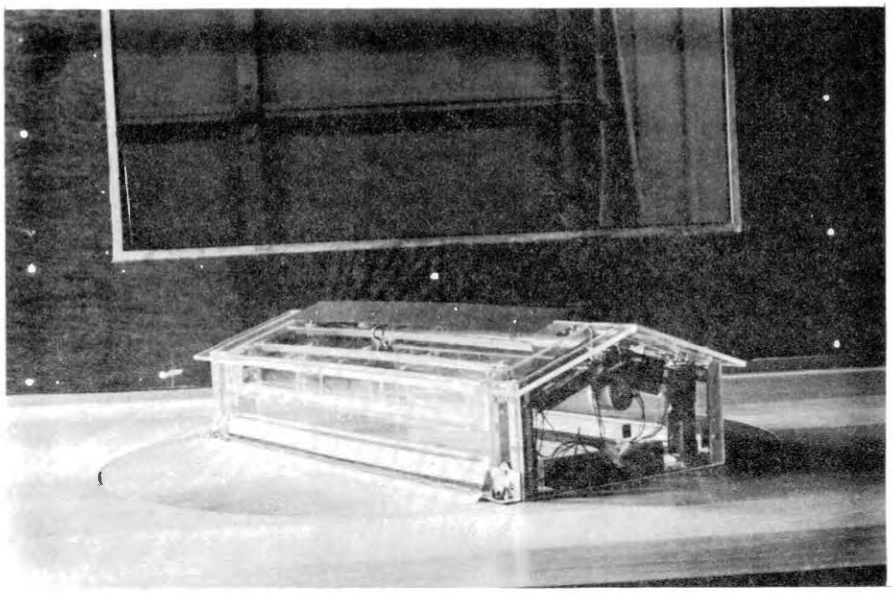

Figure 105. Airfoil $e_{2}\,d_{2}(-\beta_{3})$ on the Model

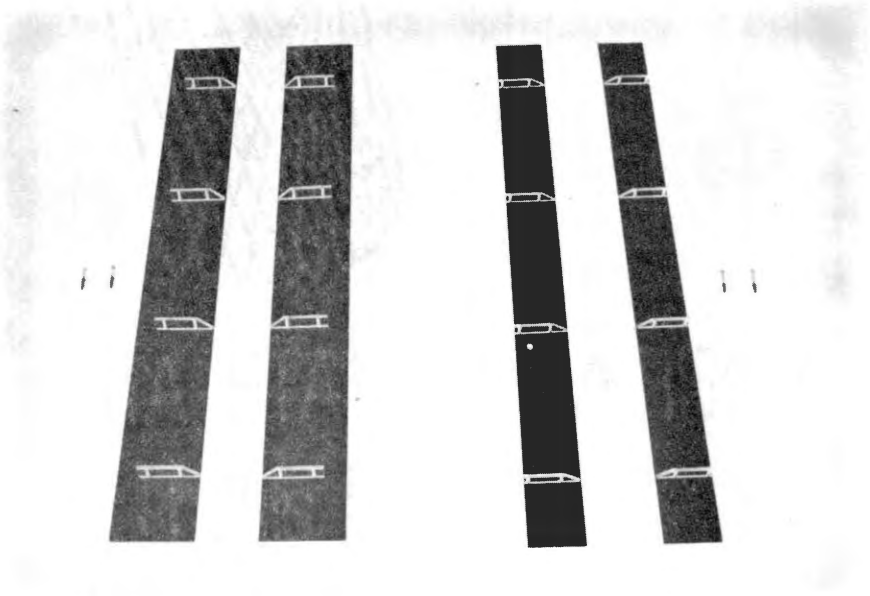

Figure 106. Airfoil Equipment Disassembled

the model with $e_2 d_2 \beta_1$ in place and in Figure 106 is displayed the equipment described. The tall risers (7/16" = d_1) are shown with e_2 (2-1/4") and the short risers (d_2 = 5/16") with e_1 (1-1/2"), however, both sets of risers were used for each of the two sets of strips.

The control for the 1-1/2" airfoil is $e_1 d_3 \beta_1$, meaning that the airfoil flat metal strip is fastened directly against the plexiglass roof using the same holes. Except for the influence of the weight of the airfoil, the building behavior should be exactly the same as that of the model with no modification. Likewise, the 2-1/4" control is $e_2 d_3 \beta_1$ and utilized the flat metal strips for the e_2 tests.

When d_1 (7/16") was used almost a 1/8" gap existed between the two strips at the highest point--i.e., directly over the ridge of the building. During the two later supplemental tests, II-9(A) and II-13 (A), the angle of -6° produced nearly a quarter inch gap between the two airfoils at the highest point. The 5/16" riser (d_2) produced no gap at these points.

Procedure. The test series listed in Figure 103 were run under "unsealed" conditions. The order of tests was selected at random and the normal procedure described earlier for the quantitative investigation was used.

To obtain the various angles, β, small shim blocks were used between the metal strips and the riser, either against the front screw or against the back screw. One-eighth inch shims produced the 6° change and 1/16" resulted in 3° of change. All the data was taken using X.1 and 5 settings of the recorder amplifiers.

Results - Airfoils, Unsealed Model. The data have again been plotted without reduction for calibrations and velocity so that a quick preliminary evaluation could be made. The only exception is that A3 and B3 were multiplied by 1.5 since the stiffness of those beams was greater by approximately that amount.

The general force pattern (Figure 107) on the unsealed control shows the highest forces to be outward on the lower leading part of the front roof (A3 and B3). Next are A6 and B6, on the lower edge of the back roof, followed by the front and back wall forces. Lowest are the forces at the top of the front roof. All are outward except the forces on the front wall.

The pattern for the alterations due to the II-8 modification ($e_1 d_1 \beta_1$) shown in Figure 107 is typical of the 12 tested. It is safe to characterize all by the following remarks.

1. All at least maintain the control level of front wall forces (A_1, A_2, B_1, B_2) or cause slight reduction.
2. All modifications cause forces of the 3's, 4's, and 5's to increase--the 5's rather drastically.
3. The forces of the 6's, 7's, and 8's are reduced.
4. All the forces on the controls and the modifications cause the front wall to be pushed inward and the other surfaces experience outward forces.
5. Forces on 7's and 8's are very similar for all tests employing d_2 and the d_1 tests are similar to each other as well--even though the controls exhibited slight differences on panel 4. The forces at 7 and 8 are not large and no further attempt at analysis will be made.

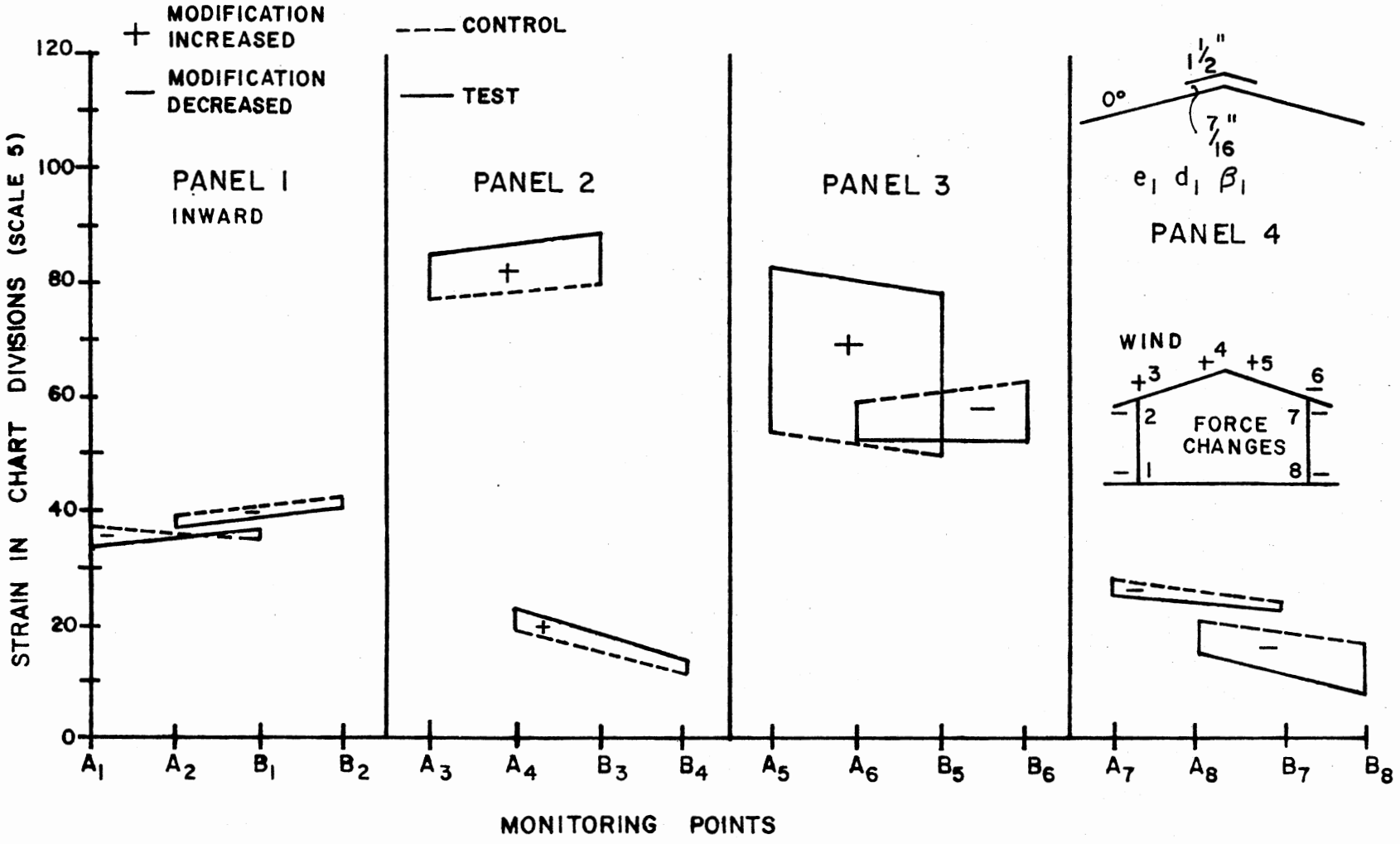

Figure 107. II-8 Versus II-7 Control

6. Both d's for e_2 (2-1/4") β_1 (0°) caused virtually no change in the A4-B4 forces.
7. There is no discernable relationship between the e values tested and the resulting forces.

The Two Additional Tests. Following the planned series two additional tests were added:

II - 9(A), $e_1 d_1$ ($-\beta_3$) and
II - 13(A), $e_2 d_1$ ($-\beta_3$)

Both involved maintaining d_1 at 7/16", however, the angle $-\beta_3$ or -6° was obtained by tilting the airfoil in the opposite direction from the first series.

The two special additions to the planned series provided some interesting and contrasting information, adding to certain of the general results in the first series, but projecting them into a new dimension for roof panels 2 and 3. Inspection of Figure 108 for II-9(A) shows panel 2 forces decrease while all others appear much the same as for II-8. The results for panels 2 and 3 for all 14 of the tests are presented in Figures 109 and 110. The forces for II-9(A) and II-13(A) on panel 1 and 4 show no significant variation from all the other modifications.

Figure 109 shows panel 2 (upwind roof) forces. Even though no data was taken for β = -3°, it is readily apparent that while all of the original series show the 3's to be higher than the control plane, the descending curves pass through the control plane somewhere between 0 and -3°. At -6° the forces for the 3's are lower than the control. The same thing is true of the 4's.

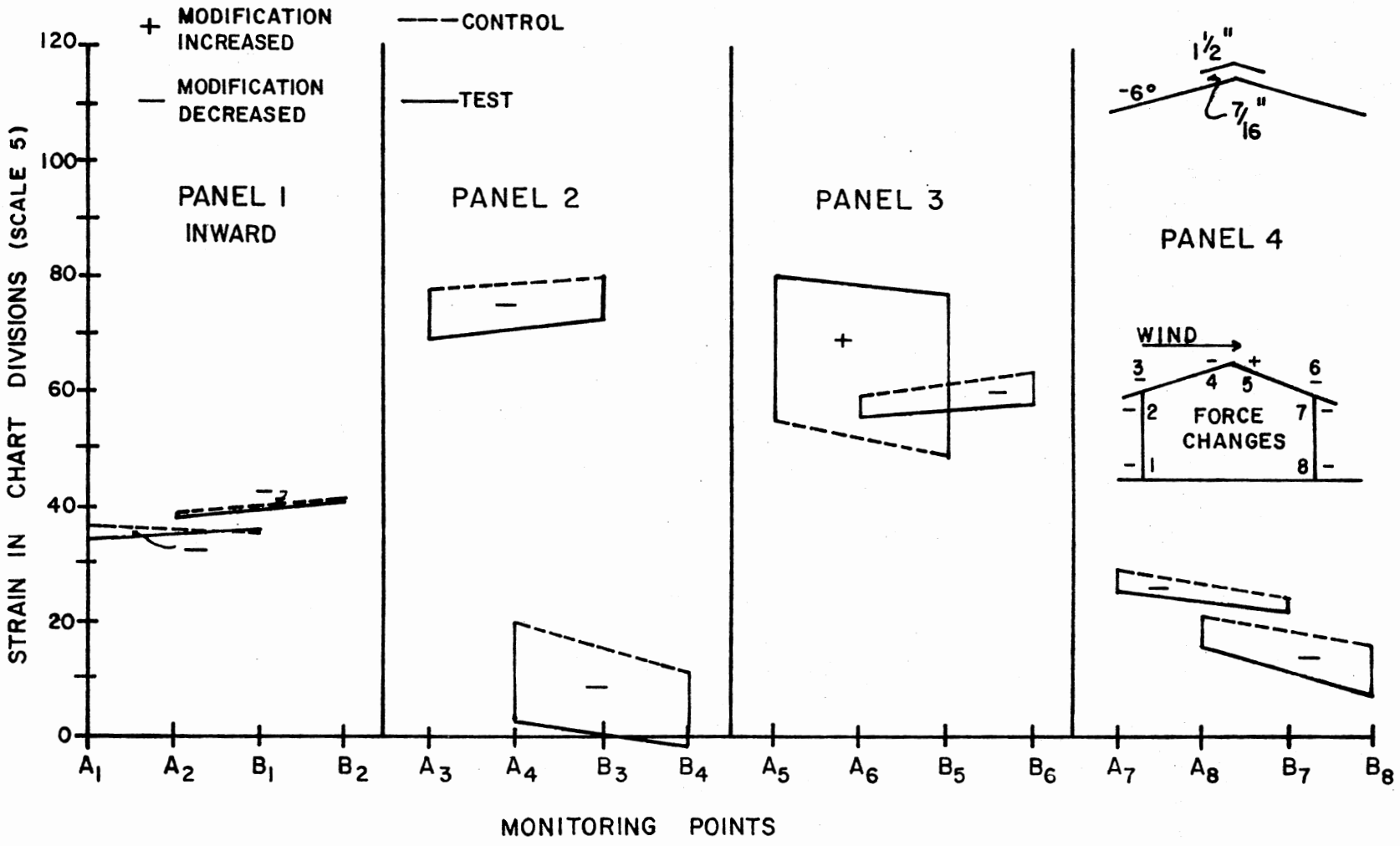

Figure 108. II-9(a) Versus II-7 Control

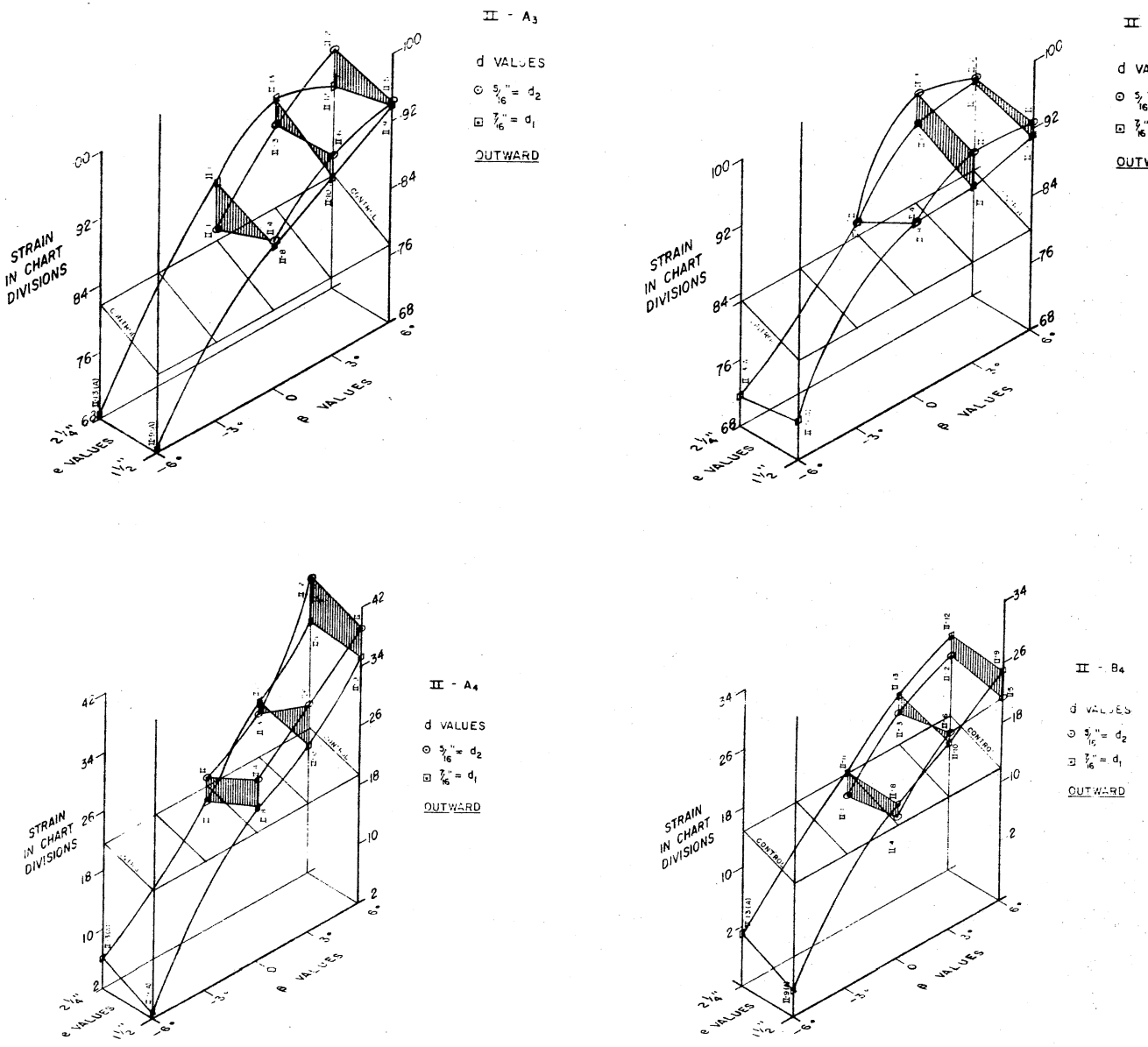

Figure 109. Panel 2 Strain Readings Due to Alternative II Modifications

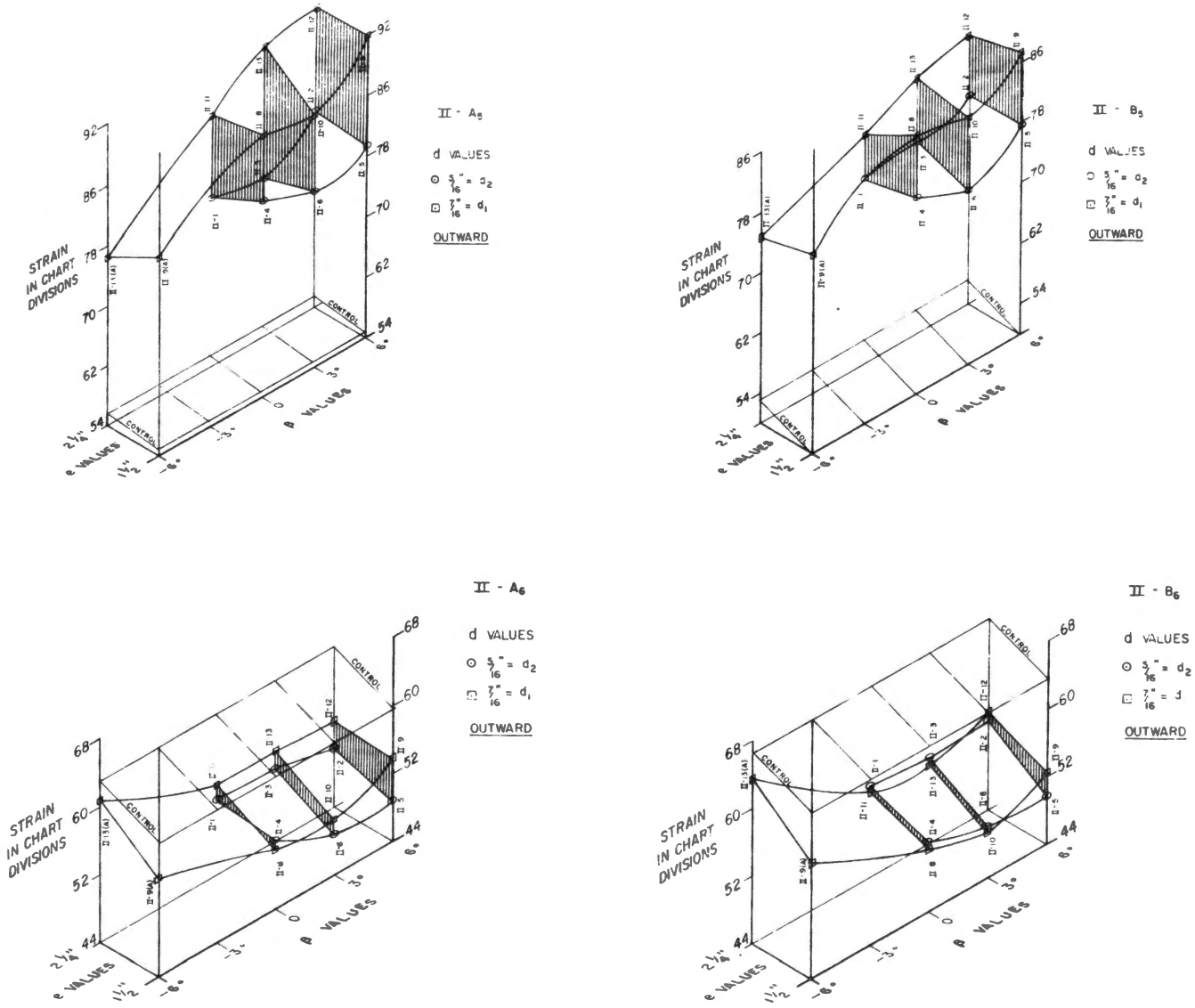

Figure 110. Panel 3 Strain Readings Due to Alternative II Modifications

It may be questionable to plot the results in this way since the data is erratic, limited, and the curves were drawn by inspection. Too, it may not be entirely proper to join the points in this fashion since the pivot point for the airfoil with positive angles is at the ridge whereas the -6° angle was obtained by putting the large shim above the top screw with the pivot point at the front or lower position of the airfoil. (Refer to Figure 104). The problem of the gap between the two halves of the airfoil mentioned earlier also introduced another variable. The trend favoring -6° is unmistakable, however, in spite of these differences.

On panel 3 (Figure 110) the forces at the 5's, though all are well above the control, do nevertheless become lower as the curves approach -6°, meaning there is less increase in the forces. Here the smaller d value (5/16") is seen to result in lesser increases at the monitoring point of the highest forces. The forces monitored for the 6's are all below the control plane but are rising after the curve passes 0° and approaches -6°. This means, of course, that they show a reduction of forces throughout but tend to lose that advantage for a β value of -6°.

The forces on the other two panels show less pronounced changes without such a readily discernable pattern.

The effect of the -6° modifications on the individual monitoring points, on panel forces and upon the model total forces is seen in Table XIII.

Conclusions - Airfoils, Unsealed Model. The original series

TABLE XIII

SUMMARY OF PARTIALLY REDUCED DATA, AIRFOILS--UNSEALED MODEL (RECORDED STRAIN IN CHART DIVISIONS)

	Control II-7	II-9(a)	% Change	Control II-14	II 13(a)	% Change
AV1*	36.33	35.1	- 3.4	35.17	37.17	+ 5.7
AV2*	40.75	39.75	- 2.5	39.42	39.58	+ 0.4
AV3**	78.75	70.50	-10.5	82.38	70.00	-15.0
AV4	15.67	0.25	-98.4	18.17	3.50	-80.7
AV5	52.33	78.83	+50.6	54.50	75.42	+38.4
AV6	61.67	56.67	- 8.1	64.67	62.00	- 4.1
AV7	26.08	23.83	- 8.6	28.42	26.08	- 8.2
AV8	18.83	11.50	-38.9	15.75	13.25	-15.9
Panel 1*	154.16	149.67	- 2.9	149.17	153.50	+ 2.9
Panel 2	188.83	141.50	-25.1	201.09	147.00	-26.9
Panel 3	228.00	271.00	+18.9	238.33	274.83	+15.3
Panel 4	89.83	70.66	-21.3	88.33	78.67	-10.9
Inward	154.16	149.67	- 2.9	149.17	153.50	+ 2.9
Outward	506.75	483.16	- 4.7	527.75	500.50	- 5.1
Abs. Panel Total	660.91	632.83	- 4.2	676.92	654.00	- 3.4
Alg. Panel Total	352.59	334.00	- 5.3	378.58	347.00	- 8.3

*Inward

**now multiplied by 1.5

Recorder Scale = 2

[i.e., without II-9(A) and II-13(A)] is not promising because of the increases on both the 3's (leading edge of roof) and the 5's (at the ridge on back roof panel).

The cause for the increase in the 5's is evident--the air channeled underneath the airfoil has to be turned down by the section of the airfoil mounted on the back side of the roof. It behaves like an inclined plate in the wind and is, in the process, lifted by the concentrated flow. Also, the air flow over the top of the airfoil is faster, creating lift, much as on an aircraft wing.

Still referring to the original series, though the increase of the 5's is large it does not occur at the building's most vulnerable point. Even with the increase, the 5's are but little higher than the original 3's for the control. Equally serious is the universal tendency for increase on the already highest forces at A3 and B3.

The angle β is the most influencial of the variables tested. The extra tests indicated that with $-\beta$ angles, the characteristic increase of the 3's becomes a decrease and the increase for the 5's becomes less. The latter does <u>not</u> exceed the original control value of the previous highest force at A3-B3. In retrospect it is regrettable that more tests were not run using $-\beta$ angles. This could certainly be the subject of future study as this type of ridge airfoil is sometimes used with eave vents for natural ventilation.

There is no conclusive evidence, from the inspection of the curves, that the range of e values tested greatly affect the results. The same is true of the d values <u>except</u> at A5-B5 where the lower value (5/16") resulted in considerably smaller force increases. The influence of the top gap is unknown as it did introduce a difference

between the modifications that was unforeseen. It has simply been noted as existing.

The airfoils definitely can cause reduction of the overall force pattern as evidenced by the two (A) tests and all the tests caused redistribution of the building forces.

For the purposes of this study on the unsealed building, alternative II was dropped in order to search for, hopefully, a more effective means of force reduction.

Other airfoils might well be the subject of further investigation.

Airfoils, Sealed Model. Subsequent to sealing the model, three modifications were rerun, one with two variations, in order to see the differences in the sealed and unsealed force patterns.

The tests run were:

II - 7(s)	control or $e_1 d_3 \beta_1$	(1-1/2, 0.0", 0°)
II - 9(A)(s)	$e_1 d_1 (-\beta_3)$	(1-1/2", 7/16", -6°)
II - 9(A)(s)(s)	$e_1 d_1 (-\beta_3)$	(1-1/2", 7/16", -6°)
II - 8(s)(s)	$e_1 d_1 \beta_1$	(1-1/2", 7/16", 0°)
II - 9(s)(s)	$e_1 d_1 \beta_3$	(1-1/2", 7/16", 6°)

where the s codes in parenthesis are sealing symbols. The first (s) designates sealing of the building model. The second (s) signals that the gap of the airfoils at the ridge was also outfitted with a flexible plastic strip simulating a roof capping. The air was free to pass through the airfoil but could not escape between the two parts of the airfoil at the highest point for the test II-9(A)(s)(s).

Results - Airfoils, Sealed Model. The first difference apparent (referring to Figure 111) is that this supplemental series was run at X.1, and 2, the greater recorder sensitivity, as shown by the higher readings. Relative positions are being compared so this is not a hindrance.

Next, the general force pattern for the control is quite different for the sealed series.

1. Panel 1 forces are now the highest, under sealed conditions, instead of A3 and B3 as with the unsealed model.
2. The next highest control forces are now on gages 3, 6, and 5 in that order.
3. Third in force level are A4 and B4 but now they are inward. Previous tests on the unsealed model resulted in all forces being inward for the front wall and outward for the other three panels.
4. Lowest forces are on the back wall and they are naer zero.

From Figure 111 the force patterns for each of the modifications can be seen. All the modifications have the same e and d values. The major difference therefore is β, the angle of the airfoil with respect to the roof. β varies from +6° to -6° in increments of 3°.

By examining Figure 111 in the sequence 9(s)(s), 8(s)(s), and 9(A)(s)(s) [ignoring for the moment 9(A)(s)] all the effects of each variation in β can be seen on the entire sealed model.

The data was further reduced to analyze the average strains (between the A end and the B end of the model), the panel strains and the model total strains. These are shown in Figures 112, 113 and 114,

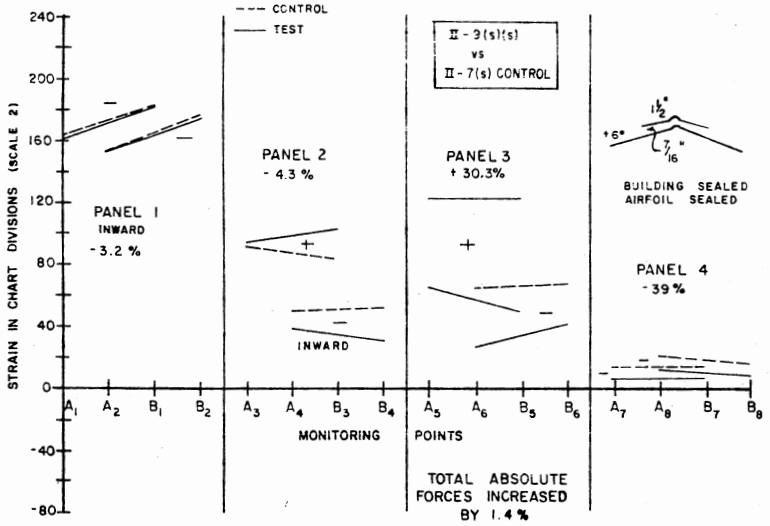

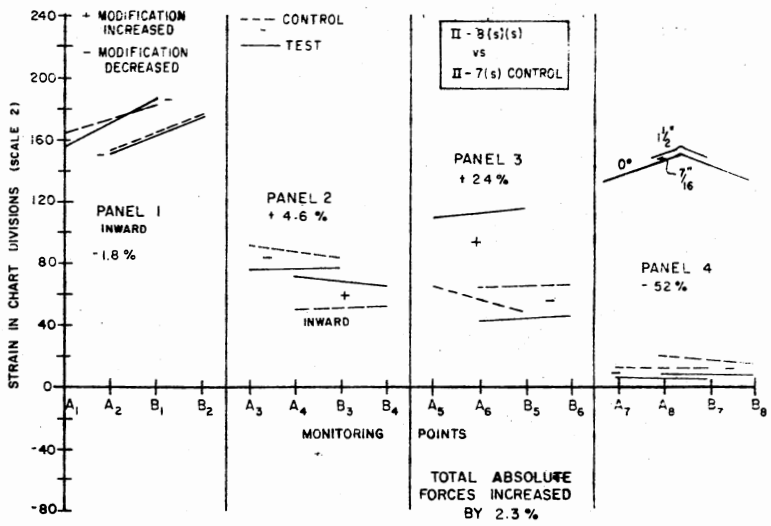

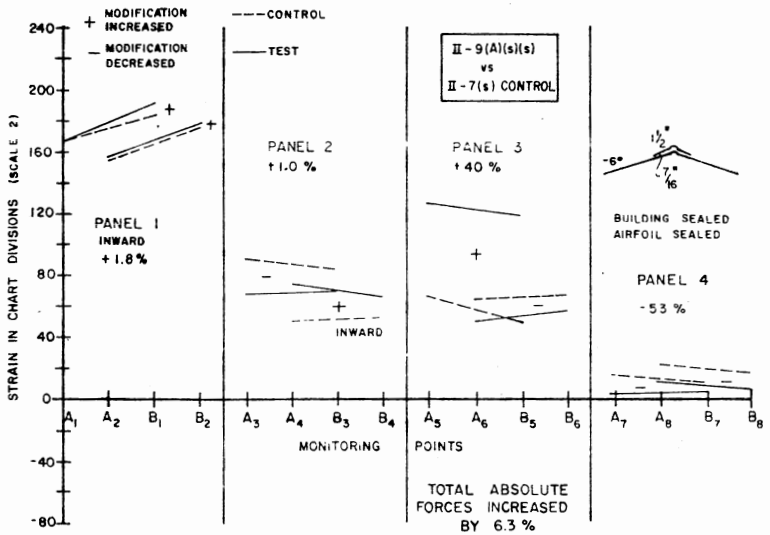

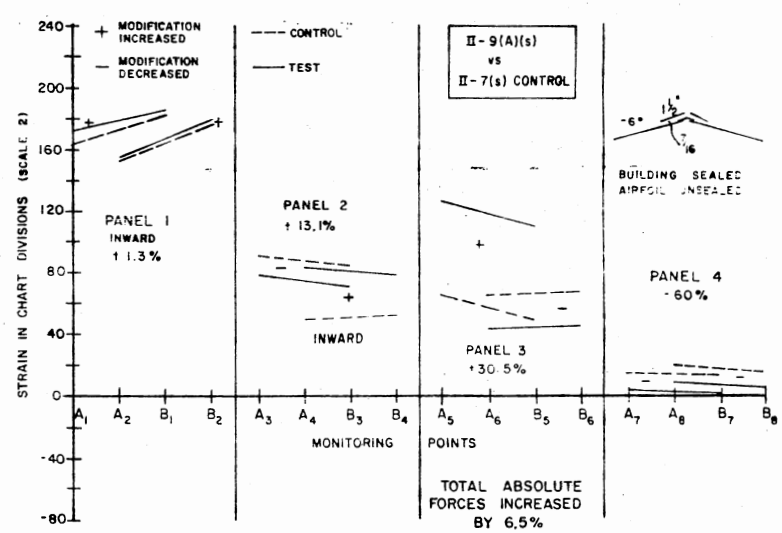

Figure 111. II-9(s)(s), II-8(s)(s), II-9(a)(s)(s), II-9 (a)(s) Versus Controls, II(s)-Series

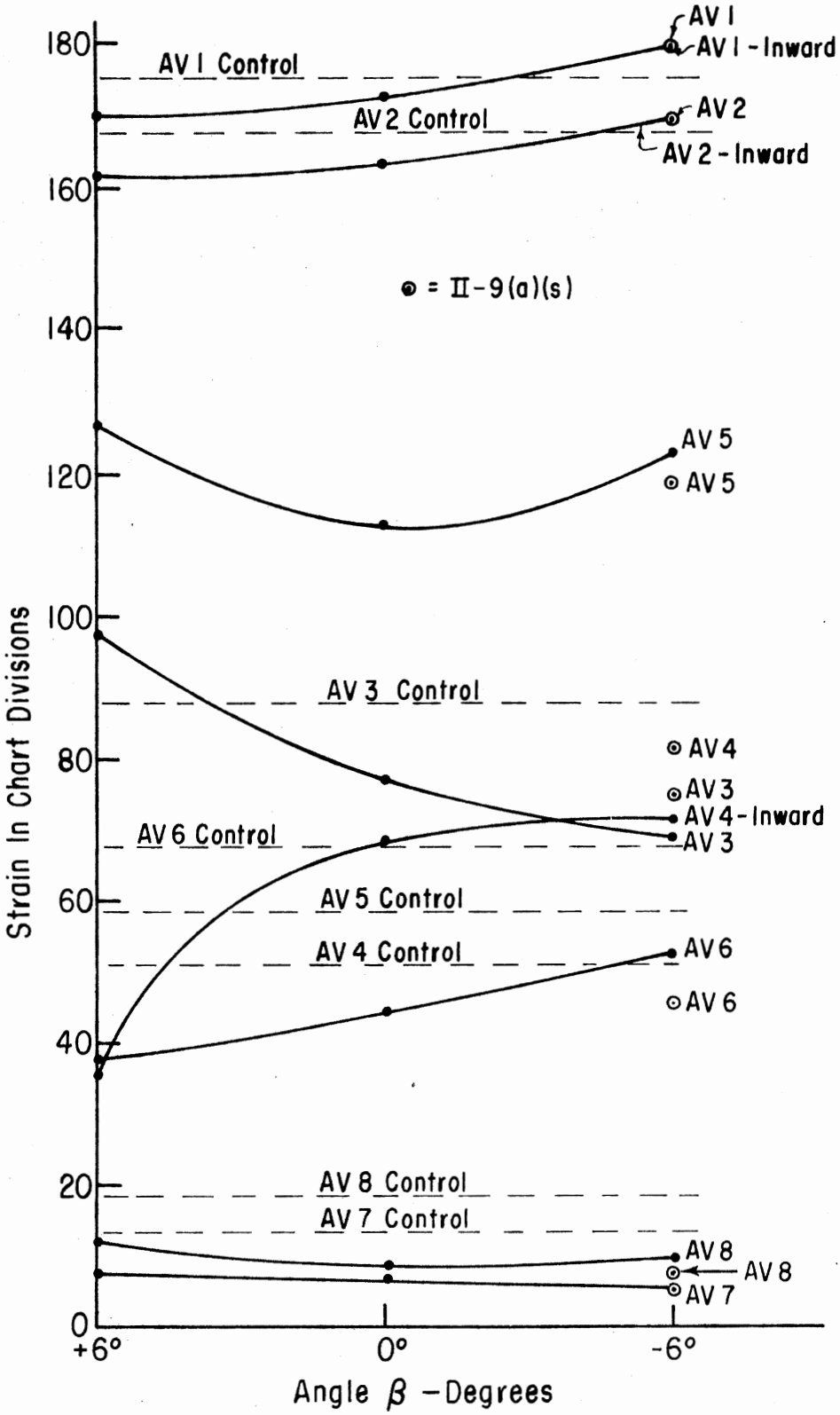

Figure 112. Average Strain Readings at Each Monitoring Point--Airfoils, Sealed

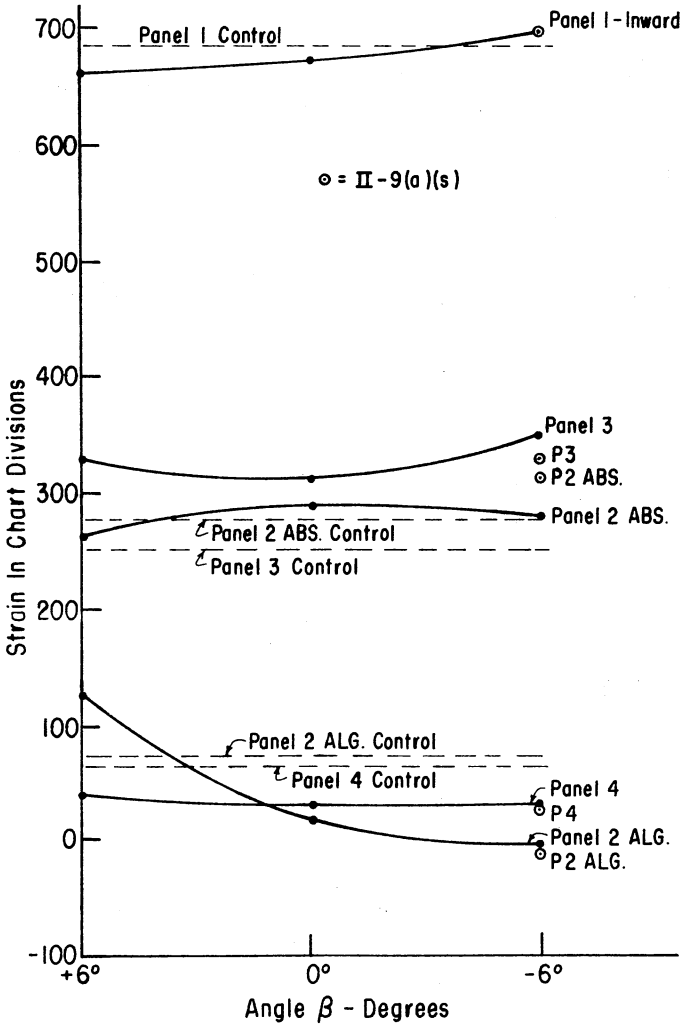

Figure 113. Panel Total Strain Readings--
Airfoils, Sealed

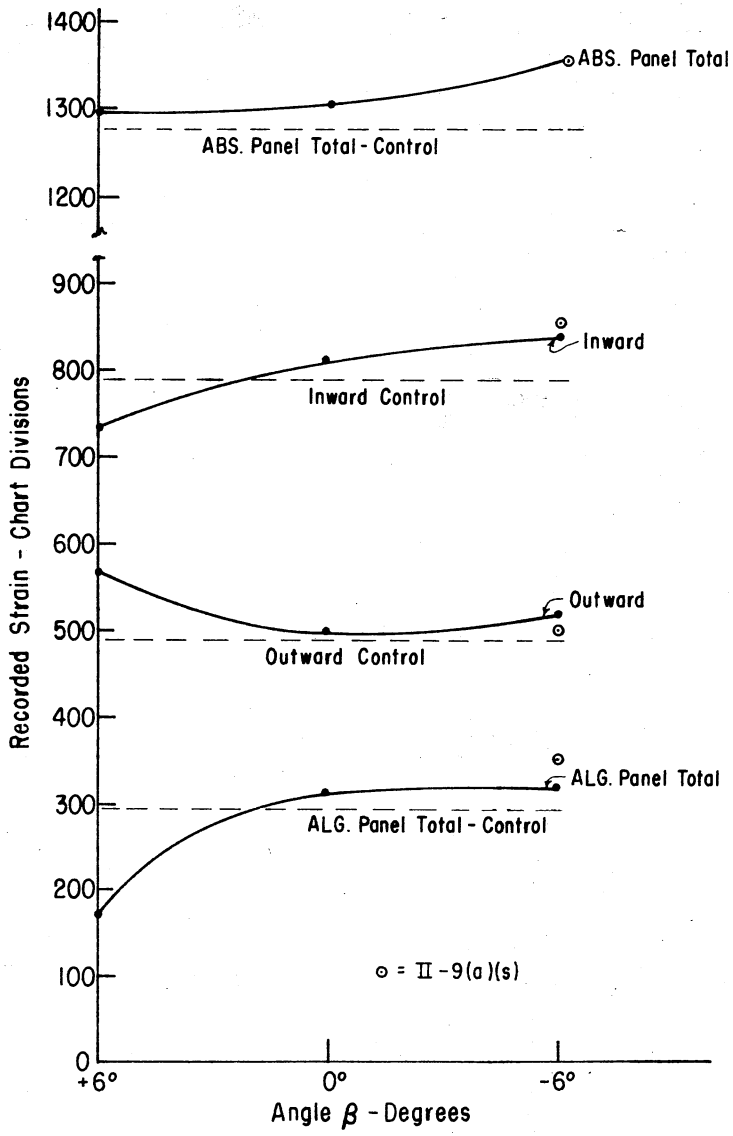

Figure 114. Total Building Strain Readings--
Airfoils, Sealed

and Table XIV.

Inward AV1 and AV2 exhibit similar behavior on the front wall. The decrease is greatest at +6° and the forces, though rising, remain less than the control until -3° and -4°, respectively, as seen in Figure 112. Panel 1 forces reflect the same pattern, as shown in Figure 113.

The outward AV3 on panel 2 is increased over the control at +6° and thereafter continually declines toward -6°, becoming less than the control at ≃+4°. AV4 (inward at the top of the roof) shows an increase as β is varied from +6° to -6°, though it levels out at -6°. The +6° modification results in a decrease with respect to the control but the increase causes it to exceed the control after about +4.5°.

Panel 2 forces are plotted in Figure 113, both absolute and algebraic, since AV3 is outward and AV4 inward. The absolute forces are lower than the control at +6°, but rise to a maximum at 0°, and then fall slightly to the -6° level. After ≃+2°, they are greater than the control. This results from the drop in the outward AV3 being cancelled by the rise of the inward AV4 as β varies from +6° to -6°. The algebraic sum of AV3 and AV4 (Panel 2 Alg. in Figure 113) is higher than the control at +6°, due to the high value of AV3 and the low value for AV4. As the angle β was varied from +6° to -6°, the two, one inward and the other outward, approach the same value as seen in Figure 112. Consequently, the panel 2 algebraic forces, Figure 113, reach the zero level.

The critical AV5 exhibits an entirely different pattern from its behavior for the unsealed model. It is higher at +6° and -6° with its low value corresponding to $\beta = 0°$. All throughout the range

TABLE XIV

SUMMARY OF PARTIALLY REDUCED DATA, AIRFOILS--SEALED MODEL (RECORDED STRAIN IN CHART DIVISIONS)

	II 7(s) Control	II-9(s)(s)	% Change	II-8(s)(s)	% Change	II-9(a)(s)(s)	% Change	II 9(a)(s)	% Change
*AV1	175.00	170.00	- 2.9	172.75	- 1.3	179.25	+ 2.4	178.75	+ 2.1
*AV2	167.50	161.50	- 3.6	163.75	- 2.2	169.25	+ 1.0	168.25	+ 0.5
AV3	87.50	97.50	+11.4	76.88	-12.1	68.63	-21.6	75.00	-14.3
*AV4	51.00	35.00	-31.4	68.00	+33.3	71.25	+39.7	81.50	+59.8
AV5	58.34	126.50	+116.85	112.25	+92.4	123.00	+110.9	118.50	+103.1
AV6	67.50	37.50	-44.4	44.50	-34.1	52.75	-21.9	45.75	-32.2
AV7	13.50	7.50	-44.4	6.75	-50.0	5.25	-61.1	4.75	-64.8
AV8	18.50	12.00	-35.1	8.50	-54.0	9.75	-47.3	7.75	-58.1
*Panel 1	685.00	663.00	- 3.2	673.00	- 1.8	697.00	+ 1.75	694.00	+ 1.3
Panel 2 (Abs.)	277.00	265.00	- 4.3	289.75	+ 4.6	279.75	+ 1.0	313.00	+13.0
Panel 2 (Alg.)	73.00	125.00	+71.2	17.75	-75.7	5.24*	-107.2	13.00*	-117.8
Panel 3	251.67	328.00	+30.3	313.50	+24.6	351.50	+39.7	328.50	+30.5
Panel 4	64.00	39.00	-39.1	30.50	-52.3	30.00	-53.1	25.00	-60.9
*Inward	787.00	733.00	- 6.9	809.00	+ 2.8	839.50	+ 6.7	857.00	+ 8.9
Outward	490.67	562.00	+14.5	497.75	+ 1.4	518.75	+ 5.7	503.50	+ 2.6
Abs. Panel Total	1277.67	1295.00	+ 1.4	1306.75	+ 2.3	1358.25	+ 6.3	1360.50	+ 6.5
*Alg. Panel Total	296.33	171.00	-43.3	311.25	+ 5.0	320.75	+ 8.4	353.50	+19.3
*Inward		$\beta = +6^{\circ}$		$\beta = 0^{\circ}$		$\beta = -6^{\circ}$		$\beta = -6^{\circ}$ Ridge of Modification Unsealed	

**now multiplied by 1.5

of values tested, its levels are greatly increased over the control. The 6's, at the lower edge of the back roof and for all values of β, are considerably less than the control. As β varies from +6° to -6°, AV6 tends to gradually lose, in a linear fashion, its advantage as seen in Figure 112. AV5 and AV6, both being outward forces, combine (panel 3), as seen in Figure 113, to result in a curve that is well above the control but which dips slightly at 0°, then rises to its highest value at -6°. This reflects the most serious fault of the modification--a significant increase in the worst outward panel forces, well beyond those of the unmodified building, due to the drastic increases in AV5 at the top of the back roof. This imposes a severe problem for the fastening tying the roof to the rest of the structure.

AV7 and AV8 (Figure 112) show an advantage but their magnitudes are low, and, though this is academically interesting, it is of no practical significance. Their values are always about one-half the magnitude of the control.

From Figure 114, the absolute total forces are increased over the control for all values of β. An increasing gradual rise exists as β is varied from +6° to -6°. The same gradual rise, though decreasing, is seen for the total inward forces, AV1, AV2 and AV4. However, from +6° to +4° the values are less than the control. These forces would collapse the structure inward, downward and backward.

The total outward forces are much higher than the control for +6°, nearly the same at 0°, and higher again at -6°. The influence of AV5 is dominant. It might be assumed from this curve alone that the 0° modification is favorable. It must be noted that, though

AV3 and AV6 are reduced, AV5 is greatly increased--now to the extent that it is the worst outward force and much higher than was AV3 originally.

The algebraic panel total simply reflects that the total inward and outward forces are better balanced at +6° than any other β value tested. After ≃+1° this is no longer true. In all cases the inward forces prevail, but less so at +6°.

The effects of not sealing the gap at the top of the -6° airfoil, II-9(a)(s), is also plotted in Figures 111, 112, 113, and 114. There it can be compared to both the control and the same modification with the gap sealed, II-9(a)(s)(s). (For both of these the roof of the model was sealed.) Removing the sealing on the airfoil had virtually no effect upon AV1 and AV2. Outward AV3 showed less decline while inward AV4 registered more increase on panel 2. No improvement resulted on either of these two panels. On panel 3, however, some gains are noted. AV5 increases less and AV6 decreases more, resulting in lower outward force for the panel--still though, not enough to change the overall picture with respect to the unmodified structure.

Conclusions - Airfoils, Sealed Model. A very significant modification of the overall force pattern was exhibited. Reductions were achieved for the worst inward forces on the front wall for positive values of β, for the worst outward forces at AV3 as well as for the outward AV6, AV7 and AV8 on the back roof and wall for all values of β. None of these reductions offset the very high increase in AV5 at the top of the back roof. Here much additional lift was generated (nearly double), to the extent that AV5 replaced AV3 as the worst

outward force, at levels higher by ≃33% than AV3 on the unmodified structure. Inward force at AV4 was increased also, though it should not be nearly as serious as the outward increase in AV5.

The d and e values were held constant (7/16" and 1-1/2") since their variation showed no significant results in the unsealed tests (except for d at AV5) and β was the dominant variable. (In retrospect a d value of 5/16" may have had more favorable results on AV5 for the sealed model as well.) The β response was entirely different for the sealed model and there is no proof that some other e and d combination would not be more successful.

Though the variation of the angle β of the airfoil does show the ability to decrease the forces on the sealed model everywhere except at monitoring points 4 and 5, indications are that for any type of airfoil to be successful, the high lift increase experienced at the ridge of the back roof will have to be avoided. A β angle of 0° would seem best because of the smaller increases in outward forces at AV5 and total forces as well. The ridge of the modification should not be sealed.

The results of the airfoil tests on both the unsealed and sealed model could be helpful indications of forces generated on structures utilizing similar natural ventilation methods, and perhaps for certain solar installations, but for the purposes of this investigation, the modification was dropped from further investigation.

Ducts

Objective. The objective of this phase of the preliminary investigation was to determine if contained "leaking" of the pressure built

up on the upwind wall into the wake area of the back wall could reduce the forces induced upon the various parts of the building.

It was hypothesized that this should tend to equalize the pressures and would thus reduce both front and back wall surface pressures. In addition, it was speculated that the flow would be reduced over the top of the building; that this in turn would influence the pressures on the roof surfaces as well.

Smoke studies during the qualitative study indicated that several versions of ducts might accomplish this purpose. Several duct configurations were eliminated as impractical for both prototype and, especially, for the type of model used in this study since it utilized movable panels.

Method. The same wind tunnel model used in the other investigations was used for this study, also. Since the two walls had to move independently, the inlets and outlets could not be rigidly fastened together with the plastic tubes to be used in simulating the necessary duct work. Some means of providing the needed flexibility, and yet maintaining the integrity of flow in the tubes, had to be found.

The tests were run only at the highest wind tunnel velocity achievable and were envisioned to be, again, a part of a larger series of tests to be run should the alternative look promising.

Equipment Unique to the Ducts Investigation. Three sizes of ducts were prepared utilizing Tygon tubing:

1. Small, 1/4" diameter, 12-1/2" full scale
2. Medium, 3/8" diameter, 18-3/4" full scale
3. Large, 1/2" diameter, 25" full scale

The original model incorporated removable sections (17-7/8" by 13/16") in the upper portion of the two walls. These were closed by a slightly larger cover panel used when testing the roof modifications. During the tests on the ducts, the covers were removed and replaced with the apparatus shown in Figure 115. The dark strips are not a part of the apparatus and serve only to support the Tygon tubes for photographing. Two sizes are shown in the photograph. On the left and bottom are the medium tubes and the right and top are the largest ones. The tubes are polyvinyl chloride and were fixed in place with epoxy glue.

The center portion consisted of sections of ballons secured on each end by rubber bands. The centers of the tubes were 3-1/8" from the floor at the wall.

The open area of the 20 tubes, installed 7/8" on center along the 17-7/8" length in the 20-19/32" long front wall panel, can be summarized as follows:

Tube Diameter	Area 1 Tube (in2)	Area 20 Tubes (in^2)	% Total Wall Area	% Panel Area
1/4"	0.0491	0.982	1.066	1.241
3/8"	0.1005	2.109	2.288	2.667
1/2"	0.1964	3.929	4.263	4.968

Procedure. The control was implemented by simply closing the holes, front and back, with a strip of masking tape.

The tests were designated as follows:

small tubes = small III

medium tubes = medium III

large tubes = big III

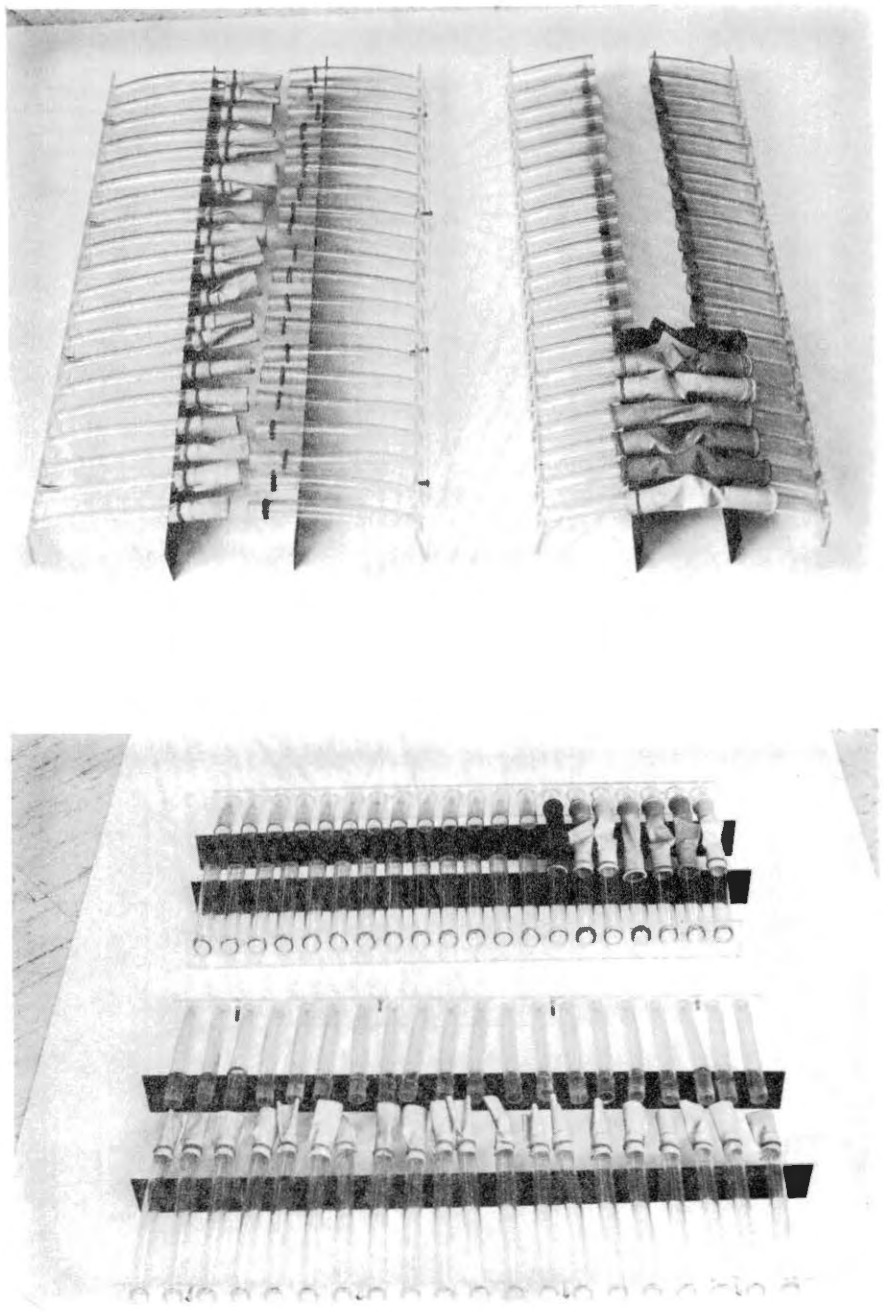

Figure 115. Duct Apparatus Medium III, Left and Bottom; Big III, Right and Top

Tests were run both on unsealed and, later, sealed models. It was during the course of running Big III that the significant differences due to sealing the small building cracks was first discovered.

Big III was run first. Procedures were as described earlier for all the preliminary tests.

Results - Ducts, Unsealed Model. Analysis of the unreduced data, corrected only approximately for the increased stiffness of beams A3 and B3 by a factor of 1.5, showed promise from a theoretical point of view.

Figure 116 illustrates the result on the unsealed model. The control forces are inward on the front wall and outward elsewhere. All show reduction except the forces at the bottom of the front wall, A1 and B1, and those forces are the same for both Big III and the control. None show increase.

The control pattern is typical of the unsealed model with the high forces being on the roof.

With an open area of ≃4.25% of the entire front wall, the forces were reduced as shown in Table XV.

Unsealed Big III was also used as a sample of how the forces would plot if reduced for the various calibration factors. Heretofore, only the "raw data" has been plotted by strain readings in chart divisions, with the 3's multiplied by 1.5 since they are stiffer beams. The comparison can also be seen in Figure 117 in terms of ounces of force.

As noted in Table XVI and marked on the two drawings, in Figures 116 and 117, the results are insignificantly different. Where comparison is the goal, instead of prediction, the more rapid approximate

TABLE XV

SUMMARY OF PARTIALLY REDUCED DATA, DUCTS--UNSEALED MODEL (RECORDED STRAIN IN CHART DIVISIONS)

	Big III Control	Big III	% Change
AV1*	85.33	85.17	---
AV2*	85.83	82.84	- 3.5
AV3	207.75	194.87	- 6.2
AV4	38.83	32.83	-15.5
AV5	148.33	141.50	- 4.6
AV6	164.33	146.83	-10.7
AV7	84.33	80.50	- 4.5
AV8	91.83	83.00	- 9.6
Panel 1*	342.33	336.00	- 1.9
Panel 2	493.17	455.40	- 7.7
Panel 3	625.33	576.67	- 7.8
Panel 4	352.33	327.00	- 7.2
Inward *	342.33	336.00	- 1.9
Outward	1470.83	1359.07	- 7.6
Abs. Panel Total	1813.17	1695.07	- 6.5
Alg. Panel Total	1128.50	1023.07	- 9.4

*Inward

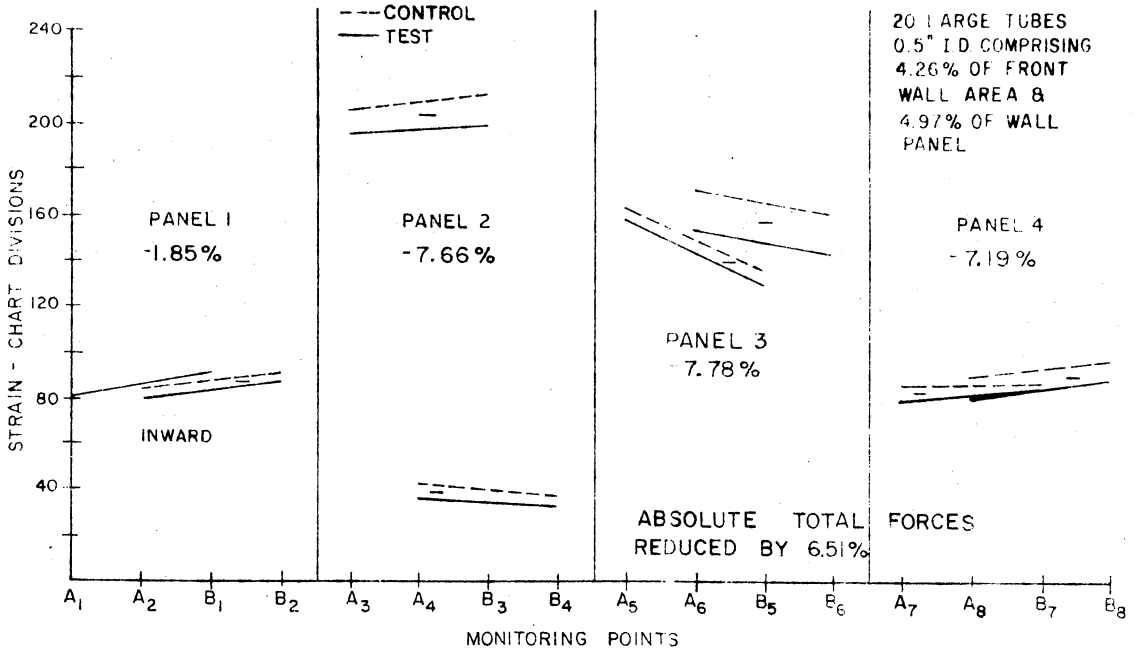

Figure 116. Big III Versus Control--Strain in Chart Divisions

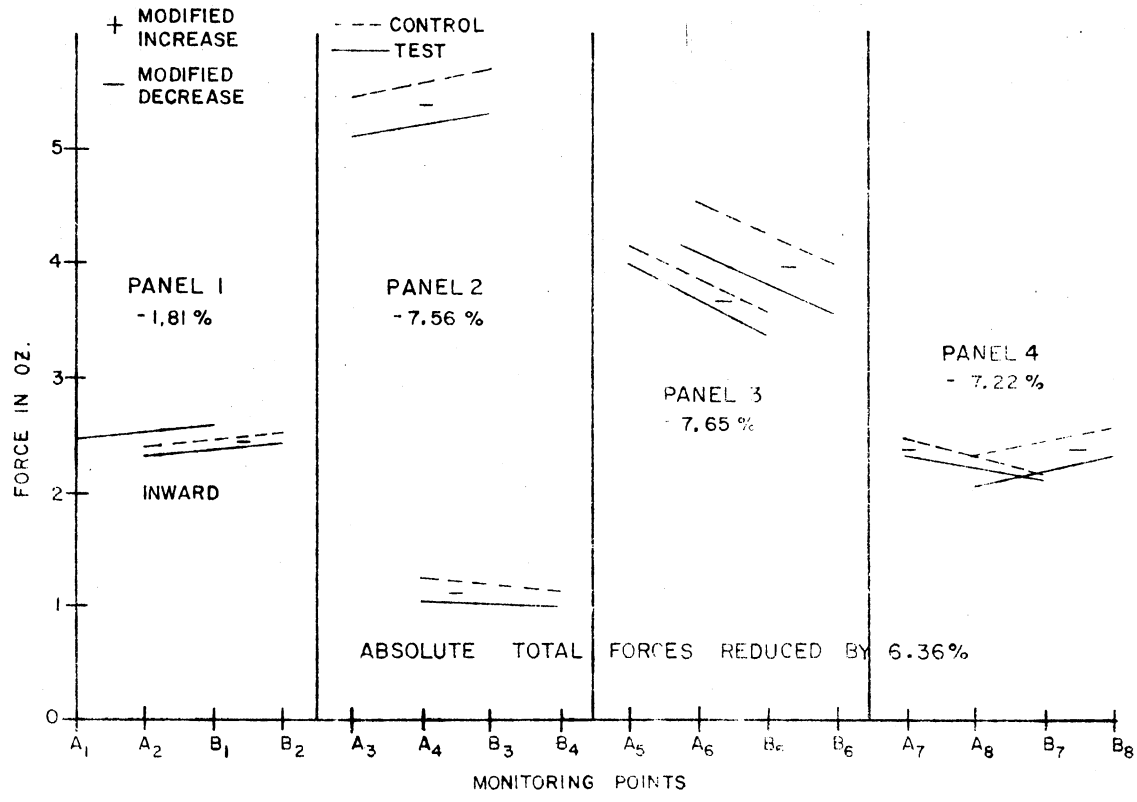

Figure 117. Big III Versus Control--Force in Ounces

TABLE XVI

COMPARISONS OF PARTIALLY AND FULLY CORRECTED DATA FOR BEAM CALIBRATION

		Uncorrected Data		Corrected Data	
	Calibration Factor Divisions/oz.	Big III Control Ch. Div.	Big III Ch. Div.	Big III Control Oz.	Big III Oz.
A_1	32.7355	80.33	80.00	2.45	2.44
A_2	34.2445	81.67	79.00	2.39	2.31
B_1	35.0395	90.33	90.33	2.58	2.58
B_2	36.0015	90.00	86.67	2.50	2.41
A_3	25.0515	136.33	128.17	5.44	5.12
A_4	33.8000	41.33	34.33	1.22	1.02
B_3	24.6685	140.67	131.67	5.70	5.34
B_4	31.7980	36.00	31.33	1.13	0.99
A_5	38.8555	161.33	154.67	4.15	3.98
A_6	37.4195	169.67	152.50	4.53	4.08
B_5	38.0700	135.53	128.33	3.55	3.37
B_6	39.8130	159.00	141.17	3.99	3.55
A_7	34.2265	84.00	78.33	2.45	2.29
A_8	38.6667	88.67	79.00	2.29	2.04
B_7	39.7555	84.67	82.67	2.13	2.08
B_8	37.4620	95.00	87.00	2.54	2.32

TABLE XVI (Continued)

	PARTIALLY CORRECTED			CORRECTED			
	Big III Control Chart Div.	Big III Chart Div.	% Change	Big III Control--oz.	Big III oz.	% Change	Difference
AV1*	85.33	85.17	- 0.2	2.515	2.510	- 0.2	----
AV2*	85.83	82.83	- 3.5	2.445	2.360	- 3.5	----
AV3	207.75**	194.88**	- 6.2	5.570	5.230	- 6.1	.1%
AV4	38.84	32.83	-15.5	1.175	1.005	-14.5	1.0%
AV5	148.33	141.50	- 4.6	3.850	3.675	- 4.6	----
AV6	164.33	146.83	-10.7	4.260	3.815	-10.5	.2%
AV7	84.33	80.50	- 4.5	2.290	2.185	- 4.6	.1%
AV8	91.83	83.00	- 9.6	2.415	2.180	- 9.7	.1%
Panel 1*	342.33	336.00	- 1.85	9.92	9.74	- 1.81	.04%
Panel 2	493.17	455.42	- 7.66	13.49	12.47	- 7.56	.10%
Panel 3	625.33	576.66	- 7.78	16.22	14.98	- 7.65	.13%
Panel 4	352.32	327.00	- 7.19	9.41	8.73	- 7.22	.03%
Inward*	342.33	336.00	- 1.85	9.92	9.74	- 1.81	.04%
Outward	1470.83	1359.08	- 7.60	39.12	36.18	- 7.52	.08%
Abs. Panel Total	1813.17	1695.08	- 6.51	49.04	45.92	- 6.36	.15%
Alg. Panel Total	1128.50	1023.08	- 9.34	29.20	26.44	- 9.45	.11%

* Inward

**now multiplied by 1.5

methods used cause no disadvantage. The only graph position to change appreciably due to the calibration factors is that of A7, and since it always registers one of the smaller forces this hardly affects the judgments being made. Assumption of 1.5 as an adjustment factor for the stiffer gages in reality assumes all the others have calibration factors of approximately 37.2. While this is not the case for a few of them, the relative error thus introduced is slight and, by elimination of the exact reduction of the data for preliminary analysis, much unnecessary work is avoided.

Conclusions - Ducts, Unsealed Model. All of the average forces show reduction with the exception of AV1, at the bottom of the upwind wall. The two worst outward forces, AV3 and AV6 are alleviated 6.2% and 10.7%, respectively. The algebraic total forces are outward for the unsealed models, therefore, the 9.4% reduction, in this case, signifies that the outward forces drop more than the inward forces.

On the basis of the results of Big III a definite very desirable pattern was found. During the course of the tests the very significant results of sealing the model were discovered. The validity of using the raw data, with only AV3 multiplied by 1.5, for rapid analysis was confirmed. Since no larger benefits could reasonably be expected from testing the smaller ducts, the tests were concluded prematurely. It was obvious that this option was one to be pursued further so a series of tests on sealed versions of Big III and Medium III followed.

Results - Ducts, Sealed Model. Of the four tests run, two utilized Big III(s) and the other two Medium III(s). Individual comparisons for each monitoring point are shown in Figures 118 and 119.

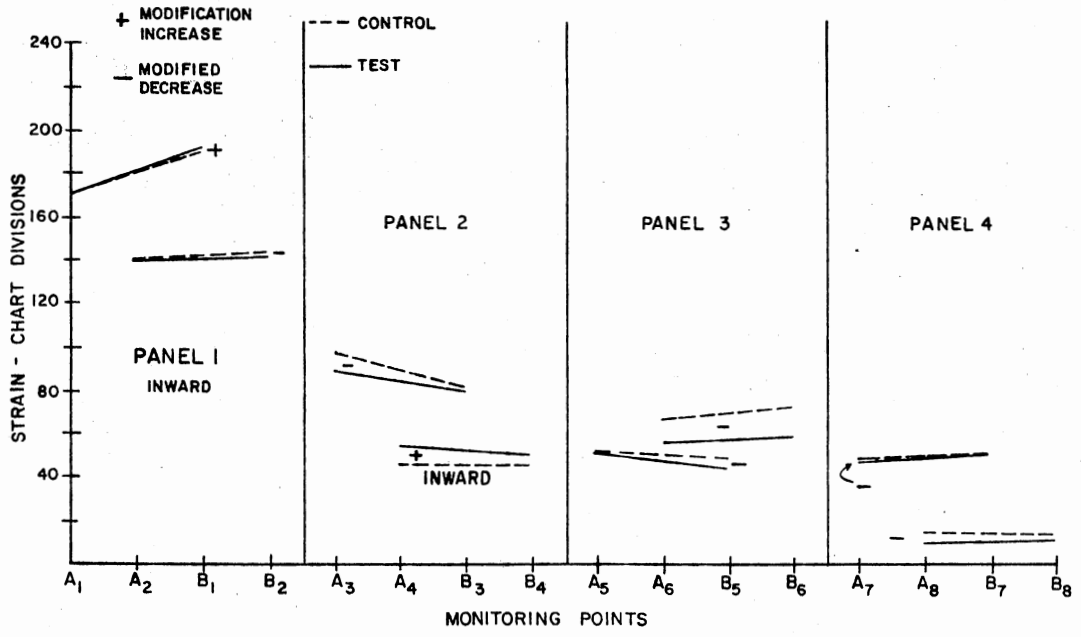

Figure 118. Medium III(s) Versus Control

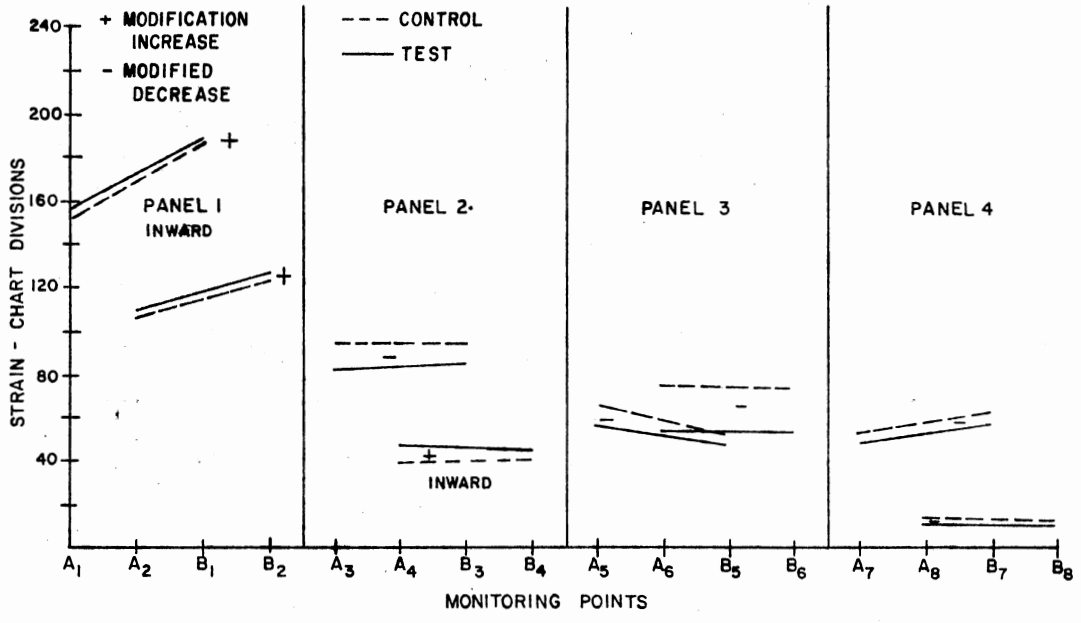

Figure 119. Big III(s) Versus Control

Typical of the controls for the other sealed models, gages A4 and B4 show inward forces rather than the outward forces of the unsealed model. The highest of the control forces are those inward on the front wall. The highest outward forces are at A3 and B3 on the front roof.

Atypical is the fact that the taped control forces for A1 and B1, at the lower corners of the front wall, differ significantly from those of A2 and B2 at the top. The lower corners of the wall experience the highest forces. The same sort of atypical result is noted for A8 and B8 where, at the bottom of the back wall, the forces are lower than A7 and B7 at the top.

There is no apparent reason for these differences except perhaps for the effects of the tubing apparatus. It was difficult to introduce the flexibility needed to allow the front wall to move independently of the back wall. The solution of using the ballon sections was not ideal, but was the best manner found.

The additional weight of the tubing apparatus would certainly exert some initial moment on the cantilever beams registering the forces at the corners of the wall panels.

Either of the above mentioned problems should have exerted the same influence on the previous unsealed tests for Big III, also. The effects are absent. Any pre-stressing of the gages due to weight of the apparatus could have affected inward A2 and B2 and outward A7 and B7. This was not the case. Interaction of the front wall and back could mask the results.

Not only is there a difference between these controls and those of the other sealed models, there is a difference between the taped

controls for the two sizes of tubes used.

Overall, the absolute totals were not greatly different; 1264.33 for Medium III(s) and 1255.00 for Big III(s). On the other hand, AV2 for Medium III(s) was 140.17 and for Big III(s) was 114.83. Several others were in the range of 5 to 10 chart divisions apart. With the holes taped on both controls, these differences were not expected. It was discovered early, however, that for the various modifications, differences in the control readings sometimes resulted. For that reason, each time a new modification was implemented which involved altering the apparatus in any way, or shutting down the equipment, a new control test was performed in order to obtain good comparisons. These two modifications are good examples of that difficulty in that the roof of the model had to be completely removed in order to change from Big III(s) to Medium III(s) by installing the tubes in the interior of the model between the two walls. The gages were so sensitive that even the weight difference of the two sets of tubes makes a single control for the two tests impossible. The two tests were eight days apart as well. Reinstallation of the sealing strips introduced another potential difference as well.

At this stage of the tests, the panel calibration procedure, to test for interaction, was not yet devised and the presence or absence of such is unknown.

A better way to test the option might have been to use very large tubes and tape closed part of the 40 tubes in order to attain at least four percentage variations of the front wall area. In this way, a single control would have been valid.

Ignoring the above, and comparing the trend exhibited by the

data, undisputable patterns can be observed.

The results are summarized in Table XVII and plotted in Figures 120, 121 and 122. Where a given change takes place for Medium III, the same change consistently takes place for Big III, only moreso. The sole exception is on the front wall at AV2 where the negative changes registered for Medium III(s) are very small, if they do indeed exist at all.

Only inward forces are slightly increased; outward forces are all reduced. The only inward forces which become significantly increased are the inward 4's at the ridge of the leading roof panel. AV3, the largest outward force, is decreased significantly. Several of the other forces show quite large decreases, percentage-wise, but the effect is not large due to the small magnitude of the forces. The large increase of the inward algebraic totals is due to the large decreases of the outward forces combined with small increases of the inward forces.

Conclusions - Ducts, Sealed Model. All the outward forces are decreased even with a small proportion of the area of the front wall open. The inward forces are not increased significantly except at the top of the ridge on the leading roof panel. The building should easily sustain such forces there.

This modification deserved further investigation and was, indeed, the basis for selecting the final modification for more extensive study. It was considerably modified in an attempt to increase the open area. As a result of some of the problems discovered an attempt was made in the final tests to document any interaction between the

TABLE XVII

SUMMARY OF PARTIALLY REDUCED DATA, DUCTS - SEALED MODEL (RECORDED STRAIN IN CHART DIVISIONS)

	Med III(s) Control	Med III(s)	% Change	Big III(s) Control	Big III(s)	% Change
AV1*	179.50	180.17	+ .4	171.00	172.67	+ 1.0
AV2*	140.17	139.00	- .8	114.83	119.00	+ 3.6
AV3**	87.75	84.00	- 4.3	95.00	84.00	- 11.6
AV4*	45.33	51.00	+12.5	40.83	47.17	+ 15.5
AV5	49.33	46.83	- 5.1	59.33	53.83	- 9.3
AV6	68.41	56.75	-17.1	74.67	54.00	- 27.7
AV7	48.83	48.33	---	56.83	54.17	- 4.7
AV8	12.83	9.75	-24.0	15.00	12.67	- 15.5
Panel 1*	639.33	638.33	- .1	571.67	583.33	+ 2.0
Panel 2 Absolute	266.17	270.00	+ 1.4	271.67	262.33	- 3.4
Panel 2 Algebraic	84.83	66.00	-22.2	108.33	73.67	- 32.0
Panel 3	235.50	207.17	-12.0	268.00	215.67	- 19.5
Panel 4	123.33	116.17	- 5.8	143.67	133.67	- 6.9
Inward*	730.00	740.33	+ 1.4	653.33	677.67	+ 3.7
Outward	534.33	491.33	- 8.1	601.67	517.33	- 14.0
Abs. Panel Total	1264.33	1231.67	- 2.6	1255.00	1195.00	- 4.8
Alg. Panel* Total	195.67	249.00	+27.3	51.67	160.33	+102.1

*Inward

** now multiplied by 1.5

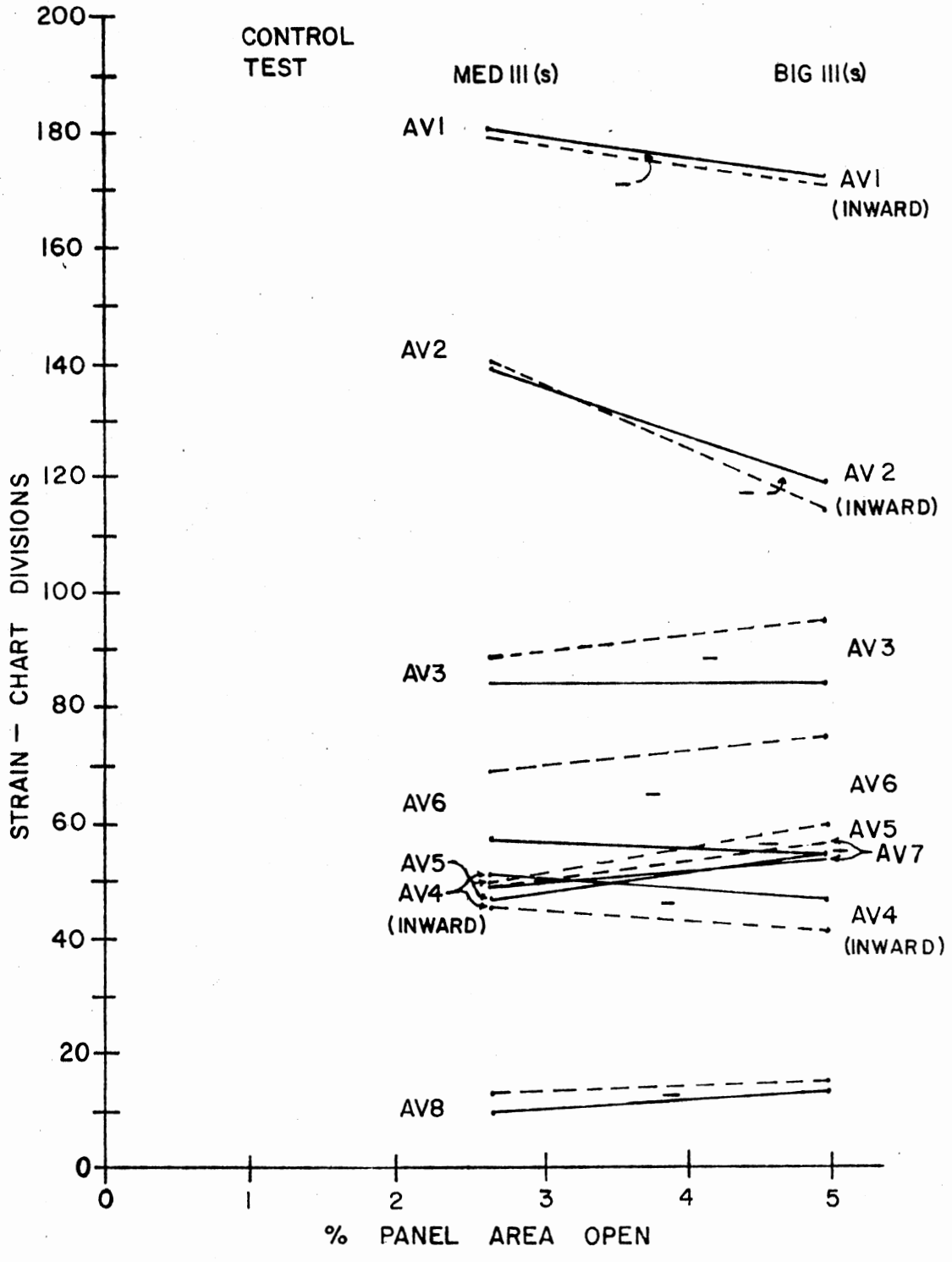

Figure 120. Average Strain Readings--Ducts, Sealed

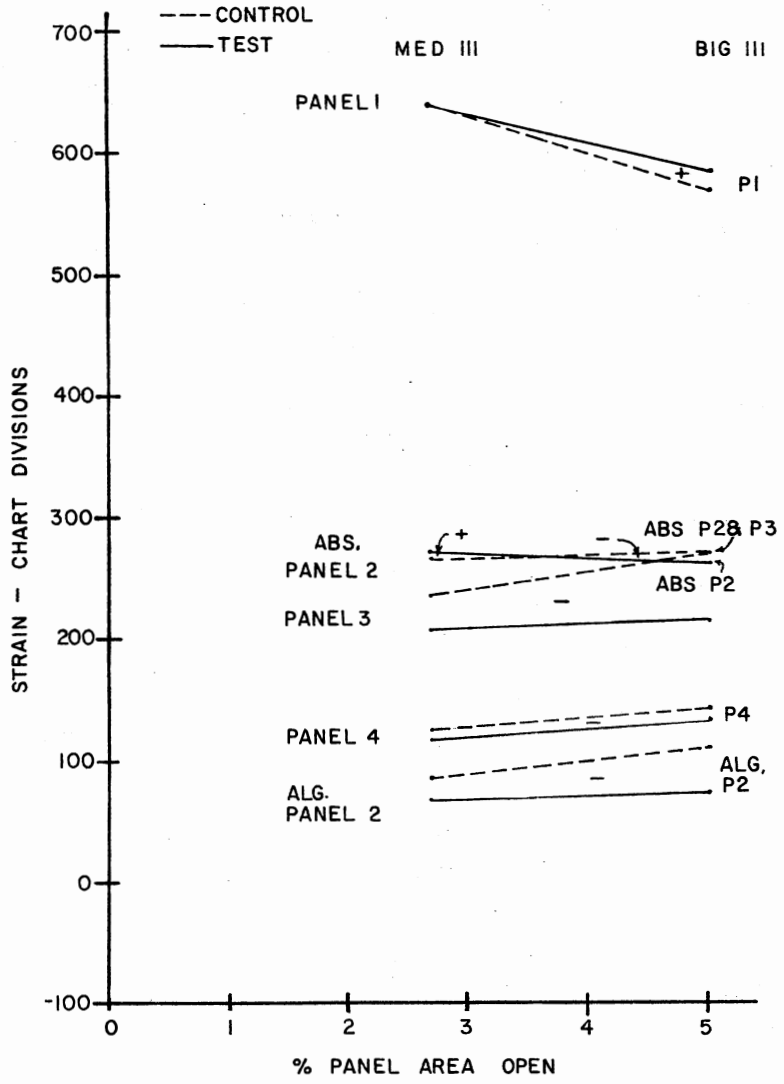

Figure 121. Panel Strain Readings--Ducts, Sealed

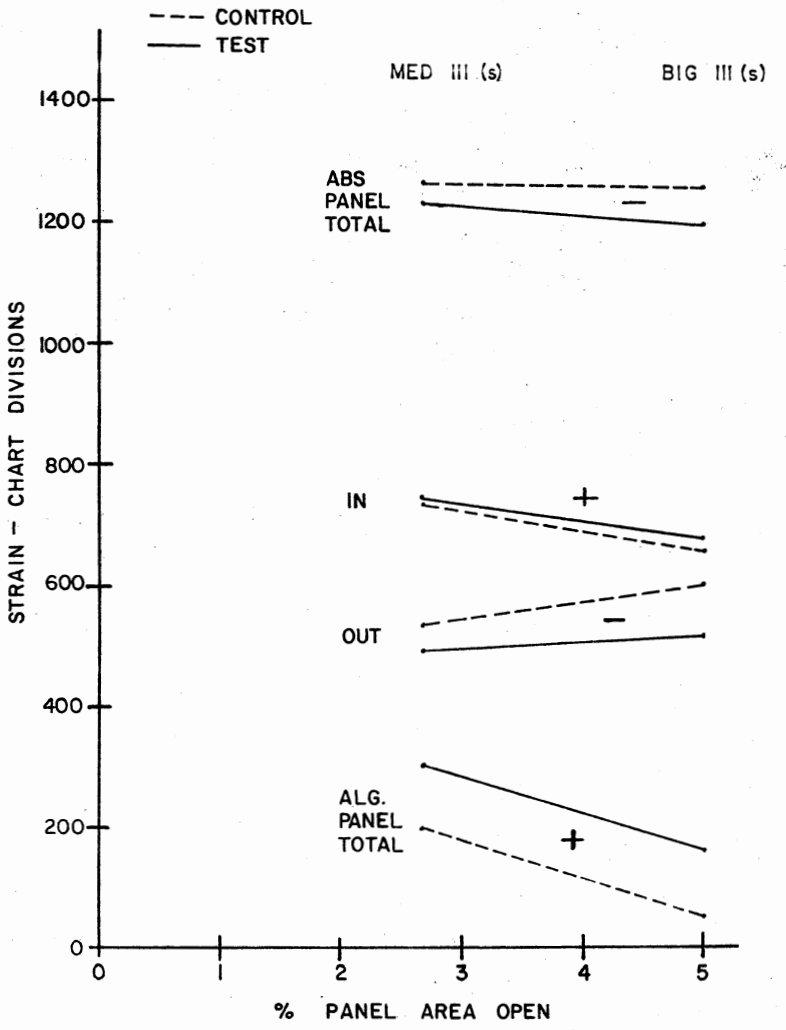

Figure 122. Building Total Strain Readings--Ducts, Sealed

panels which might result from the joint sealing and/or any deficiencies in the flexible section between the portion of the ducts on the front wall and the back wall.

Eave Overhang, Sealed Model

Objective. Several unplanned attempts were made to determine the potential beneficial effects of eave overhang modifications. As a result, some very interesting information was obtained.

Method. The normal sealed model was used for all the tests performed at high velocity only. The modifications were installed only on the upwind roof panel (No. 2).

Equipment Unique to the Eave Overhang Investigation. The equipment used consisted of metal strips - 1/16" shorter than the length of the movable panel. Some of the equipment is pictured on the model in Figure 123.

The eave overhang option with venting holes [EOHi(s)] and the bent eave overhang modification [EOB(s)] are shown. All the modifications are drawn in Figure 124.

The EOHi(s) strip was drilled with 40 9/32" holes spaced 1/2" on center and centered 1/2" from the outer edge. It was 2-1/4" wide and 20-17/32" long. The metal strip had a series of mounting holes used to install it in two positions.

The metal strip used for the EOB(s) modification was the same size with a 33.7° bend 3/4" from the outer edge. This resulted in the bent portion being at an angle of 45° with the ground plane and 1-3/16" out from the wall.

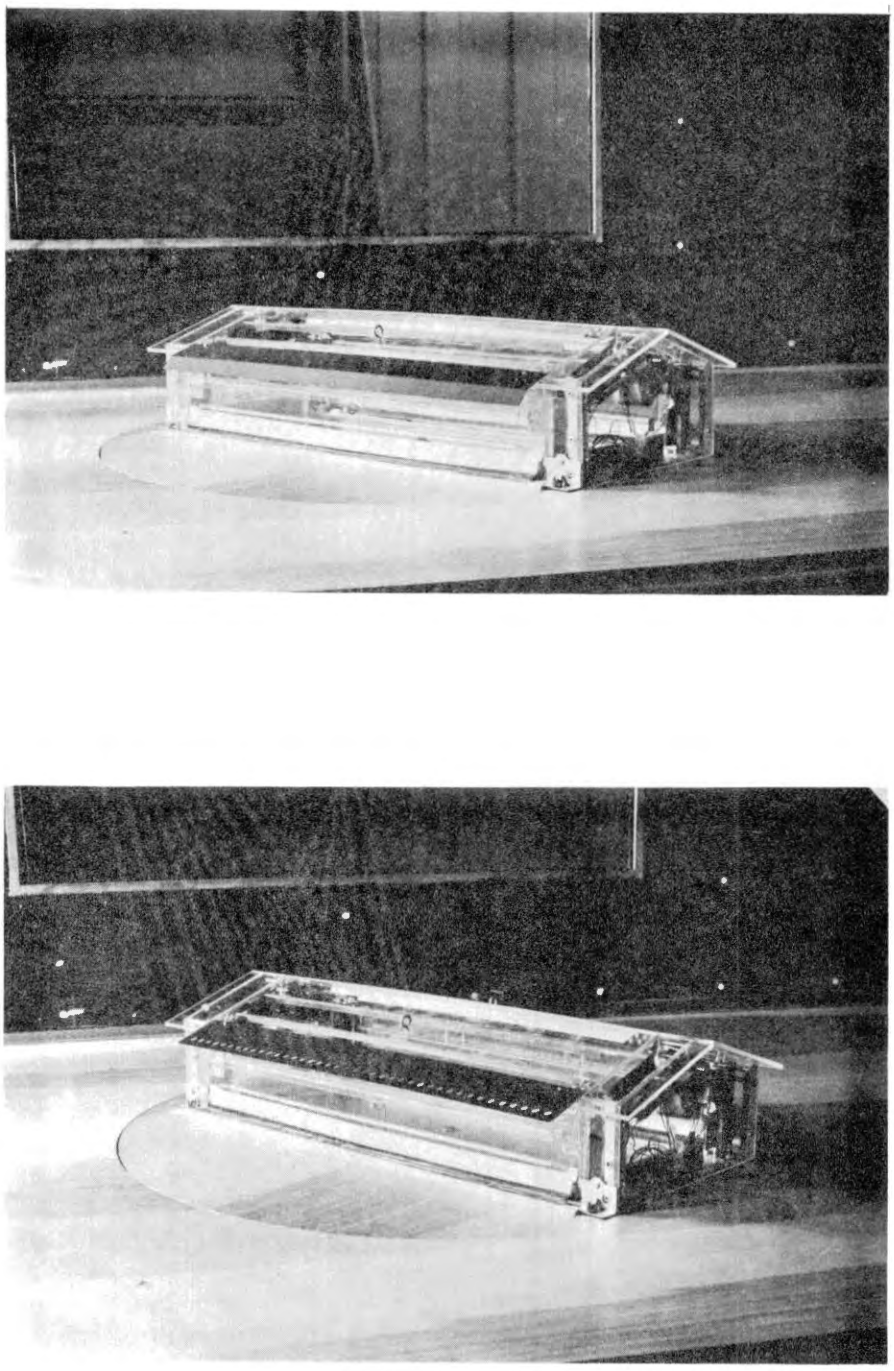

Figure 123. Eave Overhang Apparatus Installed on Model: Top, Bent Overhang--EOB(s); Bottom, Overhang with Holes--EOHi(s)

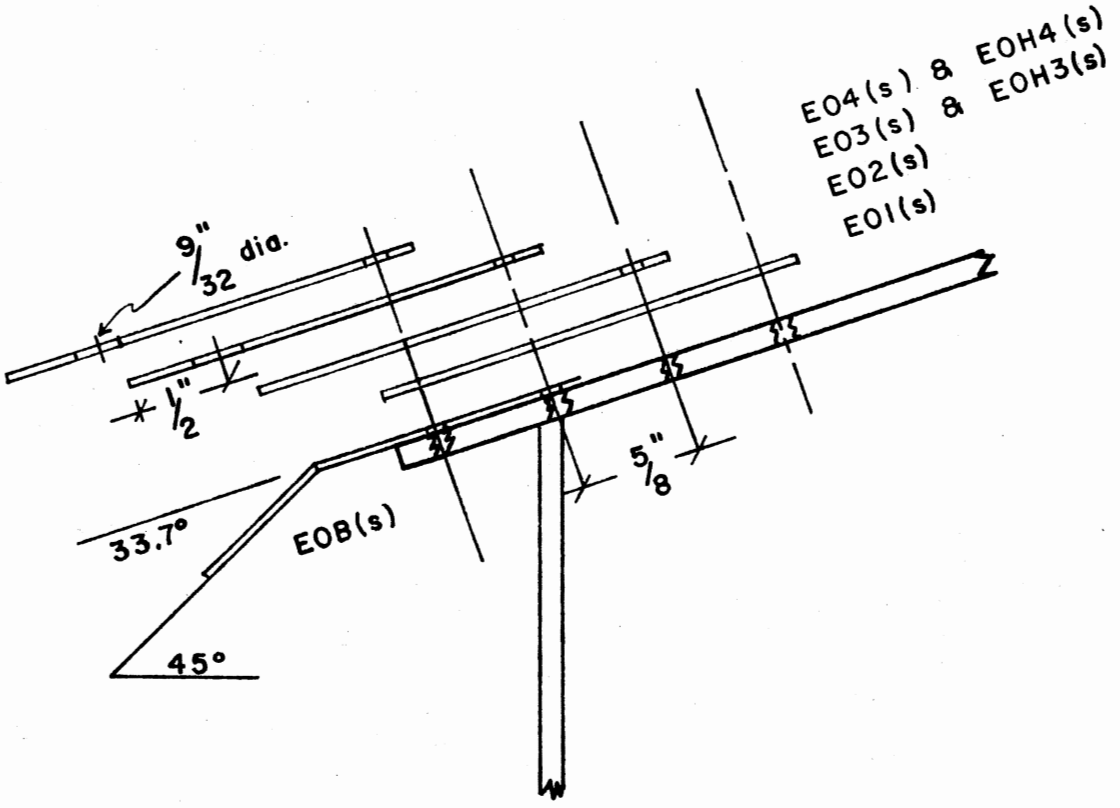

Figure 124. Eave Overhang Equipment

EOi(s), the third option tested, used a flat metal strip extended beyond the normal leading edge of the model's upwind roof panel. Four positions were possible, one being the control with only the normal overhang. Zero overhang was not possible without rebuilding the model.

Procedure. The EOHi(s) tests used overhangs of 3/4" and 1-3/8" beyond the leading edge of the regular roof panel versus its control in the same positions with the holes taped.

The positions are described as follows:

EOH3(s), with vent holes centered 3/4" from the edge of the regular roof

EOH4(s), same with holes centered 1-3/8" from roof edge

The controls were called EOH3(s) taped and EOH4(s) taped.

EOB(s) was a single test plotted against the same control as the EOi(s) series below. The bend was ≃ 33° with respect to the strip itself and mounted on the roof was inclined at ≃ 45° with respect to the ground in position 3.

The four positions utilized for EOi(s) were:

EO1(s), control strip of the same size mounted on the top of the roof panel, at the leading edge, with no overhang

EO2(s), 5/8" overhang beyond the ordinary leading edge of the roof

EO3(s), 1-1/4" beyond

EO4(s), 1-7/8" beyond

Results - Eave Overhang. The results of the end overhang tests, EOi(s), are plotted in Figures 125, 126, 127 and labeled by position 1, 2, 3, and 4. In Figure 125, the average individual forces are shown. Since the control pattern (position 1) is typical of the other sealed models, AV4, i.e., $(A_4 + B_4)/2$, is inward as is panel 1. The panel 1 inward forces are the highest of all the forces. The next highest are the outward forces on panel 2 at the point of overhang (AV3). They are followed closely by the other roof forces. Lowest of all are AV7 and AV8 on the back wall (panel 4). The forces plotted are the absolute values.

1. The decreases on the front wall, panel 1, were not expected though it is very possible that the further out the overhang (and thus lower to the ground), the less abruptly the air flow is changed.
2. The large increase on panel 2 for the 3's outward force could be expected due to the additional eave area with suction over it and pressure under it. From the data taken, the rise of AV3 appears to reach a summit at position 4. The behavior of the 4's shows large linear increases in the inward force at the top of the leading roof panel as the overhang is increased.
3. If the back roof, panel 3, had also been extended for symmetry of overhang, the results would obviously change some - most certainly for the back roof and perhaps also for the back wall. It can be anticipated that the increases would have been still more as compared to the control on these back surfaces.

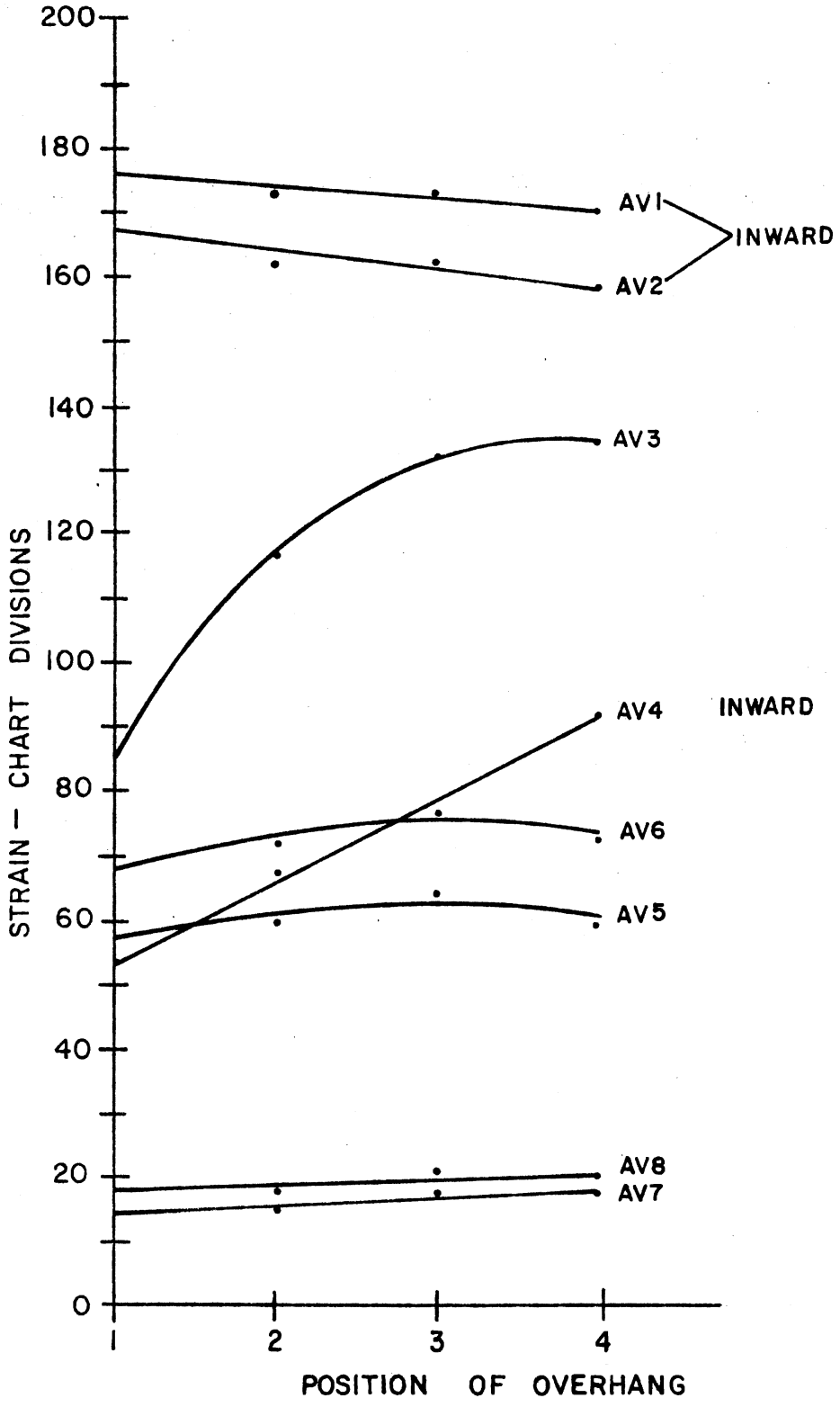

Figure 125. EOi(s) Series--Average Strain Readings of Individual Monitoring Points

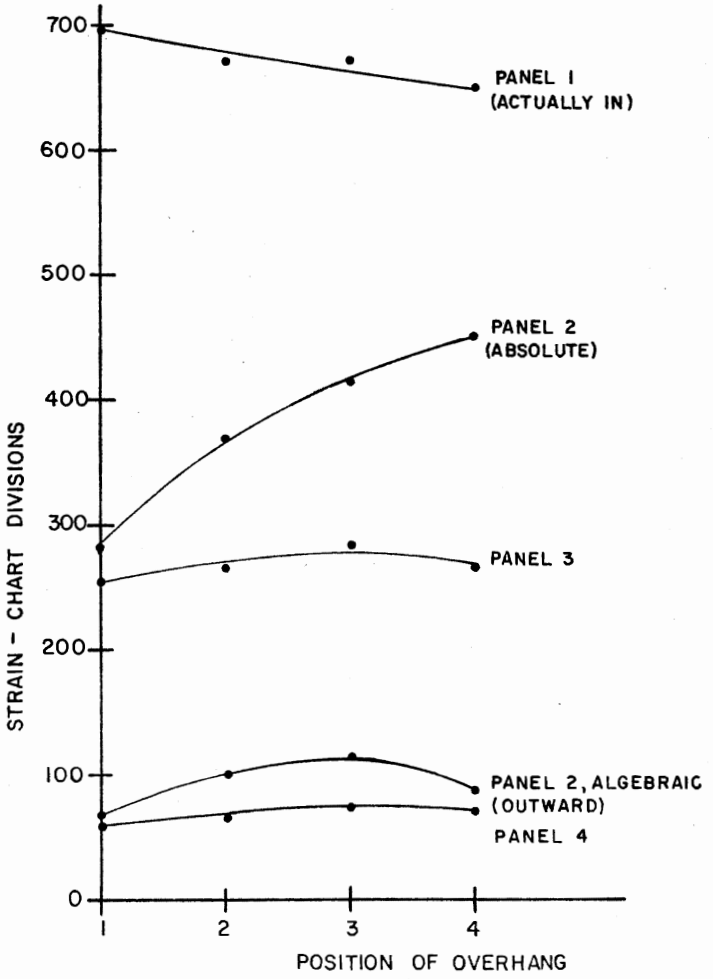

Figure 126. EOi(s) Series--Panel Total Strain Readings

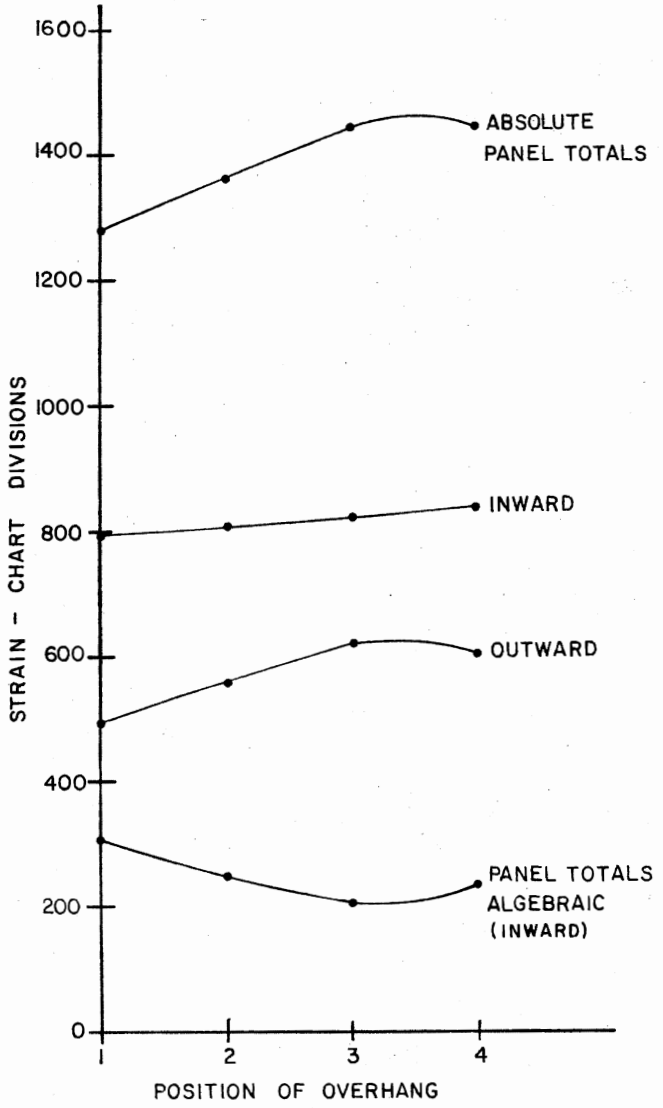

Figure 127. EOi(s) Series--Building Total Strain Readings

4. Panel 4, the back wall, also shows increase though rather insignificant in view of the small changes and the low magnitudes of the forces themselves.
5. Inward forces (combination of AV1, AV2, and AV4) show a linear, though slight, increase.
6. Outward forces appear to peak between positions 3 and 4.
7. The absolute force total for the building - simply the absolute sum of inward and outward forces - exhibits the same behavior as the outward forces, though the curve is somewhat more steep.
8. The algebraic total - being the difference between inward and outward forces - is in this case inward and almost a mirror image of the absolute forces. The decrease simply reflects the more rapid increase of the inward forces as opposed to the outward forces.

To summarize from Figures 125, 126 and 127, the actual percentages of change for each modification with respect to E01(s) are:

	E02(s)	E03(s)	E04(s)
* Panel 1	-2.7%	-2.4%	-4.5%
Panel 2 (Abs)	+31.4	+48.8	+62.2
* Panel 2 (Alg)	+52.3	+70.1	+29.3
Panel 3	+2.8	+10.6	+3.0
Panel 4	+5.8	+24.0	+20.2
Absolute Panel Total	+6.2	+12.6	+12.6
Inward	+1.1	+3.7	+5.8

	E02(s)	E03(s)	E04(s)
Outward	+14.6	+27.2	+23.9
* Algebraic Panel Total	-20.5	-33.7	-23.0

* Inward

Conclusions - Eave Overhang. In every case for the eave overhang tests:

1. The front wall forces represent decreases over the control.
2. The other surfaces all show increases.

The decreases on the front wall are significant, yet eave overhang is certainly not beneficial in view of the much higher increases in the leading roof panel forces. The building is especially vulnerable to the outward forces at the eave.

It is very difficult to justify the practice of ignoring the significance of eave overhang in calculating the wind loads incurred by a building. More study on this matter would seem to be imperative since the eave overhang is a dominant factor in determining the force patterns on all the model surfaces. It would be especially interesting to set up similar experiments with a model where zero overhang is possible and to further verify the apparent imminent peak of AV3 and the recorded peaks of AV6 and AV5 by extending the overhang farther.

Results - Eave Overhang With Holes. The two tests run were identified as EOH3(s) and EOH4(s), both with 9/32" (14" full scale) holes 1/2" on center, 1/2" in from the leading edge of the strip which was 1-1/4" and 1-7/8" out, respectively, from the edge of the roof. This adds 5.2' and 10.8' to the already existing overhang of

the normal full scale building.

They resulted in the following changes, first with respect to the controls having the holes taped closed and, second, with respect to a repeat of E01(s) with the metal strip of equivalent weight fastened on top of panel 2 at the roof's leading edge (no overhang other than normal).

	EOH3(s) [with respect to holes taped]		EOH4(s) [with respect to E01(s)]	
* Panel 1	+0.5%	+1.5%	-1.4%	-1.9%
Panel 2 (Abs)	-15.5%	-9.2%	+20.6%	+35.9%
* Panel 2 (Alg)	-10.2%	+28.3%	+21.6%	+25.5%
Panel 3	-4.1%	-4.2%	-2.4%	-4.8%
Panel 4	-5.0%	-4.9%	+8.1%	+11.4%
Absolute Panel Total	-5.3%	-3.1%	+3.9%	+6.8%
* Inward	-3.0%	-2.2%	+1.8%	+4.1%
Outward	-8.8%	-4.6%	+7.2%	+11.2%
* Algebraic Panel Total	+10.1%	+3.4%	-7.0%	-7.4%

* Inward

As would be expected, the two taped controls themselves varied only slightly from E03(s) and E04(s) previously discussed. Control forces for EOH4(s) were reduced 1.5% on the front wall when compared to the control for EOH3(s). The control front roof 3's increased by a small percentage ($\simeq$ 2.5%) and the 4's by $\simeq$ 12%. The panel 3 forces decreased by 2.5% and the back wall forces were about the same, all conforming with the forces found in the E03(s) and E04(s) tests.

The only real inaccuracy in making a comparison of EOH3(s) and EOH4(s) with control EO1(s) is that the latter was also the control for EOB and thus did not actually have holes drilled in it. There would thus be a slight weight difference as a result of the metal drilled out to make the holes.

The plots in Figures 128 and 129 reveal some interesting facts.

1. The front panel forces, though showing very slight gains for the EOH tests over their respective taped controls, reveal that the front wall forces with the EOH modification are still less than the front wall forces with only the regular eave overhang. This same air flow effect due to the longer overhang was noted in the EOi(s) series.
2. Panel 2 forces for EOH are between those of the taped controls and the dashed control line representing only the normal overhang, EO1(s). With the EOH modification, the overhang increases are not so severe - i.e., for A3 and B3, the EOH outward forces are lower than the taped controls but still higher than for the ordinary building overhang; and for A4 and B4 the EOH inward forces are less than the taped controls' and more than the forces on the ordinary model.
3. Panel 3 shows EOH to cause, in general, lower forces than either the taped controls or the unmodified model overhang.
4. Panel 4 forces are small and the changes are insignificant.
5. Inward forces (Figure 130) on the entire building are increased with respect to EO1(s), moreso at position 4 than at EOH3(s), indicating that the same tests at position 2 could have resulted in lower inward forces than the control.

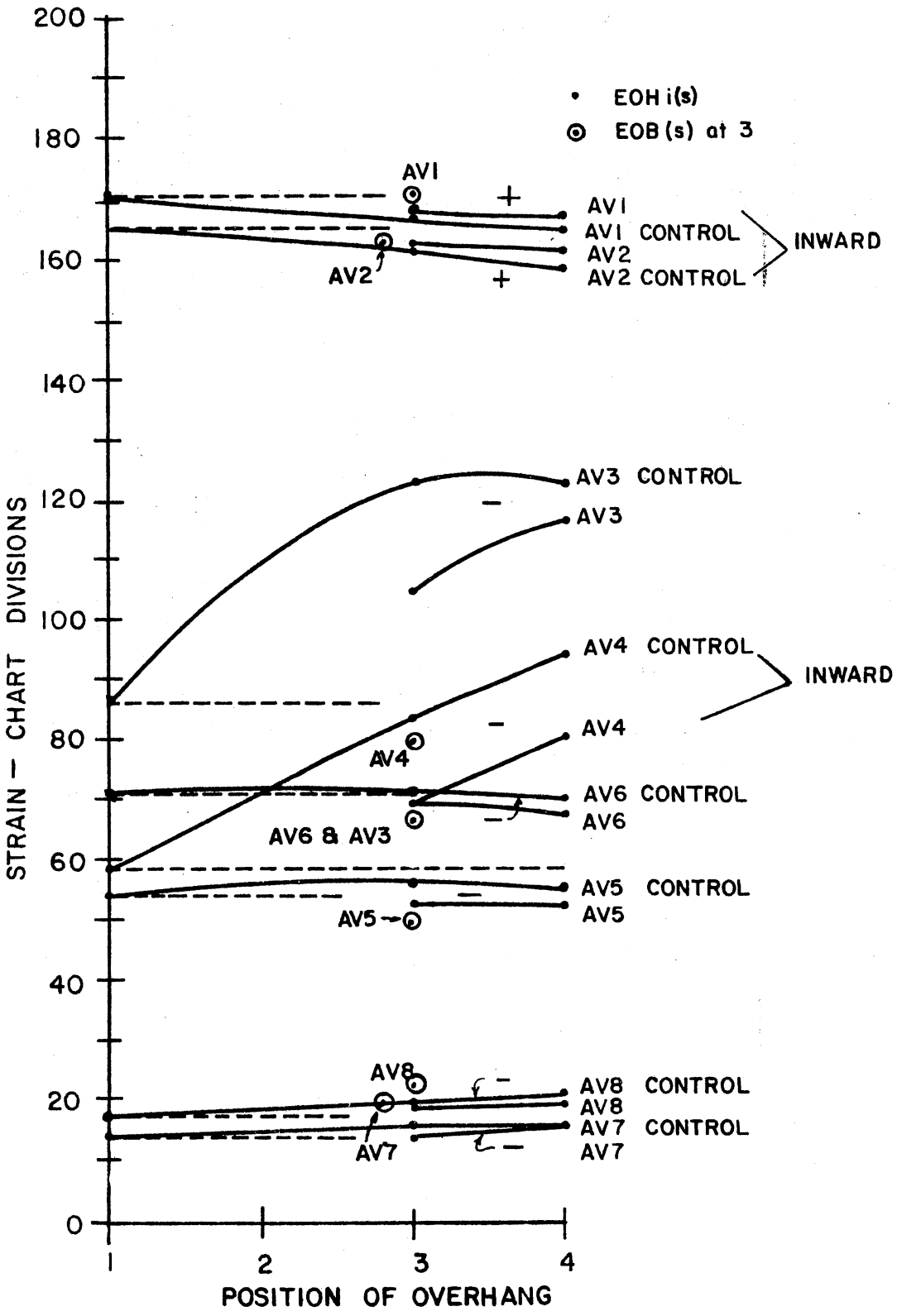

Figure 128. EOHi(s) and EOB(s) Series--Averages of Individual Monitoring Points

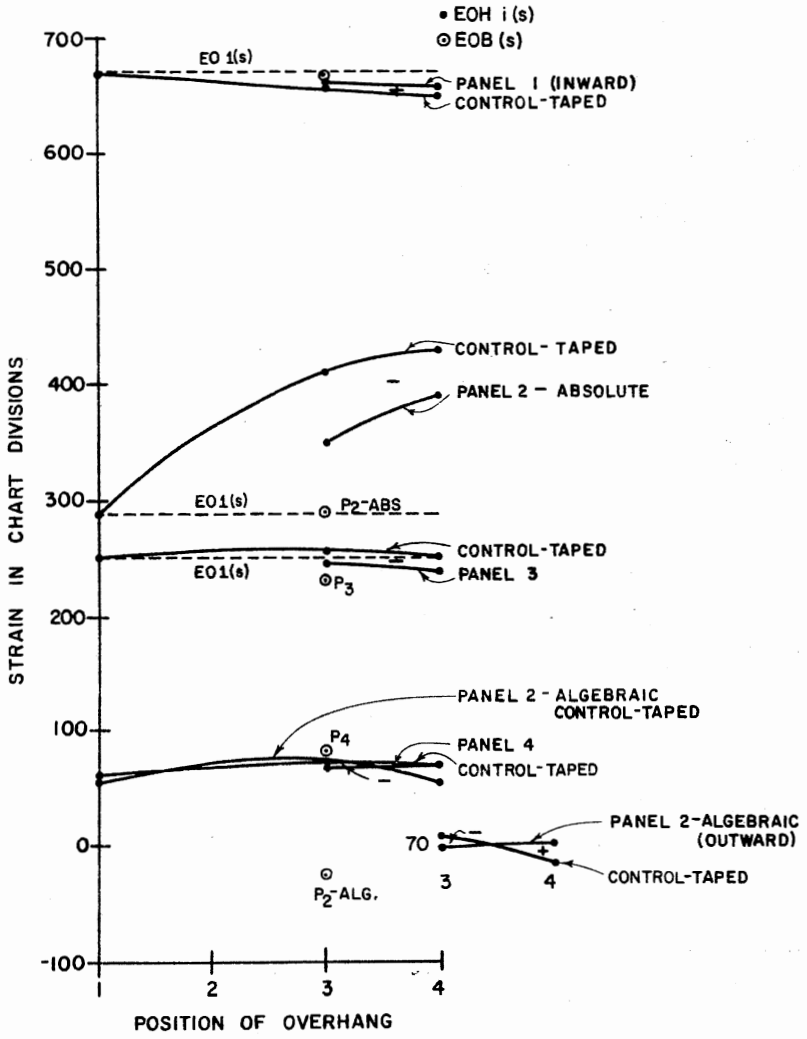

Figure 129. EOHi(s) and EOB(s) Series--Panel Totals

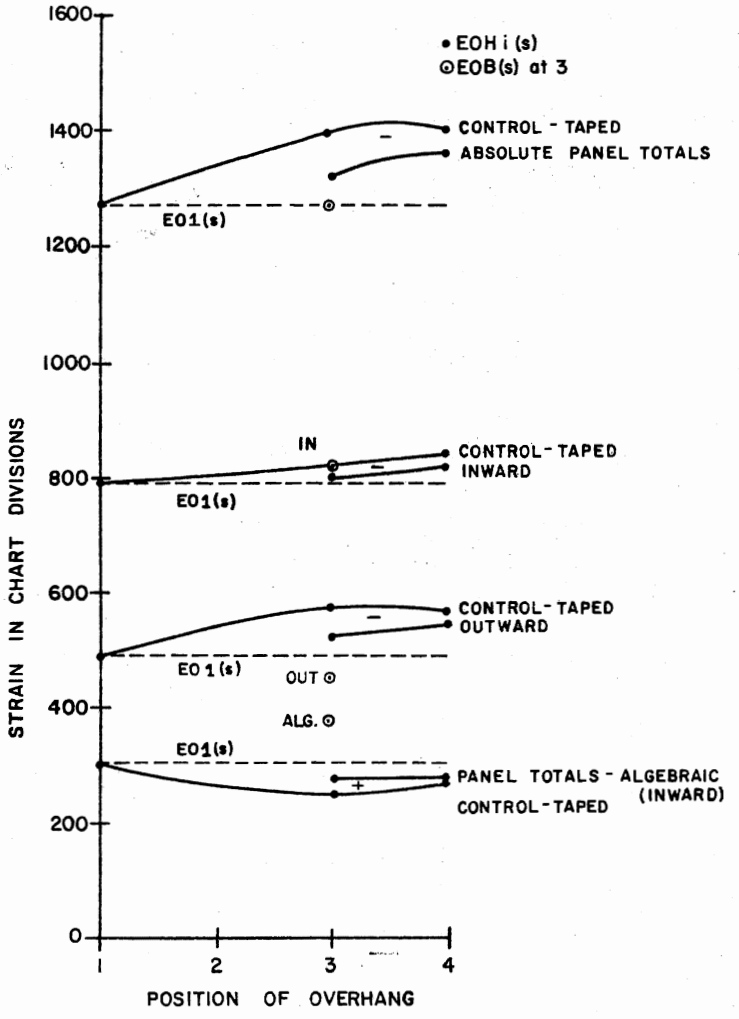

Figure 130. EOHi(s) and EOB(s) Series--Building Totals

Comparison of EOHi(s) with the taped controls at the same position shows EOHi(s) to be lower inward forces.

6. Outward forces are again greater than the EOl(s) control but less than for the two taped controls at the same position. Reductions are greater at position 3 than at position 4.
7. Absolute total forces reflect the same pattern - i.e., the forces are greater than the EOl(s) control but show decided improvement over the two taped controls. There is more reduction at 3 than at 4 and conjecture indicates position 2 to be even more favorable.
8. The algebraic force totals for EOHi(s) is a level line, indicating the same rate of increase for both inward and outward forces. Its location beneath the control EOl(s) signifies that the inward forces did not increase as much as the outward forces when compared to EOl(s). The test curve's location above the taped control's shows the inward forces did not drop as much as did the outward forces in comparison to those controls.

Conclusions - Eave Overhang with Holes. It has already been determined that the presence of an eave overhang causes lower forces on panel 1, but higher forces elsewhere - especially on panel 2. If an overhang is already present, the venting holes, as tested in this series, will reduce all the forces at each of the monitoring points except those of panel 1 which show a very slight increase of $\simeq$ 1%.

The holes cause air flow changes which tend to null out part of

the only advantage of overhang - a small reduction of the front wall forces. However, the leakage of air through the holes from under the overhang reduces the uplift on the eave, causes the air flow at the top of the upwind roof to induce less inward pressure on the roof, and reduces the outward pressure on the back roof and wall. This is especially significant at AV3, the highest outward force and a vulnerable point of the structure.

The concept shows ability to reduce the forces only when overhang is already present. Judging from the plots and the percentages, the vented holes closer to the wall (i.e., further from the overhanging roof's edge) seem to be more effective. This seems logical and it is regrettable a closer position was not tested.

The concept of venting holes in the overhang should be studied further to see if some practical means of achieving even better results could be attained. Only one size of hole and two positions were tested in this study. Smaller and larger holes at several positions should be tested to document more accurately the relationships. Intermittent slots could be included as well. It should be possible to maintain the contruction advantage of the overhang and yet vent it so as to reduce the increases in wind forces caused by overhang.

Results - Eave Overhang, Bent. The single test identification was EOB(s). The main control chosen for comparison was EO1(s) which was rerun at the same time as EOB(s). Other controls could have been chosen - an unbent strip with the same horizontal or vertical projection, for example. Since this was not the case, here the primary comparison is with EO1(s), i.e., no overhang beyond that of the

regular model. Also, EOH3(s) taped, the additional overhang without a bend (i.e., having the same overhang surface area) is used as a comparison. It was used due to minor changes in equipment since the testing of the more logical control, EO3(s). EO1(s) utilized a metal strip of the same weight fastened on top the upwind panel (2) and its leading edge with no additional overhang.

The EOB(s) results are plotted as single points with the EOHi(s) series in Figures 128, 129 and 130.

The percentages of change are as follows:

	EOB(s) with Respect to EO1(s)	EOB(s) with Respect to EOH3(s)
*Panel 1	-0.4%	+1.6%
Panel 2 (abs)	+0.4%	-29.4%
*Panel 2 (alg)	-144.6%	-132.9%
Panel 3	-7.6%	-9.2%
Panel 4	+35.7%	+19.3%
Absolute Panel Total	+0.2%	-8.6%
*Inward	+5.2%	+0.2%
Outward	-7.7%	-21.4%
*Algebraic Panel Total	+26.0%	+49.2%

* Inward

Comparing the extended bent overhang to the ordinary model with the shorter normal straight overhang, some surprising facts emerge.

1. The forces on the front wall do <u>not</u> increase.
2. The front roof panel outward forces at AV3 drop as much as

the inward AV4 rises. Here the most drastic changes take place. The bent extension significantly alters the air flow pattern and the most severe and critical outward forces on the building are greatly reduced (22-1/2%).

3. Panel 3 forces are reduced.
4. Panel 4 forces, though the smallest, do experience 35.7% increase but remain at an insignificant level.
5. Inward forces on the whole building increase 5.2% as a result of the AV4 increase.
6. Outward forces are reduced 7.7% overall due to the high decrease of AV3 and lesser decreases at AV5 and AV6. AV7 and AV8 experience some increase which offsets the other decreases.
7. Absolute forces are about the same.
8. Algebraic forces show 26% increase, meaning the inward forces increase but little while the outward forces are reduced a greater amount. The net effect is to increase the balance toward the inward forces.

If the modification is compared to that of the taped control at the same position the following is noted:

1. Front wall inward forces increase an insignificant amount.
2. The bend in the overhang causes significant reductions in both the outward AV3 (46%) and inward AV4 (5%). Absolute panel forces are reduced 29.4%.
3. Panel 3 forces drop 9.2% due to equal decreases in AV5 and AV6.
4. Panel 4 forces increase 19.3% though their magnitude makes

this charge rather insignificant.

5. Inward forces on the whole building experience offsetting changes as the reduction of AV4 is balanced by the increases at AV1.
6. The most important change is seen in a 21.4% reduction of outward forces on the building, mainly due to decrease in AV3 and some decrease at AV5 and AV6.
7. Absolute total decreases 8.6%.
8. Algebraic total increases, becoming more inward. This results from essentially no net decrease in the inward forces whereas outward forces were decreased.

Conclusions - Eave Overhang, Bent. The bent overhang has potential based upon the test. Even judging the bent extension against no extension of the normal overhang results in favorable redistribution of the forces. The most severe outward forces at the leading edge of the roof and the other back roof forces are traded for increases in outward force on the back wall and increases in the inward force at the ridge of the front roof surface. These changes are beneficial both from the standpoint of decrease of critical forces and change to force patterns which the building can more easily sustain.

In comparing the forces of the bent overhang to those of the unbent overhang of the same length, the changes are even more striking. All surfaces show either no increase or favorable changes except for the outward increases of the forces of insignificant magnitude on the backwall. Overall, the inward forces are not reduced, but the outward forces greatly decline and thus reduce the absolute total, also. Again,

the most serious outward forces are reduced in magnitude.

Further testing is indicated since only one extended position was tested with one angle of bend. It may well be that such gains could be amplified by changing the length of the bend as well.

Conclusions for the Complete Eave Overhang Series. The eave overhang of the model was influential on the wind force pattern of the entire structure. The area most affected is the leading roof surface where the outward force at AV3 increased and the inward force at AV4 likewise was greatly increased.

Venting the existing eave overhang with holes reduces the forces on all surfaces except the front wall where minimal increases occur. The holes are more effective when located nearer to the front wall. The effects are most pronounced on the front roof panel where the vents are located, but the other surfaces are also affected.

The bent overhang has potential to overcome the AV3 force increase due to overhang. Other outward roof forces at AV5 and AV6 are also reduced by the bend in the extended overhang.

Several interesting phenomena were discovered and merit further investigation. Nevertheless, more effort will not be devoted to the option during this study.

Venting

Objective. The fourth major alternative of the preliminary investigation involved venting the building itself. For the unsealed model inward forces are incurred on the front wall while suction exists on all other panels. The 4's (top of panel 2) become inward

when the model is sealed. It was felt that dangerously high wind pressure patterns might be sufficiently relieved by venting or opening the building, allowing air to pass through rather than to lose the structure altogether. The effort of this phase of the study is to determine the force changes on the building under these circumstances.

Method. Originally some method of synthesizing a prototype building with pop off panels was considered. The panels were to be less securely fastened to the structure so as to come loose and relieve the pressures before the whole structure failed. More practical would be a panel allowed to swing either inward or outward according to direction of the wind. The panels would not fly across the countryside when opened by the wind. To prevent activation except in extreme cases of loading a tripping mechanism was foreseen, perhaps utilizing springs. Due to the impracticality of installing such on the small model to be tested, a simplification, simulating a panel already open, was accepted as a compromise. It was tested at high velocity only.

Equipment Unique to the Venting Investigation. The regular model was equipped with an open section in the front and back wall panels. The section was 27/32" high and 17-7/8" long. It was centered lengthwise in the 20-19/32" movable panels and down 43/64" from the top. This left 1/4" above the opening and 2-5/8" below.

Cover panels extended approximately 1/8" beyond the opening in all directions. The cover panels were closed in order to obtain the control. The same cover panels were dropped downward on both front and back walls to achieve the following openings:

1/4 open = .211" or 27/128", 10.55" full scale

1/2 open = .422" or 27/64", 21.10" full scale

3/4 open = .633" or 81/128", 31.64" full scale

full open = .844" or 27/32", 42.19" full scale

All were 74.5' long, full scale.

Procedure. For the unsealed tests only three tests were run:

1. Fully closed.
2. 1/4" (slight deviation from 1/4 open = .211").
3. Fully open or .844".

Sealed tests utilized the standard openings. These tests included a "completely" sealed control (with the exceptions noted earlier in the discussion of sealing), though it was found to be impossible to seal the crack at the top of the front wall during tests of the openings themselves. This was not a disadvantage as the panel was open just 1/4" below the crack in question, and all the standard openings were much greater in comparison to the very small crack. The net effect could have been very little different, if at all, had the crack at the very top of the front wall been sealed.

Results - Venting, Unsealed Model. The control force pattern conforms with earlier unsealed controls - all forces on the roof and backwall are outward and the front wall forces are inward.

Examination of Figure 131, showing the strain changes that occurred, reveals surprisingly dissimilar results for the two degrees of opening. From the figure and the curves in Figure 132, on the basis of three data tests, tentative observations can be made.

1. Forces A1 and B1 decrease 12% with the .25" opening but increase 3.8% with .844". The break even point is shown as a

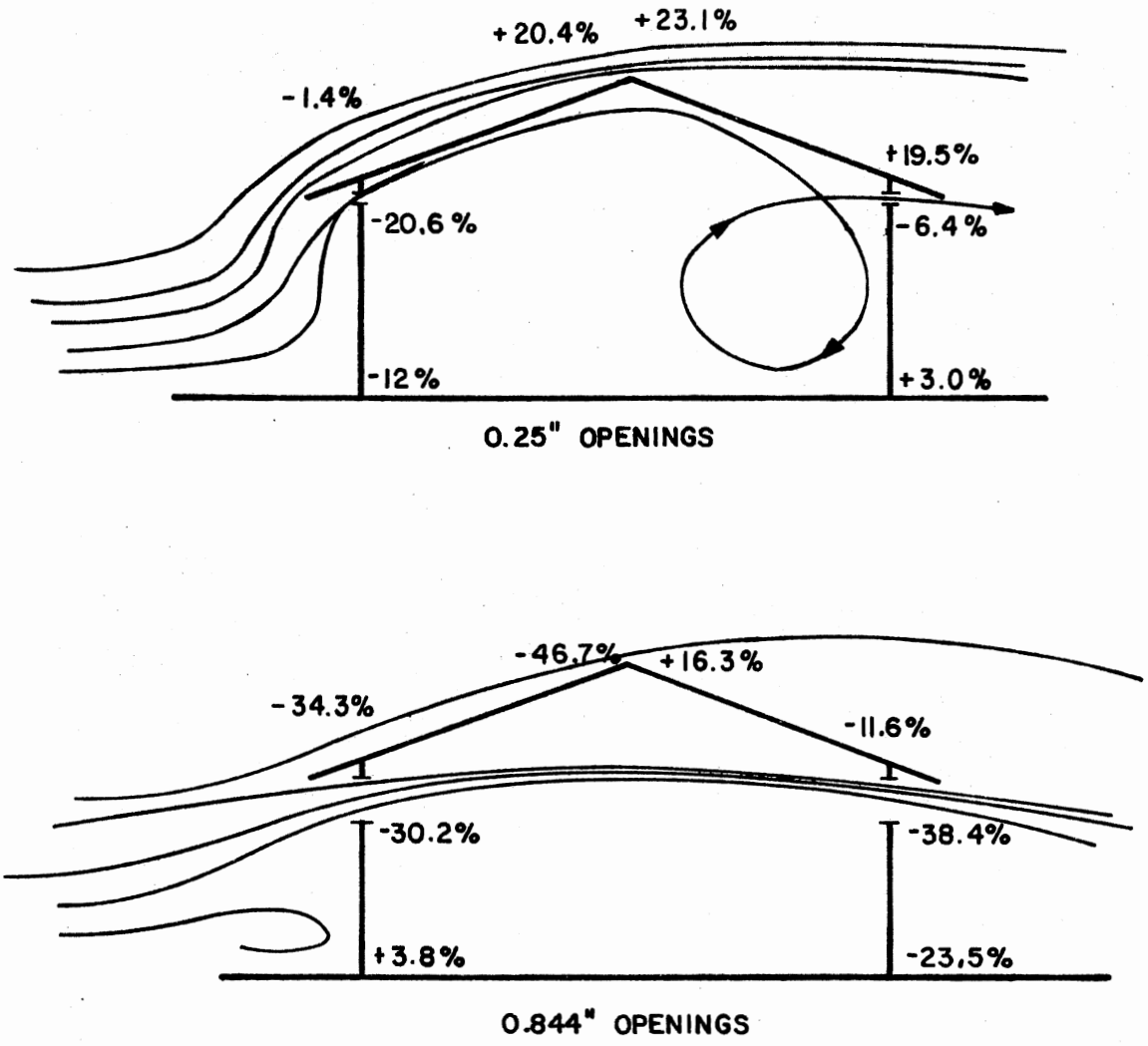

Figure 131. Unsealed Vented Model-Strain Changes with Respect to No Opening

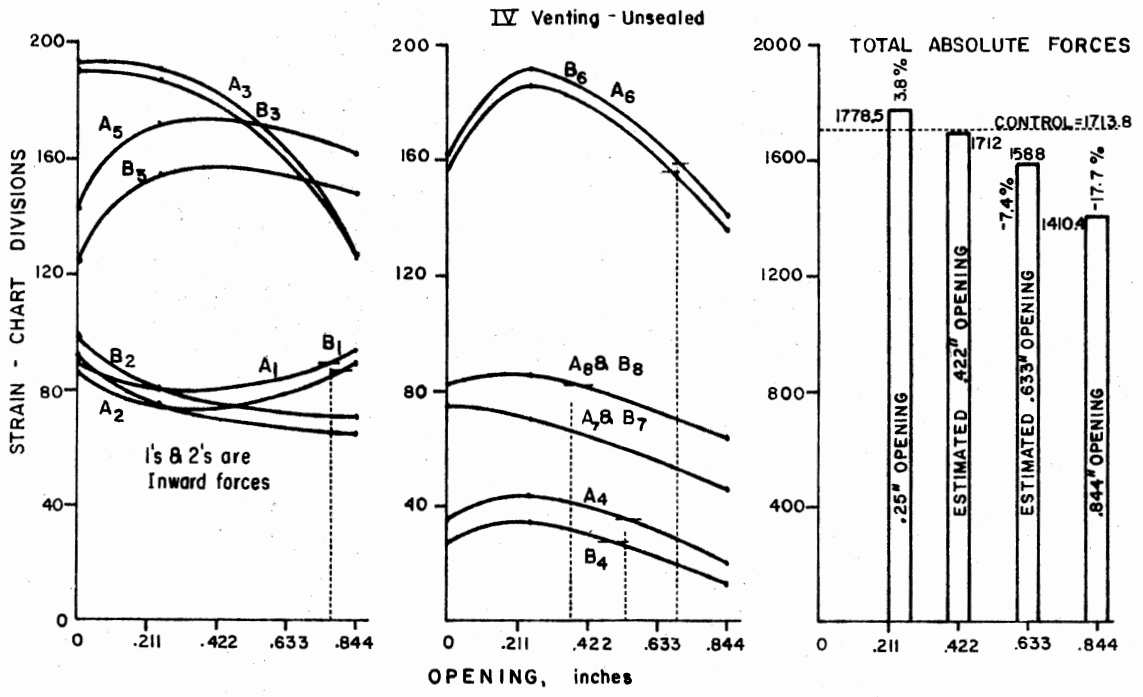

Figure 132. Individual Strain Readings Registered at Monitoring Points and Total Strain Readings for Vent Tests

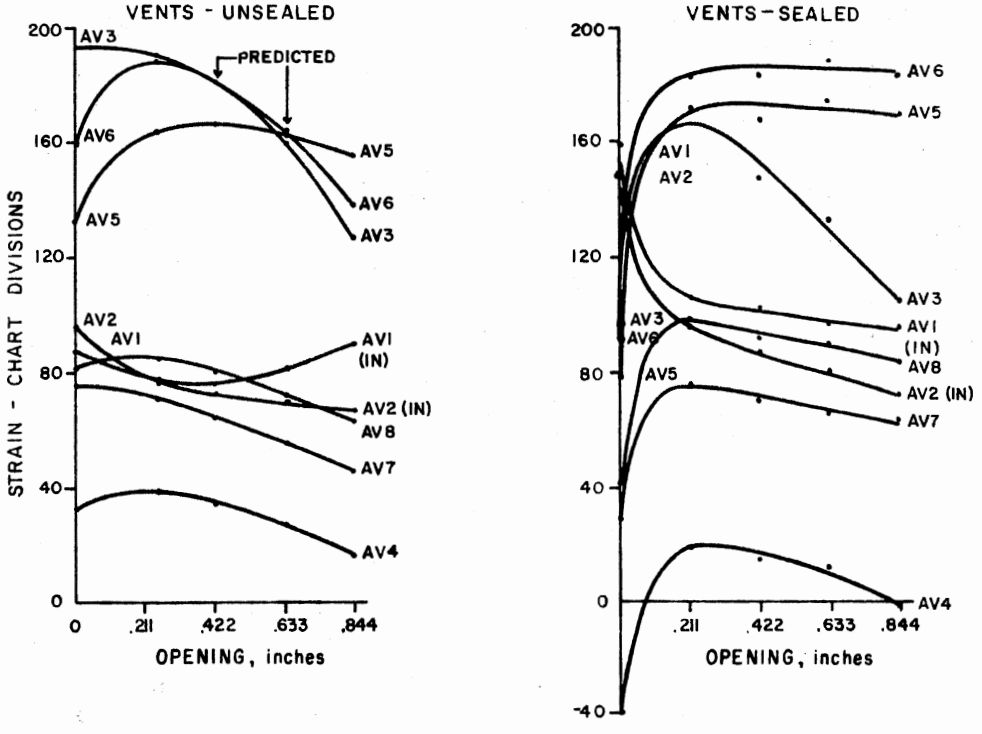

Figure 133. Average Strain at Monitoring Points for Vent Tests

dashed line at about .77" on the drawing. A2 and B2 decrease 20.6% for .25" and 30.2% for .844", likely due to decreased wall area in the immediate vicinity.

2. At the leading edge of the roof, the opening causes a slight decrease (1.4%) in A3 and B3 forces, for the .25" opening but a decrease of 34.3%, with respect to the control forces, for .844". Much of this is due to decreased uplift under the eave and less air flow over the structure. A4 and B4, at the upper edge of the same panel, first show a 20.4% rise with the .25" opening and then decline after ≃ .53" opening, considerably below the control level (-46.7%) for .844". This is likely due to added pressure inside, and then a relief of this, as the building is opened up due to more direct air flow through the structure and reduced flow over the ridge.
3. On the back roof A5 and B5 rise 23% for .25" and then slowly decline as the opening increased - still 16.3% higher than the control. A6 and B6 show the same trend, rising 19.5% for the 1/4" opening but then falling 11.6% below the control value for .844". The "break even" opening is about .7". The air flow through the building impacts most directly upon the back roof interior so the rise is not a mystery, but the failure of A5 and B5 forces to fall below the control as do the 6's when the opening is increased, remains unexplained.
4. The back wall forces at 7 continually decline to 61.6% of the original control values. At 8, bottom of the back wall, a slight rise (3.0%) is noted for .25" but after about .37"

opening, the forces are less than the control and drop to 76.5% of the control for the .844" opening.

Brief inspection of the results indicate different flow patterns for the two degrees of opening tested. This was not anticipated. It was expected that the forces would progressively rise or decline as the opening was increased. Overall, the .25" opening results in a 3.8% increase over the control forces whereas the .844" opening shows a decline of total forces of 17.7%.

The small opening, even though it existed on both walls of the model, apparently caused reactions similar to those of leakage, adding inside pressure to outside suction. Forces were relieved at the upwind eave, at the sensors nearest the openings in the two walls where the area was reduced, and even at the bottom of the front wall. Other sensors, mainly those of the roof (Figure 131) show increase as if absorbing the energy of deflecting the air flow or from additional pressure inside the building.

It is possible in the case of the larger opening (.844"), more direct air flow existed, which reduced the forces on all the surfaces except at 5 and 1. The A5 and B5 forces are diminished some, but still are higher than the control.

The slight increase in force at 1 for the larger opening is more a mystery. Separate tests on the front wall alone (other panels completely removed) revealed decreases of 18.4% at 1 and 23.3% at 2 for the largest opening, .844".

From the left-hand curves of Figure 132, the values of strain for openings of .422" and .633" at each of the monitoring points were predicted. Refer to Table XVIII. Using these, and the values

TABLE XVIII

SUMMARY OF PARTIALLY REDUCED DATA VENTING TESTS--UNSEALED MODEL
(RECORDED STRAIN IN CHART DIVISIONS)

	Openings (in.)				
	0.0"***	0.25"***	0.422"	0.633"	0.844"***
AV1*	88.0	77.5	76.0	82.0	91.3
AV2*	97.0	77.0	73.0	70.0	67.7
AV3**	192.5	189.9	181.0	161.0	126.5
AV4	32.2	38.7	35.0	28.0	17.1
AV5	132.8	163.5	166.0	162.0	154.5
AV6	156.6	187.2	181.0	163.0	138.5
AV7	75.0	70.1	64.0	56.0	46.2
AV8	82.8	85.4	80.0	72.0	63.4
Panel 1*	370.0	309.0	298.0	304.0	318.0
Panel 2	449.4	457.2	432.0	378.0	287.2
Panel 3	578.9	701.4	694.0	650.0	586.0
Panel 4	315.6	311.0	288.0	256.0	219.2
Inward*	370.0	309.0	298.0	304.0	318.0
Outward	1343.8	1469.6	1414.0	1284.0	1092.3
Panel Total (Out)	973.8	1160.6	1116.0	980.0	774.4
Total	1713.8	1778.6	1712.0	1588.0	1410.4

*Inward
**Now multiplied by 1.5
***By experimental test

measured for .25" and .844", the total absolute forces for the building over the entire range of opening were calculated. These are also plotted on the right on Figure 132.

It can be seen that the first reduction in the absolute total forces is probable only after an opening of .422" is exceeded. The opening at .25" is presumed to result in the highest total forces (+3.8%) in an absolute sense - i.e., without regard to the inward or outward direction of the forces. Opening of .844" results in the least (-17.7%).

From Figure 133, the average strain readings at each point, indication is that AV5, at least, does not peak at the .25" opening. (The comparable results for the sealed model appear on the same figure and will be discussed later.)

Figure 134 shows the panel totals with all but panel 1 indicating outward forces.

1. The combined results of AV1 and AV2 on panel 1 show total inward forces are a minimum with an opening of about .422" and are always less than the inward forces on the control with zero opening. Panel 1 forces do show a slight upward rise as the opening is increased from .422". This is due to the influence of AV1.
2. The outward forces are on panels 2, 3 and 4. Panel 2 forces quickly peak at .25" of opening and then steadily fall, continually lower than the control after about .3" of opening. Panel 3 forces rise sharply (mainly due to AV5), peaking (+22%) at about .3" and never drop below the control until the end of the range, .844" of opening. Panel 4 forces

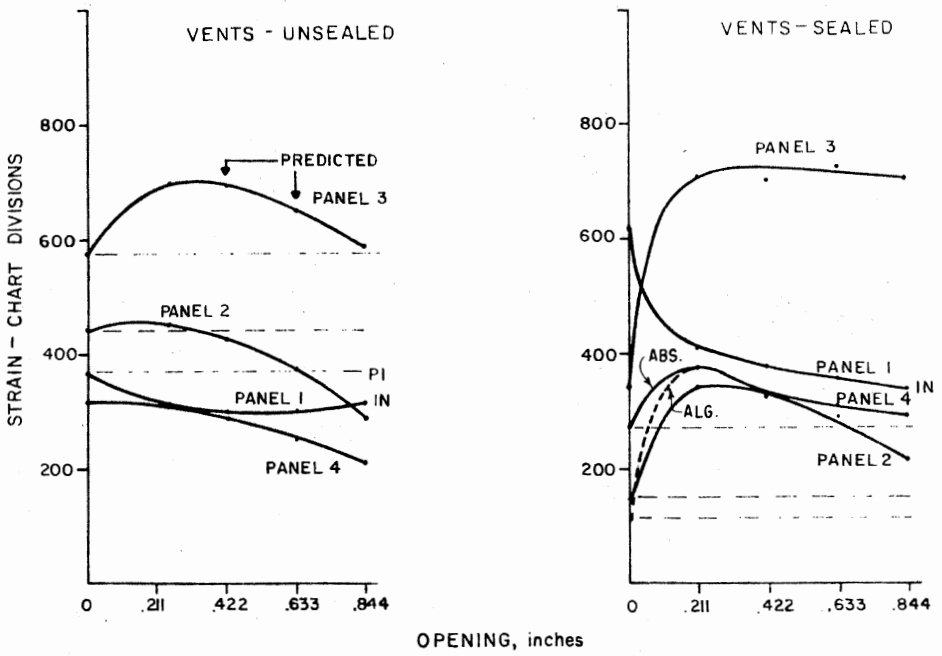

Figure 134. Panel Strain for Vent Tests

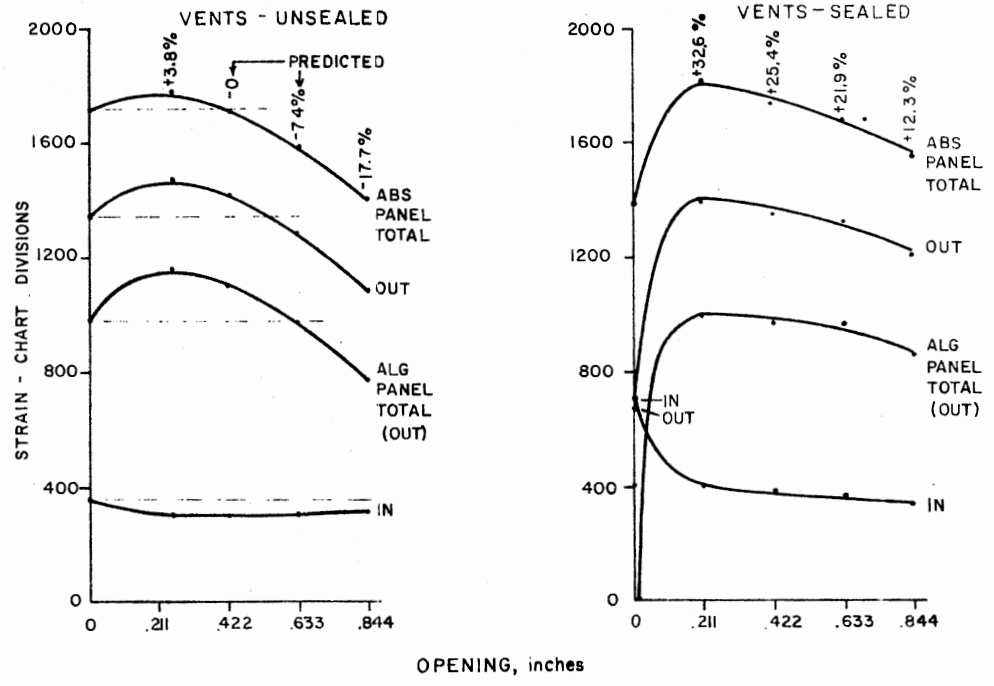

Figure 135. Building Total Strain for Vent Tests

seem to maintain the control level until .25" and then gradually fall to 66% of original value.

Figure 135 reflects the way the forces combine to obtain the total forces on the structure. Each of the two middle curves actually represent successive vector subtractions of the lower curve (panel 1 = inward) from the upper curve (total absolute forces).

In all cases the most desirable opening is .844" except for the inward forces at the base of the upwind wall which increase beyond the control value. This rise is reflected by the inward forces. Their magnitude is not critical and the structure is best able to sustain inward forces. The absolute forces show reduction after .422" as noted earlier. The outward forces indicate reduction below control values after ≃ .55" of opening. These would tend to explode the structure or its cladding. The combination of panel 2 and 3 tend to raise the roof with the vertical components and displace it backward with the difference of their horizontal components. The components of the algebraic forces, which tend to move the building off its foundation, drop below the control only after ≃ .633" of opening.

If individual and panel forces are considered, the roof forces are the most serious. Only AV5 never falls below the force level of the control. This would indicate that the fastening at the ridge of the back roof needs the most attention if venting a leaky building is attempted. The leading edge roof force at AV3 is originally the highest value but does decline. The force level, AV6, at the back edge, was initially lower but rapidly rose to the magnitude of AV3 at .25" and then declined at the same rate as AV3.

The worst original force (AV3) is therefore steadily diminished.

The counterpart on the back roof (AV6) rises but never exceeding the declining AV3. Since the wind can blow from either direction, both points on the building would have to be designed to equal strength and the individual rise of AV6 is therefore not a limitation. AV5 is critical, as is its combination with AV6 seen for panel 3 in Figure 134.

Conclusions - Venting, Unsealed Model. Venting an unsealed model profoundly affected the force pattern.

The opening with 0.25" height did not beneficially alter the forces.

At an opening height of 0.422" (1.75' on the prototype) the predicted total forces would be practically the same as for the control. The distribution would differ, however, panel 3 forces would be higher whereas the other four panels would be lower. The worst original force, at 3, would be 5% less and would equal the 6's.

The predicted forces for an opening of 0.633" would combine for a total of 7.4% below the control forces. Again, all forces would be less than the control except for panel 3. The worst forces (3's, 5's, and 6's) would be all about the same magnitude with the 3's ≃ 16% less than originally.

The largest opening, 0.844", shows the first instance of panel 3 forces being nearly the same as for the control - then only because the increased 5's are cancelled by the decreased 6's.

The "best" opening depends upon which forces or combination of forces are considered the most objectionable. At least an opening of .633" should be used (2.625' on prototype). It represents an open area of 14.4% of the movable panel and 12.4% of the entire wall. An

opening of .844" is more effective (3.50' on the prototype, 19.2% of the movable panel area and 16.5% of the area of the front wall).

This modification shows ability to reduce all the forces except those at the ridge of the back roof panel and might be pursued further. More tests should be run to verify the interpreted readings of 0.422" and 0.633". Further tests on the sealed model seem in order also. Too, it would seem beneficial to investigate the possibility of eliminating the addition of upwind pressure inside the building by containing the flow in ducts as it is conducted through the structure.

Results - Venting, Sealed Model. The control forces conform to the pattern determined earlier for other sealed models - forces are inward on the front wall and outward on the front roof and the back surfaces except for A4 and B4 which are inward.

Where the results of the unsealed model were difficult to assess as to the exact benefits of venting, the vented sealed model presents results clearly detrimental in almost every aspect. Tests were run at all the planned openings.

Examination of Figure 133, where the averages are plotted alongside of those of the unsealed model, reveals large increases over the control at .211" followed by a drop in the forces as the openings become larger for most of the monitoring points; the magnitudes are generally greater than the control for the largest opening. The 5's and 6's deviate slightly from this pattern as the drop after the 0.211" opening is missing.

AV3, after the large increase, falls to a level quite near that of the control. This would indicate an opening larger than 0.844" could

result in the sought for reduction. The 4's show the same trend as the others except the control forces being negative (inward), the subsequent rise and drop leave the forces for the largest opening near zero.

Panel 1 forces also deviate from the above pattern by steadily dropping at both 1 and 2 as the openings are increased. This would be very important, since panel 1 forces were originally the most severe, if the 3's and especially the 5's and 6's were not increased to levels beyond those of the 1's and 2's originally.

The net results is more clearly seen in the plots of the panel forces (Figure 134). Panel 1 forces decline considerably ($\simeq$ 40%) due to the steady drop in the 1's and the 2's. Panel 2 also declines ($\simeq$ 20%) due to the rapid fall in the 3's (after the large increase) and the effect of the absolute level of the 4's. Panel 4 increases would not be serious but the large increase of panel 3 forces overshadows all potential gains. This increase in lift forces for the back roof is due to internal positive pressure added to the normal suction existing above the back roof. Further, in contrast to the situation for the unsealed model, it shows no promise of decreasing even if the openings were increased.

The total forces (Figure 135) reflect also the dominance of panel 3 effects. For all openings tested, the overall forces increase when compared to the control. The only potential benefit is the reduction of inward forces on the front wall - not an especially vulnerable part of the structure.

Conclusions - Venting, Sealed Model. Contrary to popular belief,

openings in the front and back walls of a well sealed building show no promise for saving the structure from high straight winds. While true that openings will relieve the front wall, and even the front roof section if the openings are large enough, the added outward pressure on inside of the back surfaces cause the forces to exceed those formerly considered most critical. This occurs even though the back wall is also opened the same amount as the front wall.

Only in the case of the unsealed structure do openings show potential for relief. In the case of the sealed structure, the building would be more secure if it remained entirely sealed.

Though the models tested are not suitable to draw widely applicable conclusions for housing in that the models contained no ceiling, application of this prediction to buildings with no ceiling or cathedral ceilings seems in order.

It seems in retrospect that an interesting attempt for both options would have been to vent the roof - perhaps simulating spring loaded panels as in Figure 136.

For the sealed model on those portions of the roof under suction (AV3, AV5, AV6), the vents would open allowing suction to add to the outside inward forces on the front wall, but it could relieve the roof and back wall surfaces. At 4 where the force at the top of the front roof is inward, the forces would hold the vent shut. The back roof vents would add additional suction inside that would increase the inward magnitude of the AV4 forces.

For the unsealed model, the same spring loaded vents might be opened from the inside due to positive pressure inside and negative pressure outside. The lower roof portion should be vented in the

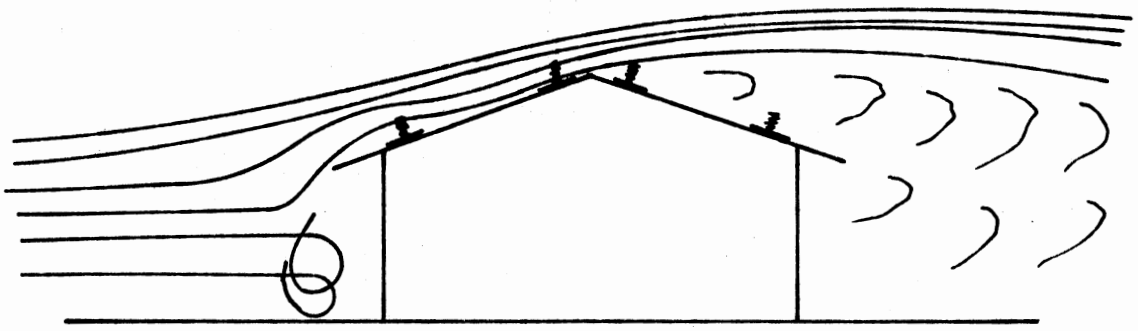

Figure 136. Spring Loaded Roof Vent Panels

area closest to the leading edge, but still inside the building, if this method is the subject of future investigation.

Ducts - Final Investigation

Based upon the favorable preliminary results of the ducts in the form of tubes, and upon the venting results, the concept of a single long duct was pursued in this final phase of the investigation. A flow visualization of the concept is shown in Figure 137. The air flow must be contained as it is conducted through the structure to avoid the additional positive pressure released into the building by the opening in the front wall - pressure which adds to the outward force already existing on the downwind exterior surfaces due to negative pressures outside the building.

Method. The same methods as used for the other preliminary tests were employed - the flow visualization tunnel and wind tunnel tests on the scaled model.

Equipment. The apparatus used to simulate the necessary ductwork is shown in Figures 138 through 141. The front and back wall were modified so as to permit attachment of two cardboard sections - one to each wall panel. The center portion was completed with a flexible section made from 2 mil plastic material taped into place so as to allow inward movement of the front panel without outward movement of the back wall panel.

For the first time, the 27" disc (Figure 140 and 141) upon which the model is constructed was utilized to rotate it around the center bolt.

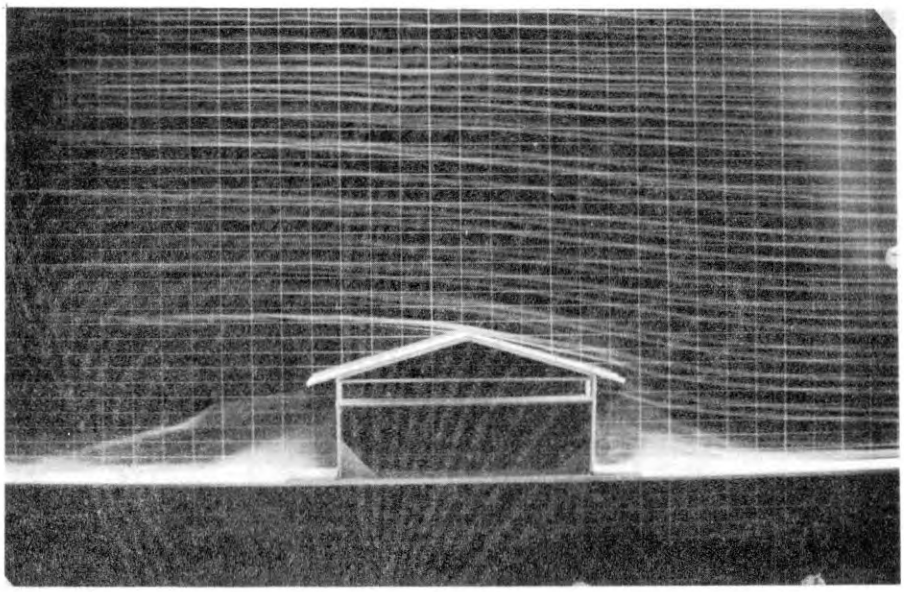

Figure 137. Air Flow Visualization for Building with Duct

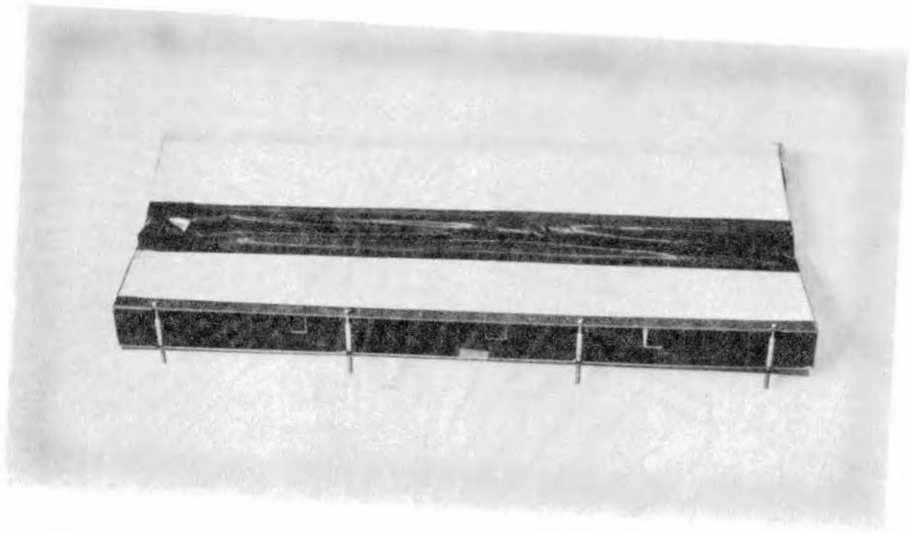

Figure 138. Cardboard Duct with Flexible Plastic Section

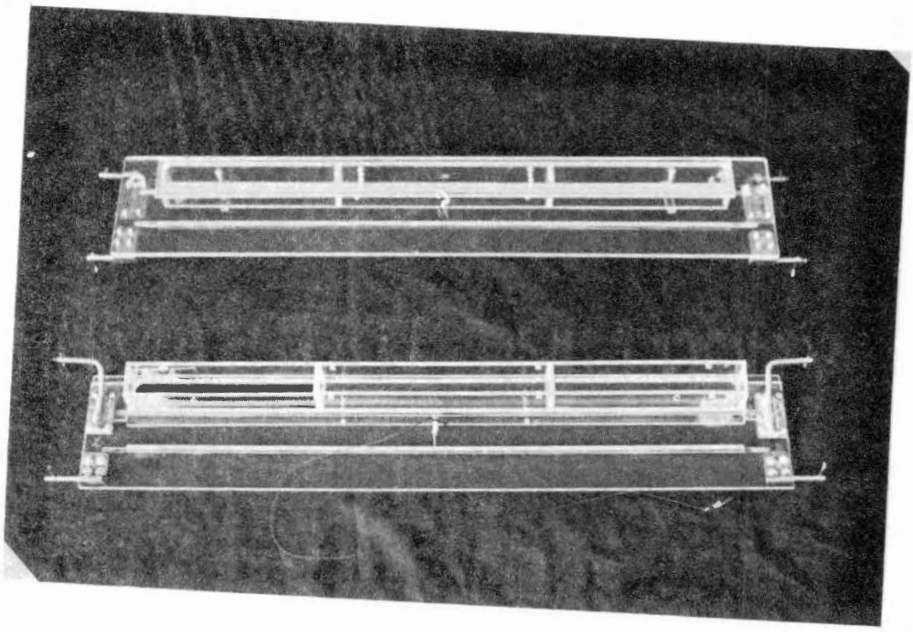

Figure 139. Modified Wall Panels

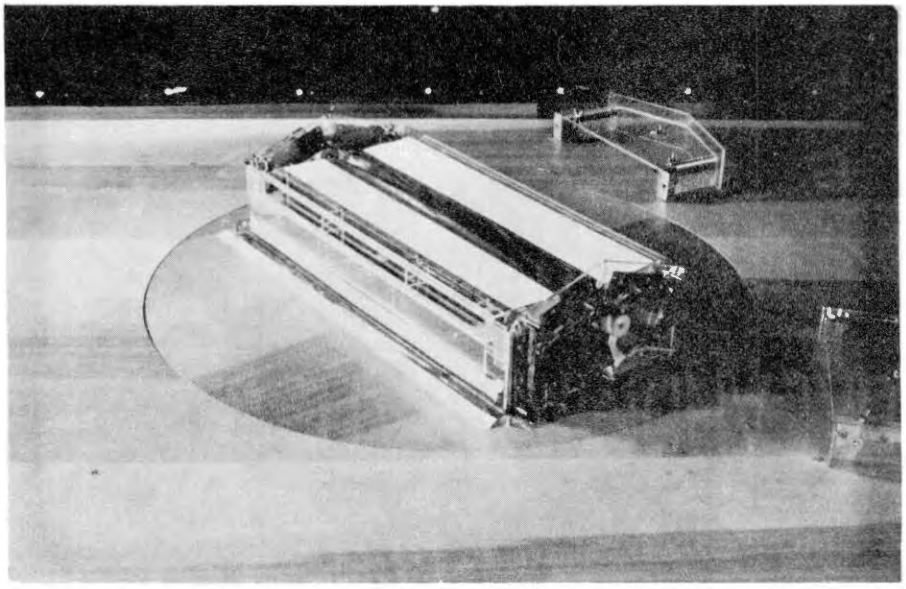

Figure 140. Model Without Roof Showing Assembled Duct Mounted Inside Model

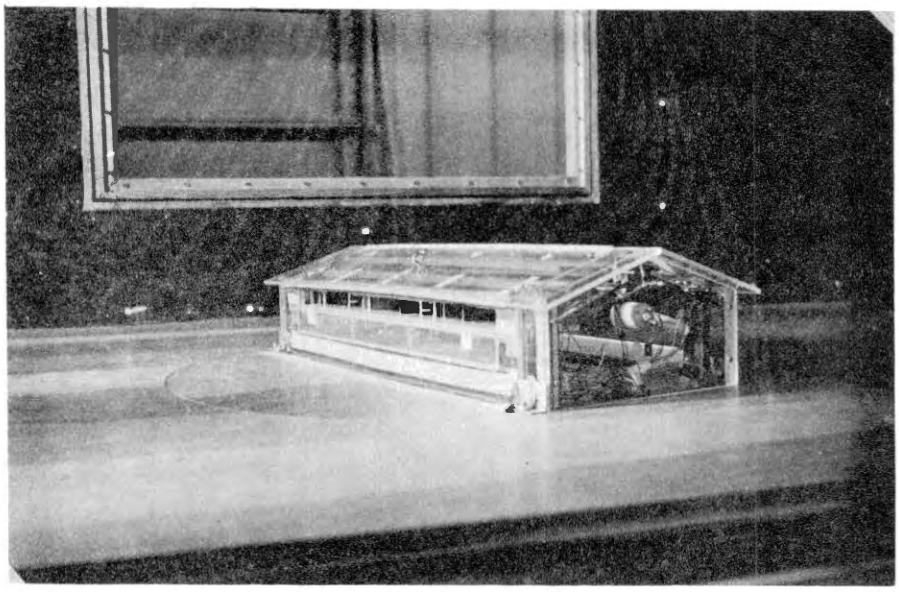

Figure 141. Completely Assembled Model with Ducts

Procedure. The procedure, as previously outlined for the full tests, was employed. The major differences from that followed for the preliminary tests were:

1. Tests were run at three velocities of air flow ranging from 25 miles per hour to 40 miles per hour at 0° orientation. (Results are not included here except for brief mention.)
2. The building was rotated with respect to the air flow in the tunnel to determine the effects of 15 and 30° orientation to the wind.
3. Only the "sealed" model was tested.

The same openings were used as for the vent tests, i.e., 0.0", .211", .422", .633" and .844". The rear opening of the duct was sealed only for the "no opening" controls. For the remainder of the tests, it was wide open with the cover still attached to the wall in the dropped position to achieve the same back wall weight for all tests. The front cover was dropped vertically to achieve the various openings and maintain the weight. Neither the size of the duct itself nor its exit were varied - only the size of the entrance opening. If the rear panel cover had not been fully open for all the tests except the controls, it would have protruded up into the air flow through the duct and caused distortion of the forces on the back wall.

The tests were run in a semi-randomized order, Table XIV, attempting not to complicate the results by loosening the center bolt an unnecessary number of times. Within a given position, 0°, for example, the order of tests was randomized as the 8, 12, 9, 11, 10 sequence indicates. The replications (three each) were not randomized as the effort to change the modification and perform the needed shake

down run explained previously required excessive time lapse and labor. For the tests at the three velocities, the three replications required at each speed were taken in the same order - i.e., the order Slow, Medium, Fast was employed.

TABLE XIX

IDENTIFICATION ORDER OF TESTS--ANGOPNG

Deviation of Wind Angle from Perpendicular to Upwind Wall--Degrees						
	30°	7		14		13
	15°	6		15		16
	0°	8	12	9	11	10
		0.0"	.211"	.422"	.633"	.844"
		Opening--In.				

Sample Calculations. For 0° orientation and the no opening control, the data obtained for panels 3 and 4 is:

Strain in Chart Divisions

	A_1	A_2	B_1	B_2	A_3	A_4	B_3	B_4	A_5	A_6	B_5	B_6	A_7	A_8	B_7	B_8
Rep 1 (of 3)	154	151	181	168									23	17	10	11

~Interaction Correction, Between 1st and 4th Panels Only~

Averages:

AV1 = (A1 + B1)/2 = (154 + 181)/2 = 167.50

AV2 = (A2 + B2)/2 = (151 + 168)/2 = 159.50

AV7 = (A7 + B7)/2 = (23 + 10)/2 = 16.50

AV8 = (A8 + B8)/2 = (17 + 11)/2 = 14.00

Panel Totals:

PAN1 = 2(AV1 + AV2) = 2(167.50 + 159.50) = 654.00

PAN4 = 2(AV7 + AV8) = 2(16.50 + 14.00) = 61.00

~Individual Strain Interactions in Chart Divisions on Panels 1 and 4~

IA1 = 7; IA2 = 10; IB1 = 1; IB2 = 5;

IA7 = 5; IA8 = 1; IB7 = 2; IB8 = 0;

~Total Panel Strain in Chart Divisions Causing Interactions, from Frame Calibration~

FPAN1 = 493.14

FPAN4 = 528.67

RA1 = PAN1/FPAN1 = 654/493.14 = 1.32620

RA4 = PAN4/FPAN4 = 61/528.67 = 0.115384

~Corrected Individual Strains in Chart Divisions~

A1 = A1 - (IA1 x RA4) = 154. - (7.0 x 0.115384) = 153.192

A2 = A2 - (IA2 x RA4) = 151. - (5.0 x 0.115384) = 149.846

B1 = B1 - (IB1 x RA4) = 181. - (1.0 x 0.115384) = 180.885

B2 = B2 - (IB2 x RA4) = 168. - (10.0 x 0.115384) = 167.423

A7 = A7 - (IA7 x RA1) = 23. - (5.0 x 1.32620) = 16.3690

A8 = A8 - (IA8 x RA1) = 17. - (1.0 x 1.32620) = 15.6738

B7 = B7 - (IB7 x RA1) = 10. - (2.0 x 1.32620) = 7.3476

B8 = B8 - (IB8 x RA1) = 11. - (0 x 1.32620) = 11.000

~Reduction of Data for Velocity Squared~

V1 = 1.300 (1st Replication Velocity)

VS1 = V1 x V1

~Adjustment of the V^2 Term to the Eave Height of Building Using the "Fast" Velocity Profile~

Eave Height = 3.84" (equivalent of 16')

Anemometer Height = 7.25" (equivalent of 30')

$$K = \left(\frac{H_2}{H_1}\right)^{2EV} = \left(\frac{3.84}{7.25}\right)^{2x.17445} = .801127$$

A1 = A1/(VS1 x K) = 153.192/(1.69 x .801127) = 113.149

A2 = A2/(VS1 x K) = 149.846/(1.69 x .801127) - 110.677

B1 = B1/(1.69 x .801127) = 180.885/1.3539 = 133.602

B2 = B2/(1.3539) = 123.659

~Linear Cantilever Beam Calibration Constants in Chart Divisions Per Oz. of Static Force -- Direction of Loading Considered~

CA1 = 32.7355 CB1 = 35.0395

CA2 = 34.2445 CB2 = 36.0115

~Calibration of the Observations for Each Opening~

A1 = A1/CA1 = 113.149/32.7355 = 3.4565 oz./volt^2

A2 = A2/CA2 = 110.677/34.2445 = 3.2320 oz./volt^2

B1 = B1/CB1 = 133.602/35.0395 = 3.8129 oz./volt^2

B2 = B2/CB2 = 123.659/36.0115 = 3.4339 oz./volt^2

~Adjustments for Frame Calibration~

Usually the response of the gages was checked before loosening the center bolt to rotate the model in the tunnel and after the bolt was retightened with the model in the new position. The response of the gages was sensitive to the pressure due to the tightened bolt. In the case of this illustration for the control, all five tests were taken

before the model was moved. There were, however, three calibration checks performed with the special loading frame.

Time Sequence of Data - Frame Calibration

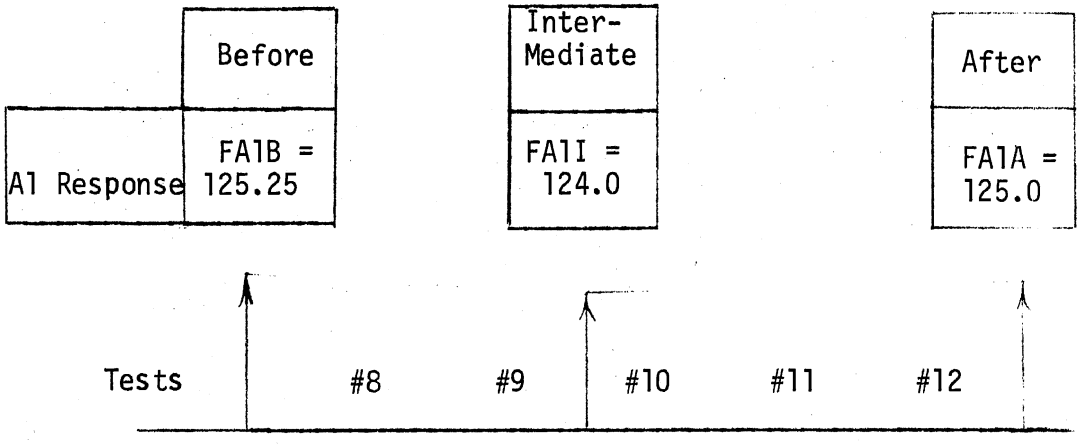

The standard performance for A1 for all the tests was set at the average of FA1B and FA1A, etc.

$$AVFA1 = (FA1B + FA1A)/2 = (125.25 + 125.00)/2 = 125.125$$

and for the other three gages:

Before	After	Intermediate
FA2B = 112.50	FA2A = 109.67	FA2I = 109.00
FB1B = 141.25	FB1A = 139.00	FB1I = 140.00
FB2B = 119.75	FB2A = 117.00	FB2I = 117.00

$$AVFA2 = (FA2B + FA2A)/2 = (112.50 + 109.67)/2 = 111.085$$

$$AVFB1 = (FB1B + FB1A)/2 = (141.25 + 139.00)/2 = 140.125$$

$$AVFB2 = (FB2B + FB2A)/2 = (119.75 + 117.0)/2 = 118.375$$

A1 and the other readings for the control (Test #8) were then adjusted each to their own standard.

$$A1 = A1\ (AVFA1/FA1B) = 3.4565\ (125.125/125.25) = 3.4530$$

$$A2 = A2\ (AVFA2/FA2B) = 3.2320\ (111.085/112.50) = 3.19135$$

$$B1 = B1\ (AVFB1/FB1B) = 3.8129\ (140.125/141.25) = 3.78253$$

$$B2 = B2\ (AVFB2/FB2B) = 3.4339\ (118.375/119.75) = 3.33945$$

All the A1's for tests 9, 10, 11 and 12 were adjusted as follows.

The intermediate frame calibration after test 9 was assumed to represent it before adjustment to the standard. The same assumption was made for Test 12 and the frame calibration after. The difference between the two was divided into thirds [(125-124)/3 = .333]. This amount was added to the 124.0 to get a distributed frame calibration value after the tenth test and twice that amount was added to 124.0 to get the value for frame calibration after the eleventh test. These numbers:

#9	124.000
#10	124.333
#11	124.667
#12	125.00

were then used to bring all the A1 readings to the common standard of AVFA1 (125.125) exactly as was done for test #8 in the previous example.

i.e., A1 (for test 11) = A1 (AVFA1/124.667)

= A1 (125.215/124.667)

a very slight increase. The examples used show slight changes because the bolt was not loosened. The other frame calibration differences (tests 6, 7, 13, 14, 15, 16) are more significant and all were normalized to remove the "bolt effect" as was A1 for test #8.

All readings now being to a common standard, two further adjustments are necessary.

~Adjustment for Difference in Length of Opening and Movable Panel~

Length of panel = 20-19/32"

Length of opening = 18"

L = (20-19/32)/18 = 20.59375/18 = 1.1441

A1 = 3.4530 x 1.1441 = 3.95056

A2 = 3.19135 x 1.1441 = 3.65125

B1 = 3.78253 x 1.1441 = 4.32759

B2 = 3.33945 x 1.1441 = 3.88361

~Readings Adjusted for Recorder Channel Calibration Constants (R_i) Reflecting Deviation from Standard of 20 -- Higher than 20 Indicates a Higher Force than Reality~

R5 = 20.0 for A_1

R6 = 20.0 for A_2

R7 = 19.9 for B_1

R8 = 20.0 for B_2

Here only B1 required any correction.

$$B1 = B1 \left(\frac{ST}{R7} \right) = 4.33144 \left(\frac{20.0}{19.9} \right)$$

$$= 4.32759 \times 1.0050 = 4.349337$$

Each of the replications of the other individual strain readings were treated in a like manner to obtain three adjusted values in ounces of load/volt^2 for the eight monitoring points on both ends of the model. One further step was needed.

~Obtain Averages of A's and B's for 0° Orientation~

At 0° orientation where A1 and B1, for example, could be expected to be the same, the average of the two was obtained for each replication in order to obtain a single curve. Since, when the model is rotated with respect to the wind, the one end is not in the same wind loading situation as the other end, the readings at the two ends of the building can only legitimately be averaged for the 0° orientation where it is symmetrically situated. These readings were averaged for the purposes of finding a common standard from which to judge the

resulting loading at the two ends of the model as the angle of orientation was changed.

$$(A1 + B1)/2 = (3.95056 + 4.34934)/2 = 4.149950$$

$$(A2 + B2)/2 = (3.65125 + 3.88361)/2 = 3.767384$$

The cause of the differences in the two readings at either end of the model is unknown since all the adjustment factors have been accounted for. It may be the remaining velocity differences across the tunnel, never completely resolved, differences in turbulence level due to the 26 additional bricks on one side or even sealing problems still lingering somewhere on the model. In any case, whatever the cause of the difference, by averaging the two readings, it is eliminated mathematically.

~Normalize the Readings at 15° and 30°~

The quantity required to bring A1, for example, at 0° orientation to the value of AV1 was next added to all the other A1 readings at other orientations. B1 was treated in the same fashion. This, in effect, normalized all the A_i and B_i readings for the orientations of 15° and 30° to those readings at 0°.

The A1's at 15° and 30° were too low by 4.149950 - 3.95056 = 0.199390. This amount was added to these readings. The B1's at 15° and 30° were too high by the same amount (4.149950 - 4.34934), therefore it was added to these readings. The resulting readings indicate the true differences in loading at the two ends of the structure, the deviation between the ends at 0° orientation having been eliminated.

The total panel forces, the inward and outward forces, the building absolute and algebraic totals are in no way affected by this

normalization as the values at the B end of the building decrease by the same amount as the A's increase.

Each of the three replications for each individual monitoring point was treated in basically the same fashion. (It was not necessary to consider interactions for the roof panels.) The mathematically derived quantities of panel forces, inward and outward total forces, etc., were maintained as individual replications for statistical analysis. The calculations explained above were written in SAS computer language in order to link the data set with SAS statistical analysis programs.

Discussion of Results. The results of the analysis of variance are listed in Table XX. The most important variable affecting the response surface is marked with an asterisk.

The experimental results are plotted in Figures 142 through 158.

The A end of the model is upwind when the prevailing wind strikes the building at an angle. The B end is downwind.

In Figure 142, at 0° with no modification, inward B1 has its highest value. A1 does not, but increases to a high at 15° and falls off a little at 30°, still higher than at 0°. The modification serves to decrease the forces in all cases--quickly at first and then steadily, as the opening is progressively increased. In general, with the exception noted, the forces at the bottom of the upwind wall progressively decline as the wind changes away from perpendicular impingement. For both, the influence of the opening is greater than that of the wind orientation. The wind angle is more influential at B than at A.

Figure 143, where A2 and B2 are shown, reveals very similar

TABLE XX

ANALYSIS OF VARIANCE--F VALUES

	OPENING	ANGLE	OPENING x ANGLE
A1	851.2*	61.0	36.6
B1	765.5*	511.9	8.6
A2	2191.4*	59.3	48.4
B2	1982.8*	750.7	36.6
Panel 1	1773.4*	335.5	35.0
A3	2972.5*	758.8	76.5
B3	3501.6*	621.0	94.9
A4	165.3	1250.4*	9.2
B4	260.5	1487.4*	12.4
Panel 2 Absolute	3614.6*	77.8	188.0
Panel 2 Algebraic	4097.4*	2416.1	104.6
A5	249.6	4389.2*	46.0
B5	207.9	1597.4*	42.8
A6	1336.2	2686.8*	144.0
B6	1156.9	1497.6*	168.4
Panel 3	835.9	4065.8*	122.4
A7	1603.4*	568.6	564.3
B7	682.6*	118.8	44.4
A8	591.9*	148.1	35.4
B8	655.9*	200.1	53.9
Panel 4	2025.2*	775.9	290.7
Outward	4132.5*	4478.3*	224.6
Inward	1157.5*	928.4	56.0
Panel Total Algebraic	1079.0	10390.9*	95.6
Panel Total Absolute	3056.6*	402.3	150.7

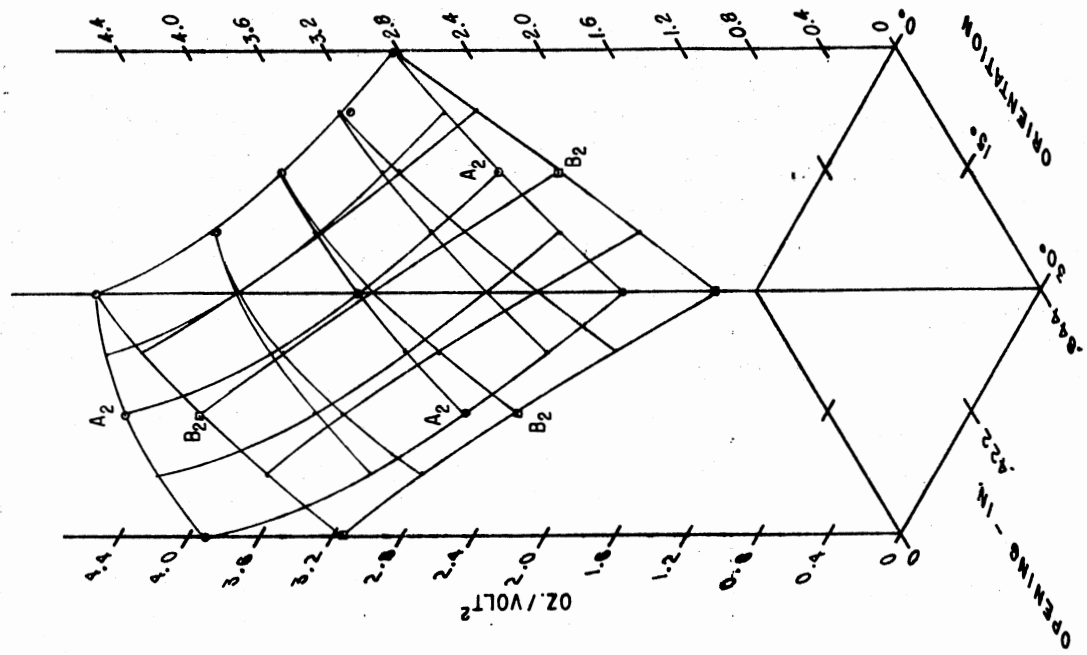

Figure 143. A2-B2, ROP1

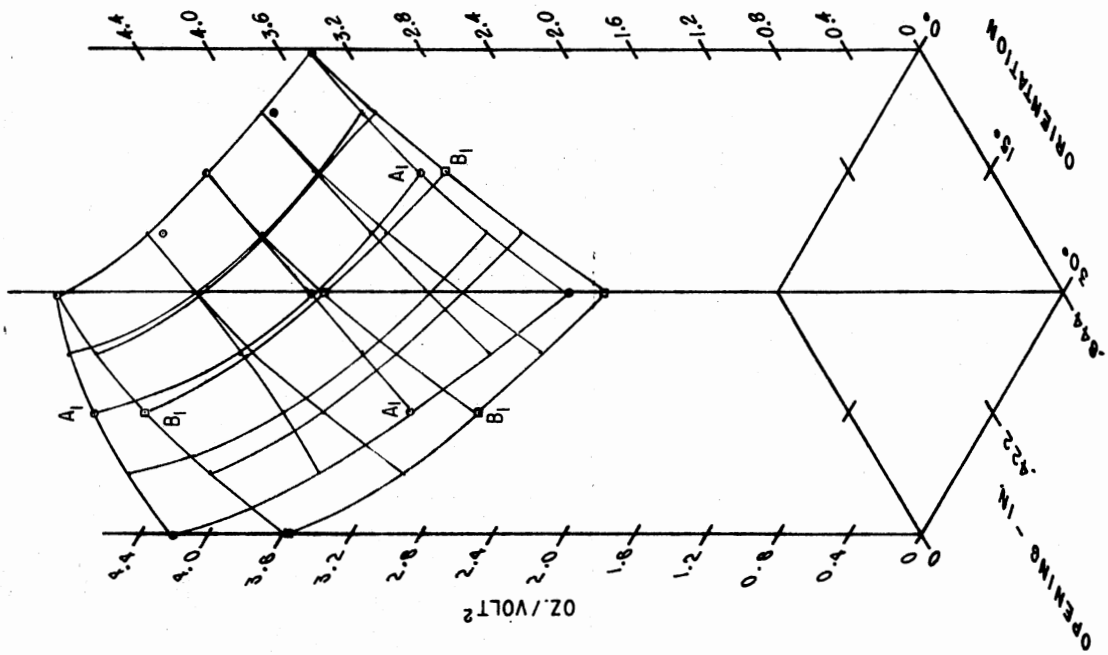

Figure 142. A1-B1, ROP1

behavior at the top of the upwind wall where the opening to the modification is located. The forces are again inward and somewhat lower than those at 1. The effects of the modification are more pronounced; the effects of the orientation for A2 are about the same or less, but for B2 are greater than for the 1's. The B2 response surface is curved the opposite direction from that of B1, with respect to the modification in the interval, from 15° to 30° orientation. B2 is rapidly falling at 30° and .844" opening.

Figure 144 shows the accumulation of inward forces for panel 1. Interestingly, the combination shows increasing decline of force for the model with modification as the opening is increased and as the wind moves toward 30°. The forces on the front panel comprise the major portion of the inward building forces of the four panels. The opening is the most influential variable.

In Figure 145, A3 and B3, even though they are located at different ends of the building, display virtually identical behavior. The orientation scale on the plot is now reversed so that 0° with no opening is on the left. Here the rise of forces incurred at the front part of the leading roof panel is overwhelming as the wind switches toward 30°. With no modification, even downwind, it appears the forces nearly double (from 2.0 to 3.4 oz./volt^2). With even an opening of .211", however, much of this rise is averted. An opening of 0.844" resulted in the least increase due to increasing the angle of orientation. The greater the wind angle, the greater the effectiveness of the modification. Opening is the dominant factor of the two.

A4 and B4 are shown together in Figure 146 where negative values are inward forces and positive are outward. The two, again, are very

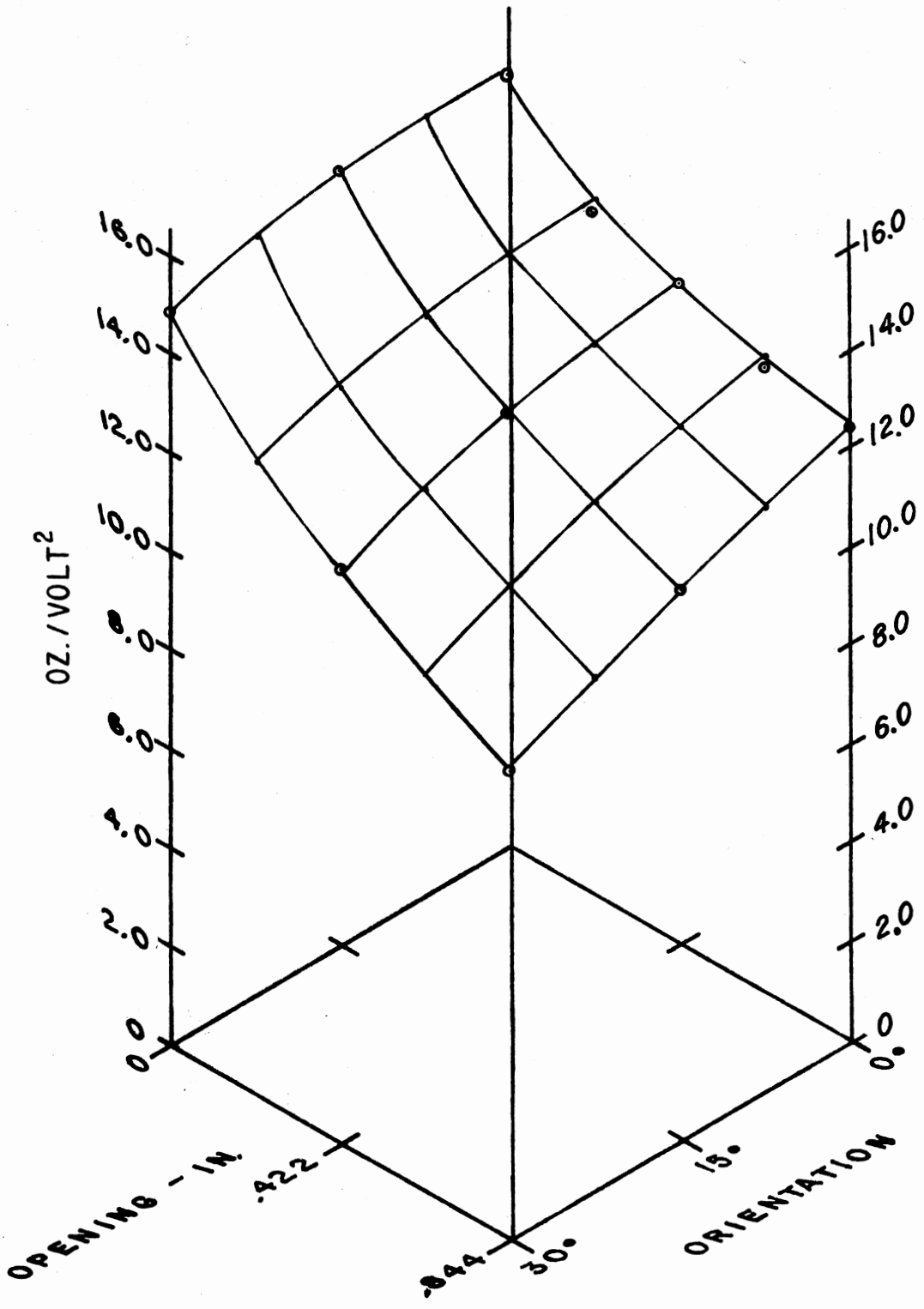

Figure 144. Panel 1, ROP1

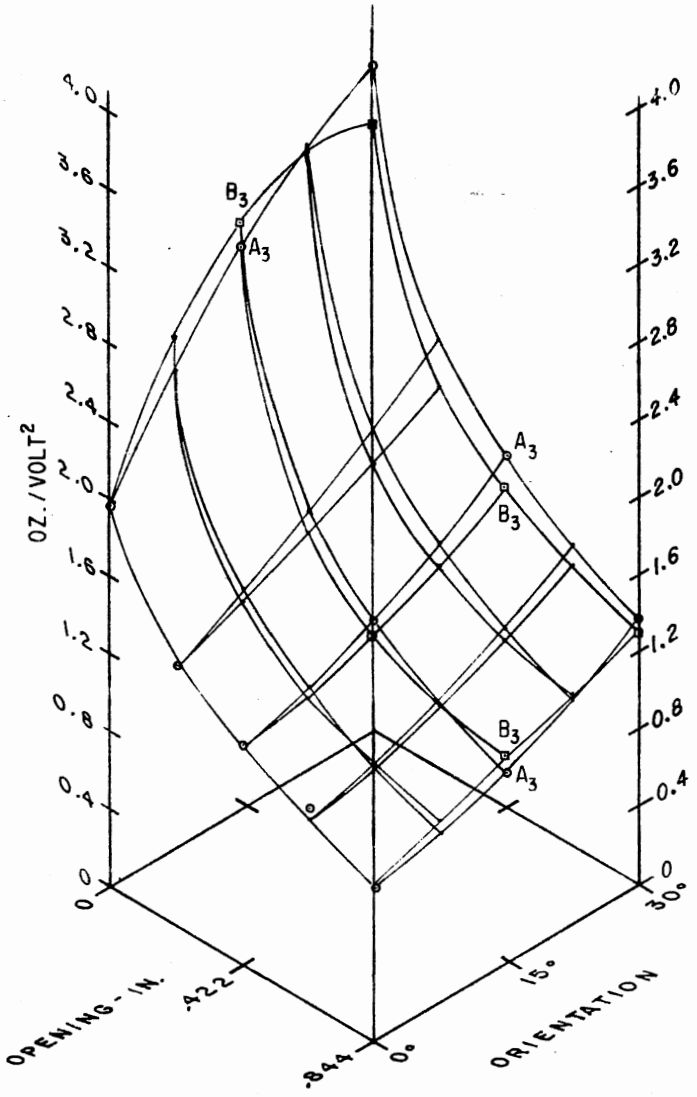

Figure 145. A3-B3, ROP1

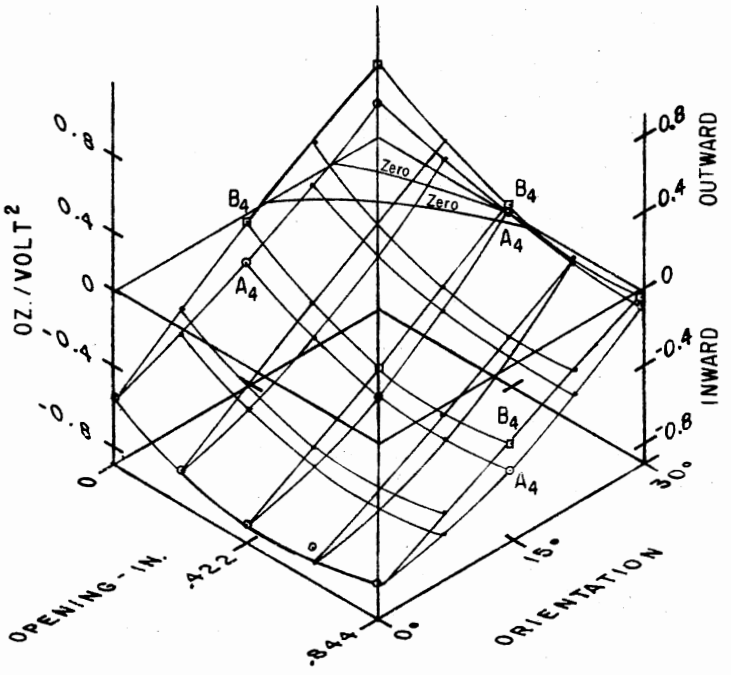

Figure 146. A4-B4, ROP1

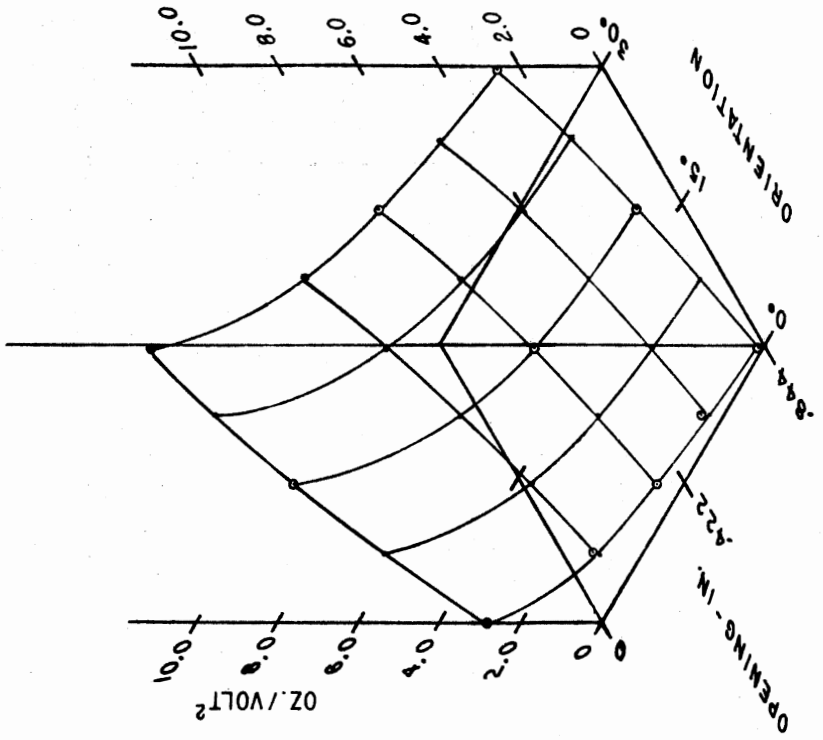

Figure 148. Panel 2 - Algebraic, ROP1

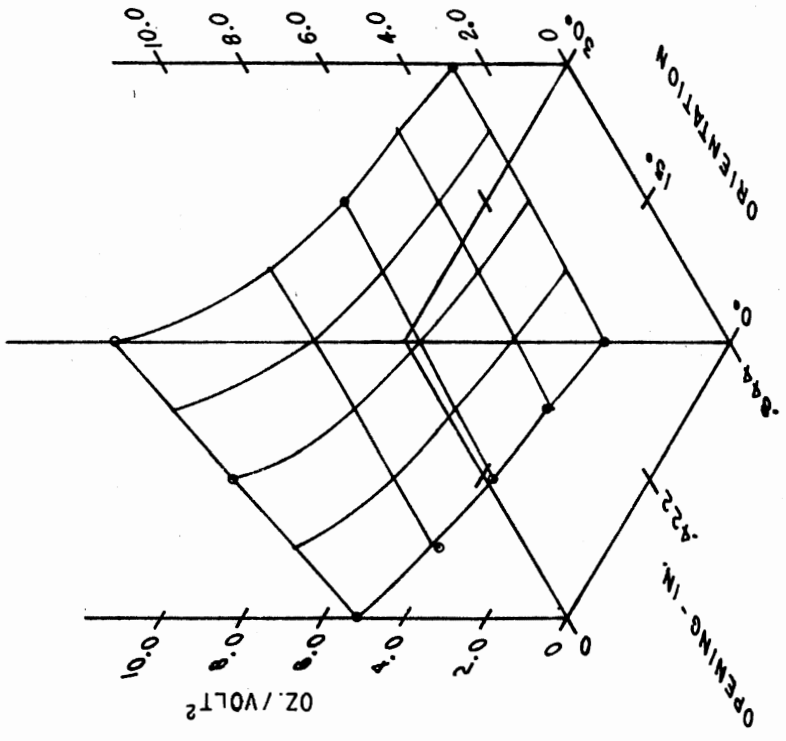

Figure 147. Panel 2 - Absolute, ROP1

similar and are also found on the front roof panel, now at the ridge. The general level of forces is quite low and this is not considered to be a critical portion of the structure by any standard. If the forces are inward, uplift is no problem, and if outward, they are still small in magnitude. It is interesting to note, however, that the forces on the downwind portion of the building (B) are more outward than at the upwind (A). The changing wind orientation from 0° to 30° causes the forces to become almost linearly more outward. Too, the modification shows to increase inward forces slightly as the opening is increased. The wind orientation is the variable most affecting the response surface.

The absolute forces on panel 2 (Figure 147) indicate that overall force levels increase linearly on the unmodified structure as the angle of wind moves from 0° to 30°. This is decreasingly true as the size of opening is increased, until with .844", the orientation has no effect on the absolute forces. Another inspection of A3-B3 and A4-B4 shows the reason--at .844" the outward increase of A3-B3 from 0° to 30° is the same as the inward decrease of A4-B4. ABSPAN2 does show the modification to be effective in reducing the forces though--somewhat moreso at 30° than at 0°. At 0°, the decrease is almost linear whereas at 30° there is a rapid drop from 0.0" to .211". Opening is the dominant variable and the F value of the cross products is higher than that of "Angle".

Panel 2 algebraic or net forces (Figure 148) mirror the pattern of A3 and B3, diminished by the nullification of some of these outward forces by the inward A4 and B4. The net forces increase as the wind orientation increases and decreases with opening. At 0° and .844"

the net forces are nearly zero because the outward value of A3 and B3 is matched by the inward value of A4 and B4. Elsewhere the net forces are outward. Opening most affects the response surface though the wind angle is nearly as important.

A5 and B5 (top of back roof panel) are outward in nature. Figure 149 reveals the great dependence of the response surface upon the angle of wind orientation, greater than any other monitoring point on the model. Here the forces more than double with an increase of the angle from 0° to 30° with no modification. The upwind "A" end of the building shows to be especially susceptible to higher forces as the A curve becomes much higher than B for all values of orientation greater than 0°. While the B forces also increase greatly with orientation, they do not approach the level of A. The differences between the A5 and B5 curves is also greater than for any other monitoring point. The modification appears to be of maximum value in reducing the forces at .844" only for 30°. The forces for the .844" opening are everywhere less than those for no opening. At 7-1/2° and 0° the .844" opening force values are the same as for no opening, however. For most of the 0° - 22-1/2° range, either an opening of .211" or .422" is best.

At the lower edge of the back roof, the A6 and B6 curves are very much alike (Figure 150), though again, the upwind A is higher than B, its counterpart away from the wind. Aside from the upward turn of A at .844", the modification does reduce these outward forces throughout. The effect of opening is more pronounced at 30° than at 0° and in most cases .633" is as beneficial as .844"--more beneficial in fact for the A end of the building. Here again, the angle of the wind is the most

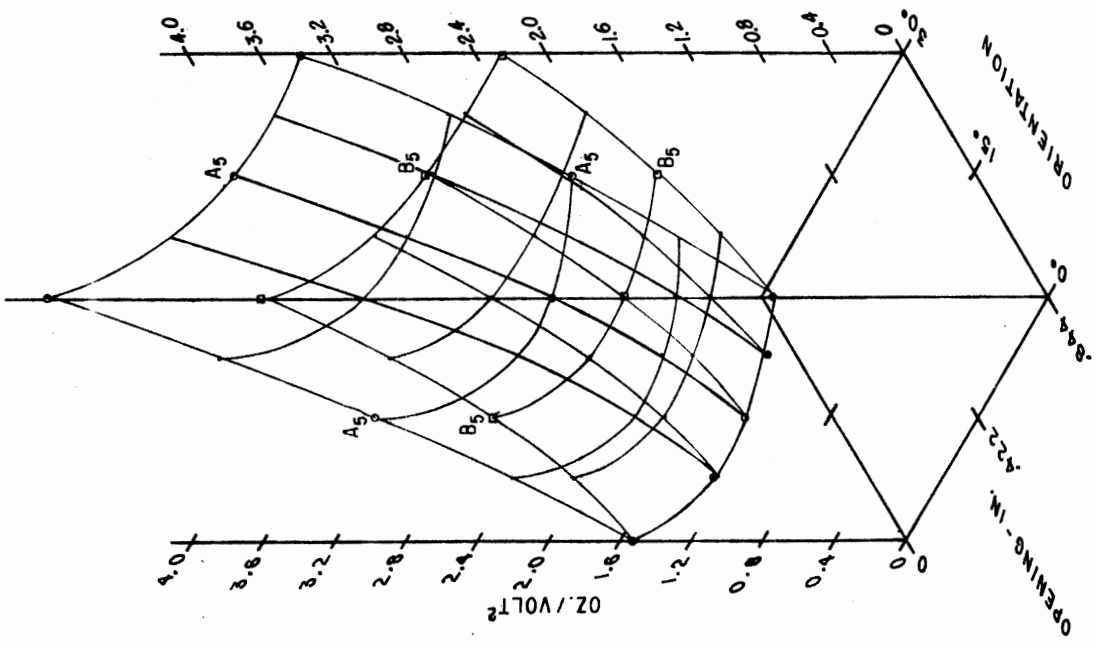

Figure 149. A5-B5, ROP1

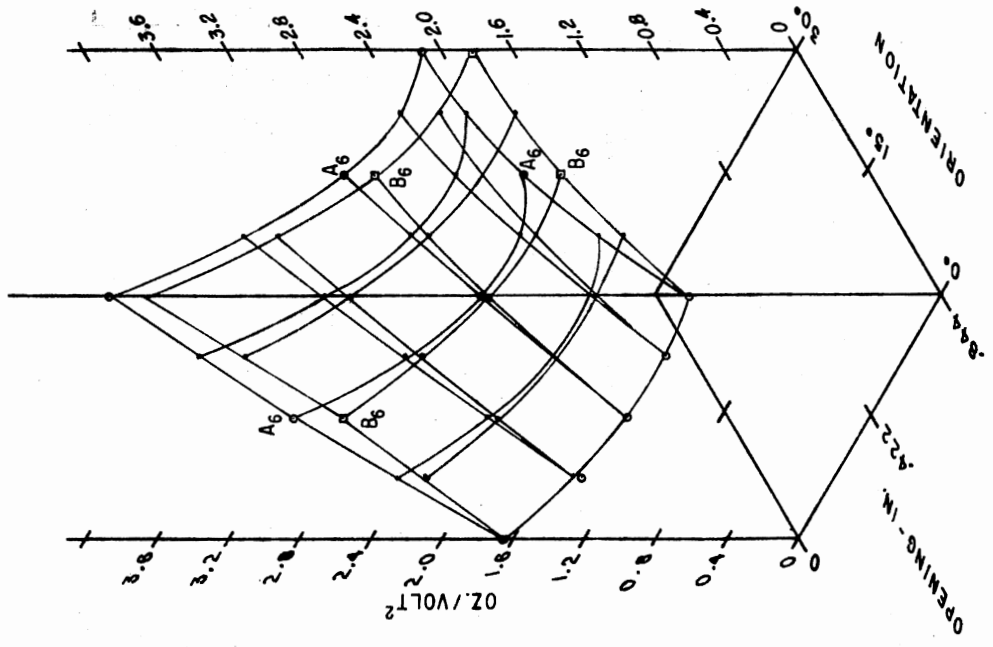

Figure 150. A6-B6, OP1

influential variable, though only slightly moreso than opening.

Panel 3 forces are all outward and Figure 151 pictures the combined effects of A5 and B5, A6 and B6. There is a slight upward turn of the forces over most of the range for the .844" opening, after a sizable drop down to .422", most of it from no opening to .211". The forces are more dependent upon orientation than opening. For each opening the increases from 0° to 30° are almost linear. At 30° the forces steadily drop with increased opening. On the back roof panel the opening effect is overshadowed by the angle of the wind. In view of the effectiveness of the .844" opening at 30°, it must still be considered the most advantageous modification.

A7 and B7 in Figure 152 are erratic and not large. The two curves are dissimilar and show mostly outward, sometimes inward forces with no discernable pattern.

A8 and B8 (Figure 153) are outward except for an opening of .844" at 0° to 7-1/2°. They, too, are of low magnitude, somewhat higher at 30° than 0°. The modifications continually reduce the forces at A but not at the B end of the model, except at 0° orientation.

Panel 4 (Figure 154) is perhaps a better indication of what is happening on the back wall, being a combination of A7 and B7, A8 and B8. The angle increase does increase the outward forces and the modification, in general, serves to decrease those same forces. The latter's effect is more pronounced.

The total outward forces (derived mathematically) shown in Figure 155 reveal great dependence upon the angle of orientation. The increases are virtually linear from 0° to 30° for all stages of opening. The increase is much more severe when no opening exists and less

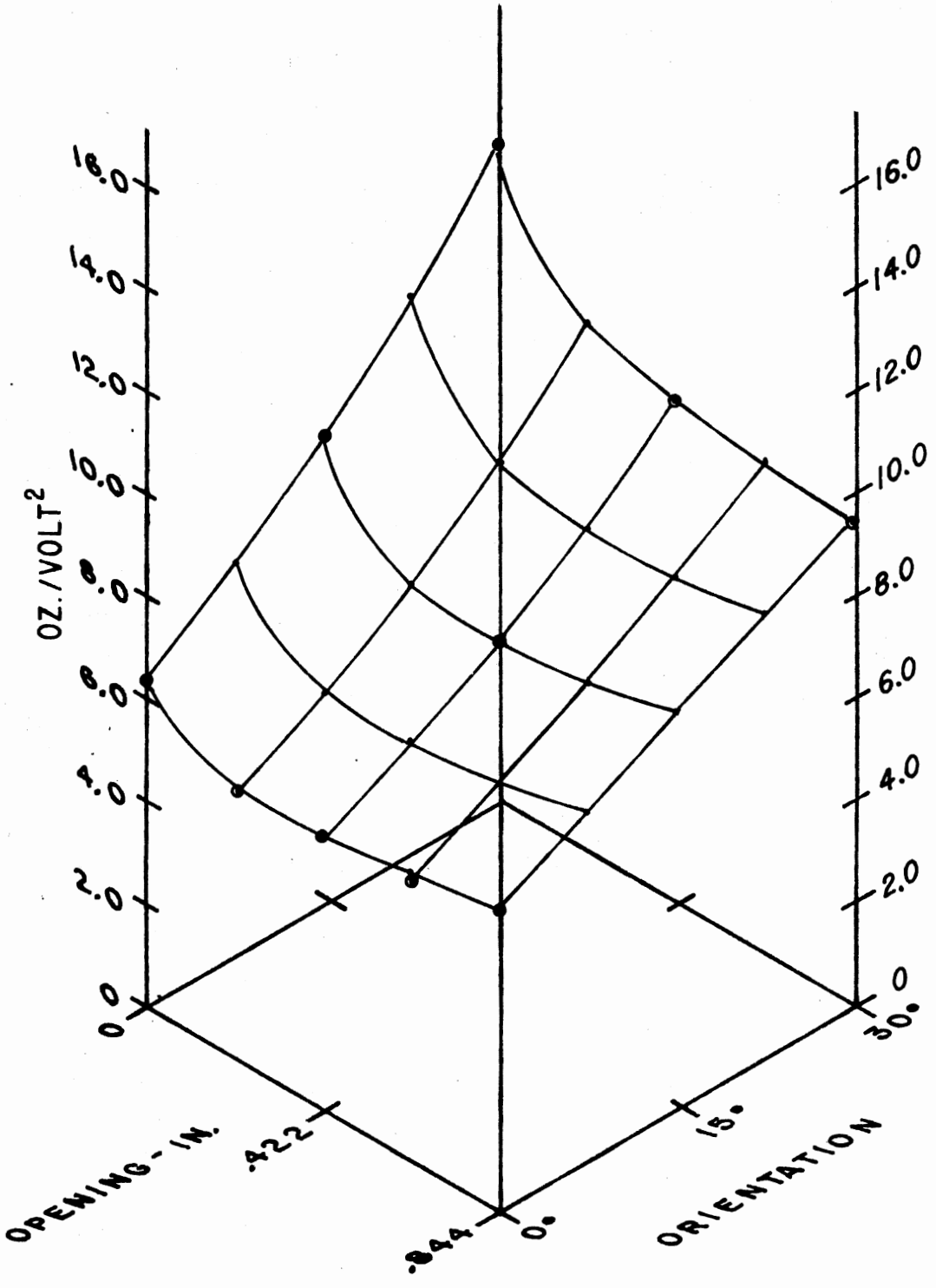

Figure 151. Panel 3, ROP1

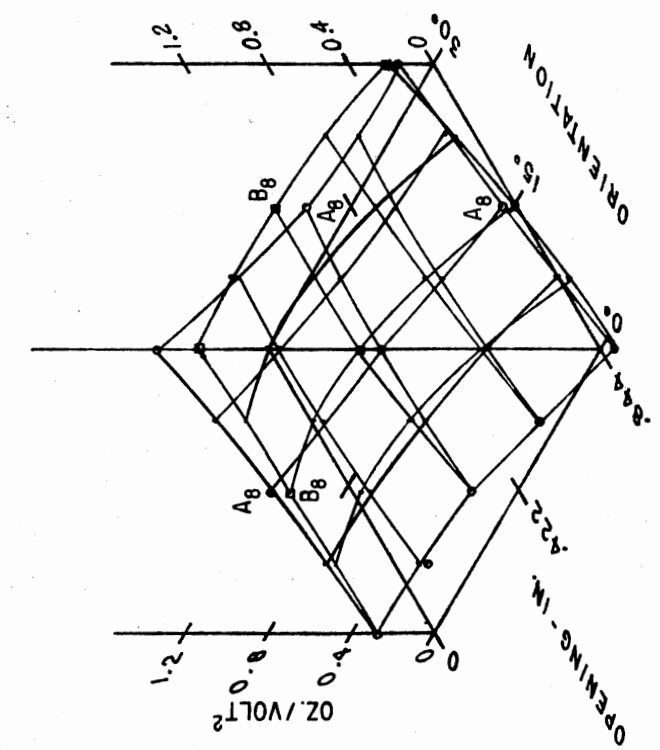

Figure 153. A8-B8, OP1

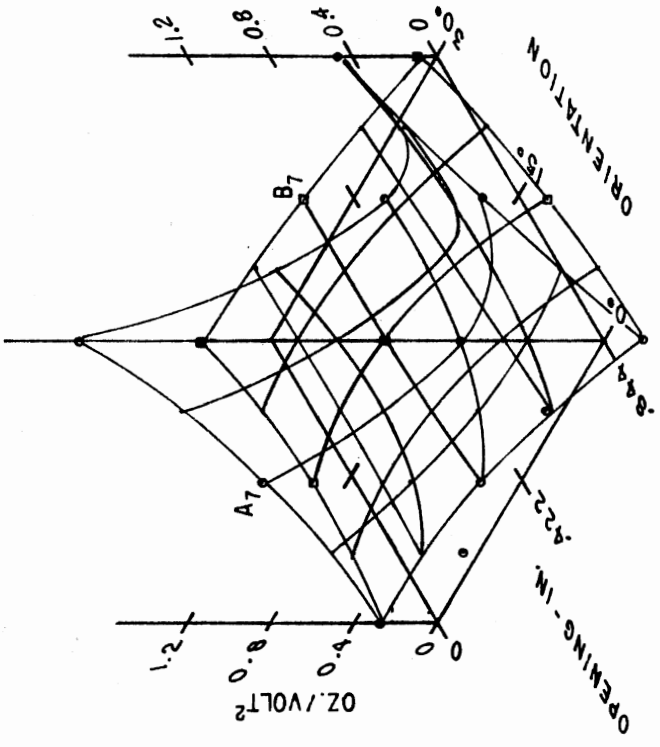

Figure 152. A7-B7, OP1

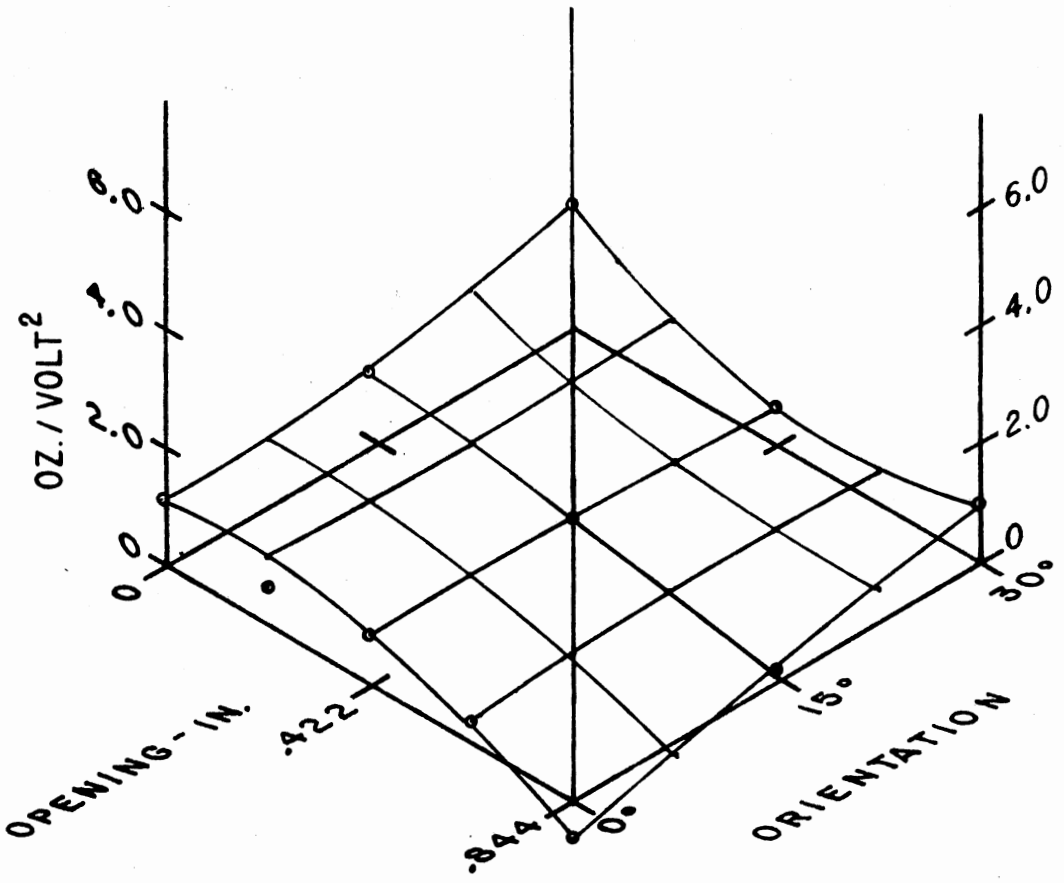

Figure 154. Panel 4, OP1

drastic with the .844" opening. The opening does help at all orientations, but the decrease in force is more pronounced from 0 to .422". The angle effects are slightly greater than those of the opening.

The total inward forces (again mathematically derived) in Figure 156 reflect largely panel 1 and A4-B4 on panel 2. That this is true is difficult to visualize because the two are oriented differently on the graphs, panel 1 being 30° to 0°, and A4 and B4 being 0° to 30°. Inward forces are at a maximum at 0° and no opening. They are, in general, reduced as the wind changed toward 30°. They are reduced, likewise, as the opening increases, for all values of wind orientation. Opening is the more influential of the two variables.

The net forces for the four panels tested were summed and shown as PANTOTA in Figure 157. It is derived mathematically from the difference of total inward and total outward forces. The orientation scale is reversed in the plot (30° to 0°). Originally the predominate forces were inward (above the zero plane). The surface is somewhat unusual in nature but reveals that the situation at 0° and 30° differs considerably.

At 0° and no opening (control point) the net forces are inward. As the opening increases to .844", the inward and outward forces are dropping; moreso for the outward totals than for the inward totals, so a slight rise in net inward force is exhibited. For each opening the change from inward toward outward is nearly linear as the wind changes from 0°to 30°. At 30° orientation the net forces, over the range of openings tested, are entirely outward. Now the effect of the modification is to cause a sudden decrease in those forces to about .422" after which a slight rise is registered. The angle is by far the

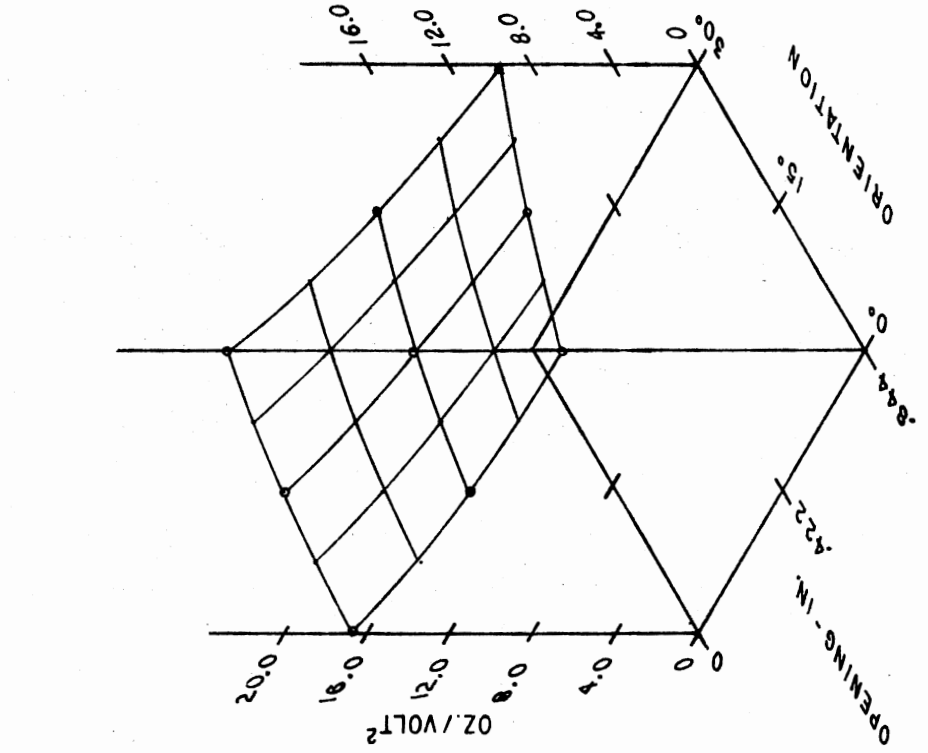

Figure 156. Inward, ROP1

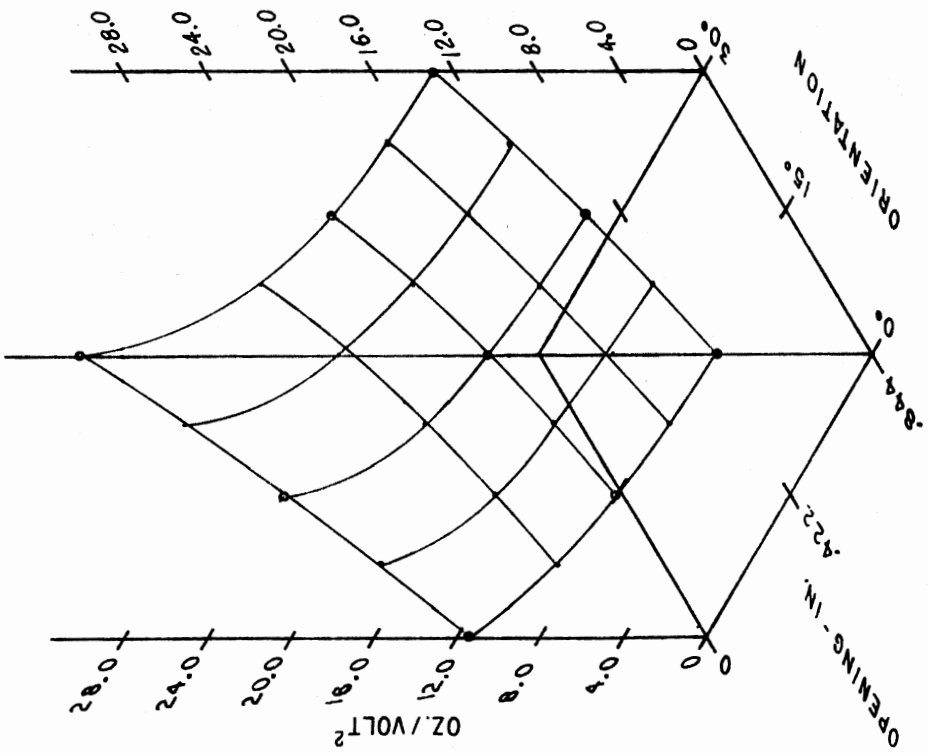

Figure 155. Outward, ROP1

dominant variable.

The absolute totals of all the panels are plotted in Figure 158. It can be seen that the opening was more effective in reducing these forces at 30° orientation. Wind angle response is almost linear as at each opening the forces increase as the angle increases. While increasing the angle with no opening increases the forces dramatically, there is little effect with an opening of .844". Interestingly, the 0° and no opening force level is about the same as 30° with .211" opening. Every other opening results in forces below the level of the original control inspite of the increases due to orientation. Overall, the effects of the opening prevail over the angle effects.

The exact mathematical description of the response of the scaled model to the variables of angle and opening usually involves the first variable squared , the square root of the other, and their cross products. In some cases, the importance of two or three terms is not significant statistically, but their elimination loses the subtleties of the curves in one way or another. Many attempts to simplify the models were made, often cutting the terms to four or five, with R values still in the 0.97 range and F values remaining high. Almost inevitably some meaningful tendency of behavior was lost, however, and there was no uniformity of pattern in the terms that could be eliminated. Often the second degree terms would be necessary, as well as a first order cross product of that same variable, but the simple term would have been eliminated. Therefore, the entire equations, as determined by regression using the Statistical Analysis System (SAS), are presented. Several mathematical models were attempted, including power series and logarithmic. The most suitable was parabolic, though the cross products

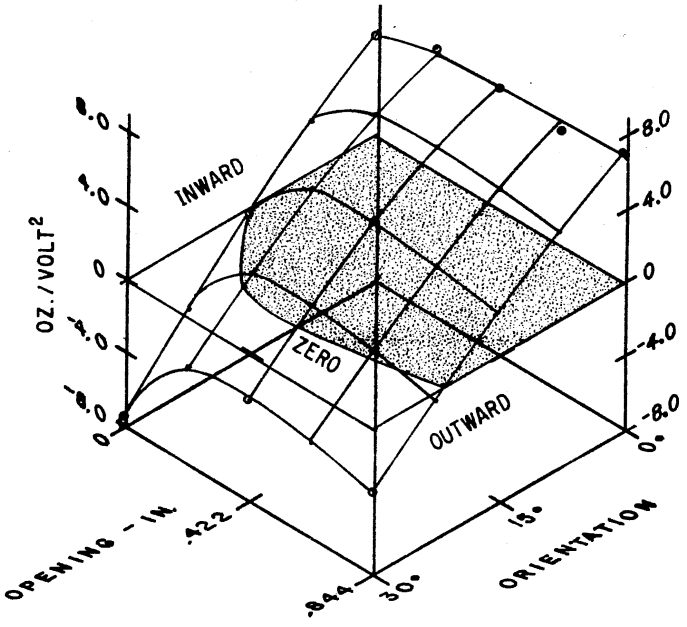

Figure 157. Panel Totals - Algebraic, ROP1

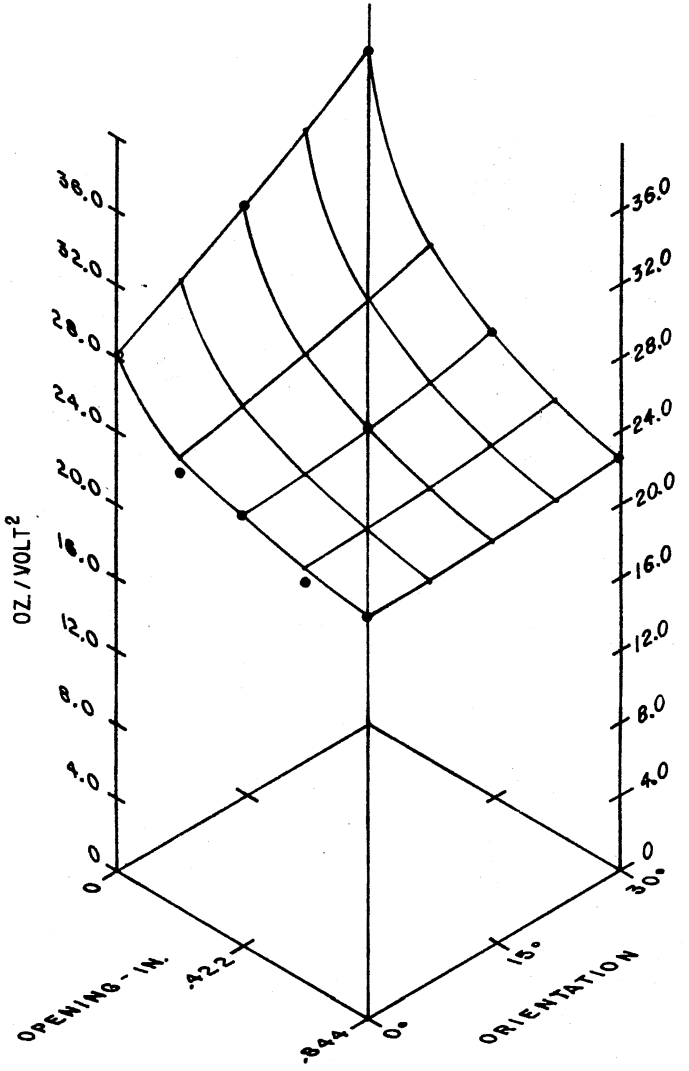

Figure 158. Absolute Panel Totals, ROP1

are essential. The earlier similitude analysis employed in the experimental design was helpful, but failed to define all the variables involved in determining the forces on the structure when rotated with respect to the prevailing wind. A very complex force pattern exists on the structure when one corner is aimed into the wind. Boundary layer separation and the ensuing reattachment make the entire situation more complex than a simple trigonometric function of the wind angle. The cosine function was not even entirely suitable for the front wall, probably because of the effects of eave overhang for the control, and the effects of overhang combined with the opening for the modifications. It is also apparent that a simple percentage of open area on the front wall does not simplify the description of the behavior displayed. Rather than continue an exhaustive search for a better manner of explaining the results in terms of trigometric functions, etc., the angle itself in degrees and the opening in inches were selected as being the simplist terms, in spite of the necessity to utilize the parabolic forms as well as the cross products.

Some of the surfaces--namely A4-B4, A -B6, A7-B7, A8-B8, panel 4 and the inward totals--were best matched by an equation utilizing the opening and the opening squared, whereas the rest resulted in a better fit using the opening and its square root as the defining terms.

Inasmuch as the eight terms were used to fit nine points, the fit is exact. Table XXI contains the equations and their coefficients for those surfaces utilizing the opening and its square foot. They are labeled in the captions of the figures as ROP1. Table XXII contains the coefficients for the models utilizing the opening and the opening squared. These surfaces are labeled OP1 in the captions.

TABLE XXI

MODELS USING ROP1

	Intercept	Angle AL	$(\text{Angle})^2$ AQ	$(\text{Opening})^{\frac{1}{2}}$ OL	Opening OQ	Angle . $(\text{Opening})^{\frac{1}{2}}$ ALOL	$(\text{Angle})^2$. $(\text{Opening})^{\frac{1}{2}}$ AQOL	Angle . Opening ALOQ	$(\text{Angle})^2$. Opening AQOQ
A_1*	4.07955	.02079	-.00056	-.68525	-.05316	-.12149	.00353	.10210	-.00381
B_1*	4.07955	.00218	-.00067	-.68525	-.05316	-.00734	.00002	-.01595	.00038
A_2*	3.73720	0.2538	-.00065	-1.01576	.01917	-.02678	.00040	-.01093	.00003
B_2*	3.73720	-.00675	-.00043	-1.01576	.01917	.12523	-.00267	-.17056	.00350
A_3	1.98812	.07215	-.00080	-1.44178	.15201	-.15513	.00335	.08953	-.00213
B_3	1.98812	.10222	-.00211	-1.44178	.15201	-.29323	.00796	.22056	-.00623
A_5	1.52730	.05777	.00086	-1.15426	1.22785	-.15104	.00461	.14825	-.00540
B_5	1.52730	.00897	.00113	-1.15426	1.22785	-.02309	.00070	.02651	-.00154
Panel 1	15.63351	.04160	-.00231	-3.40202	-.06799	-.03038	.00128	-.09534	.00011
Panel 2	2.83364	.22678	-.00275	-4.63323	1.85142	-.47466	.01306	.30449	-.00963
Abs. Panel 2	5.11884	.08345	-.00051	-1.13388	-1.24339	-.34331	.00430	.27561	-.00441
Panel 3	6.37945	.14937	.00217	-4.10950	3.78772	-.28125	.00627	.28375	-.00973
Inward	16.77611	-.03007	-.00119	-3.20573	.77585	.19063	-.00655	-.34890	.00803
Outward	11.44942	.29926	.00187	-5.60435	1.28425	-.64549	.00682	.51091	-.00751
Panel Total	5.32670	-.32932	-.00306	2.39861	-.50840	.83613	-.01337	-.85981	.01554
Abs. Panel Total	28.22553	.26919	.00069	-8.81008	2.06010	-.45486	-.00026	.16201	.00052

*Inward

TABLE XXII

MODELS USING OPT

	INT	Angle AL	(Angle)^2 AQ	Opening OL	(Opening)^2 OQ	Angle . Opening ALOL	(Angle)^2 . Opening AQOL	Angle . (Opening)^2 ALOQ	(Angle)^2 . (Opening)^2 AQOQ
A_4*	.57130	-.01625	-.00030	.96744	-.93469	.02794	-.00150	-.01415	-.00130
B_4*	.57130	-.03616	.00014	.96744	-.93469	.03001	-.00076	-.01395	.00058
A_6	1.66243	.05552	-.00027	-1.12618	.96210	-.11392	.00151	.12390	-.00252
B_6	1.66243	.02711	.00045	-1.12618	.96210	.00971	-.00238	-.00944	.00149
A_7	.26483	-.00061	.00077	.18301	-.86792	-.16972	.00029	.23995	-.00163
B_7	.26483	-.01205	.00048	.18301	-.86792	.06975	-.00275	-.06603	.00306
A_8	.28203	.00682	.00005	.14537	-.70378	-.01314	-.00086	.02451	.00076
B_8	.28203	.00062	.00003	.14537	-.70378	.06925	-.00207	-.08028	.00281
Panel 4	1.09372	-.00522	.00133	.65676	-3.14339	-.04387	-.00539	.11816	.00501

*Inward

It is possible to fit exactly either the ROP1 or the OP1 equations for the nine points. The judgment as to which is most appropriate was made by inspection of several other data runs which included all five openings at 0°, i.e., 0.0", .211", .422", .633" and .844". The main difference in the two models is the OP1 upturn, or downturn, at .844", and the greater drop near .211" for ROP1. The latter also gradually declines near .844".

The plots show two extra points at .211" and .633" opening for 0° orientation. These were analyzed as a separate series along with the other 0° orientation points of 0.0", .422" and .844". In the case of A1-B1, for example, each of these extra points show the average of six replications--three for A1 and three for B1. They are eliminated from the final analysis, since those extra points at .211" and .633" were taken only at 0° orientation, in order to eliminate SAS programming difficulty with an unbalanced matrix. The curve thus derived, however, matched quite well with the zero degree portion of the analysis of the three replications for each of the other nine points. It differs slightly, naturally, due to the influence of the two extra points. They are plotted in Figures 142 through 158 only for corroboration of the behavior at the two intermediate stages of opening, .211" and .633".

The additional series of tests (FMSDTS) were run at three decidedly different velocities on the five openings at 0° orientation. The results corroborate the general results of the Angopng series. Some difficulties were encountered during the run with the control and though many portions of the results correspond quite closely, there are differences, most of which can be resolved--the explanation of

which would be lengthy.

Sample Calculation to Obtain Drag or Lift Coefficient. In the experimental design the Drag or Lift Coefficient has the form:

$C_D = 2R_i/\rho(V)^2 h_f$ (for walls)

or

$C_L = 2R_i/\rho V^2 L_s$ (for roof)

where:

R_i indicates the panel corner reaction in terms of lbs/ft of panel length

ρ is the air density in lb-sec^2/ft^4

V is the impinging air velocity adjusted to eave height of the building in ft/sec.

h_f is the height of the wall

or

L_s is the slope length of the roof,

both in feet.

The values plotted and the numbers for which the equations are derived are all in terms of oz/volt^2, where the voltage squared is actually a measure of velocity squared.

Using the predicted value of 4.08 oz/volts^2 for AV1 on the front wall at 0° orientation and no opening

$$R_i = \frac{4.08 \text{ oz}}{(\text{volts})^2} \times \frac{1\text{b}}{16 \text{ oz}} \times \frac{1}{20.59375 \text{ in}} \times \frac{12 \text{ in}}{\text{ft}}$$

$$= 0.1486 \text{ lb/ft volt}^2$$

$$h_f = 3.84 \text{ in} \times \frac{\text{ft}}{12 \text{ in.}} = .32 \text{ ft.}$$

At 87° dry bulb and 76° wet bulb temperature,

$$\rho = \frac{1.017 \text{ lb}}{14.156 \text{ ft}^3} \times \frac{\text{sec}^2}{32.2 \text{ ft}} = .002231 \ \frac{\text{lb-sec}^2}{\text{ft}^4}$$

$$C_D = 2 \times \frac{0.1486 \text{ lb}}{\text{ft volt}^2} \times \frac{1.414 \text{ volts}}{60 \text{ ft/sec}} \times \frac{1.414 \text{ volts}}{60 \text{ ft/sec}}$$

$$\times \frac{1}{.32 \text{ ft}} \times \frac{\text{ft}^4}{(.002231)\text{lb-sec}^2} = .2312 \text{ INWARD}$$

Some abnormalities in calibration of the hot wire for the last tests were discovered, long after the data was taken, making the precise values of C_D impossible to derive. For the purpose of illustration, the approximate calibration value of 1.414 was assumed.

A similar calculation for the front roof is included for illustration also.

At AV3, 0° orientation with no opening

$$R_i = \frac{1.99 \text{ oz}}{(\text{volt})^2} \times \frac{\text{lb}}{16 \text{ oz}} \times \frac{1}{20.59375 \text{ in}} \times \frac{12 \text{ in}}{\text{ft}} = 0.07247 \text{ lb/ft-volts}$$

$$L_s = 5.8125 \text{ in} \times \frac{\text{ft}}{12 \text{ in}} = .484375 \text{ ft}$$

$$C_L = 2 \times .07247 \times (1.414)^2/60 \times 60 \times .484375 \times .002231$$

$$= .07449 \text{ OUTWARD}$$

The overall C_D or C_L for the panel would be the sum of the four corner coefficients, or the coefficient for panel 1, panel 2 algebraic, panel 3 and panel 4, found in the same fashion.

The dimensional constant employed for the walls is:

$0.056663 \text{ volts}^2/\text{oz}$

and for the roof;

$0.0374344 \text{ volts}^2/\text{oz}$.

These resulting panel coefficients are summarized in Table XXIII.

Certain difficulties during the tests had to be overcome or tolerated.

The changing of the gage readings due to the tension on the central pivot bolt was not anticipated. The 27" diameter, 3/8" thick plywood disk had been varnished only on the top side--a mistake because it became slightly concave on the bottom side requiring tension to pull it down into place. The gages, mounted on the permanently fixed portion of the endwalls, experience a very slight shift due to pulling the disk down tight. A torque wrench was not used to obtain the same tension each time the bolt was tightened. That may have helped, but the gages are much more sensitive than any torque wrench. The frame calibration apparatus had been previously built, and was being used during the tests, in order to determine if the gages were consistent in their response to given loads. Fortunately, its use allowed the changes that did occur to be removed by the normalization procedure discussed in the sample calculations. In general, the changes were not severe, however, the problem could have been avoided or at least minimized. The frame calibration method of adjustment did load the panels in the direction of wind loading, but always at the panel center. The wind's resultant forces were rarely ever applied at the centers of the panels. The method did serve to normalize the gage response differences.

The testing of the duct finally resolved to testing a large passage with varying restrictions of opening, rather than testing ducts of several sizes. It was not practical to do otherwise, given the time frame and the kind of model employed. Instead of testing

TABLE XXIII

PREDICTED VALUES OF DIMENSIONLESS FORCE COEFFICIENTS--ANGOPNG TESTS

Orientation Angle / Opening -inches	Predicted Values Oz./Volt^2 0°	15°	30°	Dimensionless Force Coefficients 0°	15°	30°	Monitoring Point	Predicted Values Oz./Volt^2 0°	15°	30°	Dimensionless Force Coefficients 0°	15°	30°	Monitoring Point
0.0	4.0796	4.2664	4.2032					1.5273	2.5865	4.0309				
0.422	3.6120	3.4152	3.2761				A1	1.2956	1.9821	3.3751				A5
0.844	3.4051	3.2159	2.7877					1.5032	2.2844	3.3039				
0.0	4.0796	3.9234	3.5455					1.5273	1.9170	2.8170				
0.422	3.6120	3.3609	2.8874				B1	1.2956	1.5840	2.2944				B5
0.844	3.4051	3.0608	2.5685					1.5032	1.7623	2.2355				
0.0	3.7372	3.9708	3.9101					1.6624	2.4347	3.0859				
0.422	3.0854	3.0509	2.8461				A2	1.3585	1.7826	2.1695				A6
0.844	2.8202	2.6358	2.3362					1.3973	1.9331	2.1119				
0.0	3.7372	3.5393	3.1481					1.6624	2.1703	2.8805				
0.422	3.0854	2.9709	2.5487				B2	1.3585	1.7365	1.9848				B6
0.844	2.8202	2.3028	1.8201					1.3973	1.7145	1.8090				
0.0	15.6335	15.7388	14.8069	.88541	.89181	.83900	Panel 1 (Upwind Wall) Inward	6.3795	9.1084	12.8143	.23881	.34097	.47970	Panel 3 (Downwind Roof) Outward
0.422	13.3948	12.7979	11.5583	.75899	.72517	.65493		5.3083	7.0852	9.8237	.19871	.26523	.36774	
0.844	12.4507	11.2153	9.5125	.70549	.63549	.53900		5.8009	7.6943	9.4603	.21715	.28803	.35414	
0.0	1.9881	2.8902	3.4321					.2648	.4282	.9365				
0.422	1.1157	1.3604	1.8201				A3	.1875	-.1206	-.1600				A7
0.844	.7919	.9781	1.3809					-.1990	.1731	.4771				
0.0	1.9881	3.0460	3.1529					.2648	.1927	.3380				
0.422	1.1157	1.2844	1.6461				B3	.1875	.2421	.2370				B7
0.844	.7919	1.0636	1.3094					-.1990	-.1250	.1034				
0.0	.5713	.2600	-.1863					.2820	.3953	.5306				
0.422	.8131	.5543	-.0129				A4	.2180	.2620	.2247				A8
0.844	.7220	.5434	.0899					-.0966	.0700	.1741				
0.0	.5713	.0594	-.3914					.2820	.2987	.3303				
0.422	.8131	.4048	-.0405				B4	.2180	.3749	.3791				B8
0.844	.7220	.3897	.0159					-.0966	-.0035	.2195				
0.0	2.8336	5.6167	7.1627	.10607	.21026	.26813	Panel 2 Algebraic (Upwind Roof) Outward	1.0937	1.3150	2.1354	.06197	.07451	.12100	Panel 4 (Downwind Wall) Outward
0.422	.6051	1.6857	3.5196	.02265	.06310	.13175		.8111	.7583	.6809	.04596	.04297	.03858	
0.844	.1397	1.1086	2.5846	.00523	.04150	.09675		-.5911	.1146	.9741	-.03349*	.00649	.05520	

*Inward

an entire duct 0.211" high, 18" long and the full width of the opening, the duct was .844" high with the bottom .633" of that height being closed off by the front cover plate to leave .211" gap at the top. The necessity to leave the back cover plate all the way down for the tests reduced the area of the back wall by the following:

(18.0" x .211")/(3.84" x 20.59375") = 3.8 in^2/79 in^2 = 4.8%

for the .211" opening

7.6 in^2/79.0 in^2 = 9.6% for the .422" opening

and

11.4 in^2/79.0 in^2 = 14.4% for the .633" opening.

This effect would largely have been sensed by the A7-B7 gages, but the readings were not adjusted for it at those openings. It could easily be done. This means the 0.0" and the .844" opening on the plots do actually reflect its behavior, but the intermediate point of .422" for Angopng and the extra points plotted at .211" and .633" are reduced. This would not, however, greatly affect the overall results, as the forces incurred on the back wall are quite low in magnitude.

Conclusions. It is obvious that the wind forces induced upon a building are affected significantly by the orientation of the building with respect to the prevailing wind direction and by the wall opening.

In general, the inward forces on the front wall drop as the wind direction switches toward 15° and 30°. Exception was noted at 15° for A1. The opening serves to reduce the forces. The opening is dominant at the upwind end, moreso than the downwind where the angle is quite influential also. At the top of the wall where the opening is located, the effects of the opening are more pronounced than at the bottom of the wall. Forces are always higher at the upwind end

when the prevailing wind is not perpendicular to the structure.

The highest outward forces are at positions 3, 5 and 6, all of which show enormous increase as the angle of the wind changes from 0°. The 3's surprisingly show virtually the same loading at either end of the building at all angles. As great as is the effect of the angle on the 3's, the ability of the opening to reduce the forces is greater. At 5 and 6 the reverse is true--the angle of the wind is most important. The opening does reduce the forces at .211" at all angles, but increasing it to .844" is effective really only at 30°. This monitoring point, at the top of the downwind roof panel, shows the greatest differences between A and B ends of the model--upwind forces on the A end are much more severe. At 6 the upwind forces are greater than at the B end, but the difference is much less pronounced. Angle is still the dominant variable. The openings were effective throughout the range for B but .633" is the most effective for the A end.

Panel 2 forces show the dominance of the opening with respect to reducing the absolute forces, in opposition to the angle's tendency to cause increase.

A redistribution on panel 2, toward a balance of outward and inward forces, takes place as the opening is increased, but rotation of the wind toward 30° opposes this.

On panel 3, the opening is least helpful though still effective. The angle change serves to increase the outward forces while opening overcomes these increases.

The lesser forces at 4, 7 and 8 all fluctuate near the breakpoint between being inward and outward and are of no great concern for the sealed structure. The opening, in general, produces desirable changes in

all. At 4 the orientation angle is dominant while at 7 and 8 the opening most influences the forces. At point 4, the inward forces decline with an increase of angle and increase with opening.

The building total forces perhaps reflect best of all that the critical angle of wind loading, at least for the outward forces, is not 0° and that the opening is beneficial. The outward increases due to angle change are largely overcome by the increased opening. The inward forces drop with a change of angle and, further still, with increased opening. The best balance of inward and outward forces is at about 15° orientation; less than that the balance is inward and beyond it, outward. The absolute total forces are increased by the angle significantly only for the unmodified building--the opening nulls out the tendency to increase.

The openings are very definitely indicated by this experiment to be effective in reducing the significant building forces. Some redistribution from inward to outward also takes place. While the angle serves to increase all the outward forces and decrease the inward forces, the opening, in general, alleviates much of the increase and heightens the decreases.

Some caution is justified in applying the exact results to a full scale building. The size of the duct was not varied--only the entrance to it. The back wall closure was always wide open except for the control. The model was not completely air tight though "nearly so". The practicality of implementing a prototype with such a system can be called into question. More study could, however, be based upon the method as it does accomplish the intended purpose.

CHAPTER IV

SUMMARY

Method, Procedure and Equipment Critique

The flow visualization studies could have resulted in limited quantitative information had they been conducted in a slightly different fashion. After the 15 cfm fan addition had been added to the smoke tunnel, it would have been advantageous to rerun all the tests utilizing the same velocity and smaller models. This would have permitted comparisons of the length and height of the wake downstream of the model and made the visualization studies more useful.

Sealing the wind tunnel model was an annoying affair. The model was excellently suited to open front studies but less suited to model closed buildings since it was necessary to allow the panels freedom to move. For the closed front sealed building, a series of pressure transducers might have been told the story in spite of all the difficulties in completely defining the pressure pattern.

The end wall covers eliminated the sensing of any wind effects on the ends of the building as well as end edge effects on the four panels tested.

It is obvious that the similitude analysis did not include all the pertinent physical quantities needed to define the behavior for all the systems. To be successful, such an analysis has to be

based upon a complete knowledge of such and, however logical the analysis seems, the relationships anticipated did not always neatly fall into place--the deflector series is a good example of this. The venting series is another. One undefined variable that had to be continually battled was the "sealing" of the model. Another factor which often made the use of a single control impossible was the necessity to move the flat control strip about on the roof to avoid differences in the readings simply due to weight location of the modification--the deflectors and airfoils are also examples of this.

The hot wire circuitry was very difficult to cope with as several wires were burnt out and replaced, making accurate reflections of minor differences of airflow very difficult to eliminate for the preliminary tests. A backup pitot tube system would have been helpful.

The strain gage circuits functioned well; though some gages showed seven percent differences in final and initial calibrations, it is likely the differences occurred during the early "break in" period of the trial runs for which data was not seriously collected nor analyzed. Hours and hours of flexing in the wind produced no failures and excellent performance.

The rotation of the model to obtain the various wind orientations in the final series of tests on the large duct was complicated by the slightly warped disk on which the model was mounted. This resulted in minor differences of the strain gage readings due to variations in tightening of the center bolt.

At times restrictions in ideally testing a specific system were imposed by the single scaled model which of necessity was used for all the tests. It would have been desirable to have removed the

eave overhang which existed on the model during the other tests in order to expand the limited range of variables investigated during the eave overhang tests.

Findings and Conclusions

Of the four systems for which tests were planned and the one unplanned series, two show greater promise for accomplishing the desired alteration of air flow and diminishing the forces the building must sustain; the eave overhang modifications and the duct systems.

The others--the deflectors on the edge of the upwind roof, the airfoils at the roof ridge and the venting systems--all have disadvantages that limit their effectiveness though indications are present that they may be successful in some situations. The knowledge gained about these systems which led to their abandonment is intriguing and should be useful if further attempts are made to utilize them. Versions of the venting modification and the airfoil modification are often seen incorporated into ventilation systems. Their effect on the air flow over a structure needs to be considered by those employing them for that purpose.

Briefly, the conclusions of each option tested are summarized below. More complete discussion on each is found in chapter III.

Deflectors, Unsealed Model

The evidence obtained points to redistribution of the forces rather than drastic reduction of the overall totals. The forces upwind of the modification are increased whereas downwind, reduction occurs. 135° orientation with a gap, high on the roof, is indicated

as the most favorable. Deflectors, sized in the 7/16" to 9/16" range, should be tested nearer to the roof ridge to attempt reduction of downwind forces without increasing those on the leading roof panel. A slight increase must be anticipated for panel 1 at best. There likely exists a delicate local boundary layer separation and reattachment relationship at the leading edge of the front roof upon which the deflector's effect is difficult to predict.

Deflectors, Sealed Model

Total force reduction of 10 percent is possible. The most successful modification was the 5/16" deflector, oriented at 135° with a gap. The only increase was at the leading edge of the roof (8-1/2 percent). The higher positions tested were the most effective in reducing the forces. Even the front wall forces were reduced. Potential for reduction of forces obviously exists, but more complete testing is needed to define precisely the most advantageous combination of components as some of the limited evidence is confusing.

Airfoils, Unsealed Model

The planned modifications with positive β angles caused great increases at the top of the back roof (AV5) due to reaction of turning the air flow down the back slope - and caused increases at the leading edge of the front roof (AV3). The latter were already the critical forces. Changing the angle β to negative values alleviated the AV3 forces but still raised AV5 to a level slightly higher than the value of AV3 before modification. Any future work should include, therefore, negative angles for β, the tilt of the airfoil. Reduction

of some forces and redistribution of others takes place with negative values of β.

Airfoils, Sealed Model

The forces were greatly modified with advantages being recorded for the front wall, the front roof and the back wall. Panel 3 showed large increases which were the least at 0° tilt of the airfoil. Panel 1 favored +6° tilt and panel 2 showed the greatest decrease at -6°. The worst outward force originally was decreased,but that at the top of the ridge for the back roof panel was greatly increased. The inward force at the ridge of the leading roof panel also increased. The ridge of the modification should not be sealed.

Ducts, Unsealed Model

The modification shows promise. Reduction occurs (with the exception of the inward forces at the bottom of the front wall) as well as redistribution of some of the forces. The reduction includes the worst forces, at AV3 (six percent) and AV6 (10 percent), the lower downwind roof force. Desirable results having been attained, the modification was used as a basis for selection of the final investigation.

Ducts, Sealed Model

Again the modification achieved desirable results. Critical outward forces were reduced and favorable redistribution occurred, to areas better able to sustain the forces. This further indicated the option as the one for more investigation during the final phase

of the study.

Eave Overhang, Sealed Model

This unplanned series is very interesting, showing increased eave overhang results in slight reduction of the inward forces on the front wall and universal increases elsewhere. The increases in outward force are high at the leading edge of the front roof where the structure is vulnerable. The addition of holes to vent the overhang creates reductions everywhere except for the nullification of the slight decreases previously noted for the front wall. The holes are naturally more effective closer to the front wall. The addition of a bend, at 45° to the ground plane, in the eave overhang on the basis of one test, seems very advantageous. Reduction and redistribution takes place - all favorable. The entire eave overhang series is fertile for future study. It is suggested the studies start with a model having no overhang and that all the modifications be pursued. This was not possible without seriously modifying the model used in this study.

Venting, Unsealed Model

Simply progressively opening up the vents in the walls did not favorably affect the force pattern. To the contrary, it creates problems unless the vent openings become fairly large. Large redistributions occur as the front wall is relieved and the inward pressure on it is transferred to the interior of the building with the back roof showing the most increase percentage wise.' The phenomenon seems to be more involved than just a simple addition of inward pressure to

the inside surfaces, however, no detailed analysis was made since the sought for reductions obviously do not occur.

Venting, Sealed Model

The venting of the sealed structure clearly shows detrimental universal increases. The addition of inward pressure, from the front wall, to the interior surfaces is the cause. Letting the air on through does not help.

Ducts, Final Option

For the sealed model the duct modification, as tested in the final phase of the study, is effective in reducing the forces on the structure at all of the critical monitoring points and at all the wind orientations tested, 0° to 30°. The inward wind forces on the front wall decrease as the wind angle of impingement changes away from perpendicular to the front wall. The outward forces increase on the other surfaces proving that for the modified, and the unmodified structure, 0° is not the critical wind angle except for the front wall. The single duct system, tested by varying the upwind opening, served to reduce the building forces at 0° and to offset the increases incurred by rotation of the model. The most advantageous is the largest (.844"), however, much benefit of the modification is obtained even with the half open position (.422").

The force prediction coefficients obtained are:

	Model Opening Inches	Orientation 0°	15°	30°
Upwind Wall (Inward)	0	.89	.89	.84
	.422	.76	.73	.66
	.844	.71	.64	.54
Upwind Roof (Outward)	0	.11	.21	.27
	.422	.02	.06	.13
	.844	.01	.04	.10
Downwind Roof (Outward)	0	.24	.34	.48
	.422	.20	.27	.37
	.844	.22	.29	.34
Downwind Wall (Outward)	0	.06	.07	.12
	.422	.05	.04	.04
	.844	-.03*	.01	.06

*Inward

where .422" opening on the model (1.75' on the prototype) resulted in 8.25 percent of the front wall area being open and .844" in 16.5 percent open.

While some doubt exists as to the practicality of the method, it is certainly effective.

Future Study

The effect of eave overhang and the modifications employing vents and/or bends in it would seem, on the basis of this investigation, to be the option to pursue first in any further study. The tests could be easily implemented in botm the smoke tunnel and the wind tunnel. This investigation shows that the air flow pattern on the entire structure is affected by the overhang configuration.

REFERENCES CITED

1. (a) "Designing Buildings to Resist Snow and Wind Loads," ASAE 2.1.2 Agricultural Engineers Yearbook, 1974, 343. Published by American Society of Agricultural Engineers, 1974, St. Joseph, Michigan.

   (b) "Designing Buildings to Resist Snow and Wind Loads," ASAE R288.3, Section 5, Figures 3 and 4, and Table I, Agricultural Engineers Yearbook, 1974, 343, 345, 346 and 347.

2. Nelson, Gordon L. "Wind Effects on Open Front Livestock Shelters." (Unpublished Ph.D. Thesis, Iowa State College, 1957).

3. Pao, Richard H. F. Fluid Mechanics. John Wiley and Sons, Inc., New York and London, 1961, 391.

4. Davenport, A. G. "Rationale for Determining Design Wind Velocities." American Society of Civil Engineers Transactions, Vol. 126, Part II, 1961, 184-213.

5. Sherlock, R. H. "Variation of Wind Velocity and Gusts with Height." American Society of Civil Engineers Transactions, ASCE, Paper 2553, 1953.

6. Pagon, W. W. "Wind Velocity in Relation to Height Above Ground." Engineering News-Record, New York: McGraw-Hill Book Company, Inc. Vol. 114, No. 21, May 23, 1935, 742-751.

7. Brunt, D. Physical and Dynamical Meteorology, 2nd edition. Cambridge: Cambridge University Press, 1952, 114.

8. Sutton, O. G. Atmospheric Turbulence. Methuen and Co., Ltd., 1949, 20.

9. Geiger, Rudolf. The Climate Near the Ground. Harvard University Press, 1950.

10. Ali, Barkat. "Variation of Wind with Height." Royal Meteorological Society Quarterly Journal, Vol. 58 (1932), 285-288.

11. Collins, G. F. "Determining Basic Wind Loads." American Society of Civil Engineers Proceedings, Vol. 81 (November, 1955).

12. Thom, H. C. S. "Distributions of Extreme Winds in the United States." Journal of the Structural Division Proceedings of the American Society of Civil Engineers, Vol. 86, Part 1. (April, 1960), 11-24, 463-466.

13. Bellman, H. E. "An Analysis of Windbreaks and Snow Barriers for Agricultural Structures." (Unpublished M. S. A. Degree, University of Guelph, Ontario, 1963).

14. Theakston, F. H., and K. H. Lin. "Shape Factors and Their Effect on Wind Currents Around Farm Structures." (Paper No. 66-002). For Presentation at the Canadian Society of Agricultural Engineering Meeting, 1967, Winnipeg, Manitoba.

15. Thomann, Hans. "Wind Effects on Buildings and Structures." American Scientist, Vol. 63 (May-June, 1975), 278-287.

16. Murphy, Glenn. Similitude in Engineering. New York: The Ronald Press Co., 1950.

17. Irminger, J. O. V., and C. Nkkentved. "Wind Pressure on Buildings, Experimental Researches." (Second Series). A, Nr. 42. Copenhagen, Denmark: Danmarks Naturvidenskabelige Samfund, Ingenirvidenskabelige Skrifter, 1936.

18. Irminger, J. O. V., and C. Nkkentved. "Wind Pressure on Buildings, Experimental Researches," (First Series). A, Nr. 23. Copenhagen, Denmark: Danmarks Naturvidenskabelige Samfund, Ingenirvidenskabelige Skrifter, 1930.

19. Jensen, Martin. Shelter Effect. Copenhagen, Denmark: The Danish Technical Press, 1954.

20. Huntley, H. E., Dimensional Analysis. New York: Dover Publications, Inc., 1967.

21. Leutheusser, Hans J., and W. Douglas Baines, "Similitude Problems in Building Aerodynamics." Journal of the Hydraulics Division, Proceedings of the American Society of Civil Engineers, Vol. 93 (May, 1967), 35-49.

22. Buckingham, E. "On Physically Similar Systems; Illustrations of the Use of Dimensional Equations." The Physical Review, Ser. II, 4 (1914), 345-376.

23. Ghaswala, S. K. "Aerodynamic Aspects of Civil Engineering." Civil Engineering and Public Works Review, Vol. 45 (Part 1), 586-589.

24. Brown, F. N. M. The Organized Boundary Layer, Proceedings of the 6th Annual Conference on Fluid Mechanics, University of Texas, September, 1959.

25. Goddard, Vincent P. Development of Supersonic Streamline Visualization. Notre Dame, Indiana: Department of Aeronautical Engineering, University of Notre Dame, March, 1962.

26. Theakston, F. H. "Advances in the Use of Models to Predict Behaviour of Snow and Wind," Transcript No. 67-433, 60th Annual Meeting of ASAE, Saskatoon, Saskatchewan, June 27-30, 1967.

27. EAI Applications Reference Library, "Continuous Data Analysis with Analog Computers Using Statistical and Regression Techniques." Bulletin No. 952015, August, 1969.

APPENDICES

APPENDIX A

SMOKE TUNNEL OPERATION

Preparation of Equipment

NO SMOKING! Both kerosene and its vapor, especially, are flammable.

Fill kerosene supply until fluid level corresponds with "Best Level" indicator. (This should bring fluid to middle of bottom heater coil). Do not spill kerosene into transformer below supply! Set up in room where no air currents exist.

Operating Instructions

a. Model Requirements

1. Both cardboard and plexiglass models have been used.
2. 1" wide-can use foam to take up slack and make model 31/32" wide for some purposes.
3. Some way to hold model in place is needed while door is closed.

b. To Place Model -- Loosen five thumbscrews at least 3/8". Slide flow chamber and contraction section to left 1/4" and turn catch to release door which will then drop down. Place model. Reassemble by first closing door. This should just barely squeeze model. Shut door catch and slide flow chamber in place to right. Next, tighten top thumbscrew near the Variac. At inlet end, push chamber forward to the front stop strip and tighten bottom thumbscrews front and back. Last, tighten top thumbscrews front and back. DO NOT OVER TIGHTEN--snug is sufficient.

c. Vapor

REMEMBER WARNING AGAINST SMOKING.

Turn on Variac. (It should be set to 35v max.) Idiot light will come on when heating coil is energized. When kerosene begins to vaporize in bottle, turn on both fans.

d. Lights

Turn on lights as master control.

1. Low, if used for demonstration only.
2. High, if used for photographs.

Lights can be switched on individually or all together as master control. Hi-Low control is possible only at master control. Light in box can cause drawdown at exit section of visualization chamber by the heat buildup in the upper portion of the box. The hot air simply forces the cooler smoke down and upsets the pattern. To avoid this, leave light in box off except when photograph is being made or when its contribution to visualization is essential, after which, turn it off.

e. Flow Regulation

Inlet adjustment of air for vapor bottle is best set for maximum circulation, and adjustment made only with the top air gap regulator. Butterfly flow regulator sets air speed through the visualization chamber. Flow settings of 75 fpm through 375 fpm are available. Best laminar flow is at the minimum flow (75 fpm).

Top hole stopped with cork on top of visualization chamber is for insertion of pitot tube or portable hot wire probe for velocity determination.

Should streamlines waver back and forth crossing over each

other, too many air currents exist in the room air. Should smoke rake jets plug up, as they seem to do on some days, the "inline" valve on top of the condensation bottle can be closed, the "outside" valve opened and air pressure may be applied to the outside valve inlet. Even blowing by mouth suffices to clear jets. Reverse valve procedure after clearing.

If smoke flow is decidedly uneven:

1. Check to see that kerosene is not too high in heating coil--too high produces "gusty" smoke and too low makes smoke too "thin". Supply bottle is adjustable.
2. Check air gap regulator

   "In" - causes smoke to get thicker and more uneven.

   "Out" - causes thinner more even smoke.
3. Voltage higher than 35 causes too much uneven vaporization (pressure spurts).

f. Photographing

1. It is best to use a room with no windows due to glare and reflections.
2. To avoid "mirror effect" on the front glass of smoke chamber, hide the camera and photographer behind a large cardboard shield. Cut a hole in it for the camera lens.
3. Use the hinged wooden panel to keep light from shining into camera lens.

g. Shut Down

Do not simply turn everything off.

1. Turn off the power to the Variac which will soon stop

the vaporization.

2. When all traces of kerosene vapor are cleared out by the fans, then turn off lights and fans.

h. Cleaning

1. Cleaning windows - use a plexiglass cleaner with anti-static additive to reduce line and dust.

2. Cleaning vapor bottle of carbon buildup. Can be put in OSU glassblowers oven overnight and carbon burns out.

APPENDIX B

CONTINUOUS DATA ANALYSIS USING THE ANALOG COMPUTER

The need for some simple and quick method for evaluation of rapidly fluctuating signals generated by strain gage transducers led to consideration of the analog computer for integration of the signals. The "mean" or "arithmetic average" is defined by:

$$\bar{f} = \frac{\sum_{i=1}^{N} f_i}{N}$$

Specifically, it was desired to compute the average or mean value, $\bar{f}$, of a signal, f_i, varying with time, or $f(t)$, over the interval $T_1 < t < T_2$. For example, it was necessary that a rapidly varying signal representing the force on any one of the monitoring strain gage transducers be compared to that same force after making the scheduled building modifications. The sensing devices generate signals proportional to the wind forces on the building.

The most obvious method of determining the arithmetic average can be represented by the following equation.

$$\bar{f}(t) = \frac{1}{T_2 - T_1} \int_{T_1}^{T_2} f(t)\, dt$$

This value can be computed with the circuit shown below.

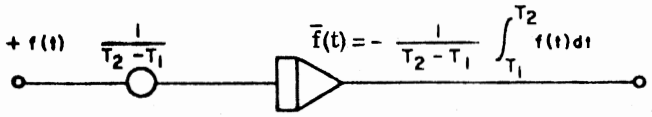

Analog Circuit for Calculation of Estimate of the Mean for a Fixed Time Interval

At time T_1, the integrator begins to function and at time T_2, its output is noted. The integrator must then be discharged and another average can be taken.

An improvement of this circuit would enable the time also to be determined electronically by incorporating a division circuit. The determination of the average could be accomplished entirely by the computer thus eliminating any possibility of error due to timing. To determine the time, a constant voltage could be integrated. A constant voltage of 1v. would accumulate x volts in x seconds. Such a circuit is shown below.

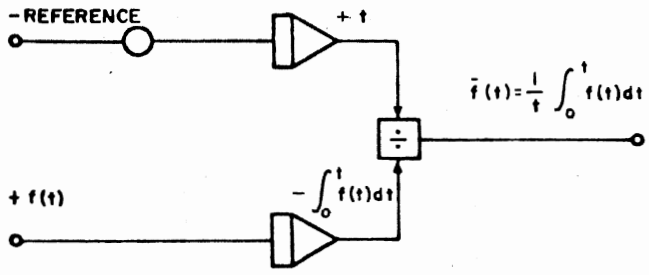

Analog Circuit for Calculation of a Continuous Estimate of the Mean for a Fixed Time Interval

The upper limit, T_2, is then a variable, t, depending upon how long the circuit is active. The lower limit, T_1, is zero. The major disadvantage of this circuit is that it is necessary to choose in advance the operating time since the integrator will eventually overload. In the case of the equipment available, an EAI TR-20 Analog Computer, the integrator capacity is 10v. and the operating limit under the convenient condition of using a 1v. signal is 10 seconds. After 10 seconds, the integrator must be discharged or reset. Working within the limits as outlined above, the average value is dependent only upon the behavior of f(t) during the preceeding 10 seconds. The information older than 10 seconds is obsolete. When the integrator is reset, the values of f(t) are lost.

A third method is possible. It avoids the resetting needed for the two previous circuits. The circuit is much simpler and eliminates worry about overloads and the complexity of division circuits. The secret to this more simple circuit lies in the fashion with which it is able to continuously "forget" values in the distant "past" while determining the average mainly from the values in its most recent "past". Past values of $\overline{f}(t)$ continuously become obsolete. Since the basic signal, f(t), can easily be continuously monitored, it is advantageous to let past information become continuously and gradually obsolete, rather than abruptly as it does in a series of runs.

$\overline{F}(t)$ must be defined so that recent values count much more heavily than earlier values. The behavior of f(t) in the remote past must have but little effect upon the value of $\overline{f}(t)$. This can be accomplished by use of a weighted average.

The following development of the Exponentially Mapped Past Method,

which will hereafter be referred to as the "EMP" concept, utilizes a weighted average and was obtained from the manufacturers of the EAI Analog TR-20 Computer used in the experiment (27).

"The weighted-average $\bar{f}(t)$ of a function, $f(t)$, over $T \leq t \leq T_2$ (with weight function $\phi(t)$ is defined by (1) where $\phi(t) \geq 0$ in the interval $T_1 \leq t \leq T_2$). Thus

$$\bar{f}(t) = \frac{\int_{T_1}^{T_2} f(t)\ \phi(t)\ dt}{\int_{T_1}^{T_2} \phi(t)\ dt} \qquad (3)$$

The integral in the denominator serves to "normalize" the expression. The function $\phi(t)$ can be chosen arbitrarily to emphasize or de-emphasize various parts of the interval from T_1 to T_2.

Remembering the requirements that the recent past must be emphasized and the remote past de-emphasized, it follows that we should choose a weighting function, $\phi(t)$, which is increasing and such that $\lim_{t \to -\infty} \phi(t) = 0$. Many functions have this property but the exponential function is a natural one and leads to a simple computer circuit. Picking an exponential weighting function, $e^{\alpha t}(\alpha > 0)$, Equation 3 becomes

$$\bar{f}(t) = \frac{\int_{T_1}^{T_2} e^{\alpha t} f(t)\ dt}{\int_{T_1}^{T_2} e^{\alpha t}\ dt} \qquad (4)$$

$$\bar{f}(t) = \alpha \frac{\int_{T_1}^{T_2} e^{\alpha t} f(t)\ dt}{e^{\alpha T_2} - e^{\alpha T_1}} \qquad (5)$$

This can be simplified by letting $T_1 \rightarrow -\infty$, or

$$\bar{f}(T) = \alpha e^{-\alpha T_2} \int_{-\infty}^{T_2} e^{\alpha t} f(t)\, dt \qquad (6)$$

The minus infinity in the lower limit serves to indicate that the average has been generated for such a long time that the effect of what happened before T_1 is negligible. In other words, since the exponential weighting function, $e^{\alpha t}$, approaches zero as $t \rightarrow -\infty$, the importance of events prior to T_1 is negligible if T_1 is suitably chosen.

Dropping the subscripts, Equation 6 can be written as

$$\bar{f}(T) = \alpha e^{-\alpha T} \int_{-\infty}^{T} f(t)\, e^{\alpha t}\, dt \qquad (7)$$

Re-arranging

$$\bar{f}(T) = \alpha \int_{-\infty}^{T} f(t)\, e^{-\alpha(T - t)}\, dt \qquad (8)$$

Otterman (2) defines this to be the "Exponentially Mapped Past" or EMP of f(t) over a time interval defined by α.

Implementation of the analog circuit for solving this equation is reasonably straightforward. Differentiating Equation 7 with respect to machine time, T, (t is a dummy variable) gives

$$\frac{d\bar{f}(T)}{dT} = \alpha \left\{ (-\alpha e^{-\alpha T}) \int_{-\infty}^{T} e^{\alpha t} f(t)\, dt + e^{-\alpha T} \left[e^{\alpha T} f(T) \right] \right\} \qquad (9)$$

$$\frac{d\bar{f}(T)}{dT} = \alpha \left[-\bar{f}(T) + f(T) \right] = \alpha f(T) - \alpha \bar{f}(T) \qquad (10)$$

Equation 10 is implemented by the simple circuit of Figure 4, which is recognized easily as the circuit for a simple filter or first order lag. Note that the input and output signals

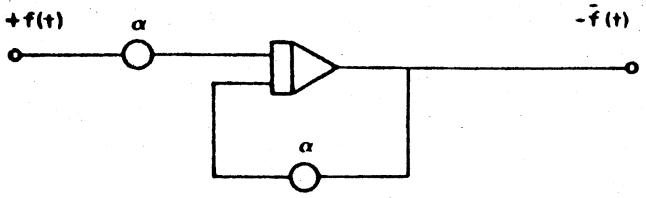

Analog Circuit for Obtaining the EMP Estimate of the Mean

Figure 4.

have been written in terms of the more familiar notation for time, t, which is not to be confused with the dummy variable of Equation 7.

The value of the constant, α, determines how fast past information becomes obsolete. It is chosen arbitrarily to be large enough to filter out non-essential random fluctuations and small enough not to obscure long term trends. A useful rule of thumb can be developed by examining the response of the circuit of Figure 4. If f(t) changes abruptly (step input), $\bar{f}(t)$ will follow gradually, making 95% of the change in 3 time constants or a time interval of $3/\alpha$. In other words, as shown in Figure 5, after three time constants, the

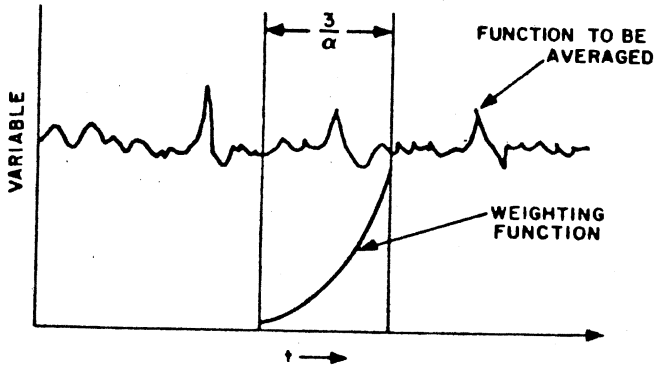

The EMP Mean of a Continuous Variable Provides a Measure of the Average of the Variable for a Continuously Updated Fixed Time Interval. Note the 95% decrease in the value of the weighting function over a period of length $3/\alpha$. This means that the weighted average at time, t, is virtually independent of values that occurred prior to time $t - 3/\alpha$.

Figure 5.

integrator has forgotten 95% of the information it had before the step change. Consequently, the EMP average defined by Equation 8 is an estimate* of the mean over a time interval approximately equal to $3/\alpha$.

In the circuit of Figure 4 it is obvious that an initial condition applied to the integrator will improve the computed average at the beginning. This value should represent a good guess as to the nominal or expected mean value of f(t). One normally would have such an estimate available. If it is a good estimate, the computed average will be reasonable from the start; if it is a bad one, it will not make any difference after about three to five time constants."

*If a 99% criterion were used, the time interval would be approximately $5/\alpha$.

REFERENCES

(1) Davenport, W. B., Jr., and W. L. Root: "An Introduction to the Theory of Random Signals and Noise". McGraw-Hill Book Company, Inc., New York, 1958.

(2) Otterman, Joseph: "The Properties and Methods for Computation of Exponentially Mapped Past Statistical Variables". IRE TRANS. on Automatic Control, Volume AC-5, Number 1, January, 1960, pp. 11-17.

APPENDIX C

ANALOG CIRCUITS

CIRCUIT DESCRIPTION	COMPUTER SYMBOL	PATCHING	COMMENTS
DUAL INTEGRATOR NETWORK 12.1116	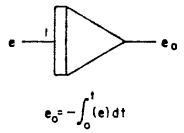 $e_o = -\int_0^t (e)\,dt$	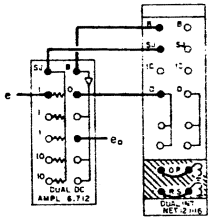	BASIC INTEGRATOR CIRCUIT

CIRCUIT DESCRIPTION	COMPUTER SYMBOL	PATCHING	COMMENTS
INVERTER	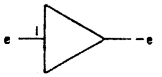	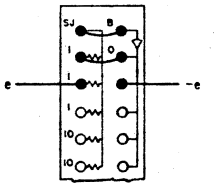	STANDARD CIRCUIT 100K INPUT IMPEDANCE

CIRCUIT DESCRIPTION	COMPUTER SYMBOL	PATCHING	COMMENTS
QUARTER-SQUARE MULTIPLIER USED AS SQUARER	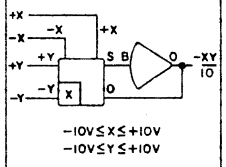 $-10V \le X \le +10V$ $-10V \le Y \le +10V$	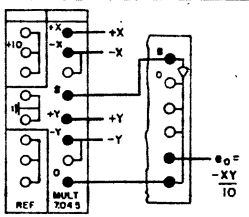	$\frac{X \cdot Y}{10}$

WHEN X = Y THEN $e_0 = -X^2/10$

CIRCUIT DESCRIPTION	COMPUTER SYMBOL	PATCHING	COMMENTS
QUARTER-SQUARE MULTIPLIER USED TO TAKE SQ. ROOT	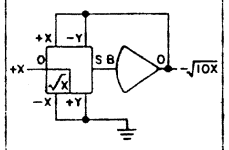	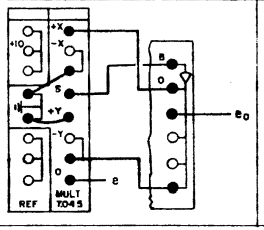	$\sqrt{X}$ POSITIVE INPUT

CIRCUIT DESCRIPTION	COMPUTER SYMBOL	PATCHING	COMMENTS
ADDITION	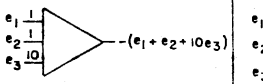 $-(e_1 + e_2 + 10e_3)$	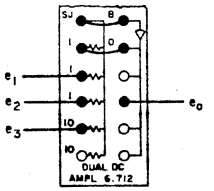	TYPICAL SUMMATION CIRCUIT

APPENDIX D

CANTILEVER BEAM CALIBRATIONS

	INITIAL CANTILEVER BEAM CALIBRATIONS Beckman Amplifier Settings of X.1 & 5 Full Scale Chart Deflection Considered 200				FINAL CANTILEVER BEAM CALIBRATIONS Beckman Amplifier Settings of X.1 & 2 Full Scale Chart Deflection Considered 40					
	As Recorded		Converted		As Recorded		Converted		$\frac{\text{Initial - Final}}{\text{Initial}}$ =	
	In	Out	In · 5/2	Out · 5/2	In	Out	In · 5	Out · 5	% Difference	
A_1	13.3050		33.2625		6.5471		32.7355		1.6	
A_2	13.7514		34.3785		6.8489		34.2445		0.4	
B_1	13.9479		34.8698		7.0079		35.0395		-0.5	
B_2	14.4305		36.0763		7.2023		36.0115		0.2	
A_3	10.3507	10.4381	25.8768	26.0953	5.0828	5.0103	25.4140	25.0515	1.8	4.2
A_4	13.9836	14.2872	34.9590	35.7180	6.7864	6.7600	33.9320	33.8000	2.9	5.4
B_3	10.4507	10.6756	26.1268	26.6890	4.9678	4.9337	24.8390	24.6685	4.9	7.6
B_4	12.6798	13.2870	31.6995	33.2175	6.3828	6.3596	31.9140	31.7980	-0.7	4.3
A_5		15.2093		38.0233		7.7711		38.5550		-1.4
A_6		15.2022		38.0055		7.4839		37.4195		1.5
B_5		16.1023		40.2558		7.6140		38.0700		5.4
B_6		15.9450		39.8625		7.9626		39.8130		0.1
A_7	13.9592	14.6164	34.8980	36.5410	6.7395	6.8453	33.6975	34.2265	3.4	6.3
A_8	15.7308	16.2166	39.3270	40.5415	7.7311	7.7340	38.6555	38.6700	1.7	4.6
B_7	16.8094	16.2666	42.0235	40.6665	7.9483	7.9511	39.7415	39.7555	5.4	2.2
B_8	15.9880	16.1880	39.9700	40.4700	7.6225	7.4924	38.1125	37.4620	4.6	7.4

APPENDIX E

TEST DATA

TABLE XXV

DEFLECTORS, UNSEALED MODEL, I-SERIES

Remarks: Scale 2 Position = α_3 (low) Date:

	Control, I-14				I-12				I-9				I-8			
	R_1	R_2	R_3	Avg.	R_1	R_2	R_3	Avg.	R_1	R_2	R_3	Avg.	R_1	R_2	R_3	Avg.
A_1*	93	93	91	92.33	95	98	98	97.00	95	100	99	98.00	104	100	101	101.67
A_2*	102	100	101	101.00	104	103	106	104.33	104	105	105	104.67	108	107	106	107.00
B_1*	99	100	102	100.33	106	111	108	108.33	105	108	104	105.67	108	109	108	108.33
B_2*	109	112	110	110.33	118	121	117	118.67	116	120	117	117.67	121	121	119	120.33
A_3	125	124	128	125.67 x 1.5 = 188.5	132	135	133	133.33 x 1.5 = 200.00	137	144	144	141.67 x 1.5 = 212.50	129	133	128	130.0 x 1.5 = 195.00
A_4	35	34	35	34.67	34	35	37	35.33	53	55	55	54.33	39	41	37	39.00
B_3	129	130	130	129.67 x 1.5 = 194.5	135	136	135	135.33 x 1.5 = 203.00	144	148	146	146.00 x 1.5 = 219.00	130	132	127	129.67 x 1.5 = 194.50
B_4	14	15	15	14.67	17	17	15	16.33	31	30	30	30.33	23	21	22	22.00
A_5	111	107	112	110.00	104	108	102	104.67	108	108	107	107.67	103	103	100	102.00
A_6	133	130	133	132.00	120	124	118	120.67	115	119	115	116.33	115	117	115	115.67
B_5	108	108	112	109.33	100	101	100	100.33	103	104	102	103.00	99	95	97	97.00
B_6	137	137	142	138.67	124	124	125	124.33	122	122	120	121.33	125	121	122	122.67
A_7	63	63	65	63.67	57	59	57	57.67	55	54	53	54.00	56	53	55	54.67
A_8	50	49	51	50.00	39	40	43	40.67	37	37	36	36.67	40	35	36	37.00
B_7	55	56	56	55.67	48	50	55	51.00	46	46	47	46.33	47	45	46	46.00
B_8	28	27	28	27.67	20	25	25	23.33	21	18	24	21.00	23	20	21	21.33
*Inward			Total	1523.33			Total	1505.67			Total	1548.17			Total	1484.17

	I-10				I-5				I-6			
	R_1	R_2	R_3	Avg.	R_1	R_2	R_3	Avg.	R_1	R_2	R_3	Avg.
A_1*	100	97	97	98.00	97	97	99	97.67	100	99	98	99.00
A_2*	105	103	103	103.67	105	105	104	104.67	106	103	102	103.67
B_1*	105	104	103	104.00	101	104	100	101.67	108	103	102	104.33
B_2*	115	115	114	114.67	112	114	112	112.67	118	115	114	115.67
A_3	134	137	135	135.33 x 1.5 = 203.00	139	133	139	137.00 x 1.5 = 205.50	125	122	121	122.67 x 1.5 = 184.00
A_4	36	36	36	36.00	40	38	39	39.00	32	29	30	30.33
B_3	134	134	137	135.00 x 1.5 = 202.50	137	137	139	137.67 x 1.5 = 206.50	128	123	123	124.67 x 1.5 = 187.00
B_4	17	15	18	16.67	22	18	18	19.33	14	10	13	12.33
A_5	107	109	111	109.00	111	115	111	112.33	110	110	108	109.33
A_6	124	123	124	123.67	125	127	124	125.33	124	128	128	126.67
B_5	105	103	104	104.00	105	108	105	106.00	101	104	103	102.67
B_6	130	129	129	129.33	132	133	130	131.67	129	132	132	131.00
A_7	58	58	59	58.33	60	57	58	58.33	65	61	62	62.67
A_8	42	41	39	40.67	46	45	43	44.67	47	47	47	47.00
B_7	53	53	50	52.00	54	50	52	52.00	49	54	53	52.00
B_8	27	23	20	23.33	35	31	30	32.00	32	33	33	32.67
*Inward			Total	1518.83			Total	1549.33			Total	1500.33

TABLE XXV (Continued)

Remarks: Scale 2 Position = a_1 (high) Date:

	Control, I-1			I-11				I-3				I-7			
	R_1	R_2	Avg.	R_1	R_2	R_3	Avg.	R_1	R_2	R_3	Avg.	R_1	R_2	R_3	Avg.
A_1*	83	87	85.00	105	97	100	100.67	103	105	100	102.67	99	99	101	99.67
A_2*	92	95	93.50	109	104	106	106.33	106	110	106	107.33	107	106	107	106.67
B_1*	94	95	94.50	109	107	105	107.00	107	109	107	107.67	105	106	106	105.67
B_2*	106	108	107.00	120	117	117	118.00	118	118	118	118.00	116	118	117	117
A_3	127	119	123.00 x 1.5 = 184.50	117	118	114	116.33 x 1.5 = 174.50	125	125	127	125.67 x 1.5 = 188.50	123	117	119	119.67 x 1.5 = 179.50
A_4	42	42	42.00	30	36	32	32.67	49	50	50	49.67	42	43	42	42.33
B_3	128	126	127.00 x 1.5 = 190.50	118	123	120	120.33 x 1.5 = 180.50	127	128	130	128.33 x 1.5 = 192.50	126	120	120	122.00 x 1.5 = 183.00
B_4	20	17	18.50	15	17½	17	16.50	33	31	34	32.67	28	28	25	27.00
A_5	115	119	117.00	103	102	102	102.33	102	108	107	105.67	107	104	107	106.00
A_6	139	142	140.50	117	120	122	119.67	115	118	119	117.33	121	117	121	119.67
B_5	118	117	117.50	98	100	98	98.67	100	105	102	102.33	104	98	102	101.33
B_6	146	146	146.00	124	126	123	124.33	119	125	122	122.00	128	125	127	126.67
A_7	68	70	69.00	58	58	58	58.00	56	56	59	57.00	60	59	60	59.67
A_8	52	55	53.50	38	42	47	42.33	46	47	46½	46.50	44	46	44	44.67
B_7	61	59	60.00	50	49	48	49.00	52	53	52	52.33	50	50	50	50.00
B_8	36	33	34.50	19	22	18	19.67	34	36	40	36.67	30	31	29	30.00
*Inward		Total	1553.50			Total	1450.17			Total	1538.83			Total	1498.83

	I-4				I-13				I-2			
	R_1	R_2	R_3	Avg.	R_1	R_2	R_3	Avg.	R_1	R_2	R_3	Avg.
A_1*	93	95	92	93.33	93	92	94	93.00	92	95	97	94.67
A_2*	100	101	98	99.67	100	102	101	101.00	102	100	103	101.67
B_1*	99	99	98	98.67	99	102	100	100.33	100	100	104	101.33
B_2*	113	111	108	110.67	110	112	113	111.67	111	110	115	112.00
A_3	124	129	131	128 x 1.5 = 192.00	126	126	131	127.67 x 1.5 = 191.50	124	122	121	122.33 x 1.5 = 183.50
A_4	40	47	46	44.33	52	50	50	50.67	44	43	42	43.00
B_3	128	132	134	131.33 x 1.5 = 197.00	133	132	135	133.33 x 1.5 = 200.00	130	125	125	126.67 x 1.5 = 190.00
B_4	25	25	25	25.00	28	29	29	28.67	30	25	25	26.67
A_5	121	121	118	120.00	110	108	111	109.67	111	109	111	110.33
A_6	133	135	133	133.67	126	124	129	126.33	128	123	128	126.33
B_5	111	115	115	113.67	109	107	113	109.67	111	106	108	108.33
B_6	138	142	142	140.67	134	131	137	134.00	135	130	134	133.00
A_7	65	63	66	64.67	59	62	63	61.33	62	60	56	59.33
A_8	56	53	54	54.33	44	45	46	45.00	53	51	48	50.67
B_7	60	60	61	60.33	52	55	51	52.67	63	56	55	58.00
B_8	42	41	44	42.33	25	23	22	23.33	48	42	39	43.00
*Inward			Total	1590.33			Total	1538.83			Total	1541.83

TABLE XXVI

DEFLECTORS, UNSEALED MODEL, I-SERIES (RECORDED STRAIN IN CHART DIVISIONS)

Date: May 19, 1973

Remarks: $c_1a_0b_2\alpha_3$ — I-26(s)

	R_1	R_2	R_3	Avg.
A_1*	162	157	161	160.0
A_2*	156	156	160	157.3
B_1*	182	182	186	183.3
B_2*	177	177	181	178.3
A_3	58	55	55	56.0 x 1.5 = 84.0
A_4*	26	24	27	25.7
B_3	59	57	59	58.3 x 1.5 = 87.45
B_4*	31	28	31	30.0
A_5	50	49	48	49.0
A_6	57	56	56	56.3
B_5	42	46	46	44.7
B_6	54	56	57	55.7
A_7	13	12	12	12.3
A_8	18	20	17	18.3
B_7	11	11	9	10.3
B_8	13	13	10	12.0

*Inward — Total 1164.83

Remarks: $c_1a_0b_2\alpha_1$ — I-28(s)

	R_1	R_2	R_3	Avg.
A_1*	162	160	161	161.0
A_2*	159	156	157	157.3
B_1*	186	185	183	184.7
B_2*	180	180	178	179.3
A_3	57	55	55	55.7 x 1.5 = 83.55
A_4*	38	41	46	41.7
B_3	57	56	57	56.7 x 1.5 = 85.05
B_4*	43	46	44	44.3
A_5	54	54	56	54.7
A_6	61	62	59	60.7
B_5	47	46	46	46.3
B_6	60	61	60	60.3
A_7	13	14	14	13.7
A_8	17	19	19	18.3
B_7	17	16	11	14.7
B_8	14	14	13	13.7

*Inward — Total 1219.16

Remarks: $c_1a_0b_1\alpha_4$ — Control I-27(s)

	R_1	R_2	R_3	Avg.
A_1*	158	161	160	159.7
A_2*	157	158	160	158.3
B_1*	185	185	187	185.7
B_2*	180	181	180	180.3
A_3	54	53	55	54.0 x 1.5 = 81.00
A_4*	59	58	56	57.7
B_3	52	52	50	51.3 x 1.5 = 76.95
B_4*	60	60	60	60.0
A_5	56	56	57	56.3
A_6	67	67	69	67.7
B_5	50	49	50	49.7
B_6	67	68	68	67.7
A_7	17	16	16	16.3
A_8	21	21	20	20.7
B_7	14	14	13	13.7
B_8	16	17	14	15.7

*Inward — Total 1267.33

TABLE XXVI (Continued)

Date: May 17, 1973

Remarks: $c_1a_3b_1\alpha_4$ — Control I-14(s)

	R_1	R_2	R_3	Avg.
A_1*	160	158	162	160
A_2*	155	153	157	155
B_1*	174	174	175	174.3
B_2*	174	173	172	173
A_3	55	53	52	53.3 x 1.5 = 80
A_4*	57	59	58	58
B_3	59	57	57	57.7 x 1.5 = 86.5
B_4*	58	62	62	60.7
A_5	59	58	59	58.7
A_6	67	69	67	67.7
B_5	51	50	49	50
B_6	63	66	66	65
A_7	14	14	15	14.3
A_8	22	21	23	22.0
B_7	13	13	12	12.7
B_8	14	16	14	14.7
*Inward			Total	1252.6

Remarks: $c_1a_3b_2\alpha_1$ — I-12(s)

	R_1	R_2	R_3	Avg.
A_1*	164	163	162	163
A_2*	156	156	155	155.7
B_1*	177	177	178	177.3
B_2*	173	175	175	174.3
A_3	68	69	71	69.3 x 1.5 = 104
A_4*	42	36	39	39
B_3	73	75	77	75 x 1.5 = 112.5
B_4*	45	43	44	44
A_5	61	55	57	57.7
A_6	63	63	62	62.7
B_5	51	49	49	49.7
B_6	60	60	59	59.7
A_7	14	12	13	13
A_8	22	18	19	19.7
B_7	10	10	10	10
B_8	11	13	10	11.3
*Inward			Total	1253.67

Remarks: $c_1a_3b_2\alpha_3$ — I-8(s)

	R_1	R_2	R_3	Avg.
A_1*	158	160	160	159.3
A_2*	157	155	155	155.7
B_1*	176	174	178	176
B_2*	174	173	175	174
A_3	73	69	71	71 x 1.5 = 105.5
A_4*	28	31	29	29.3
B_3	78	74	76	76 x 1.5 = 114
B_4*	34	37	37	36
A_5	60	59	57	58.7
A_6	66	66	66	66
B_5	53	47	49	49.7
B_6	64	59	62	61.7
A_7	14	12	12	12.7
A_8	21	19	19	19.7
B_7	10	10	11	10.3
B_8	12	11	11	11.3
*Inward			Total	1239.83

TABLE XXVI (Continued)

Remarks: $c_3a_0b_1\alpha_4$ — Control I-24(s)

	R_1	R_2	R_3	Avg.
A_1*	160	155	158	157.7
A_2*	156	153	157	155.3
B_1*	178	177	179	178.0
B_2*	177	175	178	176.7
A_3	48	48	49	48.3 x 1.5 = 72.50
A_4*	59	58	57	58.0
B_3	53	50	55	52.7 x 1.5 = 79.0
B_4*	67	66	65	66.0
A_5	55	50	52	52.3
A_6	71	68	71	70.0
B_5	51	45	52	49.3
B_6	68	64	64	65.3
A_7	18	13	17	16.0
A_8	23	19	22	21.3
B_7	16	15	12	14.3
B_8	13	14	12	13.0
			Total	1244.70

*Inward

Remarks: $c_3a_0b_1\alpha_3$ — I-18(s)

	R_1	R_2	R_3	Avg.
A_1*	152	155	155	154.0
A_2*	151	152	152	151.7
B_1*	178	178	177	177.7
B_2*	175	175	175	175.0
A_3	66	63	65	64.7 x 1.5 = 97.0
A_4	57	55	57	56.3
B_3	75	72	73	73.3 x 1.5 = 110.0
B_4	43	43	42	42.7
A_5	66	62	64	64.0
A_6	58	58	58	58.0
B_5	65	61	65	63.7
B_6	56	53	52	53.7
A_7	1	1	1	1.0
A_8	6	7	4	5.7
B_7	2	1	1	1.3
B_8	- 1*	- 1*	- 1*	- 1.0*
			Total	1210.80

*Inward

Remarks: $c_3a_0b_1\alpha_1$ — Date: May 17, 1973 — I-19(s)

	R_1	R_2	R_3	Avg.
A_1*	155	152	155	154.0
A_2*	154	152	152	152.7
B_1*	177	178	176	177.0
B_2*	179	177	174	176.7
A_3	91	91	91	91.0 x 1.5 = 136.5
A_4	40	40	45	41.7
B_3	101	103	102	102.0 x 1.5 = 153.0
B_4	28	29	30	29.0
A_5	64	60	59	61.0
A_6	54	53	52	53.0
B_5	67	66	65	66.0
B_6	50	49	47	48.7
A_7	0	0	- 1*	- 0.3*
A_8	3	3	4	3.3
B_7	0	1	4	1.7
B_8	- 2*	- 1*	1	- 0.7*
			Total	1253.30

*Inward

TABLE XXVI (Continued)

Remarks: $c_3a_2b_1\alpha_3$

I-29(s)

	R_1	R_2	R_3	Avg.
A_1*	148	148	153	149.7
A_2*	149	146	149	148.0
B_1*	176	168	172	172.0
B_2*	173	166	172	170.3
A_3	87	86	88	87.0 x 1.5 = 130.5
A_4	44	44	45	44.3
B_3	96	94	95	95.0 x 1.5 = 142.5
B_4	28	28	28	28.0
A_5	57	59	59	58.3
A_6	55	53	51	53.0
B_5	64	61	62	62.3
B_6	50	49	48	49.0
A_7	2	1	2	1.7
A_8	6	6	7	6.3
B_7	5	5	4	4.7
B_8	1	2	1	1.3

*Inward

Total 1222.00

Date: May 18, 1973

Remarks: $c_3a_2b_1\alpha_4$

Control
I-30(s)

	R_1	R_2	R_3	Avg.
A_1*	156	154		155.0
A_2*	155	154		154.5
B_1*	180	177		178.5
B_2*	180	175		177.5
A_3	43	44		43.5 x 1.5 = 65.2
A_4*	62	60		61.0
B_3	46	48		47.0 x 1.5 = 70.5
B_4*	69	68		68.5
A_5	53	49		51.0
A_6	72	71		71.5
B_5	49	48		48.5
B_6	65	66		65.5
A_7	16	16		16.0
A_8	22	20		21.0
B_7	14	16		15.0
B_8	13	15		14.0

*Inward

Total 1232.67

TABLE XXVI (Continued)

Remarks: $c_3a_3b_1\alpha_3$ — Control I-23(s)

	R_1	R_2	R_3	Avg.
A_1*	163	163	165	163.7
A_2*	156	155	157	156.0
B_1*	181	179	182	180.7
B_2*	178	172	176	175.3
A_3	50	53	51	51.3 x 1.5 = 77.0
A_4*	56	59	59	58.0
B_3	56	52	57	55.0 x 1.5 = 82.5
B_4*	63	64	62	63.0
A_5	54	55	54	54.3
A_6	69	71	71	70.3
B_5	51	52	50	51.0
B_6	65	67	65	65.7
A_7	14	14	13	13.7
A_8	20	20	20	20.0
B_7	14	12	14	13.3
B_8	16	13	13	14.0

*Inward — Total 1258.17

Remarks: $c_3a_3\alpha_3b_1$ — I-16(s)

	R_1	R_2	R_3	Avg.
A_1*	154	155	154	154.3
A_2*	148	148	150	148.7
B_1*	171	175	172	172.7
B_2*	169	171	168	169.3
A_3	104	104	105	104.3 x 1.5 = 156.5
A_4	36	34	36	35.3
B_3	108	109	112	109.7 x 1.5 = 164.5
B_4	23	23	23	23.0
A_5	74	72	73	73.0
A_6	59	57	58	58.0
B_5	69	70	71	70.0
B_6	54	53	56	54.3
A_7	3	2	3	2.7
A_8	8	7	8	7.7
B_7	4	3	4	3.7
B_8	3	3	4	3.3

*Inward — Total 1297.07

Remarks: $c_3a_3b_1\alpha_1$ — I-17(s)

	R_1	R_2	Avg.
A_1*	156	150	153.0
A_2*	146	146	146.0
B_1*	169	173	171.0
B_2*	164	167	165.5
A_3	179	171	175.0 x 1.5 = 262.5
A_4	4	4	4.0
B_3	195	189	192.0 x 1.5 = 288.0
B_4*	- 8	- 7	- 7.5
A_5	81	80	80.5
A_6	65	58	61.5
B_5	85	82	83.5
B_6	64	61	62.5
A_7*	- 2	- 2	- 2.0
A_8	2	1	1.5
B_7	1	1	1.0
B_8*	- 2	- 3	- 2.5

*Inward — Total 1479.50

TABLE XXVII

AIRFOILS, UNSEALED MODEL II-SERIES (RECORDED STRAIN IN CHART DIVISIONS)

Remarks: Scale 5

	Control, II-7				II-9(a)			
	R_1	R_2	R_3	Avg.	R_1	R_2	R_3	Avg.
A_1*	37	37	38	37.33	34	34.5	35	34.50
A_2*	40	40	38	39.33	38	38	37.5	37.83
B_1*	36	35	35	35.33	36	36	35	35.67
B_2*	43	41	42.5	42.17	42	42	41	41.67
A_3	51	52	52	51.67 x 1.5 = 77.50	45	47	45	45.67 x 1.5 = 68.50
A_4	20	20	18	19.33	2.5	3	3	2.83
B_3	53	53	54	53.33 x 1.5 = 80.00	48	47	50	48.33 x 1.5 = 72.50
B_4	13	11	12	12.00	1*	3*	3*	2.33*
A_5	55	54	55	54.67	81	80	80	80.33
A_6	62	59	58	59.67	56	55	56	55.67
B_5	51	50	49	50.00	78	76	78	77.33
B_6	65	63	63	63.67	59	57	57	57.67
A_7	27	28	29	28.00	26	25	27	26.00
A_8	20	22	21	21.00	18	15	15	16.00
B_7	26	20	26.5	24.17	21	22	22	21.67
B_8	17	17	16	16.67	8	7	6	7.00
*Inward			Total = 660.91				Total = 632.83	

	Control, II-14				II-13(a)			
	R_1	R_2	R_3	Avg.	R_1	R_2	R_3	Avg.
A_1*	34	35	32	33.67	39	33	37	36.33
A_2*	36	39.5	37	37.50	41.5	36	38	38.50
B_1*	35	39	36	36.67	42	36	36	38.00
B_2*	40	43	41	41.33	41	40	41	40.67
A_3	54	55.5	54	54.5 x 1.5 = 81.75	45	46	46	45.67 x 1.5 = 68.50
A_4	20	23	22	21.67	7	6	5	6.00
B_3	53	57	56	55.33 x 1.5 = 83.00	48	48	47	47.67 x 1.5 = 71.50
B_4	13	17	14	14.67	2	0	1	1.00
A_5	54	60	53	55.67	74	77	77.5	76.17
A_6	62	66	61	63.00	61	59	62	60.67
B_5	51	54	55	53.33	76	74	74	74.67
B_6	67	69	63	66.33	65	63	62	63.33
A_7	32	33	31	32.00	28	27.5	27	27.50
A_8	20	23	21.5	21.50	15.5	17.5	17.5	16.83
B_7	25	25.5	24	24.83	26	24	24	24.67
B_8	9	11	10	10.00	10	9	10	9.67
*Inward			Total	676.92			Total	654.00

TABLE XXVIII

DUCTS, UNSEALED MODEL, III-SERIES (RECORDED STRAIN IN CHART DIVISIONS)

REMARKS: Scale = 2 Date:

	Control				Big III			
	R_1	R_2	R_3	Avg.	R_1	R_2	R_3	Avg.
A_1*	79	80	82	80.33	80	79	81	80.00
A_2*	80	82	83	81.67	76	80	81	79.00
B_1*	90	89	92	90.33	90	91	90	90.33
B_2*	89	89	92	90.00	85	87	88	86.67
A_3	138	136	135	136.33 x 1.5 = 204.5	124.5	126	134	128.17 x 1.5 = 192.25
A_4	43	44	38	41.67	32	34	37	34.33
B_3	140	140	142	140.67 x 1.5 = 211.0	129	129	137	131.67 x 1.5 = 197.5
B_4	35	35	38	36.00	31	30	33	31.33
A_5	161	158	165	161.33	153	153	158	154.67
A_6	172	169	168	169.67	153	151.5	153	152.50
B_5	137	132	137	135.33	128	127	130	128.33
B_6	159	158	160	159.00	142	139.5	142	141.17
A_7	83	84	85	84.00	78	79	78	78.33
A_8	87	89	90	88.67	78	80	79	79.00
B_7	84	85	85	84.67	83	83	82	82.67
B_8	93	95	97	95.00	87	88	86	87.00
			Total	1813.17			Total	1695.07

*Inward

TABLE XXIX

DUCTS, SEALED MODEL, III(s)-SERIES (RECORDED STRAIN IN CHART DIVISIONS)

REMARKS: DATE: May 22, 1973

	Control				Big III(s)			
	R_1	R_2	R_3	Avg.	R_1	R_2	R_3	Avg.
A_1*	156	151	152	153.00	158	156	153	155.67
A_2*	106	105	110	107.00	111	111	110	110.67
B_1*	191	185	191	189.00	190	190	189	189.67
B_2*	123	120	125	122.67	126	130	126	127.33
A_3	62	62	66	63.33 x 1.5 = 95.00	57	56	52	55.00 x 1.5 = 82.50
A_4*	41	42	38	40.33	47	49	49	48.33
B_3	62	63	65	63.33 x 1.5 = 95.00	57	58	56	57.00 x 1.5 = 85.50
B_4*	41	41	42	41.33	45	48	45	46.00
A_5	65	69	66	66.67	61	59	57	59.00
A_6	76	74	75	75.00	54	56	55	55.00
B_5	50	53	53	52.00	47	50	49	48.67
B_6	72	75	76	74.33	52	54	53	53.00
A_7	52	54	54	53.33	50	50	50	50.00
A_8	15	15	15	15.00	14	12	12	12.67
B_7	61	61	59	60.33	58	58	59	58.33
B_8	15	15	15	15.00	14	12	12	12.67
			Total	1255.00			Total	1195.00

*Inward

TABLE XXIX (Continued)

REMARKS:	Control				Med III(s)			DATE: May 30, 1973
	R_1	R_2	R_3	Avg.	R_1	R_2	P_3	Avg.
A_1*	171	173	165	169.67	170	168	171	169.67
A_2*	140	140	135	138.33	139	137	138	138.00
B_1*	190	191	187	189.33	188	189	195	190.67
B_2*	143	143	140	142.00	140	140	140	140.00
A_3	64	63	64	63.67 x 1.5 = 95.5	57	61	60	59.33 x 1.5 = 89.00
A_4*	46	45	45	45.33	54	49	54	52.33
B_3	52	54	54	53.33 x 1.5 = 80.0	52	53	53	52.67 x 1.5 = 79.00
B_4*	45	48	43	45.33	49	48	52	49.67
A_5	50	50	53	51.00	50	51	50	50.33
A_6	65	65.5	68	66.17	55.5	55	55	55.16
B_5	46	46	51	47.67	43	43	44	43.33
B_6	70	71	71	70.67	60	58	57	58.33
A_7	49	50	47	48.67	47	47	47	47.00
A_8	15	12	11	12.67	10	9	10	9.67
B_7	47	50	50	49.00	48	52	49	49.67
B_8	12	15	12	13.00	9.5	11	9	9.83
			Total	1264.33			Total	1231.67

*Inward

TABLE XXX

VENTING, UNSEALED MODEL (RECORDED STRAIN IN CHART DIVISIONS

	Closed Control				¼" slot in walls				27/32" slot in walls (.844")			
	R_1	R_2	R_3	Avg.	R_1	R_2	R_3	Avg.	R_1	R_2	R_3	Avg.
A_1*	85	87	87	86.3	73	74	77	74.7	91	88	90	89.7
A_2*	93	94	93	93.3	72	74	75	73.7	66	64	66	65.3
B_1*	88	93	88	89.7	79	81	81	80.3	94	92	93	93.0
B_2*	100	102	100	100.7	78	81	82	80.3	70	70	70	70.0
A_3	127	128	127	127.3 x 1.5 = 191.0	123	130	122½	125.2 x 1.5 = 187.8	85	84	83	84.0 x 1.5 = 126.0
A_4	36	37	36	36.3	42	45	44	43.7	21	21	21	21.0
B_3	130	130	128	129.3 x 1.5 = 194.0	125	132	127	128.0 x 1.5 = 192.0	86	85	83	84.7 x 1.5 = 127.0
B_4	28	27	29	28.0	33	36	32	33.7	13	15	12	13.3
A_5	142	141	144	142.3	174	170	173	172.3	160	165	160	161.7
A_6	156	154	155	155.0	182	182	185	183.0	134	139	134	135.7
B_5	125	122	123	123.3	155	154	155	154.7	148	149	145	147.3
B_6	160	157	158	158.3	190	191	193	191.3	139	145	140	141.3
A_7	74	76	77	75.6	69	71	71	70.3	47	47	46	46.7
A_8	82	83	83	82.7	84	85	85	84.7	63	63	63	63.0
B_7	71	75	77	74.3	70	71	69	70.0	45	47	45	45.7
B_8	81	83	85	83.0	86	87	85	86.0	63	65	63	63.7
			Total	1713.8			Total	1778.5			Total	1410.35

* Inward

APPENDIX F

COMPUTER PROGRAM FOR

FINAL INVESTIGATION

```
TITLE 'MODEL WIND TUNNEL TESTS';
DATA WINDA;
INPUT OPNG 1-4 VEL $ 5 ANGLE 6 MODIF $ 7-9 OBS 11-12 A1 14-17 A2 18-21
B1 22-25 B2 26-29 A3 31-34 A4 35-38 B3 39-42 B4 43-46 A5 48-51 A6 52-55
B5 56-59 B6 60-63 A7 65-68 A8 69-72 B7 73-76 B8 77-80;
IF OPNG=0000 AND ANGLE=1 THEN DO=1;
IF OPNG=0000 AND ANGLE=2 THEN DO=2;
IF OPNG=0000 AND ANGLE=3 THEN DO=3;
IF OPNG=0422 AND ANGLE=1 THEN DO=4;
IF OPNG=0422 AND ANGLE=2 THEN DO=5;
IF OPNG=0422 AND ANGLE=3 THEN DO=6;
IF OPNG=0844 AND ANGLE=1 THEN DO=7;
IF OPNG=0844 AND ANGLE=2 THEN DO=8;
IF OPNG=0844 AND ANGLE=3 THEN DO=9;
CARDS
```

```
  26 OBSERVATIONS IN DATA SET WINDA         22  VARIABLES

PROC PRINT DATA=WINDA;
```

MODEL WIND TUNNEL TESTS

OBS	OPNG	VEL	ANGLE	MODIF	OBS	A1	A2	B1	B2	A3	A4	B3	B4	A5	A6	B5	B6	A7	A8	B7	B8	DO
1	0	F	1	DTS	1	154	151	181	168	67	-20	53	-25	78	78	57	73	23	17	10	11	1
2	0	F	1	DTS	2	150	151	178	167	68	-15	56	-26	74	81	57	74	22	18	10	10	1
3	0	F	1	DTS	3	151	149	179	168	70	-18	57	-25	75	79	55	72	19	17	9	10	1
4	0	F	2	DTS	1	157	157	174	158	83	-7	78	-9	126	110	78	94	29	24	9	13	2
5	0	F	2	DTS	2	156	158	174	158	83	-7	79	-9	128	112	79	95	27	21	8	14	2
6	0	F	2	DTS	3	156	156	173	157	84	-7	79	-7	129	111	80	97	28	23	8	12	2
7	0	F	3	DTS	1	142	143	144	128	96	12	77	9	168	124	110	117	43	28	13	13	3
8	0	F	3	DTS	2	143	146	146	129	96	11	79	9	169	124	109	117	42	29	13	14	3
9	0	F	3	DTS	3	142	143	142	129	98	10	81	7	164	123	105	116	42	29	13	14	3
10	422	F	1	DTS	1	147	131	167	145	39	-34	30	-34	67	67	57	66	17	12	9	11	4
11	422	F	1	DTS	2	147	130	165	143	38	-33	32	-34	67	66	58	67	16	12	9	12	4
12	422	F	1	DTS	3	146	132	166	145	39	-33	28	-33	66	67	58	68	16	11	10	11	4
13	422	F	2	DTS	1	144	137	162	147	46	-27	33	-18	99	86	71	86	2	15	13	21	5
14	422	F	2	DTS	2	140	135	162	147	43	-25	33	-21	99	85	70	85	3	15	14	21	5
15	422	F	2	DTS	3	143	135	162	148	44	-26	33	-19	101	85	71	86	3	15	14	22	5
16	422	F	3	DTS	1	138	127	136	123	57	-1	44	0	164	102	104	100	1	14	13	22	6
17	422	F	3	DTS	2	136	128	136	122	60	4	47	2	166	108	104	101	1	14	13	21	6
18	844	F	1	DTS	1	137	113	163	142	27	-30	23	-29	77	66	73	73	-17	-8	5	0	7
19	844	F	1	DTS	2	136	113	159	139	28	-32	20	-31	78	66	71	72	-14	-8	5	0	7
20	844	F	1	DTS	3	135	112	163	142	28	-30	21	-32	78	68	73	74	-14	-10	6	0	7
21	844	F	2	DTS	1	129	109	155	124	34	-26	31	-19	114	90	82	89	2	1	11	7	8
22	844	F	2	DTS	2	132	110	151	125	32	-26	28	-18	113	91	80	88	1	1	10	6	8
23	844	F	2	DTS	3	134	111	154	124	31	-26	25	-19	116	91	82	89	1	0	10	7	8
24	844	F	3	DTS	1	114	97	128	98	45	-4	38	-1	160	100	102	95	14	5	21	18	9
25	844	F	3	DTS	2	114	98	126	97	44	-5	36	-1	165	101	104	95	14	7	22	18	9
26	844	F	3	DTS	3	116	100	127	99	46	-2	37	-2	163	102	107	98	15	8	21	17	9

```
DATA WINDB; SET WINDA;
AV1=AVG(A1,B1);
AV2=AVG(A2,B2);
AV3=0; AV4=0; AV5=0; AV6=0;
AV7=AVG(A7,B7);
AV8=AVG(A8,B8);
PAN1=(AV1+AV2)*2.;
AESPAN1=0;PAN2=0; AESPAN2=0; PAN3=0; ABSPAN3=0;
PAN4=(AV7+AV8)*2.;
ABSPAN4=0;
IF ANGLE=1 THEN GO TO F1;
IF ANGLE=2 THEN GO TO F2;
IF ANGLE=3 THEN GO TO F3;
F1:;
IA1=  7;  IA2=  10;  IB1=  1;  IB2=  5;
IA7=  5;  IA8=   1;  IB7=  2;  IB8=  0;
FPAN1=  493.14;
FPAN4=  528.67;
GO TO NULL;
F2:;
IB1=1.5;  IB2=5.5;  IB7=3.5;  IB8=2;
IA1=7.5;  IA2=11;  IA7=5;  IA8=2;
FPAN1=509.25;   FPAN4=526.75;
GO TO NULL;
F3:;
IA1=7;  IA2=9.5;  IA7=5.5;  IA8=3;
IB1=0;  IB2=5;  IB7=3.5;  IB8=2;
FPAN1=498.67;   FPAN4=523.0;
NULL:;
RA1=PAN1/FPAN1;
RA4=PAN4/FPAN4;
A1=A1-IA1*RA4;
A2=A2-IA2*RA4;
B1=B1-IB1*RA4;
B2=B2-IB2*RA4;
A7=A7-IA7*RA1;
A8=A8-IA8*RA1;
B7=B7-IB7*RA1;
B8=B8-IB8*RA1;

  26 OBSERVATIONS IN DATA SET WINDB         50  VARIABLES

PROC PRINT;
DROP AV3 AV4 AV5 AV6 ABSPAN1 PAN2 ABSPAN2 ABSPAN3 PAN3 ABSPAN4;
```

MODEL WIND TUNNEL TESTS

OBS	OPNG	VEL	ANGLE	MODIF	OBS	A1	A2	B1	B2	A3	A4	B3	B4	A5	A6	B5	B6	A7	A8	B7
1	0	F	1	DTS	1	153.192	149.846	180.885	167.423	67	-20	53	-25	78	78	57	73	16.3690	15.6738	7.3476
2	0	F	1	DTS	2	149.206	149.865	177.887	166.433	68	-15	56	-26	74	81	57	74	15.4501	16.6900	7.3801
3	0	F	1	DTS	3	150.272	147.960	178.896	167.480	70	-18	57	-25	75	79	55	72	12.4400	15.6880	6.3760
4	0	F	2	DTS	1	155.932	155.434	173.786	157.217	83	-7	78	-9	126	110	78	94	22.6573	21.4629	4.5601
5	0	F	2	DTS	2	155.003	156.538	173.801	157.269	83	-7	79	-9	128	112	79	95	20.6573	18.4629	3.5601
6	0	F	2	DTS	3	154.989	154.517	172.798	156.259	84	-7	79	-7	129	111	80	97	21.6966	20.4786	3.5876
7	0	F	3	DTS	1	140.702	141.238	144.000	127.073	96	12	77	9	168	124	110	117	36.8567	24.6491	9.0906
8	0	F	3	DTS	2	141.688	144.220	146.000	128.063	96	11	79	9	169	124	109	117	35.7795	25.6070	9.0415
9	0	F	3	DTS	3	140.688	141.220	142.000	128.063	98	10	81	7	164	123	105	116	35.8677	25.6551	9.0976
10	422	F	1	DTS	1	146.351	130.073	166.907	144.537	39	-34	30	-34	67	67	57	66	11.0179	10.8036	6.6072
11	422	F	1	DTS	2	146.351	129.073	164.907	142.537	38	-33	32	-34	67	66	58	67	10.0686	10.8137	6.6274
12	422	F	1	DTS	3	145.364	131.092	165.909	144.546	39	-33	28	-33	66	67	58	68	10.0281	9.8056	7.6112
13	422	F	2	DTS	1	143.274	135.935	161.855	146.467	46	-27	33	-18	99	86	71	86	-3.7928	12.6829	8.9450
14	422	F	2	DTS	2	139.245	133.893	161.849	146.447	43	-25	33	-21	99	85	70	85	-2.7339	12.7064	9.9863
15	422	F	2	DTS	3	142.231	133.872	161.846	147.436	44	-26	33	-19	101	85	71	86	-2.7732	12.6907	9.9588
16	422	F	3	DTS	1	137.331	126.092	136.000	122.522	57	-1	44	0	164	102	104	100	-4.7794	10.8476	9.3222
17	422	F	3	DTS	2	135.344	127.110	136.000	121.532	60	4	47	2	166	108	104	101	-4.7573	10.8596	9.3363
18	844	F	1	DTS	1	137.265	113.378	163.038	142.189	27	-30	23	-29	77	66	73	73	-22.6272	-9.1254	2.7491
19	844	F	1	DTS	2	136.225	113.322	159.032	139.161	28	-32	20	-31	78	66	71	72	-19.5461	-9.1092	2.7816
20	844	F	1	DTS	3	135.238	112.340	163.034	142.170	28	-30	21	-32	78	68	73	74	-19.5968	-11.1194	3.7613
21	844	F	2	DTS	1	128.701	108.561	154.940	123.781	34	-26	31	-19	114	90	82	89	-3.0761	-1.0304	7.4467
22	844	F	2	DTS	2	131.744	109.624	150.949	124.812	32	-26	28	-18	113	91	80	88	-4.0859	-1.0344	6.4399
23	844	F	2	DTS	3	133.744	110.624	153.949	123.812	31	-26	25	-19	116	91	82	89	-4.1350	-2.0540	6.4055
24	844	F	3	DTS	1	113.224	95.946	128.000	97.446	45	-4	38	-1	160	100	102	95	9.1802	2.3710	12.9329
25	844	F	3	DTS	2	113.184	96.892	126.000	96.417	44	-5	36	-1	165	101	104	95	9.2022	4.3830	18.9469
26	844	F		DTS	3	115.184	98.892	127.000	98.416	46	-2	37	-2	163	102	107	98	10.1250	5.3409	17.8477

OBS	B4	DO	AV1	AV2	AV7	AV8	PAN1	PAN4	IA1	IA2	IB1	IB2	IA7	IA8	IB7	IB8	FPAN1	FPAN4	RA1	RA4
1	11.0000	1	167.5	159.5	16.5	14.0	654	61	7.0	10.0	1.0	5.0	5.0	1	2.0	0	493.14	528.67	1.32620	.115384
2	10.0000	1	164.0	159.0	16.0	14.0	646	60	7.0	10.0	1.0	5.0	5.0	1	2.0	0	493.14	528.67	1.30997	.113492
3	10.0000	1	165.0	158.5	14.0	13.5	647	55	7.0	10.0	1.0	5.0	5.0	1	2.0	0	493.14	528.67	1.31200	.104035
4	10.4629	2	165.5	157.5	19.0	18.5	646	75	7.5	11.0	1.5	5.5	5.0	2	3.5	2	509.25	526.75	1.26853	.142363
5	11.4629	2	165.0	158.0	17.5	17.5	646	70	7.5	11.0	1.5	5.5	5.0	2	3.5	2	509.25	526.75	1.26853	.132890
6	9.4786	2	164.5	156.5	18.0	17.5	642	71	7.5	11.0	1.5	5.5	5.0	2	3.5	2	509.25	526.75	1.26068	.134789
7	10.7661	3	143.0	135.5	28.0	20.5	557	97	7.0	9.5	0.0	5.0	5.5	3	3.5	2	498.67	523.00	1.11697	.185468
8	11.7380	3	144.5	137.5	27.5	21.5	564	98	7.0	9.5	0.0	5.0	5.5	3	3.5	2	498.67	523.00	1.13101	.187380
9	11.7701	3	142.0	136.0	27.5	21.5	556	98	7.0	9.5	0.0	5.0	5.5	3	3.5	2	498.67	523.00	1.11497	.187380
10	11.0000	4	157.0	138.0	13.0	11.5	590	49	7.0	10.0	1.0	5.0	5.0	1	2.0	0	493.14	528.67	1.19641	.092685
11	12.0000	4	156.0	136.5	12.5	12.0	585	49	7.0	10.0	1.0	5.0	5.0	1	2.0	0	493.14	528.67	1.18628	.092685
12	11.0000	4	156.0	138.5	13.0	11.0	589	48	7.0	10.0	1.0	5.0	5.0	1	2.0	0	493.14	528.67	1.19439	.090794
13	18.6829	5	153.0	142.0	7.5	18.0	590	51	7.5	11.0	1.5	5.5	5.0	2	3.5	2	509.25	526.75	1.15857	.096820
14	18.7064	5	151.0	141.0	8.5	18.0	584	53	7.5	11.0	1.5	5.5	5.0	2	3.5	2	509.25	526.75	1.14678	.100617
15	19.6907	5	152.5	141.5	8.5	18.5	588	54	7.5	11.0	1.5	5.5	5.0	2	3.5	2	509.25	526.75	1.15464	.102515
16	19.8984	6	137.0	125.0	7.0	18.0	524	50	7.0	9.5	0.0	5.0	5.5	3	3.5	2	498.67	523.00	1.05080	.095602
17	18.9064	6	136.0	125.0	7.0	17.5	522	49	7.0	9.5	0.0	5.0	5.5	3	3.5	2	498.67	523.00	1.04678	.093699
18	0.0000	7	150.0	127.5	-6.0	-4.0	555	-20	7.0	10.0	1.0	5.0	5.0	1	2.0	0	493.14	528.67	1.12544	-.037831
19	0.0000	7	147.5	126.0	-4.5	-4.0	547	-17	7.0	10.0	1.0	5.0	5.0	1	2.0	0	493.14	528.67	1.10922	-.032156
20	0.0000	7	149.0	127.0	-4.0	-5.0	552	-18	7.0	10.0	1.0	5.0	5.0	1	2.0	0	493.14	528.67	1.11936	-.034048
21	4.9696	8	142.0	116.5	6.5	4.0	517	21	7.5	11.0	1.5	5.5	5.0	2	3.5	2	509.25	526.75	1.01522	.039867
22	3.9656	8	141.5	117.5	5.5	3.5	518	18	7.5	11.0	1.5	5.5	5.0	2	3.5	2	509.25	526.75	1.01718	.034172
23	4.9460	8	144.0	117.5	5.5	3.5	523	18	7.5	11.0	1.5	5.5	5.0	2	3.5	2	509.25	526.75	1.02700	.034172
24	16.2473	9	121.0	97.5	17.5	11.5	437	58	7.0	9.5	0.0	5.0	5.5	3	3.5	2	498.67	523.00	0.87633	.110899
25	16.2554	9	120.0	97.5	18.0	12.5	435	61	7.0	9.5	0.0	5.0	5.5	3	3.5	2	498.67	523.00	0.87232	.116635
26	15.2273	9	121.5	99.5	18	12.5	442	61	7	9.5	0	5	5.5	3	3.5	2	498.67	523	.886358	.116635

```
DATA WINDC; SET;
IF ANGLE=1 THEN GO TO VEL1;
IF ANGLE=2 THEN GO TO VEL2;
IF ANGLE=3 THEN GO TO VEL3;
VEL1:;
V1=  1.300;  V2=  1.300;  V3=  1.310;
V4=  1.350;  V5=  1.360;  V6=  1.350;
V7=  1.370;  V8=  1.360;  V9=  1.355;
GO TO OVER;
VEL2:;
V1=1.290;  V2=1.300;  V3=1.300;
V4=1.355;  V5=1.360;  V6=1.355;
V7=1.360;  V8=1.365;  V9=1.370;
GO TO OVER;
VEL3:;
V1=1.240;  V2=1.230;  V3=1.240;
V4=1.355;  V5=1.370;  V6=0;
V7=1.375;  V8=1.370;  V9=1.375;
OVER:;
V1S=V1**2;  V2S=V2**2;  V3S=V3**2;  V4S=V4**2;  V5S=V5**2;  V6S=V6**2;
V7S=V7**2;  V8S=V8**2;  V9S=V9**2;
IF OBS=1. AND OPNG=0000 THEN VS=V1S;
IF OBS=2. AND OPNG=0000 THEN VS=V2S;
IF OBS=3. AND OPNG=0000 THEN VS=V3S;
IF OBS=1. AND OPNG=0422 THEN VS=V4S;
IF OBS=2. AND OPNG=0422 THEN VS=V5S;
IF OBS=3. AND OPNG=0422 THEN VS=V6S;
IF OBS=1. AND OPNG=0844 THEN VS=V7S;
IF OBS=2. AND OPNG=0844 THEN VS=V8S;
IF OBS=3. AND OPNG=0844 THEN VS=V9S;
IF VEL='S'      THEN GO TO EV1;
IF VEL='M'      THEN GO TO EV2;
IF VEL='F'      THEN GO TO EV3;
EV1: EV=.17337;
GO TO AHEAD;
EV2: EV=.17626;
GO TO AHEAD;
EV3: EV=.17445;
AHEAD: K=(3.84/7.25)**(2*EV);
NEXT:A1=A1/(VS*K); A2=A2/(VS*K); A3=A3/(VS*K); A4=A4/(VS*K);
A5=A5/(VS*K); A6=A6/(VS*K); A7=A7/(VS*K); A8=A8/(VS*K);
B1=B1/(VS*K); B2=B2/(VS*K); B3=B3/(VS*K); B4=B4/(VS*K);
B5=B5/(VS*K); B6=B6/(VS*K); B7=B7/(VS*K); B8=B8/(VS*K);
```

```
  26 OBSERVATIONS IN DATA SET WINDC         71  VARIABLES
```

```
PROC PRINT DATA=WINDC;
DROP V1 V2 V3 V4 V5 V6 V7 V8 V9;
DROP V1S V2S V3S V4S V5S V6S V7S V8S V9S ;
DROP AV1 AV2 AV7 AV8 PAN1 PAN4 FPAN1 FPAN4 IA1 IA2 IA7 IA8 IB1 IB2 IB7 IB8;
DROP PA1 PA4;
DROP AV3 AV4 AV5 AV6 ABSPAN1 PAN2 ABSPAN2 ABSPAN3 PAN3 ABSPAN4;
```

MODEL WIND TUNNEL TESTS

OBS	OPNG	VEL	ANGLE	MODIF	OBS	A1	A2	B1	B2	A3	A4	B3	B4
1	0	F	1	DTS	1	113.149	110.677	133.602	123.659	49.4865	-14.7721	39.1460	-18.4651
2	0	F	1	DTS	2	110.204	110.691	131.388	122.928	50.2251	-11.0791	41.3619	-19.2037
3	0	F	1	DTS	3	109.303	107.622	130.124	121.820	50.9160	-13.0927	41.4602	-18.1843
4	0	F	2	DTS	1	116.965	116.591	130.357	117.928	62.2583	-5.2507	58.5078	-6.7509
5	0	F	2	DTS	2	114.486	115.620	128.370	116.160	61.3042	-5.1702	58.3498	-6.6474
6	0	F	2	DTS	3	114.476	114.127	127.629	115.413	62.0428	-5.1702	58.3498	-5.1702
7	0	F	3	DTS	1	114.223	114.659	116.901	103.159	77.9339	9.7417	62.5095	7.3063
8	0	F	3	DTS	2	116.902	118.991	120.460	105.660	79.2063	9.0757	65.1802	7.4256
9	0	F	3	DTS	3	114.212	114.644	115.277	103.963	79.5576	8.1181	65.7568	5.6827
10	422	F	1	DTS	1	100.237	89.088	114.316	98.994	26.7113	-23.2868	20.5472	-23.2868
11	422	F	1	DTS	2	98.768	87.108	111.291	96.194	25.6451	-22.2708	21.5959	-22.9456
12	422	F	1	DTS	3	99.561	89.786	113.632	99.001	26.7113	-22.6019	19.1774	-22.6019
13	422	F	2	DTS	1	97.406	92.417	110.039	99.578	31.2736	-18.3562	22.4354	-12.2375
14	422	F	2	DTS	2	93.973	90.361	109.227	98.833	29.0195	-16.8718	22.2708	-14.1723
15	422	F	2	DTS	3	96.697	91.015	110.033	100.236	29.9139	-17.6764	22.4354	-12.9174
16	422	F	3	DTS	1	93.366	85.725	92.461	83.298	38.7521	-0.6799	29.9139	0.0000
17	422	F	3	DTS	2	90.011	84.535	90.447	80.825	39.9033	2.6602	31.2576	1.3301
18	844	F	1	DTS	1	91.289	75.403	108.429	94.564	17.9565	-19.9517	15.2963	-19.2866
19	844	F	1	DTS	2	91.934	76.477	107.326	93.916	18.8964	-21.5959	13.4974	-20.9210
20	844	F	1	DTS	3	91.943	76.376	110.841	96.656	19.0361	-20.3958	14.2771	-21.7556
21	844	F	2	DTS	1	86.857	73.265	104.565	83.536	22.9456	-17.5467	20.9210	-12.8226
22	844	F	2	DTS	2	88.260	73.441	101.126	83.616	21.4380	-17.4183	18.7582	-12.0589
23	844	F	2	DTS	3	88.947	73.571	102.384	82.342	20.6167	-17.2914	16.6264	-12.6360
24	844	F	3	DTS	1	74.753	63.346	84.509	64.336	29.7102	-2.6409	25.0886	-0.6602
25	844	F	3	DTS	2	75.273	64.438	83.797	64.123	29.2624	-3.3253	23.9420	-0.6661
26	844	F	3	DTS	3	76.047	65.291	83.848	64.977	30.3704	-1.3204	24.4284	-1.3204

OBS	A5	A6	B5	B6	A7	A8	B7	B8	DO	VS	EV	K
1	57.611	57.611	42.1005	53.9181	12.0902	11.5767	5.4270	8.1247	1	1.69000	.17445	.801127
2	54.657	59.827	42.1005	54.6567	11.4115	12.3273	5.4509	7.3860	1	1.69000	.17445	.801127
3	54.553	57.462	40.0054	52.3707	9.0485	11.4110	4.6377	7.2737	1	1.71610	.17445	.801127
4	94.513	82.511	58.5078	70.5094	16.9953	16.0994	3.4206	7.8483	2	1.66410	.17445	.801127
5	94.541	82.724	58.3498	70.1674	15.2576	13.6368	2.6295	8.4666	2	1.69000	.17445	.801127
6	95.280	81.985	59.0884	71.6447	16.0252	15.1256	2.6498	7.0010	2	1.69000	.17445	.801127
7	138.384	100.665	89.2993	94.9820	29.9207	20.0104	7.3799	8.7400	3	1.53760	.17445	.801127
8	139.436	102.308	89.9322	96.5327	29.5204	21.1274	7.4598	9.6846	3	1.51290	.17445	.801127
9	133.137	99.853	85.2402	94.1702	29.1178	20.8271	7.3856	9.5551	3	1.53760	.17445	.801127
10	45.889	45.989	39.0397	45.2038	7.5462	7.3994	4.5253	7.5340	4	1.82250	.17445	.801127
11	45.216	44.542	39.1425	45.2164	6.7950	7.2979	4.4727	8.0985	4	1.84960	.17445	.801127
12	45.204	45.889	39.7246	46.5736	6.8683	6.7159	5.2130	7.5340	4	1.82250	.17445	.801127
13	67.306	58.468	48.2701	58.4681	-2.5786	8.6226	6.0814	12.7018	5	1.83602	.17445	.801127
14	66.812	57.364	47.2410	57.3641	-1.8450	8.5752	6.7394	12.6244	5	1.84960	.17445	.801127
15	68.666	57.788	48.2701	58.4681	-1.8854	8.6279	6.7706	13.3870	5	1.83602	.17445	.801127
16	111.497	69.346	70.7056	67.9861	-3.2493	7.3749	6.3378	13.5282	6	1.83602	.17445	.801127
17	110.399	71.826	69.1657	67.1706	-3.1639	7.2223	6.2091	12.5739	6	1.87690	.17445	.801127
18	51.209	43.894	48.5490	48.5490	-15.0483	-6.0689	1.8283	0.0000	7	1.87690	.17445	.801127
19	52.640	44.542	47.9159	48.5907	-13.1911	-6.1475	1.8772	0.0000	7	1.84960	.17445	.801127
20	53.029	46.231	49.6299	50.3097	-13.3231	-7.5596	2.5572	0.0000	7	1.83602	.17445	.801127
21	76.935	60.738	55.3394	60.0635	-2.0760	-0.6954	5.0256	3.3538	8	1.84960	.17445	.801127
22	75.703	60.964	53.5949	58.9544	-2.7373	-0.6930	4.3143	2.6567	8	1.86322	.17445	.801127
23	77.146	60.520	54.5345	59.1899	-2.7500	-1.3660	4.2690	3.2894	8	1.87690	.17445	.801127
24	105.636	66.023	67.3432	62.7216	6.0610	1.5654	11.8397	10.7269	9	1.89063	.17445	.801127
25	109.734	67.171	69.1657	63.1802	6.1200	2.9150	12.6007	10.8107	9	1.87690	.17445	.801127
26	107.617	67.343	70.6443	64.7023	6.6848	3.5262	11.8166	10.0535	9	1.89063	.17445	.801127

```
DATA WINDE; SET;
PI=3.141592654;
IF DO=1 OR DC=4 OR DC=7 THEN C=COS(0);
IF DO=2 OR DC=5 OR DO=8 THEN C=COS(PI/12.);
IF DO=3 OR DO=6 OR DO=9 THEN C=COS(PI/6.);
COMMENT
       LINEAR CANTILEVER BEAM CALIBRATION CONSTANTS IN CHART DIVISIONS
       PER OZ. OF STATIC FORCE.  DIRECTION OF LOADING CONSIDERED
                                                                  ;
CA1=32.7355; CB1=35.0395; CA2=34.2445; CB2=36.0115;
CA3=25.0515; CB3=24.6685; CA4=33.9320; CB4=31.9140;
CA5=38.8555; CB5=38.0700; CA6=37.4195; CB6=39.8130;
CA7=34.2265; CB7=39.7555; CA8=38.6700; CB8=37.4620;
COMMENT
       CALIBRATION OF AVG OBSERVATIONS FOR EACH OPENING

A1=A1/CA1;  A2=A2/CA2;  A3=A3/CA3;  A4=A4/CA4;
A5=A5/CA5;  A6=A6/CA6;  A7=A7/CA7;  A8=A8/CA8;
B1=B1/CB1; B2=B2/CB2; B3=B3/CB3; B4=B4/CB4;
B5=B5/CB5; B6=B6/CB6; B7=B7/CB7; B8=B8/CB8;
FA1B=125.25; FA1A=125.00; FA1I=124.00; FB1B=141.25; FB1A=139.00; FB1I=140.00;
FA2B=112.50; FA2A=109.67; FA2I=109.00; FB2B=119.75; FB2A=117.00; FB2I=117.00;
FA3B=119.00; FA3A=105.67; FA3I=108.33; FB3B=115.50; FB3A=105.33; FB3I=107.00;
FA4B=078.50; FA4A=082.00; FA4I=077.33; FB4B=076.33; FB4A=082.67; FB4I=078.67;
FA5B=120.75; FA5A=131.00; FA5I=124.33; FB5B=108.75; FB5A=125.67; FB5I=112.50;
FA6B=153.25; FA6A=152.33; FA6I=151.00; FB6B=160.75; FB6A=162.00; FB6I=161.50;
FA7B=118.33; FA7A=126.33; FA7I=122.33; FB7B=121.67; FB7A=130.00; FB7I=124.33;
FA8B=138.67; FA8A=131.00; FA8I=138.67; FB8B=148.00; FB8A=139.67; FB8I=147.00;
AVFA1=AVG(FA1B,FA1A);   AVFB1=AVG(FB1B,FB1A);
AVFA2=AVG(FA2B,FA2A);   AVFB2=AVG(FB2B,FB2A);
AVFA3=AVG(FA3B,FA3A);   AVFB3=AVG(FB3B,FB3A);
AVFA4=AVG(FA4B,FA4A);   AVFB4=AVG(FB4B,FB4A);
AVFA5=AVG(FA5B,FA5A);   AVFB5=AVG(FB5B,FB5A);
AVFA6=AVG(FA6B,FA6A);   AVFB6=AVG(FB6B,FB6A);
AVFA7=AVG(FA7B,FA7A);   AVFB7=AVG(FB7B,FB7A);
AVFA8=AVG(FA8B,FA8A);   AVFB8=AVG(FB8B,FB8A);
STA1=AVFA1;  STB1=AVFB1;
STA2=AVFA2;  STB2=AVFB2;
STA3=AVFA3;  STB3=AVFB3;
STA4=AVFA4;  STB4=AVFB4;
STA5=AVFA5;  STB5=AVFB5;
STA6=AVFA6;  STB6=AVFB6;
STA7=AVFA7;  STB7=AVFB7;
STA8=AVFA8;  STB8=AVFB8;
IF OPNG=0000 AND ANGLE=2 THEN ORD=6;
IF OPNG=0000 AND ANGLE=3 THEN ORD=7;
IF OPNG=0000 AND ANGLE=1 THEN ORD=8;
IF OPNG=0422 AND ANGLE=1 THEN ORD=9;
IF OPNG=0844 AND ANGLE=1 THEN ORD=10;
IF OPNG=0844 AND ANGLE=3 THEN ORD=13;
IF OPNG=0422 AND ANGLE=3 THEN ORD=14;
IF OPNG=0422 AND ANGLE=2 THEN ORD=15;
IF OPNG=0844 AND ANGLE=2 THEN ORD=16;
IF ANGLE=1 THEN GO TO ANG1;
IF ANGLE=2 THEN GO TO ANG2;
IF ANGLE=3 THEN GO TO ANG3;
ANG1:;
DA1=(FA1I-FA1A)/3.;      DB1=(FB1I-FB1A)/3.;
```

```
DA2=(FA2I-FA2A)/3.;       DB2=(FB2I-FB2A)/3.;
DA3=(FA3I-FA3A)/3.;       DB3=(FB3I-FB3A)/3.;
DA4=(FA4I-FA4A)/3.;       DB4=(FB4I-FB4A)/3.;
DA5=(FA5I-FA5A)/3.;       DB5=(FB5I-FB5A)/3.;
DA6=(FA6I-FA6A)/3.;       DB6=(FB6I-FB6A)/3.;
DA7=(FA7I-FA7A)/3.;       DB7=(FB7I-FB7A)/3.;
DA8=(FA8I-FA8A)/3.;       DB8=(FB8I-FB8A)/3.;
IF ORD=8 THEN GO TO IS8;
GO TO GT8;
IS8:A1=A1*AVFA1/FA1B;       B1=B1*AVFB1/FB1B;
    A2=A2*AVFA2/FA2B;       B2=B2*AVFB2/FB2B;
    A3=A3*AVFA3/FA3B;       B3=B3*AVFB3/FB3B;
    A4=A4*AVFA4/FA4B;       B4=B4*AVFB4/FB4B;
    A5=A5*AVFA5/FA5B;       B5=B5*AVFB5/FB5B;
    A6=A6*AVFA6/FA6B;       B6=B6*AVFB6/FB6B;
    A7=A7*AVFA7/FA7B;       B7=B7*AVFB7/FB7B;
    A8=A8*AVFA8/FA8B;       B8=B8*AVFB8/FB8B;
GO TO CAB;
GT8:A1=A1*(AVFA1/(FA1I-(ORD-9)*DA1)); B1=B1*(AVFB1/(FB1I-(ORD-9)*DB1));
    A2=A2*(AVFA2/(FA2I-(ORD-9)*DA2)); B2=B2*(AVFB2/(FB2I-(ORD-9)*DB2));
    A3=A3*(AVFA3/(FA3I-(ORD-9)*DA3)); B3=B3*(AVFB3/(FB3I-(ORD-9)*DB3));
    A4=A4*(AVFA4/(FA4I-(ORD-9)*DA4)); B4=B4*(AVFB4/(FB4I-(ORD-9)*DB4));
    A5=A5*(AVFA5/(FA5I-(ORD-9)*DA5)); B5=B5*(AVFB5/(FB5I-(ORD-9)*DB5));
    A6=A6*(AVFA6/(FA6I-(ORD-9)*DA6)); B6=B6*(AVFB6/(FB6I-(ORD-9)*DB6));
    A7=A7*(AVFA7/(FA7I-(ORD-9)*DA7)); B7=B7*(AVFB7/(FB7I-(ORD-9)*DB7));
    A8=A8*(AVFA8/(FA8I-(ORD-9)*DA8)); B8=B8*(AVFB8/(FB8I-(ORD-9)*DB8));
GO TO CAB;
ANG2:;
IF ORD=6 THEN GO TO NO6;
IF ORD=15 OR ORD=16 THEN GO TO NO15_16;
NO6::
A1=A1*STA1/124.25;  B1=B1*STB1/142.00;
A2=A2*STA2/111.25;  B2=B2*STB2/119.75;
A3=A3*STA3/103.50;  B3=B3*STB3/104.75;
A4=A4*STA4/103.25;  B4=B4*STB4/96.25;
A5=A5*STA5/127.00;  B5=B5*STB5/119.50;
A6=A6*STA6/151.00;  B6=B6*STB6/159.67;
A7=A7*STA7/122.25;  B7=B7*STB7/127.75;
A8=A8*STA8/132.00;  B8=B8*STB8/141.00;
GO TO CAB;
NO15_16:;
A1=A1*STA1/126.75;  B1=B1*STB1/145.75;
A2=A2*STA2/113.50;  B2=B2*STB2/123.25;
A3=A3*STA3/103.33;  B3=B3*STB3/100.00;
A4=A4*STA4/89.00;   B4=B4*STB4/88.33;
A5=A5*STA5/122.75;  B5=B5*STB5/111.25;
A6=A6*STA6/147.75;  B6=B6*STB6/159.50;
A7=A7*STA7/119.75;  B7=B7*STB7/123.00;
A8=A8*STA8/137.75;  B8=B8*STB8/146.25;
GO TO CAB;
ANG3:;
IF ORD=7 THEN GO TO NO7;
IF ORD=13 OR ORD=14 THEN GO TO NO13_14;
NO7::
A1=A1*STA1/126.0;  B1=B1*STB1/144.0;
A2=A2*STA2/113.67; B2=B2*STB2/120.0;
A3=A3*STA3/112.17; B3=B3*STB3/111.5;
A4=A4*STA4/78.33;  B4=B4*STB4/72.5;
A5=A5*STA5/120.0;  B5=B5*STB5/118.33;
A6=A6*STA6/147.33; B6=B6*STB6/159.67;
```

```
A7=A7*STA7/115.33; B7=B7*STB7/118.33;
A8=A8*STA8/140.33; B8=B8*STB8/149.67;
GO TO CAR;
NO13_14:;
A1=A1*STA1/126.33;  B1=B1*STB1/140.67;
A2=A2*STA2/113.67;  B2=B2*STB2/118.00;
A3=A3*STA3/103.33;  B3=B3*STB3/104.00;
A4=A4*STA4/86.33;   B4=B4*STB4/84.67;
A5=A5*STA5/119.75;  B5=B5*STB5/110.75;
A6=A6*STA6/148.75;  B6=B6*STB6/161.75;
A7=A7*STA7/118.00;  B7=B7*STB7/121.33;
A8=A8*STA8/137.33;  B8=B8*STB8/146.33;
CAR:;
COMMENT
                    ADJUSTMENT FOR DIFFERENCE IN LENGTH OF
                     OPENING AND MOVEABLE PANEL
     ;
I=(20+19/32)/18.;
A1=A1*L; A2=A2*L; A3=A3*L; A4=A4*L;
A5=A5*L; A6=A6*L; A7=A7*L; A8=A8*L;
B1=B1*L; B2=B2*L; B3=B3*L; B4=B4*L; B5=B5*L;
B6=B6*L; B7=B7*L; B8=B8*L;
COMMENT
       RECORDER CHANNEL CALIBRATION CONSTANTS FOR TESTS AND STANDARD
                                                                      ;
R5=  20  ;R6=  20.00;R7=  19.9 ;R8=  20.0 ;
ST=20.;
COMMENT
       CHANNEL CALIBRATION ADJUSTMENTS,HIGHER THAN STANDARD INDICATES
       A HIGH READING FOR THAT CHANNEL (COMMON TO 4 MONITORING POINTS)
                                                                      ;
A1=A1*ST/R5;  B1=B1*ST/R7;
A2=A2*ST/R6;  B2=B2*ST/R8;
A3=A3*ST/R5;  B3=B3*ST/R7;
A4=A4*ST/R6;  B4=B4*ST/R8;
A5=A5*ST/R5;  B5=B5*ST/R7;
A6=A6*ST/R6;  B6=B6*ST/R8;
A7=A7*ST/R5;  B7=B7*ST/R7;
A8=A8*ST/R6;  B8=B8*ST/R8;
AV1=(A1+B1)/2.0;
AV2=(A2+B2)/2.0;
AV3=(A3+B3)/2.0;
AV4=(A4+B4)/2.0;
AV5=(A5+B5)/2.0;
AV6=(A6+B6)/2.0;
AV7=(A7+B7)/2.0;
AV8=(A8+B8)/2.0;
PAN1=(AV1+AV2)*2.; ABSPAN1=(ABS(AV1)+ABS(AV2))*2.;
PAN2=(AV3+AV4)*2.; ABSPAN2=(ABS(AV3)+ABS(AV4))*2.;
PAN3=(AV5+AV6)*2.; ABSPAN3=(ABS(AV5)+ABS(AV6))*2.;
PAN4=(AV7+AV8)*2.; ABSPAN4=(ABS(AV7)+ABS(AV8))*2.;
PANTOT=(PAN1 + PAN2 + PAN3 + PAN4);
ABSPANTO=ABSPAN1+ABSPAN2+ABSPAN3+ABSPAN4;
```

26 OBSERVATIONS IN DATA SET WINDE 194 VARIABLES

MODEL WIND TUNNEL TESTS

OBS	OPNG	VEL	ANGLE	MODIF	A1	A2	B1	B2	A3	A4	B3	B4	A5	A6	B5
1	0	F	1	DTS	3.87154	3.61773	4.28756	3.85668	2.16462	-.447452	1.81162	-.695152	1.70684	1.77717	1.34777
2	0	F	2	DTS	4.05840	3.85129	4.17039	3.65876	3.06671	-.136196	2.86947	-.183276	2.76601	2.54944	1.73745
3	0	F	3	DTS	3.99522	3.79058	3.75355	3.26755	3.60862	.310153	2.97639	.267504	4.21042	3.20066	2.63745
4	422	F	1	DTS	3.50983	3.01878	3.71411	3.15210	1.24817	-.794979	0.98316	-.831235	1.35449	1.40578	1.23676
5	422	F	2	DTS	3.31304	2.98422	3.46305	3.03760	1.49292	-.536141	1.15185	-.422972	2.04099	1.82983	1.52512

OBS	B6	A7	A8	B7	B8	DC	AV1	AV2	AV3	AV4	AV5	AV6	AV7	AV8
1	1.54768	0.37495	.338647	.154707	.225419	1	4.07955	3.73720	1.98812	-.571302	1.52730	1.66243	.264828	.282033
2	2.05553	0.53829	.451932	.082619	.242129	2	4.11439	3.75503	2.96809	-.159736	2.25173	2.30249	.310453	.347030
3	2.76578	1.04665	.587173	.227863	.273731	3	3.87439	3.52906	3.29250	.288828	3.42394	2.98322	.637257	.430452
4	1.31124	0.23633	.205338	.138666	.230758	4	3.61197	3.08544	1.11567	-.813107	1.29563	1.35851	.187496	.218048
5	1.68924	-0.07181	.249305	.193234	.387595	5	3.38804	3.01091	1.32238	-.479557	1.78305	1.75953	.060711	.318450

OBS	PAN1	ABSPAN1	PAN2	ABSPAN2	PAN3	ABSPAN3	PAN4	ABSPAN4	ORD	PANTOT	ABSPANTO
1	15.6335		2.83364	5.11884	6.3795		1.09372		8	25.9403	28.2255
2	15.7388		5.61671	6.25566	9.1084		1.31497		6	31.7789	32.4179
3	14.8069		7.16266		12.8143		2.13542		7	36.9193	
4	13.3948		0.60512	3.85755	5.3083		0.81109		9	20.1193	23.3717
5	12.7979		1.68566	3.60388	7.0852		0.75832		15	22.3271	24.2453

MODEL WIND TUNNEL TESTS

OBS	OPNG	VEL	ANGLE	MODIF	A1	A2	B1	B2	A3	A4	B3	B4	A5	A6	B5
6	422	F	3	DTS	3.17393	2.77948	2.98351	2.61541	1.95261	.031035	1.51360	.022386	3.43395	2.21677	2.23551
7	844	F	1	DTS	3.22608	2.58531	3.58422	3.05510	0.88955	-.708220	0.69417	-.735789	1.53150	1.38467	1.47498
8	844	F	2	DTS	3.03688	2.40093	3.23985	2.53766	1.07575	-.529574	0.96595	-.403508	2.31275	1.92050	1.73395
9	844	F	3	DTS	2.60862	2.10130	2.74753	2.05502	1.47862	-.076128	1.21176	-.029686	3.33226	2.09930	2.20723

OBS	B6	A7	A8	B7	B8	DC	AV1	AV2	AV3	AV4	AV5	AV6	AV7	AV8
6	1.93748	-.111121	.212014	.188184	.391784	6	3.08172	2.69745	1.73311	.026710	2.83473	2.07713	.038532	.301899
7	1.40986	-.458114	-.193201	.060194	.000000	7	3.40515	2.82021	0.79186	-.722005	1.50319	1.39726	-.198960	-.096601
8	1.72711	-.086089	-.026589	.134138	.093110	8	3.13836	2.46930	1.02085	-.466541	2.02335	1.82380	.024025	.033261
9	1.82155	.217924	.077527	.362533	.316116	9	2.67807	2.07816	1.34519	-.052907	2.76975	1.96043	.290228	.196822

OBS	PAN1	ABSPAN1	PAN2	ABSPAN2	PAN3	ABSPAN3	PAN4	ABSPAN4	ORD	PANTOT	ABSPANTO
6	11.5583		3.51963	3.54094	9.82372		.680861		14	25.5825	25.6039
7	12.4507		0.13971	3.02773	5.80091		-.591121	.591121	10	17.8002	21.8705
8	11.2153		1.10862	2.97479	7.69429		.114571		16	20.1328	21.9990
9	9.5125		2.58457	2.79619	9.46034		.974100		13	22.5315	22.7431

```
DATA WI; SET WINDE;

  26 OBSERVATIONS IN DATA SET WI           194  VARIABLES


DATA SUPP;
INPUT OPNG 1-4 VEL $ 5 ANGLE 6 MODIF $ 7-9 OBS 11-12;
IF ANGLE=3 AND    OPNG=0422 THEN GO TO DEF;
DEF:;
OBS=3;
A1=3.17392640;
A2=2.77948487;
B1=2.98951144;
B2=2.61541      ;
A3=1.95261372;
A4=.03103493;
B3=1.51359895;
B4=.02238602;
A5=3.43395485;
A6=2.21677087;
B5=2.23550923;
B6=1.93748117;
A7=-.11112077;
A8=.21201354;
B7=0.188184384;
B8=.391783835;
PAN1=11.5583      ;
PAN2=3.51963362;
ABSPAN2=3.54094232;
PAN3=9.8237161;
PAN4=0.68086098;
PANTOT=25.5825     ;
ABSPANTO=25.6039    ;
CARDS


   1 OBSERVATIONS IN DATA SET SUPP          28  VARIABLES

DATA WISUPP; SET WI ;     SET SUPP;
  27 OBSERVATIONS IN DATA SET WISUPP       194  VARIABLES


DATA WIN; SET WISUPP;

  27 OBSERVATIONS IN DATA SET WIN          194  VARIABLES


PROC SORT DATA=WIN;
BY ANGLE OPNG;
```

```
1   DATA SWIM; SET WIM;
    IF ANGLE>1 THEN GO TO EIT;
    IF OPNG=0 THEN GO TO OPZERO;
    IF OPNG=422 THEN GO TO OPFOUR;
    IF OPNG=844 THEN GO TO OPATE;
    OPZERO:
    IF OBS=1 THEN GO TO POP1;
    IF OBS=2 THEN GO TO POP2;
    IF OBS=3 THEN GO TO POP3;
    POP1:
    ODI11=A1-((A1+B1)/2);
    ODI12=A2-((A2+B2)/2);
    ODI13=A3-((A3+B3)/2);
    ODI14=A4-((A4+B4)/2);
    ODI15=A5-((A5+B5)/2);
    ODI16=A6-((A6+B6)/2);
    ODI17=A7-((A7+B7)/2);
    ODI18=A8-((A8+B8)/2);
    GO TO EIT;
    POP2:
    ODI21=A1-((A1+B1)/2);
    ODI22=A2-((A2+B2)/2);
    ODI23=A3-((A3+B3)/2);
    ODI24=A4-((A4+B4)/2);
    ODI25=A5-((A5+B5)/2);
    ODI26=A6-((A6+B6)/2);
    ODI27=A7-((A7+B7)/2);
    ODI28=A8-((A8+B8)/2);
    GO TO EIT;
    POP3:
    ODI31=A1-((A1+B1)/2);
    ODI32=A2-((A2+B2)/2);
    ODI33=A3-((A3+B3)/2);
    ODI34=A4-((A4+B4)/2);
    ODI35=A5-((A5+B5)/2);
    ODI36=A6-((A6+B6)/2);
    ODI37=A7-((A7+B7)/2);
    ODI38=A8-((A8+B8)/2);
    GOTO EIT;
    OPFOUR:
    IF OBS=1 THEN GO TO POP4;
    IF OBS=2 THEN GO TO POP5;
    IF OBS=3 THEN GO TO POP6;
    POP4:
    FDI11=A1-((A1+B1)/2);
    FDI12=A2-((A2+B2)/2);
    FDI13=A3-((A3+B3)/2);
    FDI14=A4-((A4+B4)/2);
    FDI15=A5-((A5+B5)/2);
    FDI16=A6-((A6+B6)/2);
    FDI17=A7-((A7+B7)/2);
    FDI18=A8-((A8+B8)/2);
    GO TO EIT;
    POP5:
    FDI21=A1-((A1+B1)/2);
    FDI22=A2-((A2+B2)/2);
    FDI23=A3-((A3+B3)/2);
    FDI24=A4-((A4+B4)/2);
```



```
2   FDI25=A5-((A5+B5)/2);
    FDI26=A6-((A6+B6)/2);
    FDI27=A7-((A7+B7)/2);
    FDI28=A8-((A8+B8)/2);
    GO TO EIT;
    POP6:
    FDI31=A1-((A1+B1)/2);
    FDI32=A2-((A2+B2)/2);
    FDI33=A3-((A3+B3)/2);
    FDI34=A4-((A4+B4)/2);
    FDI35=A5-((A5+B5)/2);
    FDI36=A6-((A6+B6)/2);
    FDI37=A7-((A7+B7)/2);
    FDI38=A8-((A8+B8)/2);
    GO TO EIT;
    OPATE:
    IF OBS=1 THEN GO TO POP7;
    IF OBS=2 THEN GO TO POP8;
    IF OBS=3 THEN GO TO POP9;
    POP7:
    EDI11=A1-((A1+B1)/2);
    EDI12=A2-((A2+B2)/2);
    EDI13=A3-((A3+B3)/2);
    EDI14=A4-((A4+B4)/2);
    EDI15=A5-((A5+B5)/2);
    EDI16=A6-((A6+B6)/2);
    EDI17=A7-((A7+B7)/2);
    EDI18=A8-((A8+B8)/2);
    GO TO EIT;
    POP8:
    EDI21=A1-((A1+B1)/2);
    EDI22=A2-((A2+B2)/2);
    EDI23=A3-((A3+B3)/2);
    EDI24=A4-((A4+B4)/2);
    EDI25=A5-((A5+B5)/2);
    EDI26=A6-((A6+B6)/2);
    EDI27=A7-((A7+B7)/2);
    EDI28=A8-((A8+B8)/2);
    GO TO EIT;
    POP9:
    EDI31=A1-((A1+B1)/2);
    EDI32=A2-((A2+B2)/2);
    EDI33=A3-((A3+B3)/2);
    EDI34=A4-((A4+B4)/2);
    EDI35=A5-((A5+B5)/2);
    EDI36=A6-((A6+B6)/2);
    EDI37=A7-((A7+B7)/2);
    EDI38=A8-((A8+B8)/2);
    EIT:
    IF OPNG=0 THEN GO TO DIFZERO;
    IF OPNG=422 THEN GO TO DIFOUR;
    IF OPNG=844 THEN GO TO DIFATE;
    DIFZERO:
    IF OBS=1              THEN GO TO POOF1;
    IF OBS=2              THEN GO TO POOF2;
    IF OBS=3              THEN GO TO POOF3;
    POOF1:
    A1=A1-ODI11;
    B1=B1+ODI11;
    A2=A2-ODI12;
```

```
3
      B2=B2+CDI12;
      A3=A3-CDI13;
      B3=B3+ODI13;
      A4=A4-ODI14;
      B4=B4+CDI14;
      A5=A5-ODI15;
      B5=B5+CDI15;
      A6=A6-ODI16;
      B6=B6+CDI16;
      A7=A7-CDI17;
      B7=B7+ODI17;
      A8=A8-CDI18;
      B8=B8+CDI18;
      GO TO TIP;
      POOP2:
      A1=A1-ODI21;
      B1=B1+ODI21;
      A2=A2-CDI22;
      B2=B2+ODI22;
      A3=A3-CDI23;
      B3=B3+ODI23;
      A4=A4-ODI24;
      B4=B4+CDI24;
      A5=A5-ODI25;
      B5=B5+ODI25;
      A6=A6-ODI26;
      B6=B6+ODI26;
      A7=A7-CDI27;
      B7=B7+ODI27;
      A8=A8-CDI28;
      B8=B8+ODI28;
      GO TO TIP;
      POOP3:
      A1=A1-ODI31;
      B1=B1+ODI31;
      A2=A2-CDI32;
      B2=B2+ODI32;
      A3=A3-CDI33;
      B3=B3+ODI33;
      A4=A4-ODI34;
      B4=B4+CDI34;
      A5=A5-ODI35;
      B5=B5+CDI35;
      A6=A6-CDI36;
      B6=B6+ODI36;
      A7=A7-CDI37;
      B7=B7+ODI37;
      A8=A8-CDI38;
      B8=B8+CDI38;
      GO TO TIP;
      DIFCUR:
      IF OBS=1          THEN GO TO POOP4;
      IF OBS=2          THEN GO TO POOP5;
      IF OBS=3          THEN GO TO POOP6;
      POOP4:
      A1=A1-FDI11;
      B1=B1+FDI11;
      A2=A2-FDI12;
      B2=B2+FDI12;

4
      A3=A3-FDI13;
      B3=B3+FDI13;
      A4=A4-FDI14;
      B4=B4+FDI14;
      A5=A5-FDI15;
      B5=B5+FDI15;
      A6=A6-FDI16;
      B6=B6+FDI16;
      A7=A7-FDI17;
      B7=B7+FDI17;
      A8=A8-FDI18;
      B8=B8+FDI18;
      GO TO TIP;
      POOP5:
      A1=A1-FDI21;
      B1=B1+FDI21;
      A2=A2-FDI22;
      B2=B2+FDI22;
      A3=A3-FDI23;
      B3=B3+FDI23;
      A4=A4-FDI24;
      B4=B4+FDI24;
      A5=A5-FDI25;
      B5=B5+FDI25;
      A6=A6-FDI26;
      B6=B6+FDI26;
      A7=A7-FDI27;
      B7=B7+FDI27;
      A8=A8-FDI28;
      B8=B8+FDI28;
      GO TO TIP;
      POOP6:
      A1=A1-FDI31;
      B1=B1+FDI31;
      A2=A2-FDI32;
      B2=B2+FDI32;
      A3=A3-FDI33;
      B3=B3+FDI33;
      A4=A4-FDI34;
      B4=B4+FDI34;
      A5=A5-FDI35;
      B5=B5+FDI35;
      A6=A6-FDI36;
      B6=B6+FDI36;
      A7=A7-FDI37;
      B7=B7+FDI37;
      A8=A8-FDI38;
      B8=B8+FDI38;
      GO TO TIP;
      DIFATE:
      IF OBS=1          THEN GO TO POOP7;
      IF OBS=2          THEN GO TO POOP8;
      IF OBS=3          THEN GO TO POOP9;
      POOP7:
      A1=A1-EDI11;
      B1=B1+EDI11;
      A2=A2-EDI12;
      B2=B2+EDI12;
      A3=A3-EDI13;
      B3=B3+EDI13;

5
      A4=A4-EDI14;
      B4=B4+EDI14;
      A5=A5-EDI15;
      B5=B5+EDI15;
      A6=A6-EDI16;
      B6=B6+EDI16;
      A7=A7-EDI17;
      B7=B7+EDI17;
      A8=A8-EDI18;
      B8=B8+EDI18;
      GO TO TIP;
      POOP8:
      A1=A1-EDI21;
      B1=B1+EDI21;
      A2=A2-EDI22;
      B2=B2+EDI22;
      A3=A3-EDI23;
      B3=B3+EDI23;
      A4=A4-EDI24;
      B4=B4+EDI24;
      A5=A5-EDI25;
      B5=B5+EDI25;
      A6=A6-EDI26;
      B6=B6+EDI26;
      A7=A7-EDI27;
      B7=B7+EDI27;
      A8=A8-EDI28;
      B8=B8+EDI28;
      GO TO TIP;
      POOP9:
      A1=A1-EDI31;
      B1=B1+EDI31;
      A2=A2-EDI32;
      B2=B2+EDI32;
      A3=A3-EDI33;
      B3=B3+EDI33;
      A4=A4-EDI34;
      B4=B4+EDI34;
      A5=A5-EDI35;
      B5=B5+EDI35;
      A6=A6-EDI36;
      B6=B6+EDI36;
      A7=A7-EDI37;
      B7=B7+EDI37;
      A8=A8-EDI38;
      B8=B8+EDI38;

  27 OBSERVATIONS IN DATA SET SWIM
                                  266  VARIABLES
      TIP:
      PROC PRINT;
      VAR OBS OPNG ANGLE A1 B1  A2 B2
                                A3 B3
                                A4 B4
                                A5 B5
                                A6 B6
                                A7 B7
                                A8 B8
```

OBS	OBS	OPNG	ANGLE	A1	B1	A2	B2	A3	B3	A4	B4	A5	B5	A6	B6
1	1	0	1	4.14995	4.14995	3.76738	3.76738	1.93890	1.93890	-.599317	-.599317	1.56943	1.56943	1.65581	1.65581
2	2	0	1	4.06250	4.06250	3.75613	3.75613	2.00419	2.00419	-.549459	-.549459	1.52409	1.52409	1.70024	1.70024
3	3	0	1	4.02620	4.02620	3.68810	3.68810	2.02127	2.02127	-.565130	-.565130	1.48839	1.48839	1.63122	1.63122
4	1	422	1	3.64487	3.64487	3.10768	3.10768	1.12666	1.12666	-.829222	-.829222	1.29824	1.29824	1.35884	1.35884
5	2	422	1	3.56930	3.56930	3.02897	3.02897	1.12663	1.12663	-.805265	-.805265	1.28984	1.28984	1.33818	1.33818
6	3	422	1	3.62173	3.62173	3.11967	3.11967	1.09371	1.09371	-.804833	-.804833	1.29881	1.29881	1.37851	1.37851
7	1	844	1	3.39034	3.39034	2.80087	2.80087	0.79850	0.79850	-.685703	-.685703	1.48507	1.48507	1.37330	1.37330
8	2	844	1	3.38354	3.38354	2.80872	2.80872	0.77745	0.77745	-.743013	-.743013	1.49643	1.49643	1.38389	1.38389
9	3	844	1	3.44155	3.44155	2.85103	2.85103	0.79963	0.79963	-.737297	-.737297	1.52808	1.52808	1.43460	1.43460
10	1	0	2	4.31606	4.02190	4.00569	3.58740	2.89148	3.06921	-.227740	-.109761	2.55934	1.93220	2.45232	2.14821
11	2	0	2	4.24419	3.94218	3.96158	3.54357	2.87763	3.02800	-.303068	-.029261	2.60552	1.88218	2.43578	2.16139
12	3	0	2	4.23896	3.92305	3.94502	3.48690	2.90154	3.04070	-.249332	-.039256	2.59457	1.93656	2.41599	2.20123
13	1	422	2	3.47052	3.36180	3.09627	2.96413	1.41438	1.29302	-.572479	-.380447	1.96254	1.60577	1.78780	1.76977
14	2	422	2	3.32828	3.35998	3.01774	2.95269	1.35293	1.23408	-.538943	-.431279	1.95927	1.56138	1.77391	1.70765
15	3	422	2	3.44675	3.36093	3.03864	2.99600	1.31393	1.32596	-.551386	-.402807	2.02458	1.58479	1.78597	1.74110
16	1	844	2	3.17621	3.11942	2.63443	2.31024	1.08034	1.13564	-.534821	-.412368	2.30832	1.77569	1.93974	1.72700
17	2	844	2	3.19511	3.04045	2.61152	2.34136	0.93956	1.09026	-.531834	-.386614	2.24057	1.75072	1.93749	1.70414
18	3	844	2	3.27651	3.02245	2.66153	2.25671	0.91429	0.96502	-.563421	-.369991	2.30441	1.76036	1.92205	1.71239
19	1	0	3	4.16374	3.53357	3.85980	3.11681	3.36990	3.07990	.246380	.377354	4.01351	2.87055	3.09152	2.85898
20	2	0	3	4.27207	3.63185	3.98953	3.20692	3.46155	3.16972	.145936	.459479	4.15311	2.84414	3.12051	2.92713
21	3	0	3	4.17387	3.47122	3.88084	3.12049	3.46491	3.20904	.166592	.337229	3.92605	2.73627	3.04573	2.85545
22	1	422	3	3.34182	2.91259	2.87326	2.58046	1.76569	1.61870	-.035713	.014404	3.38121	2.32986	2.11699	2.01001
23	2	422	3	3.20193	2.87054	2.82312	2.51294	1.89332	1.63472	.057379	.070772	3.35886	2.26900	2.21590	1.96560
24	3	422	3	3.28445	2.87899	2.84206	2.55284	1.78132	1.68489	.017055	.036366	3.38520	2.28426	2.17560	1.97865
25	1	844	3	2.76720	2.58297	2.30701	1.81173	1.41620	1.30047	-.084133	-.020864	3.25495	2.16734	2.09279	1.77891
26	2	844	3	2.75569	2.5892	2.31399	1.83359	1.32804	1.30965	-.106497	-.020112	3.35114	2.25614	2.11944	1.80146
27	3	844	3	2.84018	2.5332	2.38760	1.81507	1.39857	1.31821	-.079106	-.006728	3.30587	2.28315	2.12347	1.84649

OBS	A7	B7	A8	B8
1	.290071	.290071	.287092	.287092
2	.278703	.278703	.286928	.286928
3	.225709	.225709	.272080	.272080
4	.192360	.192360	.219001	.219001
5	.179034	.179034	.225974	.225974
6	.191094	.191094	.209169	.209169
7	-.222441	-.222441	-.088935	-.088935
8	-.191030	-.191030	-.090087	-.090087
9	-.183409	-.183409	-.110780	-.110780
10	.440743	.225183	.440602	.290453
11	.394705	.190562	.344422	.331474
12	.449048	.162474	.400930	.274301
13	-.147943	.239836	.255845	.375375
14	-.111109	.247522	.264368	.363157
15	-.102875	.238833	.265831	.386123
16	.204271	-.126455	.068796	.011800
17	.151686	-.117500	.070019	-.010290
18	.163238	-.131092	.071220	-.011981
19	.933137	.354719	.522902	.302462
20	.931030	.345092	.532899	.351943
21	.945423	.314142	.535875	.336628
22	-.172492	.250005	.220364	.399974
23	-.157745	.234359	.225826	.361430
24	-.149615	.226678	.227979	.375818
25	.485197	.079995	.134408	.233082
26	.457239	.132824	.174763	.234445
27	.488798	.097317	.213212	.191020

```
DATA TIP; SET;
ANGL=(ANGLE-1)*15;
CP1=CENG;
PANTOTA=(2.*PAN1)-PANTOC;
IN=(ABSPANTO+PANTOTA)/2.;
OUT=(ABSPANTO-PANTOTA)/2.;
```

27 OBSERVATIONS IN DATA SET TIP 271 VARIABLES

```
DATA WINA;SET; KEEP A1 A2 A3 A4 A5 A6 A7 A8 B1 B2 B3 B4 B5 B6 B7 B8
PAN1 PAN2 ABSPAN2 PAN3 PAN4 PANTOTA IN OUT ABSPANTO ANGL CP1;
```

27 OBSERVATIONS IN DATA SET WINA 27 VARIABLES

```
DATA COMP; SET;
CI=CP1/1000;
AL=ANGL;
AQ=AI*AL;
OQ=CI*CL;
AQCL=AQ*CL;
ALCL=AL*CL;
AICQ=AI*CQ;
AQOQ=AQ*OQ;
```

27 OBSERVATIONS IN DATA SET COMP 35 VARIABLES

```
PROC REGR DATA=COMP;
ID CP1 ANGL;
MODEL A1=AL AQ CL CQ ALCL AQCL ALCQ AQCQ/P CLM;
MODEL B1=AL AQ CL CQ ALCL AQCL ALCQ AQCQ/P CLM;
MODEL A2=AL AQ CL CQ ALCL AQCL ALCQ AQCQ/P CLM;
MODEL B2=AL AQ CL CQ ALCL AQCL ALCQ AQCQ/P CLM;
MODEL A3=AL AQ CL CQ ALCL AQCL ALCQ AQCQ/P CLM;
MODEL B3=AL AQ CL CQ ALCL AQCL ALCQ AQCQ/P CLM;
MODEL A4=AL AQ CL CQ ALCL AQCL ALCQ AQCQ/P CLM;
MODEL B4=AL AQ CL CQ ALCL AQCL ALCQ AQCQ/P CLM;
MODEL A5=AL AQ CL CQ ALCL AQCL ALCQ AQCQ/P CLM;
MODEL B5=AL AQ CL CQ ALCL AQCL ALCQ AQCQ/P CLM;
MODEL A6=AL AQ CL CQ ALCL AQCL ALCQ AQCQ/P CLM;
MODEL B6=AL AQ CL CQ ALCL AQCL ALCQ AQCQ/P CLM;
MODEL A7=AL AQ CL CQ ALCL AQCL ALCQ AQCQ/P CLM;
MODEL B7=AL AQ CL CQ ALCL AQCL ALCQ AQCQ/P CLM;
MODEL A8=AL AQ CL CQ ALCL AQCL ALCQ AQCQ/P CLM;
MODEL B8=AL AQ CL CQ ALCL AQCL ALCQ AQCQ/P CLM;
MODEL PAN1=AL AQ CL CQ ALCL AQCL ALCQ AQCQ/P CLM;
MODEL PAN2=AL AQ CL CQ ALCL AQCL ALCQ AQCQ/P CLM;
MODEL ABSPAN2=AL AQ CL CQ ALCL AQCL ALCQ AQCQ/P CLM;
MODEL PAN3=AL AQ CL CQ ALCL AQCL ALCQ AQCQ/P CLM;
MODEL PAN4=AL AQ CL CQ ALCL AQCL ALCQ AQCQ/P CLM;
MODEL IN       =AL AQ CL CQ ALCL AQCL ALCQ AQCQ/P CLM;
MODEL OUT      =AL AQ CL CQ ALCL AQCL ALCQ AQCQ/P CLM;
MODEL PANTOTA =AL AQ CL CQ ALCL AQCL ALCQ AQCQ/P CLM;
MODEL ABSPANTO=AL AQ CL CQ ALCL AQCL ALCQ AQCQ/P CLM;
```

VITA[2]

Ronald Jay Gaddis

Candidate for the Degree of

Doctor of Philosophy

Thesis: INVESTIGATION OF WIND PROTECTIVE SYSTEMS ON MODELS OF SINGLE STORY STRUCTURES

Major Field: Agricultural Engineering

Biographical:

Personal Data: Born in Oklahoma City, Oklahoma, February 14, 1934, the son of Mr. and Mrs. Allen Dillon Gaddis. Married September 4, 1955, to Mary Lou Shaver. Four children: Sheryl Anne, Valerie Elizabeth, Marc Allen and Michael Jay.

Education: Graduated from Putnam City High School, Oklahoma City, Oklahoma, in 1952; received the degree of Bachelor of Science in Agricultural Engineering from Oklahoma A & M College in 1957; completed requirements for the Master of Science degree at Oklahoma State University in July, 1971; completed requirements for Doctor of Philosophy at Oklahoma State University in July, 1977.

Professional Experience: Civil Engineer Trainee for Bureau of Land Management, Farmington, New Mexico, summer of 1955; Civil Engineer for A. M. Brenneke Consulting Engineers in Dallas, Texas, summer 1957; Minister, Construction Engineer, Teacher of Agricultural Mechanics and Construction, Mathematics and French at Institut Polytechnique au Congo, Sandoa, Democratic Republic of the Congo for the Board of Missions of the United Methodist Church from 1959 to 1969; Assistant Professor of Agricultural Engineering, University of Nebraska, from 1973 to 1977.

Professional and Honorary Societies: Member, American Society of Agricultural Engineers; Member, Phi Kappa Phi; Member, Sigma Tau; Member, Alpha Zeta; Soil Conservation Society of America.